

**Dark Matter in Galaxy Clusters: Shape, Projection, and Environment**

A Thesis

Submitted to the Faculty

of

Drexel University

by

Austen M. Groener

in partial fulfillment of the

requirements for the degree

of

Doctor of Philosophy

September 2015

© Copyright 2015  
Austen M. Groener.

## Dedications

I dedicate this thesis to my family, and to my wife,  
who supported me unconditionally throughout my  
career as a scientist.

## Acknowledgments

I have many people to thank for making this work a possibility. Firstly, I would like to thank my advisor, Dr. David Goldberg. His guidance, support, and most of all his patience provided the framework for which I was able to build my work from. I would also like to thank my dissertation committee members, Dr. Michael Vogeley, Dr. Gordon Richards, Dr. Luis Cruz, and Dr. Andrew Hicks, for their constructive criticism and support of my research.

I would also like to acknowledge fellow graduate students for their assistance and support. A special thanks to Justin Bird, Markus Rexroth, Frank Jones, Crystal Moorman, and Vishal Kasliwal for allowing me to bounce ideas off of them, which was a truly important but time consuming process.

## Table of Contents

LIST OF TABLES . . . . .	vi
LIST OF FIGURES . . . . .	vii
ABSTRACT . . . . .	ix
1. INTRODUCTION . . . . .	1
1.1    The Radial Density Profile . . . . .	2
1.2    Cluster Scaling Relations . . . . .	5
1.3    Clusters and Environment . . . . .	7
1.4    Outline . . . . .	11
2. CLUSTER SHAPE AND ORIENTATION . . . . .	12
2.1    Introduction . . . . .	12
2.2    Triaxial Projections . . . . .	14
2.3    Sample and Methods . . . . .	15
2.3.1    Simulation Sample . . . . .	15
2.3.2    Methods . . . . .	18
2.3.3    Non-Virialized Halos . . . . .	19
2.4    Results . . . . .	21
2.5    Summary and Conclusions . . . . .	28
2.6    Future Work . . . . .	37
3. THE OBSERVED C-M RELATION . . . . .	38
3.1    Introduction . . . . .	38
3.2    Reconstruction Techniques . . . . .	41
3.2.1    Weak Lensing (WL) . . . . .	41
3.2.2    Strong Lensing (SL) . . . . .	42
3.2.3    Weak+Strong Lensing (WL+SL) . . . . .	43

3.2.4	X-ray . . . . .	43
3.2.5	Line-of-sight Velocity Dispersion (LOSVD) . . . . .	44
3.2.6	The Caustic Method (CM) . . . . .	44
3.2.7	Hybrid Techniques . . . . .	45
3.3	The Sample . . . . .	45
3.3.1	Normalization Procedure . . . . .	48
3.4	The Observed c-M Relation . . . . .	51
3.5	Projection and Shape . . . . .	56
3.6	Conclusions And Discussions . . . . .	61
4.	CLUSTERS AND THE LSS ENVIRONMENT . . . . .	66
4.1	Introduction . . . . .	66
4.2	Data . . . . .	67
4.3	Galaxies Around Clusters . . . . .	70
4.3.1	Quantifying Structure . . . . .	71
4.4	Results And Future Work . . . . .	74
5.	CONCLUSIONS . . . . .	79
	BIBLIOGRAPHY . . . . .	82
	APPENDIX A: ANALYTICAL PROJECTION OF PROLATE SPHEROIDAL HALOS . . . . .	90
	APPENDIX B: LENSING COSMOLOGY CORRECTION . . . . .	92
	APPENDIX C: FULL OBSERVATIONAL DATASET . . . . .	94
	VITA . . . . .	127

## List of Tables

2.1	Prolate Spheroidal Geometry . . . . .	15
2.2	Cluster Halo Geometry . . . . .	23
2.3	Concentration Enhancements . . . . .	30
3.1	Population Overview . . . . .	47
3.2	Best-Fit Concentration-Mass Relation Parameters . . . . .	54
C.1	Cluster concentrations and masses . . . . .	96
C.2	A Summary of The References . . . . .	123

## List of Figures

1.1	X-ray Gas in Abell 383 . . . . .	2
1.2	The NFW Profile . . . . .	3
1.3	c-M Relations: Then and Now . . . . .	8
1.4	Cluster Formation . . . . .	9
1.5	Bolshoi Simulation . . . . .	10
2.1	Analytical concentration and shape relations. . . . .	16
2.2	The MultiDark MDR1 Mass Function. . . . .	17
2.3	Examples of Virialized and Non-Virialized Halos . . . . .	20
2.4	The Virial $\beta$ Parameter . . . . .	22
2.5	Low Mass Shape Results . . . . .	24
2.6	Medium Mass Shape Results . . . . .	25
2.7	High Mass Shape Results . . . . .	26
2.8	MDR1 Intrinsic Concentration Parameters . . . . .	27
2.9	The Intrinsic MDR1 c-M Relation . . . . .	29
2.10	Low Mass Concentration Enhancements . . . . .	31
2.11	Medium Mass Concentration Enhancements . . . . .	32
2.12	A Summary of The Change in Shape for the Low Mass Sample . . . . .	33
2.13	Low Mass Isodensity Alignment . . . . .	34
2.14	Medium Mass Isodensity Alignment . . . . .	35
2.15	High Mass Isodensity Alignment . . . . .	36
3.1	Cluster Population Overview . . . . .	48
3.2	Concentration/Mass Cosmology Correction . . . . .	49
3.3	The Normalized Data . . . . .	52
3.4	Observed c-M Fits . . . . .	55

3.5	CLASH Comparison . . . . .	56
3.6	The Full c-M Relation . . . . .	58
3.7	Lensing Relations and MDR1 Halos . . . . .	59
3.8	Comparison of Theory with Observations . . . . .	60
3.9	WL and WL+SL Cluster Measurements . . . . .	61
3.10	X-ray and WL Cluster Measurements . . . . .	62
3.11	CM and LOSVD Cluster Measurements . . . . .	62
4.1	The SDSS DR10 Footprint . . . . .	67
4.2	The Galaxy Sample Defined . . . . .	68
4.3	Galaxy Clusters In SDSS . . . . .	69
4.4	Selecting Galaxies Around Clusters . . . . .	72
4.5	Mass - $A_l^m$ Correlation . . . . .	76
4.6	Concentration - $A_l^m$ Correlation . . . . .	77
4.7	Redshift Scaled Concentration - $A_l^m$ Correlation . . . . .	78

## Abstract

Dark Matter in Galaxy Clusters: Shape, Projection, and Environment

Austen M. Groener  
Dr. David Goldberg

We explore the intrinsic distribution of dark matter within galaxy clusters, by combining insights from the largest  $N$ -body simulations as well as the largest observational dataset of its kind.

Firstly, we study the intrinsic shape and alignment of isodensities of galaxy cluster halos extracted from the MultiDark MDR1 cosmological simulation. We find that the simulated halos are extremely prolate on small scales and increasingly spherical on larger ones. Due to this trend, analytical projection along the line of sight produces an overestimate of the concentration index as a decreasing function of radius, which we quantify by using both the intrinsic distribution of 3D concentrations ( $c_{200}$ ) and isodensity shape on weak and strong lensing scales. We find this difference to be  $\sim 18\%$  ( $\sim 9\%$ ) for low (medium) mass cluster halos with intrinsically low concentrations ( $c_{200} = 1 - 3$ ), while we find virtually no difference for halos with intrinsically high concentrations. Isodensities are found to be fairly well-aligned throughout the entirety of the radial scale of each halo population. However, major axes of individual halos have been found to deviate by as much as  $\sim 30^\circ$ . We also present a value-added catalog of our analysis results, which we have made publicly available to download.

Following that, we then turn to observational measurements galaxy clusters. Scaling relations of clusters have made them particularly important cosmological probes of structure formation. In this work, we present a comprehensive study of the relation between two profile observables, concentration ( $c_{\text{vir}}$ ) and mass ( $M_{\text{vir}}$ ). We have collected the largest known sample of measurements from the literature which make use of one or more of the following reconstruction techniques: Weak gravitational lensing (WL), strong gravitational lensing (SL), Weak+Strong Lensing (WL+SL), the Caustic Method (CM), Line-of-sight Velocity Dispersion (LOSVD), and X-ray. We find that the concentration-mass (c-M) relation is highly variable depending upon the reconstruction technique used. We also find concentrations derived from dark matter only simulations (at approximately  $M_{\text{vir}} \sim 10^{14} M_\odot$ ) to be inconsistent with the WL and WL+SL relations at the  $1\sigma$  level, even after the projection of triaxial halos is taken into account. However, to fully determine consistency between simulations and observations, a volume-limited sample of clusters is required, as selection effects become increasingly more important in answering this. Interestingly, we also find evidence for a steeper WL+SL relation as compared to WL alone, a result which could perhaps be caused by the

varying shape of cluster isodensities, though most likely reflects differences in selection effects caused by these two techniques. Lastly, we compare concentration and mass measurements of individual clusters made using more than one technique, highlighting the magnitude of the potential bias which could exist in such observational samples.

Finally, we explore the large-scale environment around galaxy clusters using spectroscopically confirmed galaxies from the Sloan Digital Sky Survey (SDSS) Data Release 10. We correlate the angular structure of the distribution of galaxies (out to a distance of  $10h^{-1}$  Mpc) around 92 galaxy clusters with their corresponding mass and concentration measurements. We find that the orientation of the cluster environment on this scale has little impact on the value of cluster measurements.



## Chapter 1: Introduction

Clusters of galaxies are some of the most interesting and complex systems in the universe. Clusters are gravitationally bound collections of at least several hundred to a few thousand galaxies within a region of a few megaparsecs, and are the most massive and recent objects to form. Clusters also trap and heat large amounts of gas to  $10^7 - 10^8$  K, causing them to emit strongly in the X-ray (Figure 1.1) via free-free electron-ion interactions (*bremstrahlung*). However, a diffuse “halo” of dark matter surrounds (and extends well beyond) the luminous portions of clusters. This dark matter halo dominates the cluster by mass ( $\sim 85\%$ ), and is the primary driver of cluster formation and dynamics.

Because clusters are the largest collapsed objects known, they are outstanding probes of cosmology generally. The mass function of nearby galaxy clusters provides constraints on the amplitude of the power spectrum at the cluster scale, while its evolution can be used to measure the matter and Dark Energy density parameters (Rosati et al., 2002; Voit, 2005). The evolution of clustering properties of the large-scale distribution of clusters, specifically the correlation function and power spectrum, are highly sensitive to the value of the density parameters through linear growth rate perturbations (Borgani & Guzzo, 2001; Moscardini et al., 2001). Furthermore, due to the incredibly deep gravitational potential wells produced, the baryon fraction of the universe ( $\Omega_b/\Omega_{\text{tot}}$ ) may be estimated by observing in optical wavelengths, if clusters are assumed to be effective containers of baryons (Fabian, 1991; White et al., 1993). Measuring the baryonic content of clusters can also be done by making use of the Sunyaev-Zel'dovich (SZ) Effect (Sunyaev & Zeldovich, 1972). This effect causes the energies of photons arriving from the cosmic microwave background to be shifted to higher values, due to inverse-Compton scattering between these photons and highly energetic electrons located between the galaxies in clusters (for a review, see Birkinshaw 1999).

In this work, we focus on the *internal* distribution of dark matter, called the radial density profile, and how its properties may be measured.



**Figure 1.1:** Optical image of Abell 383, with X-ray (purple) from Chandra showing the location of the hot gas. **Credit:** X-ray: NASA/CXC/Caltech/A.Newman et al/Tel Aviv/A.Morandi & M.Limousin; Optical: NASA/STScI, ESO/VLT, SDSS **Scale:** 7.26 arcmin across (4.84 million light years)

## 1.1 The Radial Density Profile

Large scale  $N$ -body simulations are an incredibly powerful tool to investigate the distribution of mass within clusters (Navarro et al., 1996; Bullock et al., 2001a; Springel et al., 2005; Klypin et al., 2011; Prada et al., 2012a). Unlike observed clusters (which are limited to a single vantage point), simulated clusters can be studied from any angle and at any epoch. The radial density profile of dark matter halos as predicted by simulations seems to be remarkably self-similar (down to the dwarf galaxy scale,  $\sim 10^8 M_\odot$ ), a prediction first made by Navarro et al. (1996), and has been come to be known as the Navarro-Frenk-White (hereafter NFW) profile (Figure 1.2):

$$\rho_{\text{NFW}}(r) = \frac{\rho_s}{\frac{r}{r_s} \left(1 + \frac{r}{r_s}\right)^2} \quad (1.1)$$

The scale density,  $\rho_s$ , is typically expressed in terms of the critical density of the universe, and

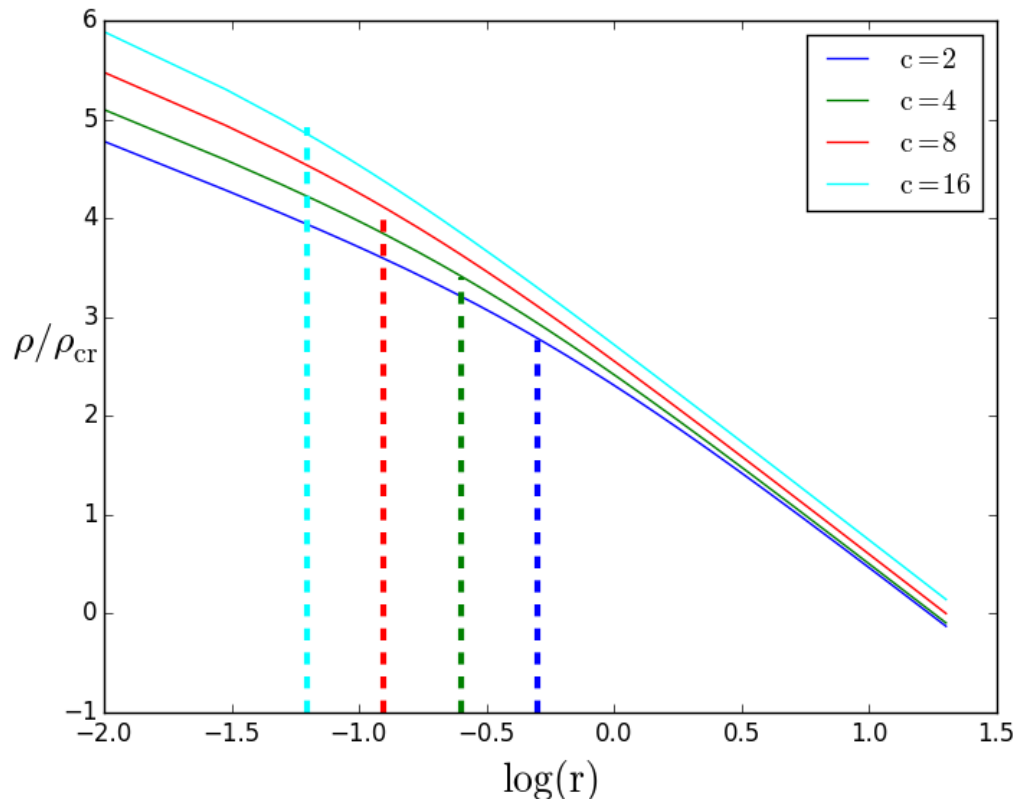


**Figure 1.2:** A cartoon depicting the Navarro-Frenk-White (NFW) density profile, for a select few values of concentration. Larger values of concentration cause the density to rise more rapidly, giving rise to a “cuspier” profile. The scale radius,  $r_s$ , is shown for each value for reference.

the characteristic overdensity parameter,  $\delta_c$ .

$$\rho_s = \rho_{cr} \delta_c \quad (1.2)$$

Furthermore, the critical density of the universe is both an epoch and cosmology-dependent quantity:

$$\rho_{cr} = \frac{3H(z)^2}{8\pi G} \quad (1.3)$$

with the hubble parameter,  $H(z)$ :

$$H(z) = H_0 \sqrt{\Omega_{\gamma,0}(1+z)^4 + \Omega_{m,0}(1+z)^3 + \Omega_{k,0}(1+z)^2 + \Omega_\Lambda} \quad (1.4)$$

where the Hubble constant today,  $H_0$ , measures the rate of expansion of the local universe, and is equal to  $100 h \text{ km/s Mpc}$  (the most up-to-date value is  $h = 0.678 \pm 0.09$ , Planck Collaboration et al. 2015). Cosmological density parameters,  $\Omega_{X,0}$ , represent the fraction of the critical density of the universe (as measured today), from each component we are considering.

The scale radius,  $r_s$ , is defined as the radius within the halo at which the density scales as  $\rho \propto r^{-2}$ . The NFW profile asymptotically behaves as two independent power-law profiles ( $\rho \propto r^{-1}$  in the inner region;  $\rho \propto r^{-3}$  in the outer), with an intermediate region connecting the two. This intermediate region, defined by the scale radius, is an incredibly important property of the halo, as it defines the relative compactness of the halo; we shall call this the concentration parameter. Throughout, we define this quantity as follows:

$$c_x \equiv \frac{r_x}{r_s} \quad (1.5)$$

The concentration parameter is an aperture-based quantity, meaning it has to be defined relative to some outer radius,  $r_x$ . In the following chapters, we will focus on one of two commonly used scales. The first is the virial radius,  $r_{vir}$ , which represents the outer-most radius within the cluster for which its member galaxies follow the virial theorem. The second is  $r_{200}$ , which is the radius inside which

the average density is 200 times the critical density of the universe (Eq. 1.3). The overdensity of the cluster can also be conveniently defined in terms of the concentration parameter:

$$\delta_c = \frac{200}{3} \frac{c^3}{\ln(1+c) - \frac{c}{1+c}} \quad (1.6)$$

Typical values of the overdensity for clusters varies from  $\sim 200 - 10000$ , for corresponding profiles with concentrations of  $c \sim 2 - 8$ .

Qualitatively, the concentration can be thought of as a re-scaled distance, indicating where the steepness of the density profile occurs. Larger concentrations give rise to a steeper (“cuspier”) inner density profile, and conversely, smaller concentrations produce a more well-defined central core, indicating a shallower inner density profile.

Galaxy clusters are *not* spherical systems. Observations suggest that cluster halos exhibit triaxial geometry (see Limousin et al. 2013a for a general discussion) in the optical distribution of light (Carter & Metcalfe, 1980; Binggeli, 1982) in X-ray (Fabricant et al., 1985; Lau et al., 2012) and in weak (Evans & Bridle, 2009; Oguri et al., 2010, 2012a) and strong lensing (Soucail et al., 1987). Observational evidence for triaxiality is matched by theory in large scale N-body simulations of structure formation, exhibiting a preference for prolateness over oblateness (Frenk et al., 1988a; Dubinski & Carlberg, 1991a; Warren et al., 1992a; Cole & Lacey, 1996a; Jing & Suto, 2002a; Hopkins et al., 2005; Bailin & Steinmetz, 2005; Kasun & Evrard, 2005a; Paz et al., 2006; Allgood et al., 2006a; Bett et al., 2007a; Muñoz-Cuartas et al., 2011; Gao et al., 2012; Despali et al., 2014).

## 1.2 Cluster Scaling Relations

The scaling relations between observable properties and the total mass of clusters are key to understanding the physical processes behind their formation and evolution (Vikhlinin et al., 2009a; Giordini et al., 2013). They are yet another test of the  $\Lambda$ CDM cosmological model, providing a means of comparison between theory and observations.

Important relations between observables like the line-of-sight velocity dispersion of galaxies,  $\sigma_v$ , optical richness,  $\lambda$ , bolometric X-ray luminosity,  $L_X$ , and the integrated SZ Compton signal,

$Y_{\text{SZ}}$ , to the total mass of a cluster have been well-studied observationally (Sereno & Ettori, 2015), theoretically (Giordini et al., 2013), and through simulations (Stanek et al., 2010). These relations also evolve with time, and thus also scale with redshift.

It was found early on that the concentration parameters of simulated clusters were highly correlated with their total mass (Navarro et al., 1996; Bullock et al., 2001b). Hereafter, we will call this relation the concentration-Mass (c-M) relation (Figure 1.3). The standard explanation for this anti-correlation between concentration and mass is that low-mass halos tend to collapse and form relaxed structures earlier than their larger counterparts, which are still accreting massive structures until much later. A consequence of early formation is that halos will have collapsed during a period of higher density, leading to a larger central density (and hence larger concentration) as compared to halos which formed later.

Many studies (most recently, e.g., Correa et al. 2015a) focus on quantifying the physical motivation behind this relationship, and suggest that the mass accretion history (MAH) of halos is the key to understanding the connection between cluster observables and the environment in which they formed (Bullock et al., 2001a; Wechsler et al., 2002; Zhao et al., 2003). These studies have found that while the mass accretion rate onto the halo is slow, the concentration tends to scale with the virial radius,  $c \propto r_{\text{vir}}$  (caused by a constant scale radius). However, the concentration remains relatively constant for epochs of high mass accretion. The MAH itself depends upon the physical properties of the initial density peak (Dalal et al., 2008), which is a function of cosmology, redshift, and mass (Diemer & Kravtsov, 2015).

With time however, as more cluster profiles became available, it became clear that cluster concentrations found for halos which form in  $\Lambda\text{CDM}$  simulations were significantly lower than ones observed by approximately a factor of  $\sim 2$  (Comerford & Natarajan, 2007a; Broadhurst et al., 2008a; Oguri et al., 2009a), and has come to be known as “the over-concentration problem”. Bahé et al. (2012a) have shown that when observed in near alignment with their major axes, weak lensing reconstructed concentrations are systematically larger by up to a factor of 2 for Millennium Simulation cluster halos. Similarly, Oguri & Blandford (2009a) find in their semi-analytic study that the most massive

triaxial halos ( $\sim 10^{15} h^{-1} M_{\odot}$ ) produce the largest Einstein radii if viewed preferentially along their major axes, thereby increasing their effectiveness as strong gravitational lenses. Through ray-tracing of high-resolution N-body simulations, Hennawi et al. (2007a) have shown that strong lensing clusters tend to have their principle axes aligned along the line of sight.

### 1.3 Clusters and The Large Scale Structure of the Universe

The standard concordance model of cosmology ( $\Lambda$ CDM) consists primarily of cosmological constant and cold dark matter components, with Gaussian initial conditions (Planck Collaboration et al., 2015). It predicts that the formation of structure is a hierarchical process (White & Frenk, 1991; Kauffmann et al., 1993; Lacey & Cole, 1993a). Small initial perturbations are gravitationally amplified over time, as collections of mass continually merge to form larger ones. Ultimately, galaxy clusters are the end result of this process and sit atop this hierarchy of mass (Figure 1.4).

Clusters are not isolated collections of galaxies. Living in the densest regions of the universe outlined by large-scale environments such as filaments and voids (Figure 1.5), the distribution of mass within clusters is strongly influenced by their surroundings. Clusters acquire most of their mass from major mergers along the filaments, giving rise to an alignment between the major axis of the halo and the large-scale filament (Bailin & Steinmetz, 2005; Altay et al., 2006; Patiri et al., 2006; Aragón-Calvo et al., 2007; Brunino et al., 2007). After these merging events occur, halos undergo violent relaxation, ultimately reaching a state of quasi-equilibrium, whereby halos are left with a “universal” (triaxial) density profile.

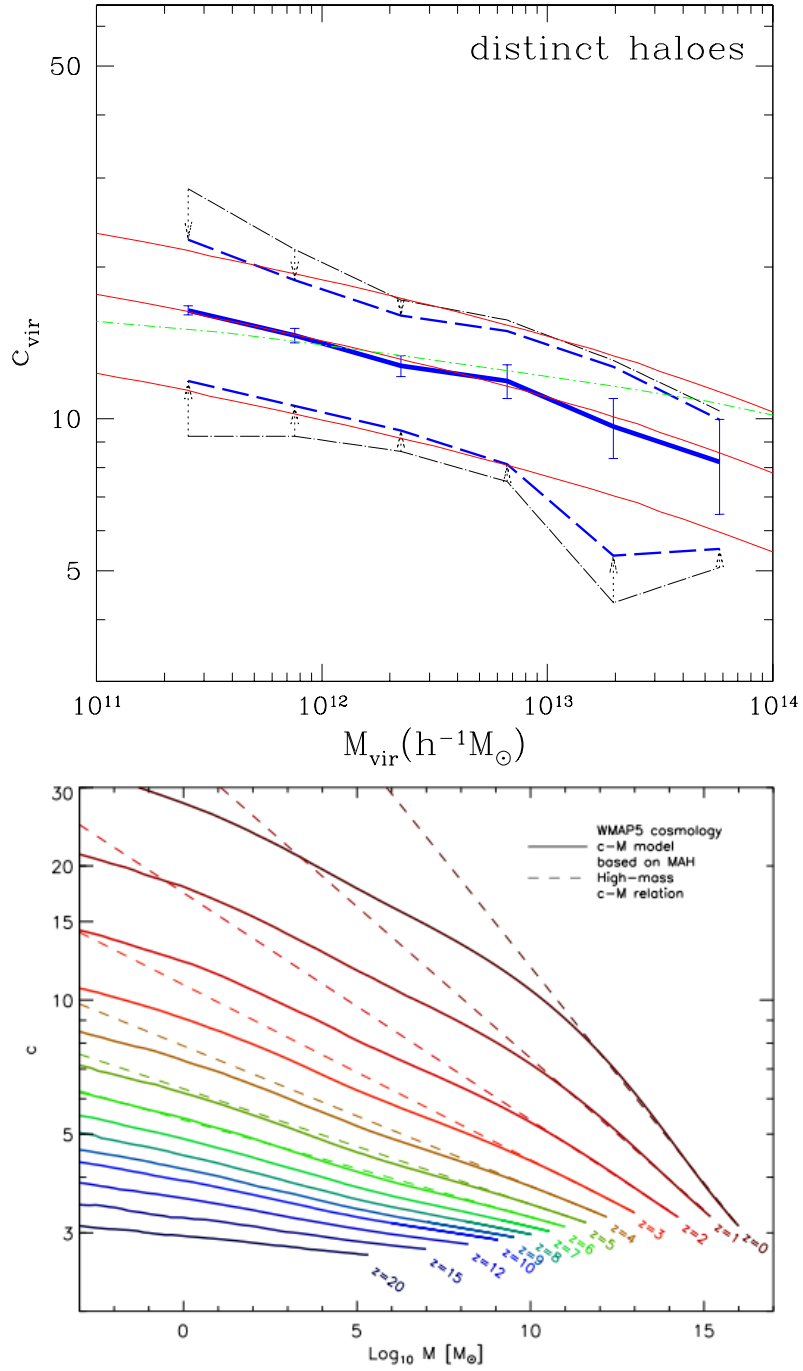


**Figure 1.3:** *Top:* One of the first works to model the cluster c-M scaling relation as found by simulations (Bullock et al., 2001b). Scatter in concentration roughly follows a log-normal distribution, with typical values of  $\Delta(\log c_{\text{vir}}) \sim 0.24$ . Thick blue curve represents the median concentration, while thin dashed blue lines encompass 68% of the  $c_{\text{vir}}$ . *Bottom:* One of the most recent studies to quantify this relation found in simulations (Correa et al., 2015a). Typical values of the concentration are  $c_{\text{vir}} \sim 5$  for halos with masses  $M_{\text{vir}} \sim 10^{14} M_{\odot}$ .

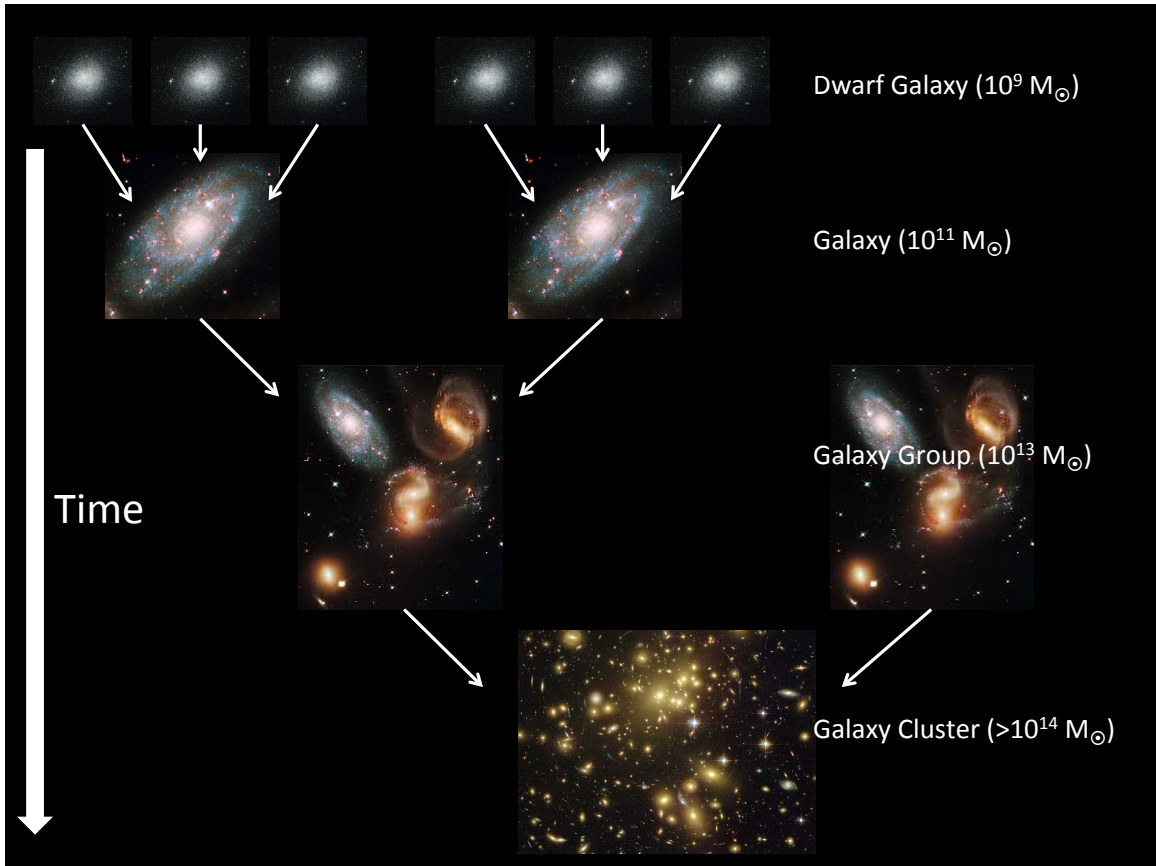


**Figure 1.4:** A schematic of the hierarchical cluster formation process. Over time, smaller structures merge into larger ones, ultimately leading to bound galaxy clusters ( $>10^{14} M_\odot$ ) which have formed relatively recently.

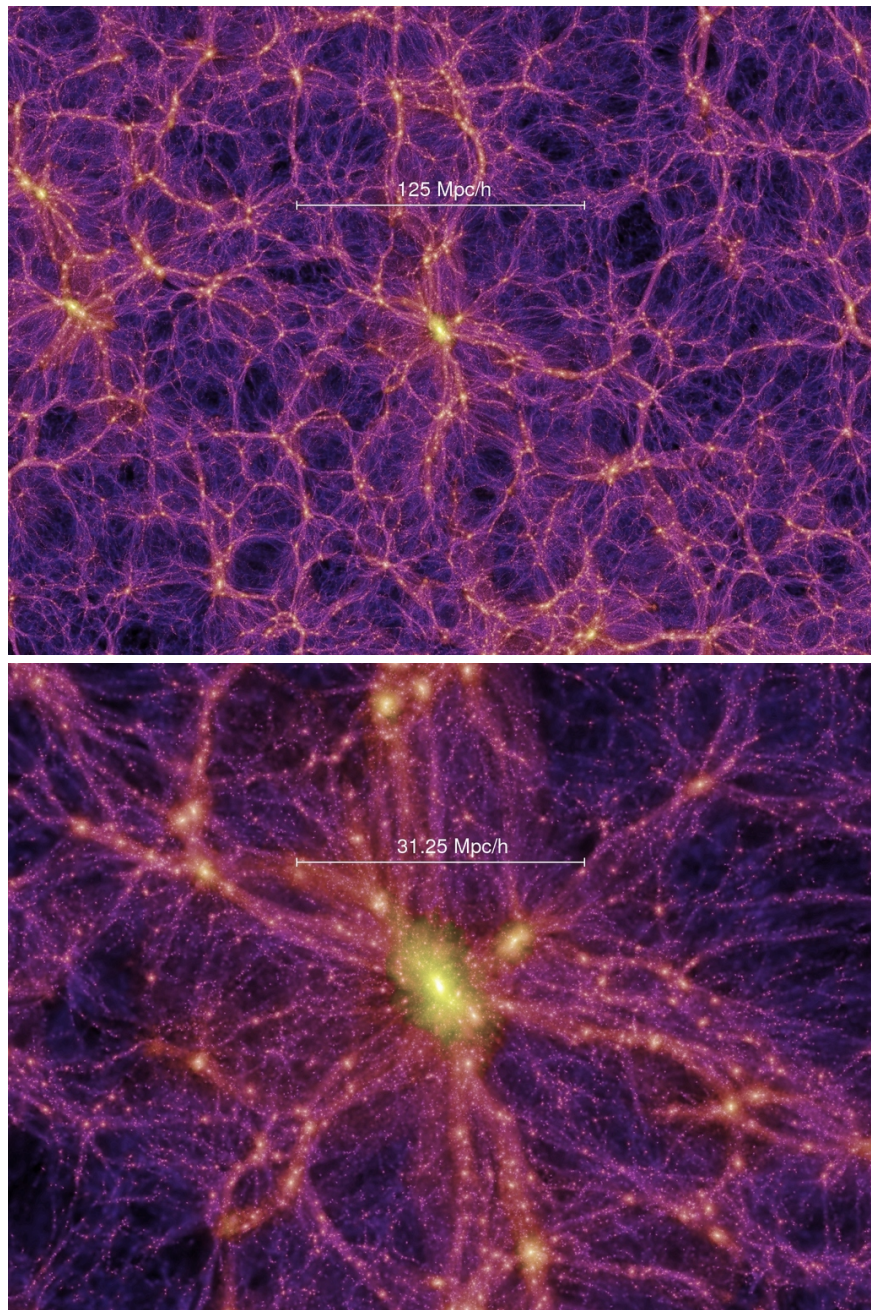


**Figure 1.5:** The formation of dark matter halos within the Bolshoi Simulation (Klypin et al., 2011). Cluster halos embedded within the large-scale structure of the universe (*Top:* 125 Mpc/h, *Bottom:* 31.25 Mpc/h) are shown in yellow.

## 1.4 Outline

In the following chapters, we explore the internal distribution of mass of galaxy clusters in a number of ways. In Chapter 2, we explore the relationship between the shape and orientation of isodensity surfaces to the projected (2D) cluster concentration parameter, with a sample of clusters formed in the MultiDark MDR1 simulation. In Chapter 3, we then observationally explore the scaling relation between cluster concentration and mass, as determined by six mass reconstruction techniques (Weak, strong, and weak+strong lensing, X-ray, the caustic method, and line-of-sight velocity dispersion), for a comprehensive sample of clusters collected from the literature. Moreover, we compare contentiously steep observed lensing relations to projected relations obtained from a number of large cosmological simulations. We then attempt to shed some light on the relationship between the projected profile parameters, like concentration and mass, with the angular distribution of the large-scale environment surrounding clusters in Chapter 4. Finally, in Chapter 5, we summarize our findings and discuss potential future work.

## Chapter 2: Shape Profiles and Orientation Bias for Weak and Strong Lensing Cluster Halos

### 2.1 Introduction

Gravitational lensing has proven an incredibly useful tool in creating detailed maps of projected density without requiring any assumptions regarding either a halo's dynamical state or hydrostatic equilibrium of its gas. Recently, strong and weak gravitational lensing methods have been used side by side to constrain the distribution of mass on different scales within the same cluster lens (for Abell 1689 for example, see Broadhurst et al., 2005a; Halkola et al., 2006a; Deb et al., 2012).

Furthermore, galaxy cluster halos are both predicted and observed to be prolate spheroidal in shape (see section 1.3). However, clusters are often modeled using spherically symmetric distributions of mass, which seriously alter their utility as cosmological probes.

Additional complications arise in this picture of cluster halos in that halo axis ratios change as a function of radius. Frenk et al. (1988a) and Cole & Lacey (1996a) found that simulation halos become more spherical towards the center, whereas Dubinski & Carlberg (1991a), Warren et al. (1992a), and Jing & Suto (2002a) have concluded the opposite. Nearly all are in agreement that there is good alignment between isodensity (or isopotential) surfaces on most scales. More recent work done by Hayashi et al. (2007a) show that axis ratios of both isopotential and isodensity surfaces consistently increase with radius for seven galaxy-scale simulations.

Though lensing concentrations are systematically higher than their predicted values simply due to orientation bias, there are other reasons to believe that clusters identified by their strong lensing features are a biased population. For one, the most massive clusters are simply more effective gravitational lenses, preferentially sampling the highest region of the cluster mass hierarchy (Comerford & Natarajan, 2007a).

Many studies have employed joint weak and strong lensing reconstruction techniques in order to probe much larger regions of the radial density profile. However, weak and strong lensing can

sometimes independently produce vastly different results, and are rather sensitive to the a priori assumptions made regarding the distribution of mass within the cluster lens. Broadhurst et al. (2005a) and Halkola et al. (2006a) both find weak lensing concentrations to be much larger than ones produced by strong lensing of the well-known cluster Abell 1689, when a spherical model is used. Weak + strong lensing analyses of Abell 1689 have generally been in agreement with one another, however, concentrations remain inconsistent with what theory predicts (Clowe, 2003; Halkola et al., 2006a; Limousin et al., 2007a). Only when a triaxial halo model is employed do theory and observation come into agreement (Oguri et al. 2005a; for a complete overview of the cluster Abell 1689, see §5 of Limousin et al. 2013a). The model assumptions and priors used in weak and strong lensing methods can produce large uncertainty in reconstructed parameters. However, physical features of the cluster halos, for example the combination of an orientation bias together with an intrinsic trend in halo shape as a function of radius could perhaps also lay at the heart of discrepancies of this nature, and work to diminish the accuracy of lensing techniques as stand-alone tools as well as joint techniques.

Lastly, ongoing baryonic physics within galaxy clusters (specifically cooling, star formation, and AGN feedback) has the potential to significantly alter the distribution of mass within clusters, and is absent from many simulations of structure formation. Kazantzidis et al. (2004) show that the addition of gas cooling to simulations of clusters has the potential to significantly increase axial ratios in the inner-most regions when compared to corresponding clusters formed in adiabatic simulations.

The lensing cross-section also depends sensitively on the addition of baryons to cluster simulations, and can be boosted by a factor of a few (Puchwein et al., 2005a; Wambsganss et al., 2008a; Rozo et al., 2008a). Studies which do not include AGN feedback suffer from over-cooling, and the addition of this component reduces the enhancement of the lensing cross-section to at most a factor of two (Mead et al., 2010a). Killelendar et al. (2012) find Einstein radii of clusters to be larger only by 5% when AGN feedback is included for  $z_s = 2$  (increasing to 10 – 20% for lower source redshifts).

In this chapter we present a study of the shape and alignment of isodensity surfaces from simulated cluster halos of the MDR1 cosmological simulation (Prada et al., 2012a) throughout a range

of radial scales. Differences between the concentration parameter on weak and strong lensing scales will be quantified by the analytical projection of NFW halos, for the specific case that their major axes point along our line of sight. This chapter is organized as follows. In section §2.2, we discuss the extension of the spherical NFW model and present prolate spheroidal simplifications of halo properties upon projection of the 3D NFW profile along the line of sight. In §2.3 we define our samples and methods we will use to analyze halo intrinsic properties. In §2.4 we present our findings on weak and strong lensing scales within clusters, and discuss our results in §2.5. And lastly, in §2.6 we add a general discussion of future work.

## 2.2 Projections of Triaxial NFW Halos

The Navarro-Frenk-White density profile (Navarro et al., 1996) has been shown accurately describe the density profiles of simulation halos over many decades of mass. Throughout this chapter, we will focus on the NFW profile, parameterized by the following definition of the concentration parameter:

$$c_{200} \equiv r_{200}/r_s. \quad (2.1)$$

The characteristic overdensity of the cluster is also defined in terms of this particular definition of the concentration (by direct substitution of Eq. 2.1 into Eq. 1.6).

Following that, the mass can now be defined in terms of  $r_{200}$  and the cosmology-dependent critical density of the universe at the redshift of the halo.

$$M_{200}(z) = \frac{4}{3}\pi r_{200}^3 \cdot 200\rho_{\text{cr}}(z) \quad (2.2)$$

Simulations show that halos deviate from spherical symmetry by a considerable amount, with a preference for prolate over oblate spheroids. Doroshkevich (1970) has made the case that triaxial collapse is a necessary outcome of structure formation models which are seeded by Gaussian random initial conditions. The spherical NFW profile can be extended to accommodate triaxial halos by

**Table 2.1:** Prolate Spheroidal Geometry

Projected Quantity	Prolate Spheroidal Expression
$Q$	$\frac{q}{\sqrt{\sin^2 \theta + q^2 \cos^2 \theta}}$
$R_s$	$\frac{q}{Q} r_s$
$\delta_C$	$\frac{Q^2}{q} \delta_c$

Shown here are the analytical expressions for projected quantities expressed in terms of intrinsic quantities and halo orientation used throughout this study. As a general rule, projected quantities will be capitalized while intrinsic quantities will not be.

redefining the radial coordinate as an ellipsoidal coordinate:

$$\zeta^2 = \frac{x^2}{c^2} + \frac{y^2}{b^2} + \frac{z^2}{a^2} \quad (2.3)$$

where  $a, b, c$  are the semi-major, -intermediate, and -minor axes of the ellipsoidal shell under consideration. Each set of semi-axes is unique to a specific radial value within each halo by the relationship  $abc = r^3$ .

The projection of an arbitrary triaxial halo onto a 2-dimensional plane is a unique process. However, the reverse process is degenerate. To understand the limits of projection biases due to orientation, we simplify the generalized projection of triaxial halos found in Sereno et al. (2010a) assuming a prolate spheroidal geometry. The following observed (projected) parameters can be expressed in terms of the angle  $\theta$  between the line-of-sight and the major axis of a prolate spheroid, as well as a single axial ratio intrinsic to the cluster (Table 2.1; see then Figure 2.1).

## 2.3 Sample and Methods

### 2.3.1 Simulation Sample

We aim to quantify the effect which line-of-sight alignment of triaxial cluster halos has upon projected concentrations on both weak and strong lensing scales in the presence of slowly evolving isodensity shapes. We study clusters from the MDR1 cosmological simulation (Prada et al., 2012a) of the MultiDark Project<sup>1</sup>. MDR1 is a dark matter only simulation which uses  $2048^3$  particles in a box

$1 \text{ h}^{-1}\text{Gpc}$  on a side. The mass of simulation particles is  $8.721 \times 10^9 \text{ h}^{-1}\text{M}_\odot$ , with a resolution

---

<sup>1</sup><http://www.multidark.org/MultiDark/>

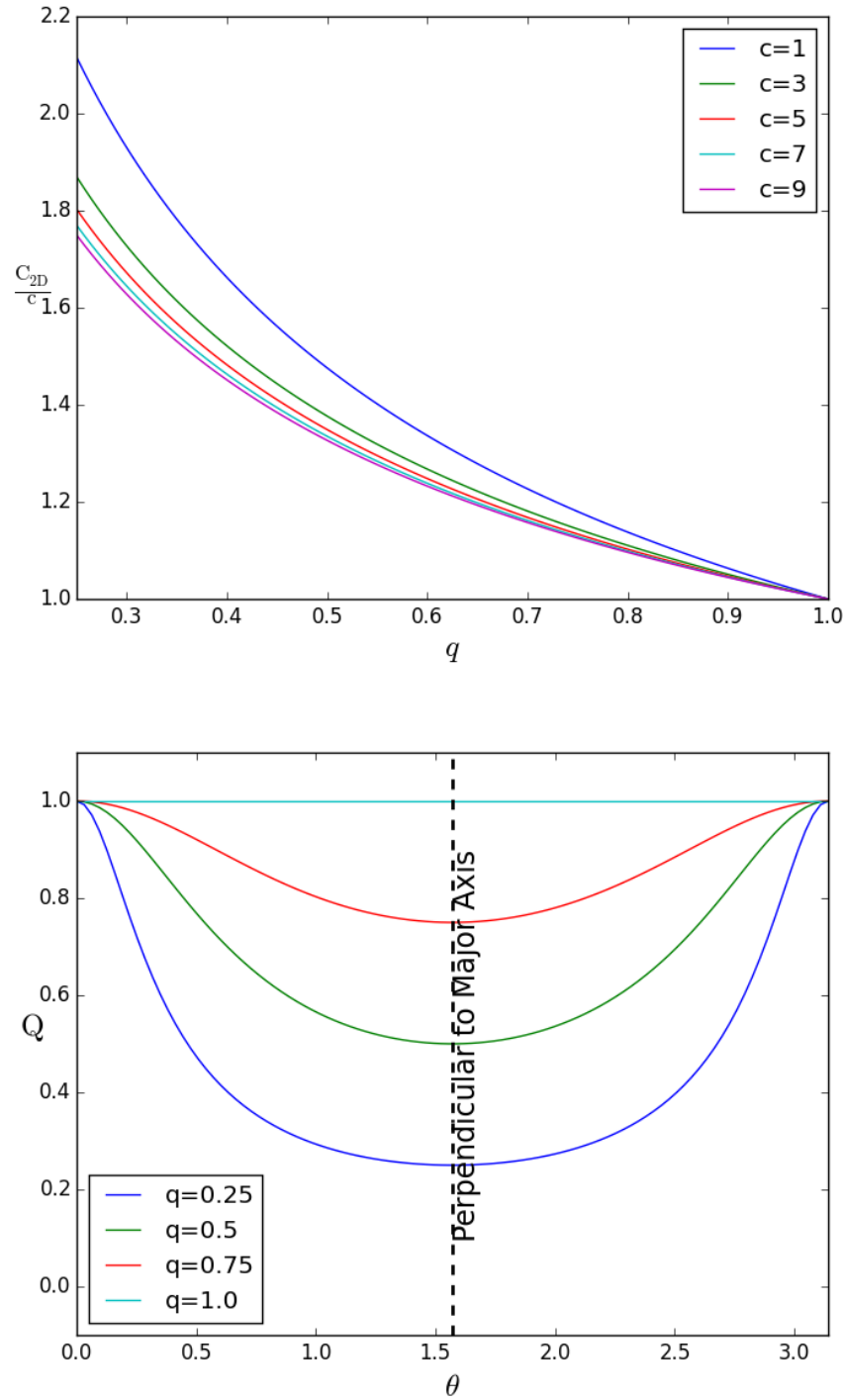


**Figure 2.1:** *Top Panel:* The ratio of projected concentration,  $C_{2D}$ , to the intrinsic concentration,  $c$ , as a function of prolateness,  $q$  (these curves assume line-of-sight alignment of the major axis). *Bottom Panel:* The projected axis ratio,  $Q$ , as a function of the degree of line-of-sight alignment,  $\theta$ , for prolate spheroidal halos.

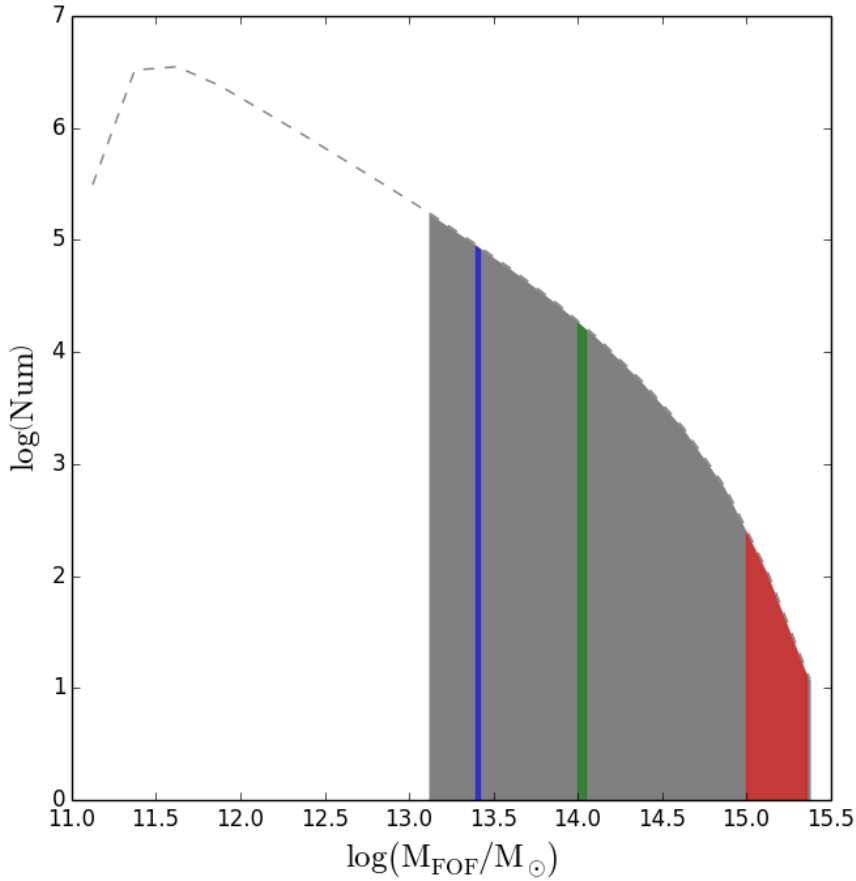


**Figure 2.2:** The MDR1 mass function (dashed black) using the FOF algorithm. The gray shaded region shows the cluster halo regime. Overplotted are the low (blue), medium (green), and high (red) mass samples extracted from the database.

of  $7 \text{ h}^{-1}\text{kpc}$ . The simulation uses results from WMAP5 as its cosmology and was run with the Adaptive-Refinement Tree (ART) code (Kravtsov et al., 1997a).

The MDR1 simulation database (Riebe et al., 2013) contains halo catalogs which are found using two different halo finding algorithms (“Bound Density Maximum” BDM, and “Friends-of-Friends” FOF) taken at 85 redshift snapshots. The masses of halos found through these two methods range from  $1.7 \times 10^{11}\text{h}^{-1}\text{M}_{\odot}$  -  $1.6 \times 10^{15}\text{h}^{-1}\text{M}_{\odot}$ . We impose a lower cutoff in halo mass of  $1 \times 10^{13}\text{h}^{-1}\text{M}_{\odot}$  to mark the beginning of the cluster halo regime which are considered for this study. Figure 2.2 shows the mass function of the sample at redshift  $z = 0$ .

In our study, three halo samples were extracted from the MDR1 FOF table (relative linking length of 0.17) of the MultiDark Database for further study. Smaller linking lengths (e.g. halo substructures) are available, however these were purposefully left out since it is beyond the scope of this study.

- Low Mass:  $2.5 - 2.6 \times 10^{13} h^{-1} M_{\odot}$  [6007 halos]
- Medium Mass:  $1.0 - 1.1 \times 10^{14} h^{-1} M_{\odot}$  [2905 halos]
- High Mass:  $> 1.0 \times 10^{15} h^{-1} M_{\odot}$  [121 halos]

It should be noted here that our results are derived using one particular agglomerative, single-linkage clustering algorithm (FOF). Studies have been conducted which compare various halo-finding algorithms for simulation data (see Knebe et al. (2011) for a general review of such algorithms and how they perform in identifying structures from simulations). Despali et al. (2013) have shown that halo shape can depend upon the choice of method used to identify halos from the overall simulation volume.

### 2.3.2 Methods

Following, for example, Warren et al. (1992a) and Shaw et al. (2006), we compute the moment of inertia tensor, from which we obtain the average shape of the halo at a given radius:

$$I_{ij} = \sum_{n=1}^{N} m_p (r_{i,n} - \bar{r}_i)(r_{j,n} - \bar{r}_j) \quad (2.4)$$

where  $r_{i,n}$  is the coordinate of the  $n^{\text{th}}$  particle in the  $i^{\text{th}}$  direction (where  $i, j \in x, y, z$ ), and  $m_p$  is the mass of the simulation particle. Finding the eigenvalues and eigenvectors of  $I$  can uniquely determine the orientation and axis ratios.

This method of determining shape has its drawbacks. Shaw et al. (2006), Jing & Suto (2002b), and Bailin & Steinmetz (2004) have all found that this approach often fails to converge in high resolution simulations with substantial substructure. Additionally, substructures of fixed mass will affect the components of the moment of inertia tensor on larger scales than it will on small scales. In

order to correct for this potential bias, we apply a Gaussian weighting function,  $w_g(\zeta)$ , (to Equation 2.6) which matches both the shape and orientation of each bounding ellipsoid within the iterative process.

We find good convergence with this method for MDR1 halos. For our purposes, calculating the shape of each halo using the inertia tensor, with the addition of a triaxial, Gaussian weighting function, will be more than adequate to describe the macrostructure of the parent halo.

### 2.3.3 Non-Virialized Halos

Mergers are common physical processes in the formation of galaxy clusters (Press & Schechter, 1974; Bond et al., 1991; Lacey & Cole, 1993b). Special care is taken to separate out halos which are better fit by more than one halo for each mass sample, since parameters like concentration and scale radius are only properly defined for a single halo profile (Figure 2.3). The Mean Shift clustering algorithm (Fukunaga & Hostetler, 1975) is used on low and medium mass clusters, while the K-Means (Hartigan & Wong, 1979) clustering algorithm is used for high mass halos.

The Mean Shift algorithm is a non-parametric algorithm which requires no initial guess for the number of clusters, making it ideal for handling clusters of arbitrary shape or number. It locates local density maxima and uses a tuning parameter to associate each particle's membership to a corresponding maximum. Conversely, the K-Means algorithm necessarily requires k-clusters to group particles into. K-Means scales as  $O(knT)$  (where  $k$  is the number of clusters,  $n$  is the number of points, and  $T$  is the number of iterations) and therefore was chosen for the high mass sample of 121 halos.

Additionally, to prevent contamination of each sample by unrelaxed or actively merging structures which may *still* be well-fit by a single model, halos are checked for virialization using the following (Shaw et al., 2006):

$$\beta = \frac{2T_0 - E_s}{W_0} + 1 \quad (2.5)$$

where  $T_0$  is the total kinetic energy,  $W_0$  is the total potential energy, and  $E_s$  comes from the pressure of the outer perimeter of the halo, an important contribution which comes from the fact that cluster

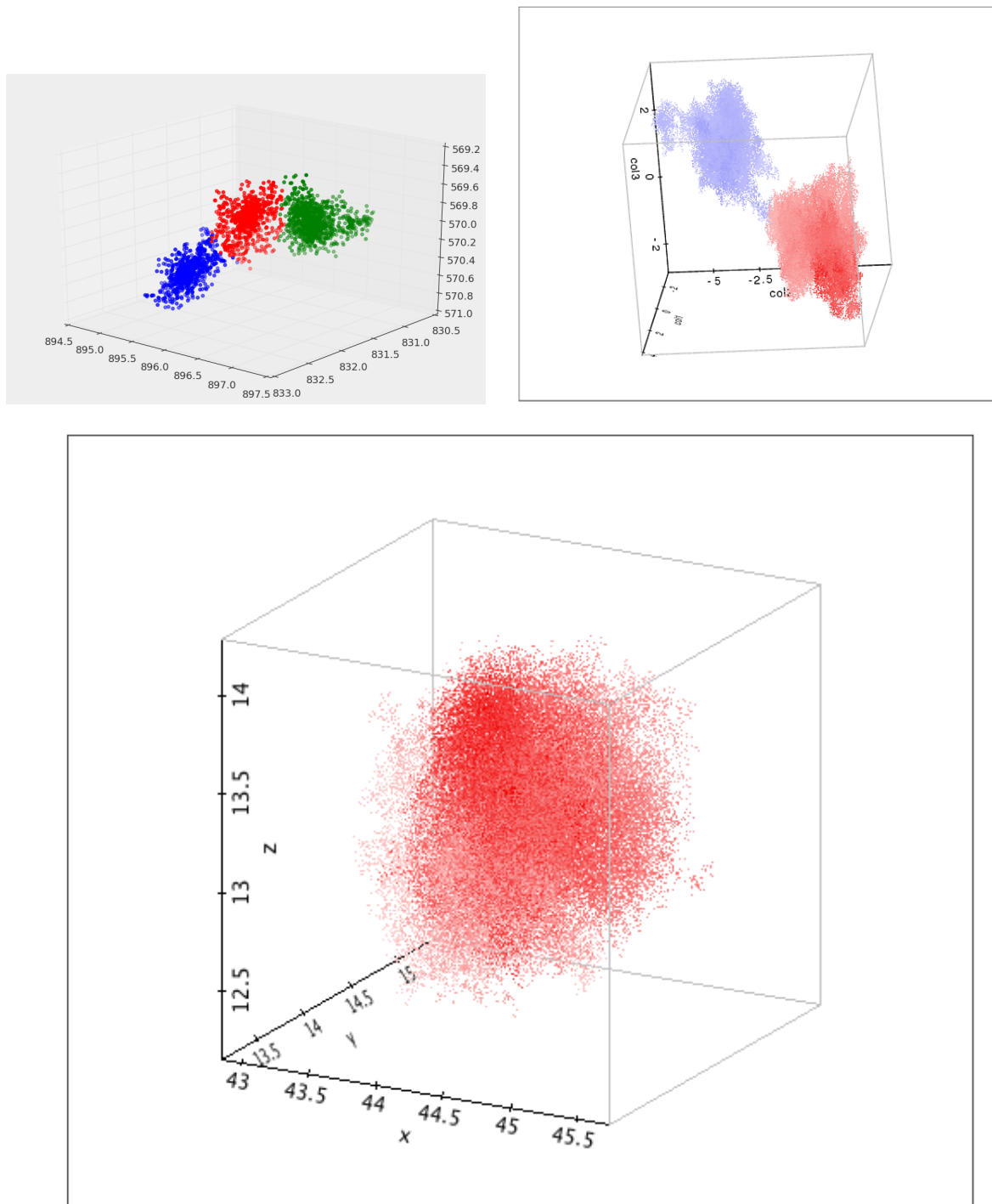


**Figure 2.3:** *Upper Row:* Examples of actively merging system of halos, which are excluded from our study. Mean-shift (left) and K-means (right) algorithms are applied to each halo (depending on mass) in order to determine if a single parent halo is present. *Bottom:* A dynamically relaxed, single-model dark matter halo.

halos are not isolated systems. This term is calculated by assuming an ideal gas of particles, where one can approximate surface pressure as being:

$$P_s = \frac{1}{3} \frac{\sum_i m_i v_i^2}{V} \quad (2.6)$$

where the summation is carried out over particles which lay in the outermost 20% of the halo ( $> R_{0.8}$ ). The volume occupied, is then:

$$V = \frac{4\pi R_{vir}^3}{3} - \frac{4\pi R_{0.8}^3}{3} \quad (2.7)$$

where  $R_{vir}$  is the outermost radius, and  $R_{0.9}$  is the median of the outermost particles. Therefore the energy  $E_s$  can be approximated by:

$$E_s \approx 4\pi R_{0.9}^3 P_s \quad (2.8)$$

A cut is made at  $\beta > -0.2$  in order to remove halos which have sufficient surface pressure at their virial radii, indicating that they are currently in a state of collapse (Shaw et al., 2006). Figure 2.4 displays the distributions of  $\beta$  for each mass sample.

All analysis results for each cluster halo within this study have been stored in a downloadable database<sup>2</sup>.

## 2.4 Results

Based upon the above criteria, that a halo must be both virialized and best fit by a single component halo model, we find that 55.3%, 42.0%, and 17.4% of halos in the low, medium, and high mass samples make it through our selection criteria. This tendency of finding higher mass halos in an un-relaxed state is a natural prediction of hierarchical structure formation models, since the largest halos are the last structures to form and must undergo major merging events. Additionally, nearly all of these cluster halos can be described as being prolate ellipsoids, becoming marginally more spherical with increasing distance from the cluster center (See Figure 2.5-2.7; See Table 2.2 for a summary of these

---

<sup>2</sup>[http://www.physics.drexel.edu/~groenera/zodb\\_file.fs](http://www.physics.drexel.edu/~groenera/zodb_file.fs)

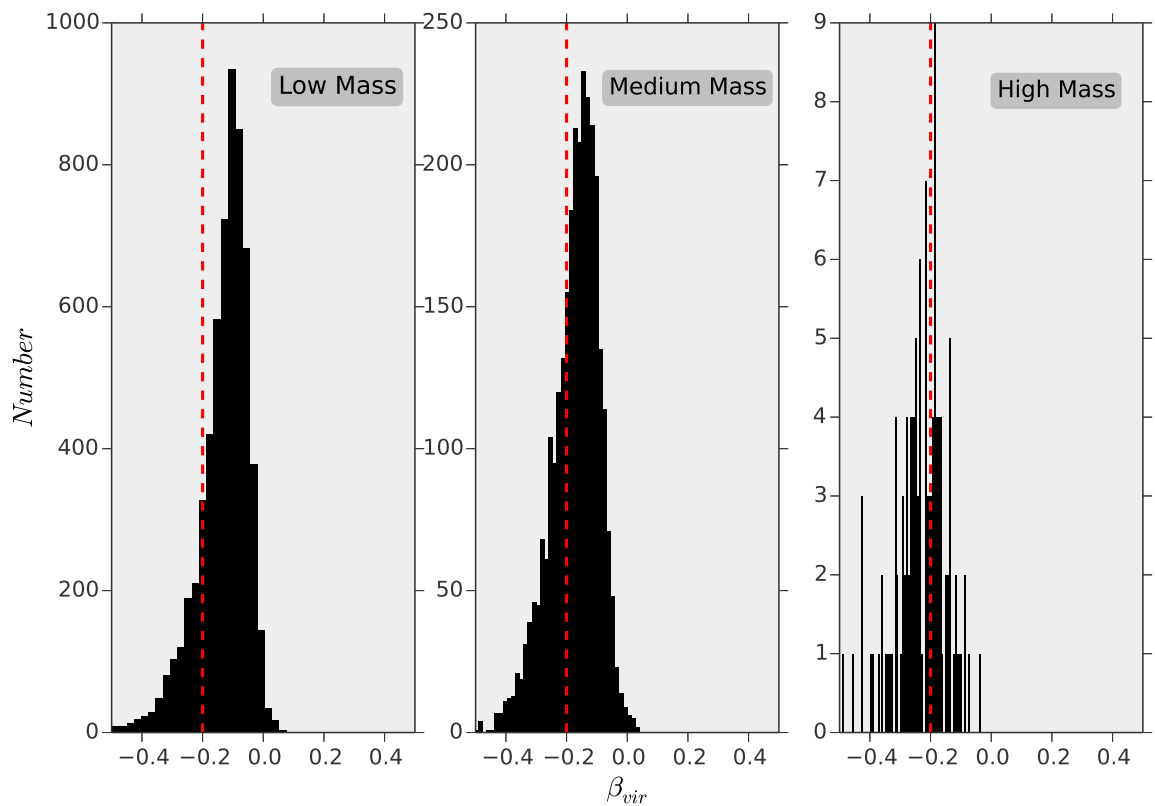


**Figure 2.4:** The distributions of virial  $\beta$  parameters, for the low, medium, and high mass samples.

**Table 2.2:** Cluster Halo Geometry

Radial Scale		Low	Medium	High
0.5 · $r_{200}$	$\bar{p} \pm \sigma_p$	$0.67 \pm 0.15$	$0.62 \pm 0.14$	$0.56 \pm 0.13$
	$\bar{q} \pm \sigma_q$	$0.53 \pm 0.12$	$0.49 \pm 0.11$	$0.42 \pm 0.06$
$r_{200}$	$\bar{p} \pm \sigma_p$	$0.71 \pm 0.13$	$0.66 \pm 0.13$	$0.54 \pm 0.15$
	$\bar{q} \pm \sigma_q$	$0.57 \pm 0.11$	$0.52 \pm 0.10$	$0.42 \pm 0.08$
$2 \cdot r_{200}$	$\bar{p} \pm \sigma_p$	$0.69 \pm 0.12$	$0.67 \pm 0.12$	$0.54 \pm 0.12$
	$\bar{q} \pm \sigma_q$	$0.55 \pm 0.10$	$0.53 \pm 0.10$	$0.43 \pm 0.08$

Reported here are the sample mean (standard deviation) values of the semi-intermediate to semi-major axis ratio  $p$ , and semi-minor to semi-major axis ratio  $q$  for each mass sample (virialized, non-mergers) at various physical scales of interest.

shape results).

Intrinsic NFW concentrations are shown in Figure 2.8 and are consistent with those produced in previous simulations as well as previous studies of the MultiDark simulation (Prada et al., 2012a). As expected, halo concentrations decrease with increasing halo mass. This concentration-mass relationship is generally fit with a power-law model which takes the form:

$$c_{200} = \frac{c_0}{(1+z)^\beta} \left( \frac{M_{200}}{M_*} \right)^\alpha \quad (2.9)$$

where for our sample  $z = 0$ , and we use  $M_* = 10^{14} h^{-1} M_\odot$  (Figure 2.9). We first compute  $r_{200}$  from the cumulative density profile of each halo, and thus establishing  $M_{200}$ . Next, by fitting NFW profiles to these density profiles we obtain concentration parameters. For MDR1 cluster halos, we find a concentration-mass relation of

$$c_{200} = (4.775 \pm 0.022) \left( \frac{M_{200}}{10^{14} h^{-1} M_\odot} \right)^{-0.056 \pm 0.007} \quad (2.10)$$

From the intrinsic distributions of shape and concentration found for each sample population, we find that solely due to line-of-sight orientation (that is, perfectly aligned with the major axis), analytically projected concentrations tend to be systematically higher by about 20% – 50% for virialized, single model halos. Halos with intrinsically low concentrations have been found to suffer from a larger orientation bias  $\sim 50\%$ , whereas higher intrinsic concentrations tend to produce an

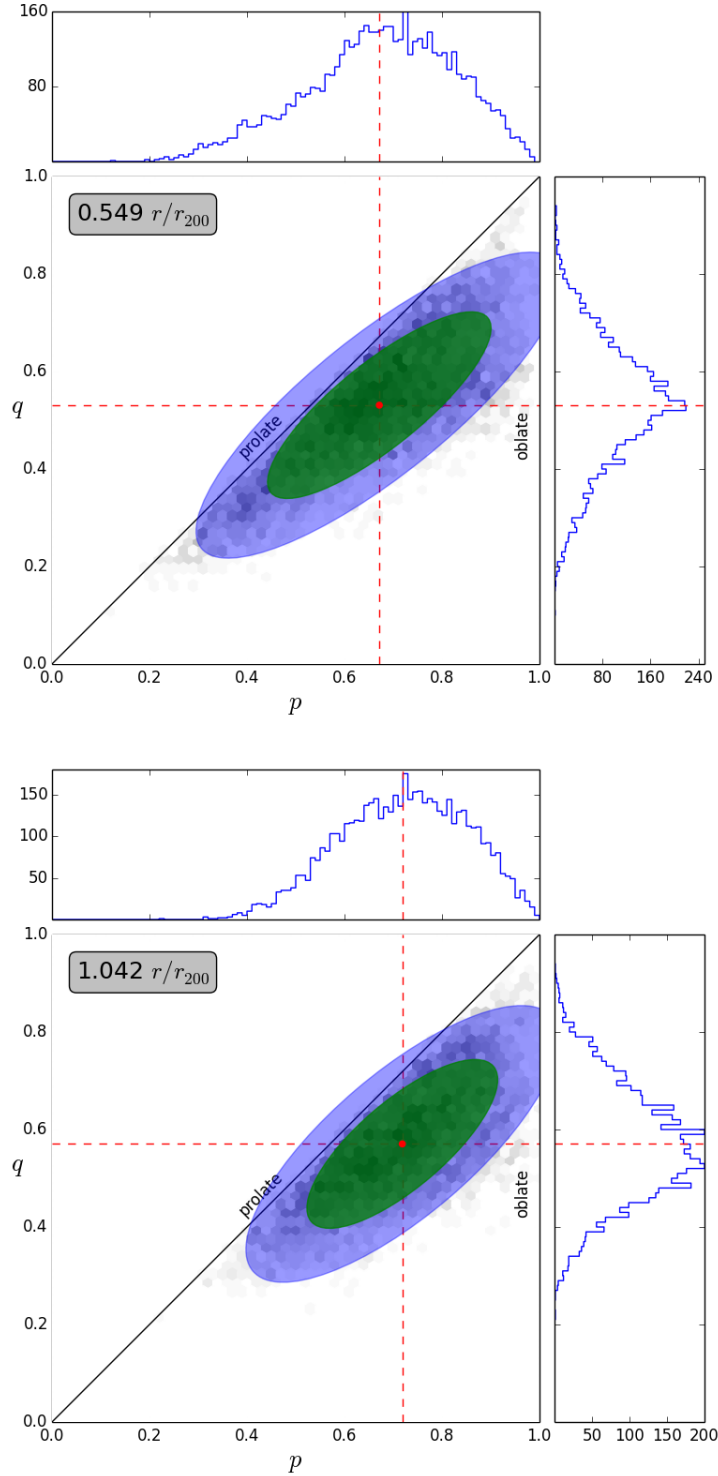


**Figure 2.5:** The distribution of isodensity shapes for the low mass halo sample at a radial scale of  $\sim 0.5r_{200}$ . The green and blue shaded regions are the 1- and 2- $\sigma$  gaussian error ellipses, and red indicates the sample mean.

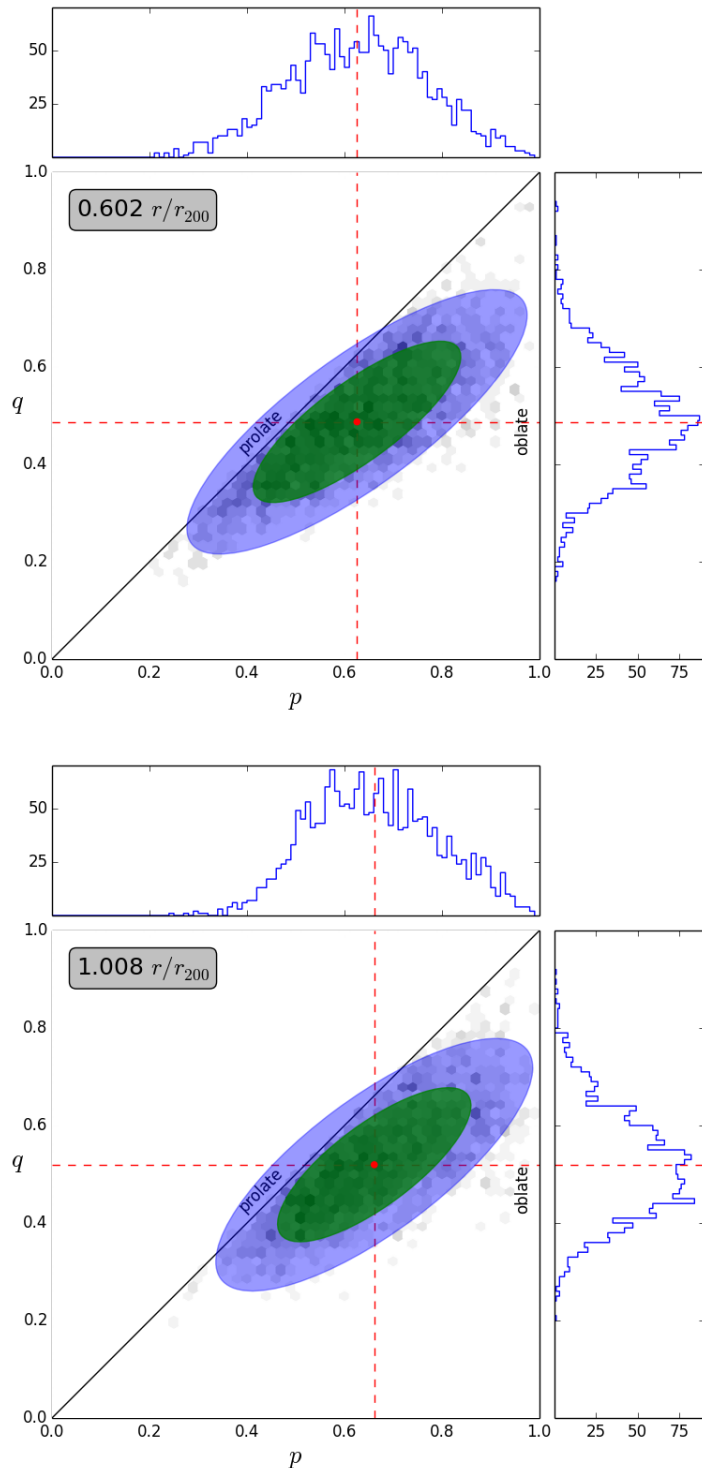


**Figure 2.6:** Same as Figure 2.5, but for the medium mass halo sample.

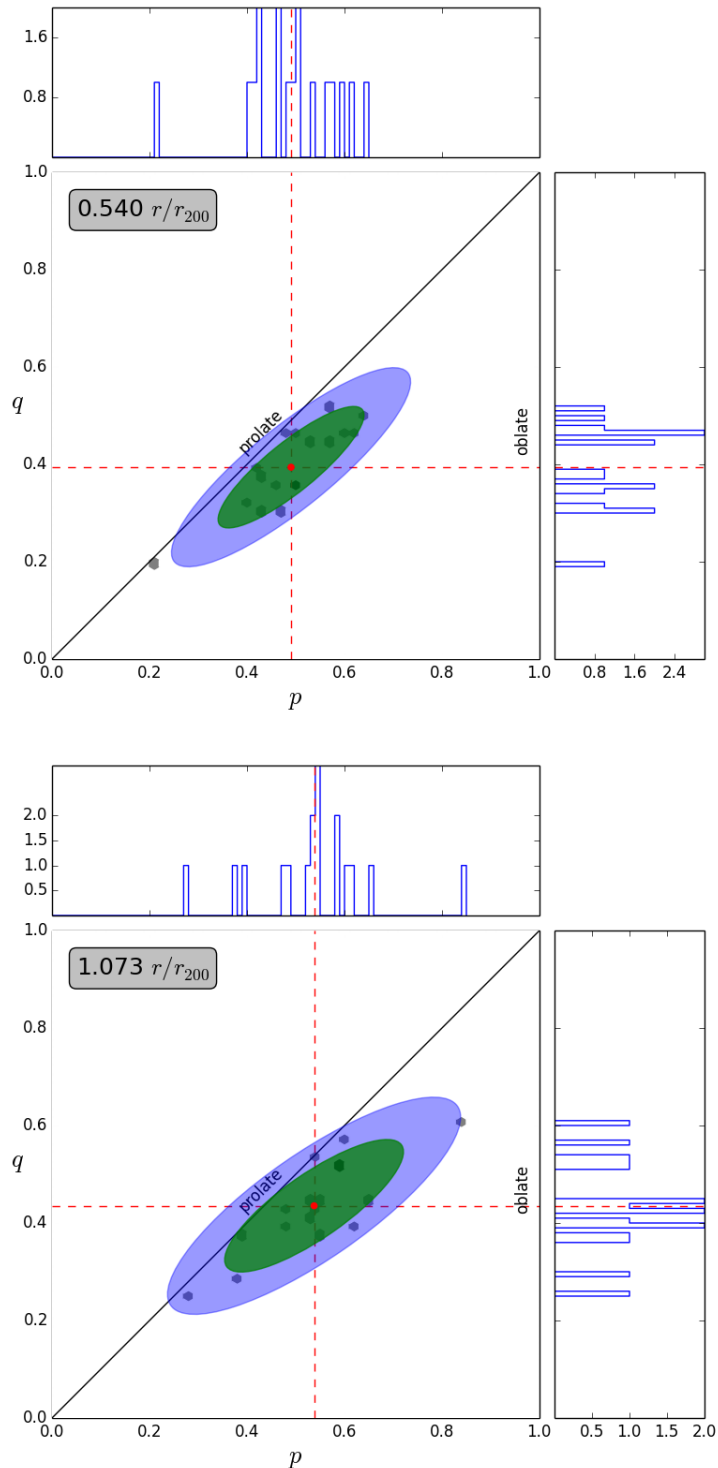


**Figure 2.7:** Same as Figure 2.5, but for the medium mass halo sample.

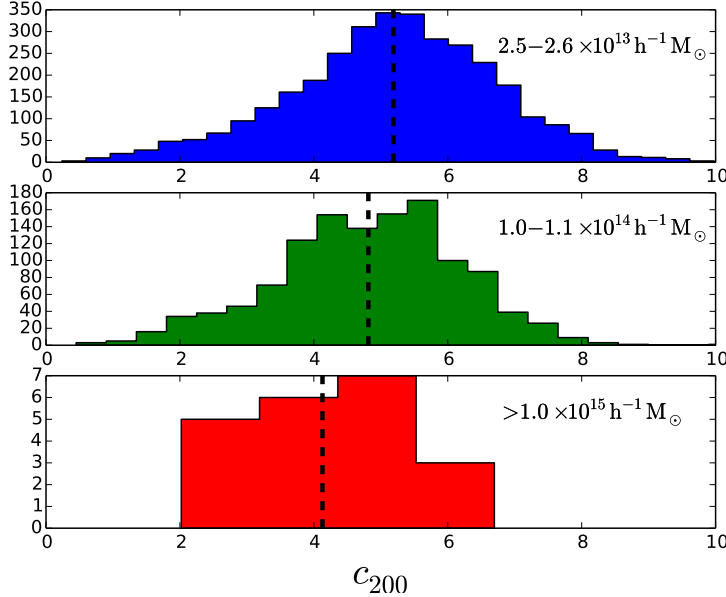


**Figure 2.8:** The distributions of intrinsic concentrations for all single virialized halos of each mass sample. From top to bottom: 1) Low Mass, 2) Medium Mass, and 3) High Mass.

over-concentration of  $\sim 20\%$ , albeit with much lower scatter. Additionally, this trend tends to flatten out with increasing distance from the cluster center. This implies that, for a fixed halo concentration, inner regions of halos (those probed on or near strong lensing scales) will bias higher than outer regions of halos (those probed on weak lensing scales) if viewed along the major axis. This information is most saliently captured for relaxed, low mass halos (Figure 2.10; See also Figure 2.11 for medium mass halos, and Table 2.3 for a complete summary).

The underlying cause for this mismatch in over-concentration between halos with low and high intrinsic concentrations is due to the magnitude of the change in shape as a function of radius. Low concentration halos are shown to significantly change their shape between  $0.5 \cdot r_{200}$  and  $r_{200}$ , increasing in p and q, 81% and 80% of the time with median differences of  $\Delta p = 0.14$  and  $\Delta q = 0.11$  (Figure 2.12). Halos with high intrinsic concentrations increase in p and q  $\sim 65\%$  of the time, however, the median value of the difference in axial ratio drops to  $\sim 0.03$ .

On the extreme end, we have shown that although a systematic bias exists, certain low concentration halos ( $c_{200} \sim 1 - 3$ ) with extreme axis ratios can produce upwards of a factor of two higher

in projected concentration on a case-by-case basis. This can be seen most notably in the low and medium mass samples at  $r \sim 0.5 \cdot r_{200}$ .

Additionally, we also find that concentric ellipsoidal shells are well described as being coaxial with one another, that is to say there is insignificant amounts of twisting of isodensity surfaces for each mass population. Alignment becomes even better with increasing radius, where the misalignment is a maximum at the innermost radial value (Figures 2.13-2.15). It should be noted, however, that alignment results are expected to be biased low due to correlation between each ellipsoidal surface and ones interior to it. Though the aggregate shows relatively good alignment, it is again possible for individual cluster halos to produce significant ( $\lesssim 30^\circ$ ) offsets between projected isodensities located at strong and weak lensing scales. This fact alone complicates things; however, in the limit of large numbers of cluster halos, this effect should be minimal in biasing reconstructed concentrations for the population as a whole.

## 2.5 Summary and Conclusions

We have shown that relaxed MultiDark MDR1 simulation (FOF) cluster halos, which are well described by a single NFW density profile, are primarily prolate spheroidal in geometry and become increasingly more spherical with increasing radius from the cluster center of mass. Using shape on weak and strong lensing scales as well as derived concentrations, we analytically project these halos along the line of sight. In doing so, we find that low mass clusters are typically over-concentrated by about 56% and 20% at half  $r_{200}$  for concentrations between 1-3 and 7-10, respectively. At  $r_{200}$  this enhancement drops to 38% and 19%. What this tells us is that the average projected concentration differs by about 18% for halos with intrinsically low concentrations simply due to differences in halo geometry as a function of radius. Clusters which do not meet this criteria show the opposite trend in shape, becoming more prolate with increasing radius.

Strong lensing clusters are usually identified by their hard to miss tangential or radial arcs, and are expected to represent a biased population simply because large mass and alignment along the line of sight are key ingredients in producing large Einstein radii. If these lensing clusters are in fact preferentially aligned along the line of sight (and are relaxed), we would expect that all else being

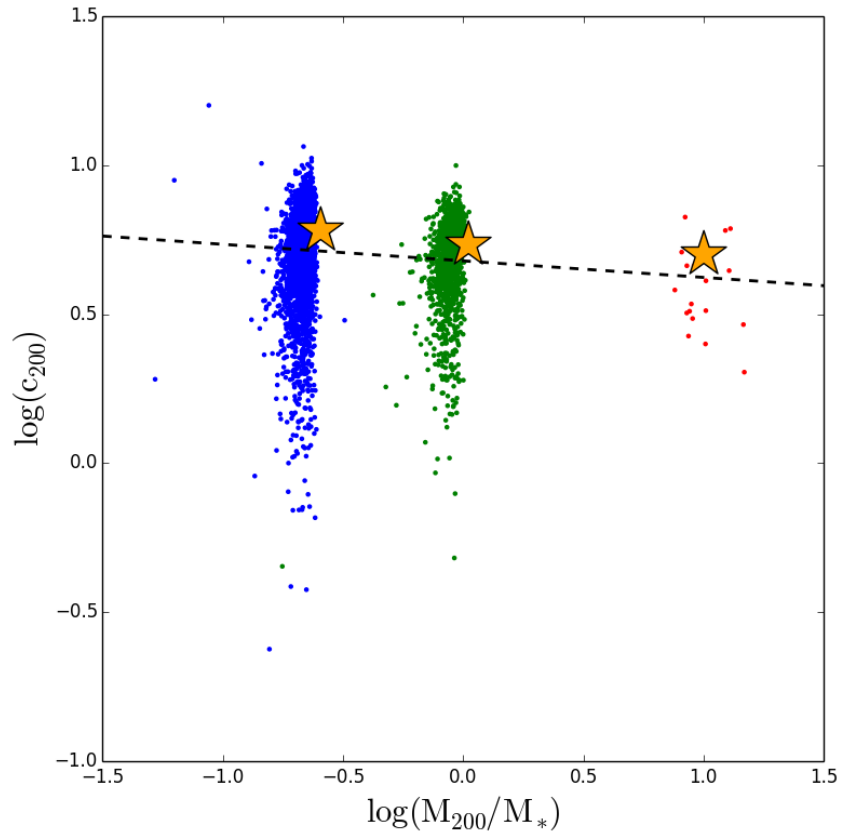


**Figure 2.9:** Shown here is the intrinsic concentration-mass relationship for the MDR1 cosmological simulation run. Orange stars represent values of concentration from the analytical expression found in Prada et al. (2012a) at redshift  $z = 0$  for values of halo mass corresponding to the sample used in this study.

**Table 2.3:** Concentration Enhancements

<b>Radial Scale</b>	<b>Low Mass</b>		<b>Medium Mass</b>	
	$c_{200}$	$\bar{\Delta}_{c_{200}} \pm \sigma_{\Delta}$	$c_{200}$	$\bar{\Delta}_{c_{200}} \pm \sigma_{\Delta}$
$0.5 \cdot r_{200}$	[1 – 3]	$1.56 \pm 0.29$	[1 – 3]	$1.52 \pm 0.25$
	[7 – 10]	$1.20 \pm 0.07$	[6 – 9]	$1.26 \pm 0.09$
$r_{200}$	[1 – 3]	$1.38 \pm 0.16$	[1 – 3]	$1.43 \pm 0.15$
	[7 – 10]	$1.19 \pm 0.09$	[6 – 9]	$1.24 \pm 0.09$
$1.5 \cdot r_{200}$	[1 – 3]	$1.30 \pm 0.12$	[1 – 3]	$1.34 \pm 0.11$
	[7 – 10]	$1.17 \pm 0.07$	[6 – 9]	$1.22 \pm 0.09$
$2 \cdot r_{200}$	[1 – 3]	$1.28 \pm 0.11$	[1 – 3]	$1.31 \pm 0.10$
	[7 – 10]	$1.18 \pm 0.07$	[6 – 9]	$1.23 \pm 0.09$

Average Concentration Enhancement ( $\Delta_{c_{200}} \equiv C_{200}/c_{200}$ ) on Weak and Strong Lensing Scales for Low and Medium Mass Samples.

equal weak lensing reconstructions should under-estimate the concentration for a population of such objects.

Projection effects aside, additional complications arise in measuring halo concentration using strong and weak lensing. For example, halo substructure can play a significant role in altering the shape of the lens as seen by strong lensing (Meneghetti et al., 2007), along with massive objects unassociated with the halo which lay along the line of sight (Puchwein & Hilbert, 2009). Redlich et al. (2012) also find that cluster mergers bias high the distribution of Einstein Radii, highlighting another source of potential bias. The weak lensing signal can be diminished by things like atmospheric PSF, correlations in the orientation of background galaxies due to large scale structure, among the usual sources of uncertainty in measuring galaxy shapes (for a review of galaxy shape measurement and correlation of galaxy shapes, see Hoekstra & Jain 2008; for a discussion of cluster triaxiality and projections of large scale structure see Becker & Kravtsov 2011). Lastly, Giocoli et al. (2014) conclude through simulations that the use of a generalized NFW model reduces mass and concentration reconstruction biases for clusters containing a BCG and adiabatic contraction of the dark matter. They also find that halo parameters differ between WL and WL+SL reconstruction methods, and that strong lensing selected clusters can have concentrations 20-30% in excess of the expected average at fixed mass.

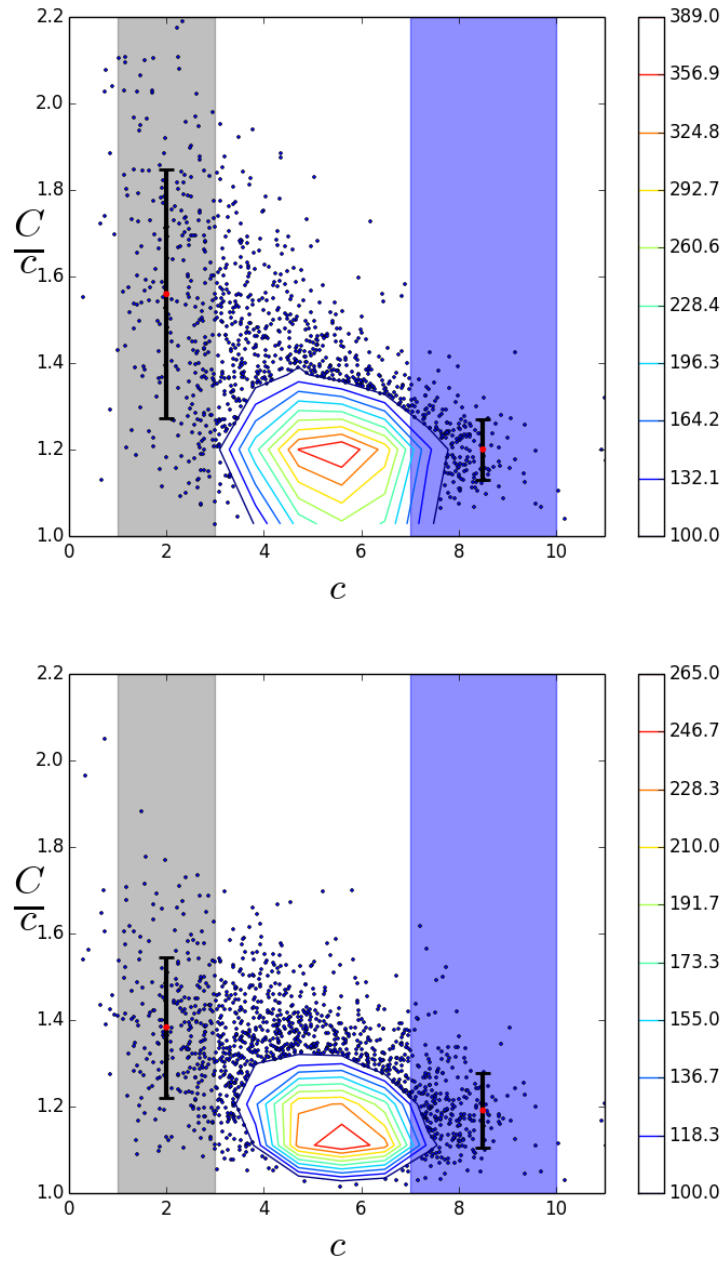


**Figure 2.10:** Shown here are concentration enhancements against intrinsic halo concentrations for line-of-sight oriented halos for the low mass, single-model, relaxed halo population. In the top (bottom) panel, we show the population at  $\sim 0.5 \cdot r_{200}$  ( $\sim 1 \cdot r_{200}$ ). Overplotted are the mean and standard deviation of low ( $1 \leq c_{200} \leq 3$ ) and high ( $7 \leq c_{200} \leq 10$ ) concentration halos for comparison. We find two novel trends: 1) the concentration enhancement is a function of the radial scale within the halo, where inner regions are found to be significantly higher than outer regions; this feature is most noticeable for halos with intrinsically low concentrations, and 2) the concentration enhancement is a function of the intrinsic halo concentration (albeit with some scatter).

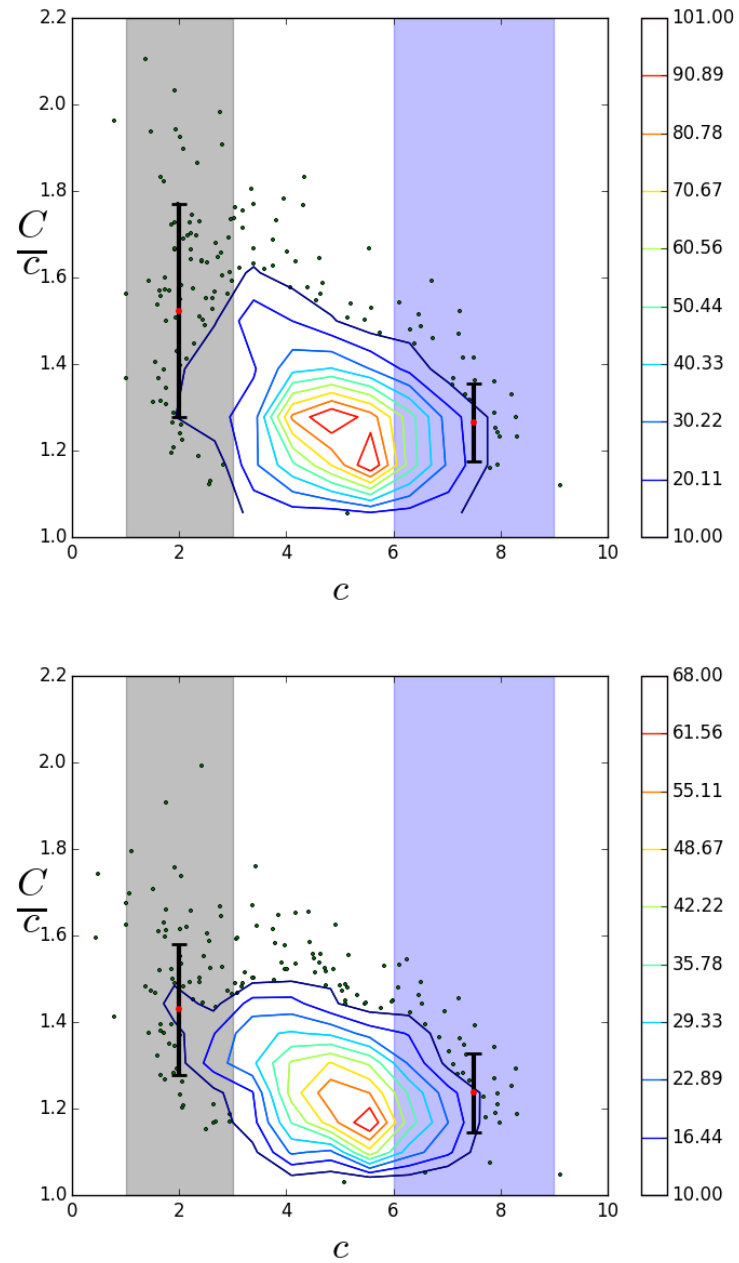


**Figure 2.11:** The concentration enhancements against intrinsic halo concentrations for line-of-sight oriented halos the the medium mass, single-model, relaxed halo population.

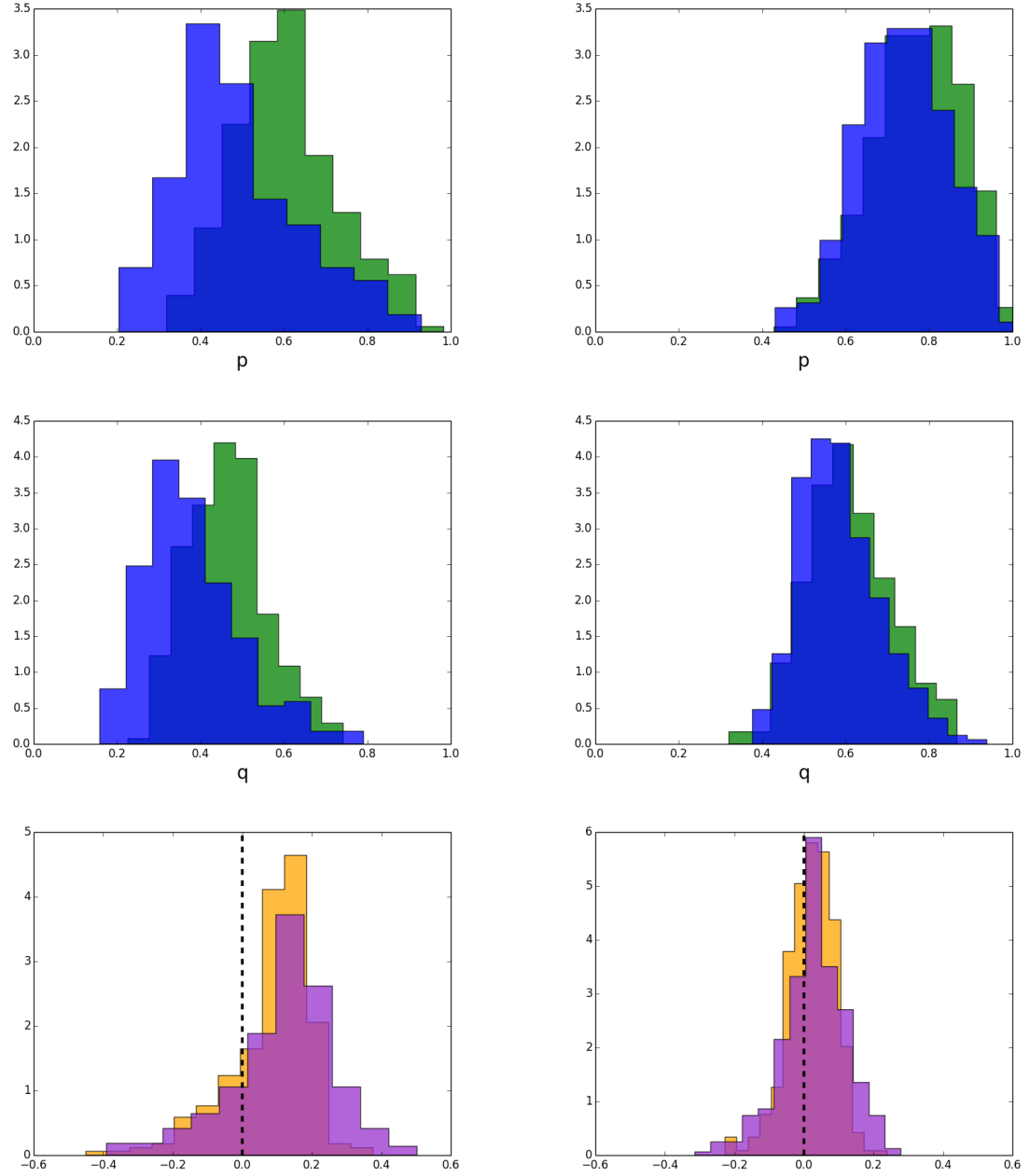


**Figure 2.12:** Halos with intrinsically low concentrations exhibit a much larger change in shape as a function of radius. *Upper left and middle*: Normalized distributions of axial ratios  $p$  and  $q$  for low-mass, low-concentration (1-3) halos at half  $r_{200}$  (blue) and  $r_{200}$  (green). *Bottom left and middle*: The distributions of axial ratios  $p$  and  $q$  for low-mass, high-concentration (7-10) halos at half  $r_{200}$  and  $r_{200}$ . *Upper right, (Lower right)*: Distributions of the differences in axial ratios  $p$  (purple) and  $q$  (orange) for low-concentration (high-concentration) low-mass cluster halos.

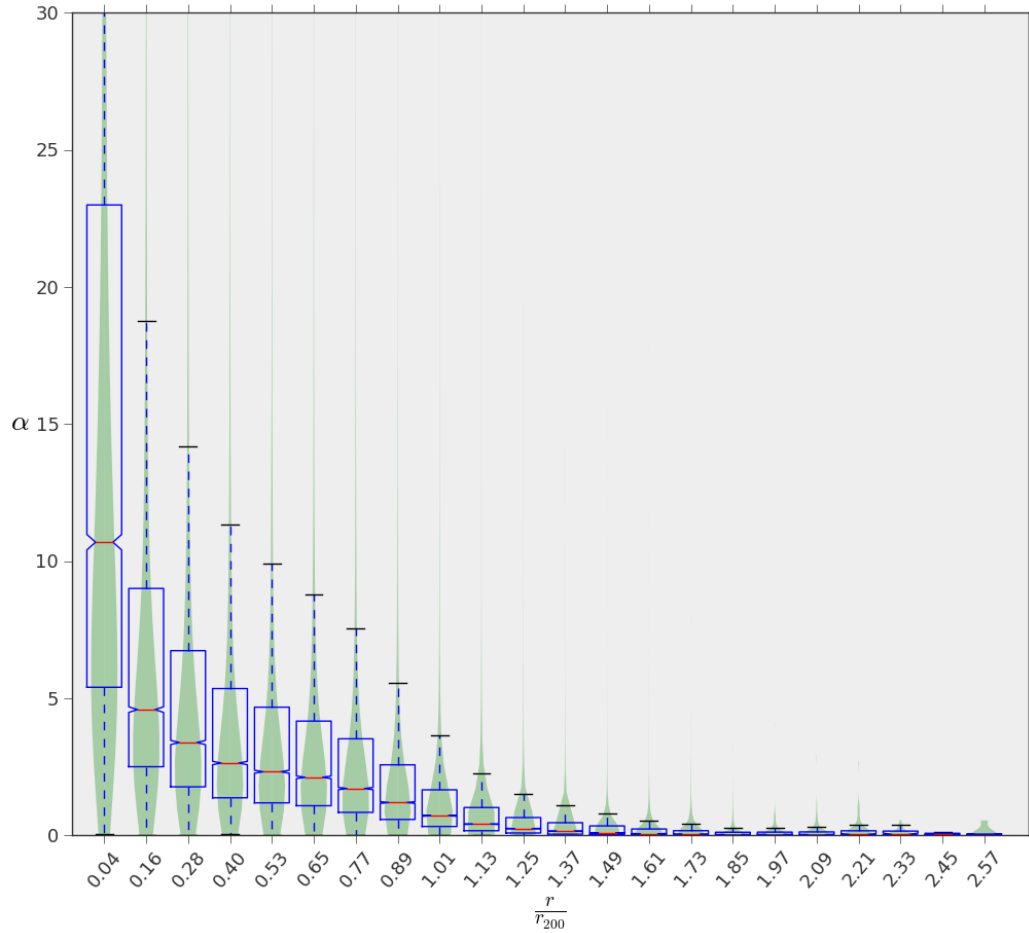


**Figure 2.13:** A ‘violin plot’ for the low mass sample, showing the distribution of angles between the major axis of an isodensity at radial coordinate  $r_i$ , and one at  $r_i + \Delta r$ . Green shaded regions represent the distributions of angles, and overplotted is a box plot showing the location of the quartiles (25%, 50%, and 75%).

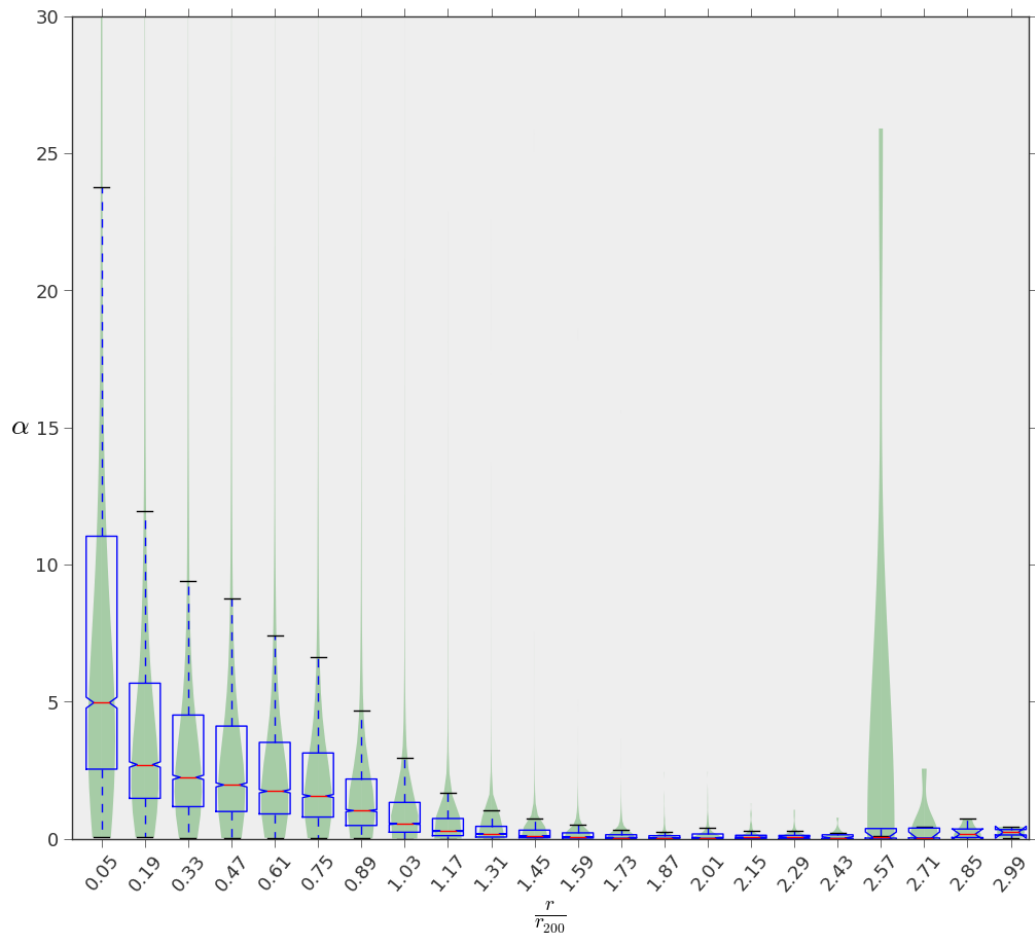


**Figure 2.14:** A ‘violin plot’ for the medium mass sample.

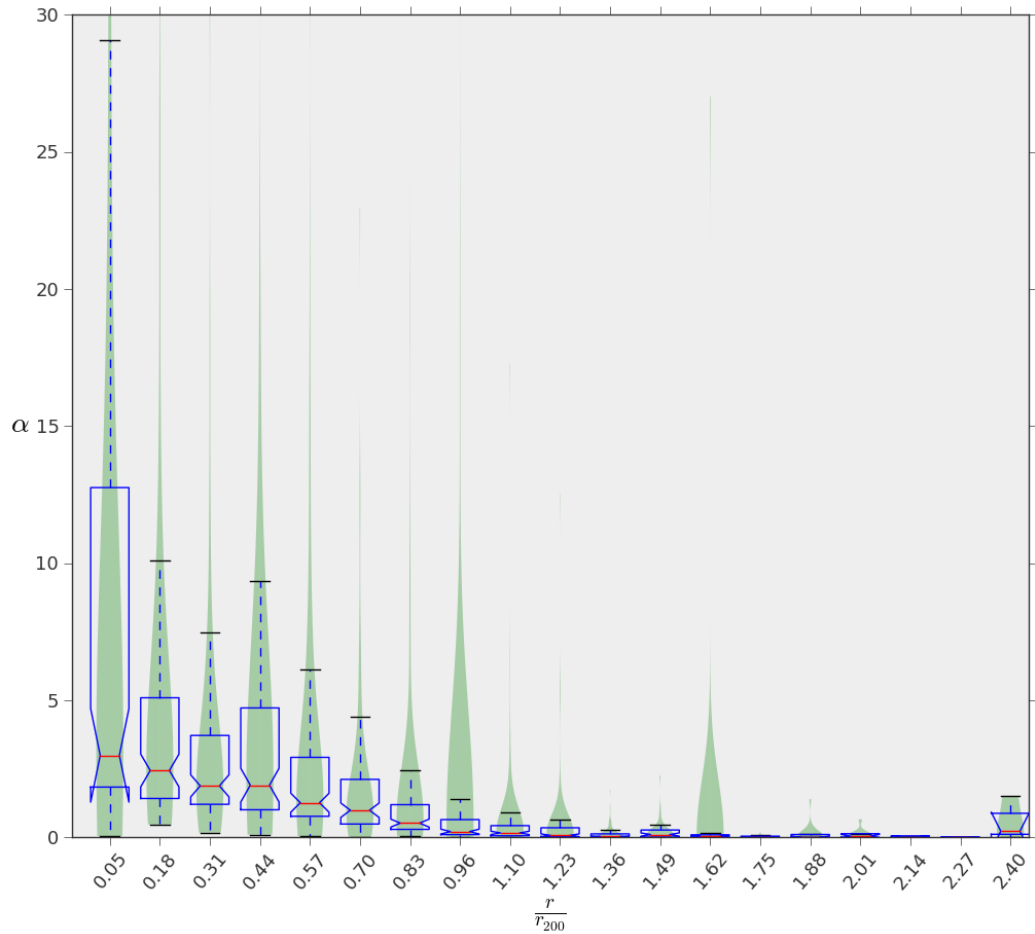


**Figure 2.15:** A ‘violin plot’ for the high mass sample.

## 2.6 Future Work

An explicit prediction has been made regarding the discrepancy between projected halo concentrations of cluster halos on characteristic lensing scales. A natural next step would be to simulate the signal produced from gravitational lensing by conducting mock weak and strong lensing analyses. However, one would realistically need to include the effects of baryons. Additionally, we plan to summarize the current state of the field of galaxy cluster mass reconstructions in each of the methods used. In future work, we will aggregate all measured NFW mass/concentration pairs from these methods in order to shed light on potential systematic observational biases, particularly on strong and weak lensing scales.

It has yet to be determined if this effect manifests itself in a measurable way for the cluster halo population. Follow-up observations of strong lensing clusters could be proposed as a way of testing the veracity of this prediction. Knowing the intrinsic distribution of cluster concentrations is difficult if not impossible due to the degenerate nature of the reverse-projection process. However, the shape of the distribution of measured concentrations due to lensing could possibly contain hallmark characteristics which could indicate the level of line of sight biasing of the population. With this information known, ultimately a correction procedure could then be proposed.

## Chapter 3: The Galaxy Cluster Concentration-Mass Scaling Relation

### 3.1 Introduction

Galaxy clusters have long been used as probes of cosmology. Cluster observables, like X-ray luminosity,  $L_X$ , optical richness, and line-of-sight galaxy dispersion,  $\sigma_v$ , are closely tied to the formation and evolution of large scale structures, and scale with redshift and the mass of the host halo (Sereno & Ettori, 2015). Scaling relations of clusters also provide a way of testing cosmology (Vikhlinin et al., 2009b; Rozo et al., 2010; Mantz et al., 2010, 2014), though are imperfect proxies for mass, due to the 2-Dimensional view they provide for us. Large cosmological simulations provide a detailed 3-dimensional view of the hierarchical process of structure formation, one that is unattainable by even the most accurate reconstruction techniques available.

The radial density profiles of clusters, well-modeled by the universal NFW profile (Navarro et al. 1997; Eq. 1.1), appears to be a prevailing outcome of simulations regardless of cosmology (Navarro et al., 1997; Craig, 1997; Kravtsov et al., 1997b; Bullock et al., 2001a). However, the details of the relationship between the two model parameters, halo mass,  $M$ , and concentration,  $c$ , is sensitive to small changes in initial parameters (Macciò et al., 2008; Correa et al., 2015b).

Tensions exist between cluster concentrations derived from simulations and observational measurements (see section 1.3), have been found to differ the most for gravitational lensing techniques (Comerford & Natarajan, 2007b; Broadhurst et al., 2008b; Oguri et al., 2009b; Umetsu et al., 2011a). This over-concentration of clusters (in favor of observational measurements) can be partially explained by the orientation of triaxial structure along our line-of-sight (Oguri et al., 2005b; Sereno & Umetsu, 2011), which has the effect of enhancing the lensing properties (Hennawi et al., 2007b). Neglecting halo triaxiality (Corless et al., 2009) and substructure (Meneghetti et al., 2010; Giocoli et al., 2012) also each have significant effects on halo parameters. For its effect on WL and X-ray mass estimates, see Sereno & Ettori (2014).

Discrepancies in how measurements of the intrinsic concentration are made using simulations also

exist, along with studies who disagree on the inner slope of the density profile (Moore et al., 1999; Ghigna et al., 2000; Navarro et al., 2004). However, the most puzzling and potentially interesting disparity between simulations is the existence of the upturn feature in the c-M relation (see for example, Fig. 12 of Prada et al. 2012b) at high redshift (Prada et al., 2012b; Dutton & Macciò, 2014; Klypin et al., 2014; Diemer & Kravtsov, 2015), which some argue is an artifact caused by the selection of halos which are dynamically unrelaxed (Ludlow et al., 2012). This novel feature only shows up when the concentration is expressed as a profile-independent halo property (in terms of the ratio of the maximum circular velocity and the virial velocity,  $V_{\max}/V_{\text{vir}}$ ). In terms of the classical definition of concentration, this feature disappears (see Meneghetti & Rasia 2013).

The connection between the observed concentration,  $c_{2D}$ , and the intrinsic concentration,  $c_{3D}$ , is further complicated, since it has been shown that relaxed cluster isodensities are not constant on all scales (Frenk et al., 1988b; Cole & Lacey, 1996b; Dubinski & Carlberg, 1991b; Warren et al., 1992b; Jing & Suto, 2002c; Hayashi et al., 2007b; Groener & Goldberg, 2014). Indeed, in a previous study by Groener & Goldberg (2014) (Chapter 2), it has been shown that a halo's concentration is an ill-defined 2-dimensional quantity, without first specifying the scale on which the measurement was made. Using the MultiDark MDR1 Cosmological Simulation, Groener & Goldberg (2014) found a systematic shift of about  $\sim 18\%$  in the mean value of the projected concentration,  $c_{2D}$ , between weak and strong lensing scales, for low-mass cluster halos ( $2.5 - 2.6 \times 10^{13} h^{-1} M_{\odot}$ ) observed with their major axes aligned with the line-of-sight direction. Though this difference is notably smaller than the intrinsic scatter of the concentration parameter ( $c_{3D}$ ) for a given halo mass, the origin of this systematic effect is solely due to the changing shape of cluster isodensities as a function of radius.

For many objects, not only do observed concentrations seem to differ substantially from those obtained in cosmological simulations, but concentrations can also vary depending on which method is used. Since different reconstruction methods probe varying scales within the halo, it is not unreasonable to suspect that there exist systematic differences in the observed c-M relation caused by shape.

In this chapter, we focus on three main objectives.

1. We present the current state of the observational concentration-mass relation for galaxy clusters by aggregating all known measurements from the literature. The raw data are reported in Table A-1, and have been made publicly available (see Appendix A). We also provide an additional table (available only online), where data have been normalized over differences in assumed cosmology, overdensity convention, and uncertainty type found in the original studies.
2. We model the observed concentration-mass relation for each method, and compare these to one another, highlighting potential differences which exist, caused by the projection of structure along the line-of-sight, the varying shape of cluster isodensities, and the selection of clusters from the cosmic population.
3. Using the largest cluster sample to date, we determine if the observed c-M relation is consistent with theory, when taking halo triaxiality and elongation of structure along the line-of-sight into account.

In section 3.2, we summarize many of the most common mass reconstruction techniques which are used throughout the cluster community, and include a discussion regarding physical scales probed within the cluster using these methods. In section 3.3, we discuss the procedure for collecting our sample from the literature, and normalizing over convention, cosmology, and uncertainties. In section 3.4, we present results for the observed c-M relation for each method, and in section 3.5, we discuss the projection of triaxial halos from simulations to the observed lensing relations. Lastly, in section 3.6, we conclude and discuss our findings.

Throughout this chapter we adopt a flat  $\Lambda$ CDM cosmology,  $\Omega_m = 0.3$ ,  $\Omega_\Lambda = 0.7$ , and  $H_0 = 70 \text{ km s}^{-1}\text{Mpc}^{-1}$ . Generally speaking, we reserve the following colors within plots to represent the various methods:

- Caustic Method (CM): blue
- Line-of-sight velocity dispersion (LOSVD): orange

- X-ray: green
- Weak Lensing (WL): purple
- Strong Lensing (SL): red
- Weak + Strong Lensing (WL+SL): black

Unless otherwise stated, throughout the study, uncertainties are reported as  $1-\sigma$  (68.3%) Gaussian uncertainties.

## 3.2 Cluster Mass Reconstruction Techniques

In this section, we present a brief overview of common mass reconstruction techniques and modeling of the cluster density profile.

### 3.2.1 Weak Lensing (WL)

Weak gravitational lensing is the process by which images of background galaxies are distorted by massive foreground objects. Though these distortions cannot be detected for any given source, it is possible to obtain a signal by locally averaging the shapes (ellipticities) of galaxies. This shear measurement within a given bin can be used as a direct proxy for the lens density profile at intermediate to large radii.

For a symmetric distribution, the azimuthally averaged tangential shear,  $\langle \gamma_t \rangle$ , as a function of radius from the cluster center can then be calculated, and relates to the convergence,  $\kappa$ :

$$\langle \gamma_t \rangle(r) = \frac{\bar{\Sigma}(< r) - \bar{\Sigma}(r)}{\Sigma_{\text{cr}}} = \bar{\kappa}(< r) - \bar{\kappa}(r) \quad (3.1)$$

where the critical surface mass density is defined in terms of cosmology-dependent angular diameter distances  $D_s$  (source),  $D_{ds}$  (lens to source), and  $D_d$  (lens):

$$\Sigma_{\text{cr}} = \frac{c^2 D_s}{4\pi G D_{ds} D_d} \quad (3.2)$$

Expressions, specifically for the NFW profile, for the convergence (Bartelmann, 1996) and the tangential shear (Oaxaca Wright & Brainerd, 1999) have been derived, and can be used for model fitting.

Weak lensing comes with its own intrinsic biases in that more massive clusters produce larger distortions of background galaxies. As a result, in a survey of detected clusters, the expectation is that nearly all of the most massive clusters would be *selected* from the population. However, in the low mass region, clusters which are highly triaxial and elongated along the line-of-sight (i.e. - larger 2D concentrations) are more likely to pass the observational signal-to-noise threshold than ones which are not. The net effect here is an artificial steepening of the c-M relation due to selection. Furthermore, lensing geometry plays an additional role in how clusters are selected. Clusters which are too distant lack the requisite number density of background galaxies to obtain high signal-to-noise (Bartelmann & Schneider, 2001). Table 3.1 presents the range in redshift for weak lensing clusters, where most measurements are found to lie in the redshift range of  $z = 0.2 - 0.6$ , with  $M_{\text{vir}} \gtrsim 1 \times 10^{14} M_{\odot}$ .

### 3.2.2 Strong Lensing (SL)

A natural extreme of the phenomenon of gravitational lensing can occur if a background galaxy is serendipitously aligned with the core of a cluster. In such cases, the projected surface mass density is so high that multiple images of the object are produced, commonly distorting them so much that they appear arc-like.

A density profile can be obtained by fitting a model to the observed image positions, orientations, and fluxes, though this technique constrains the cluster profile on small scales (approximately the Einstein radius,  $\theta_E$ <sup>1</sup>, which is typically  $\sim 5\%$  of the virial radius,  $r_{\text{vir}}$ , or  $\sim 50\%$  of the scale radius,  $r_s$  (Oguri & Blandford, 2009b)).

Due to the irregular occurrence of multiple images and arcs, cluster measurements made with strong lensing are particularly prone to selection effects, and likely represent a biased sampling

---

<sup>1</sup>The Einstein radius for a point mass is  $\theta_E = \left( \frac{4GM}{c^2} \frac{D_{LS}}{D_L D_S} \right)^{1/2}$ . Though there is no corresponding functional form for an NFW profile, typical values for clusters lie in the range: 10"-45" (Kneib et al., 2003; Broadhurst et al., 2005c).

of the cosmic population. In fact, the efficiency of lensing is increased with increasing mass and concentration, and a preferential line-of-sight alignment of the triaxial halo (Oguri & Blandford, 2009b). Concentrations derived from this method have been contentiously high as compared to X-ray studies (Comerford & Natarajan, 2007b).

### 3.2.3 Weak+Strong Lensing (WL+SL)

Combining weak and strong gravitational methods constrains the density profile over a wide range of scales, and also has the ability to break the mass-sheet degeneracy (Schneider & Seitz, 1995). Recent efforts to combine these methods have become more prevalent in the literature (Merten et al. (2014) - CLASH; Oguri et al. (2012b) - SGAS), and work to reconstruct the lensing potential by minimizing a combined least-squares approach.

$$\chi^2(\psi) = \chi_w^2(\psi) + \chi_s^2(\psi). \quad (3.3)$$

### 3.2.4 X-ray

Massive clusters are significant sources of X-ray radiation, due to the hot diffuse plasma ( $k_B T_e \sim 10 \text{ keV}$ ) emitting via thermal bremsstrahlung, and can be used to determine the total distribution of mass. Under assumptions of spherical symmetry and hydrostatic equilibrium with the underlying potential (Evrard et al., 1996), temperature and gas density information,  $\rho_g$ , are used to determine the total mass of the cluster, typically at intermediate scales ( $\sim r_{500}$ , corresponding to the radius at which the average density inside is 500 times  $\rho_{cr}$ ).

$$M(r) = \frac{kT(r)}{G\mu m_p} r \left( \frac{d \log \rho_g(r)}{d \log r} + \frac{d \log T(r)}{d \log r} \right) \quad (3.4)$$

These assumptions are often violated due to non-thermal pressure sources, temperature inhomogeneity, and to the presence of substructures further out (Rasia et al., 2012), and bias low mass estimates by 25-35%.

### 3.2.5 Line-of-sight Velocity Dispersion (LOSVD)

The distribution of mass within clusters can also be obtained by using the kinematics of cluster galaxies, specifically, by using the moments of the velocity distribution. Reconstruction methods, developed by Lokas (2002) and Lokas & Mamon (2003), use the second (dispersion) and fourth (kurtosis) moments of the velocity distribution, which relies on the underlying gravitational potential. Assuming the distribution of mass follows an NFW profile, free parameters, which include  $M_{\text{vir}}$  and  $c_{\text{vir}}$ , can be fit to the observed data.

The business of identifying clusters as mass over-densities, determining cluster membership, removal of interlopers, and reconstruction details vary from technique to technique. For a more complete review of the reconstruction methods and their impact on cluster observables, see Old et al. (2014).

### 3.2.6 The Caustic Method (CM)

With the exception of weak lensing, the caustic method is the only other standalone method which has been successful in probing the density profile at large distances from the cluster center ( $\gtrsim r_{\text{vir}}$ ). Cluster galaxies, when plotted in line-of-sight velocity versus projected cluster-centric distance phase-space, create a characteristic “trumpet shape”, the boundaries of which form what is referred to as caustics (Kaiser, 1987; Regos & Geller, 1989). The existence of these caustics mark an important boundary which envelops a volume of space in which galaxies are gravitationally bound to the cluster. Outside of this turnaround radius, galaxies are ultimately carried away in the Hubble flow.

The width of the caustic (velocity) at any given projected radius,  $\mathcal{A}(R)$ , can then be related to the escape velocity due to the gravitational potential of the cluster, under the assumption of spherical symmetry (Diaferio & Geller, 1997). Through simulations of structure formation, Diaferio (1999) has shown that the caustic amplitude can be related to the mass interior to radius  $r$  by:

$$GM(< r) = \frac{1}{2} \int_0^r \mathcal{A}^2(R) dR. \quad (3.5)$$

The success of the caustic method is independent of any assumptions regarding dynamical equi-

librium of the cluster, and has been used to reconstruct profiles over a larger range of scales: from the inner regions to a few times the virial radius (CAIRNS: Rines et al. 2003; CIRS: Rines & Diaferio 2006; HeCS: Rines et al. 2013). However, this technique requires the measurements of at least 30-50 cluster members, and thus limits this method to clusters at relatively low redshifts compared to lensing and X-ray techniques. More recently, Rines et al. (2013) make use of this technique using  $\sim 200$  cluster members.

### 3.2.7 Hybrid Techniques

The aforementioned methods represent the most commonly applied techniques for constructing a density profile, however, they do not represent them all. Novel combinations of methods have also been used, but could not be included in a study of this kind. For instance, Lemze et al. (2008) combine joint lensing and X-ray methods to make a determination of Abell 1689. Thanjavur et al. (2010) and Verdugo et al. (2011) use a combination of lensing and dynamics. Additionally, In an attempt to only compare methods used in Comerford & Natarajan (2007b), we consciously leave out measurements made with the Sunyaev-Zel'dovich (SZ) effect, or which use combinations of techniques one of which uses SZ.

Previous studies have even employed these multi-technique reconstructions to clusters in an attempt to break the line-of-sight mass degeneracy (for a review of these techniques, see section 2 of Limousin et al. (2013b); see also Ameglio et al. (2007), Sereno et al. (2012)). However, it is unclear if techniques such as this can adapt to arbitrarily complicated profiles, where shape is scale-dependent, or where isodensities are not co-axial with one another (isodensity twisting).

## 3.3 The Sample

The sample of clusters collected from the literature consists of a total of 781 cluster measurements, reported by 81 studies (Table A-2), representing the largest known collection of cluster concentration measurements to date. Of these, there are 361 unique clusters, giving us a sizable sampling of the cluster population as a whole, in addition to multiple measurements of individual clusters (often coming from more than one category of reconstruction technique).

This study builds off of work done by Comerford & Natarajan (2007b), which aggregated 182 cluster measurements of 100 unique cluster objects. In accordance with that study, we also report measurements of concentration (and mass) in the most popular conventions,  $c_{200}$ , and  $c_{vir}$ .

Table 3.1 presents population averages of masses and concentration, as well as their range in redshift for the six reconstruction techniques we reference throughout this study. This information highlights the importance of the selection function of clusters, though we make no attempt in this chapter to distinguish between whether a lack of measurements of certain values for a given method is due to its inability to make these determinations, or whether it is simply a preferential selection effect. In Figure 3.1, we show the locations of galaxy clusters on the sky, as well as distributions in mass-redshift space for each method.

**Table 3.1:** Population Overview

Method	N <sub>meas</sub>	N <sub>cl</sub>	min(M <sub>vir</sub> ) (10 <sup>14</sup> M <sub>⊙</sub> )	$\langle M_{\text{vir}} \rangle$ (10 <sup>14</sup> M <sub>⊙</sub> )	max(M <sub>vir</sub> ) (10 <sup>14</sup> M <sub>⊙</sub> )	min(c <sub>vir</sub> )	$\langle c_{\text{vir}} \rangle$	max(c <sub>vir</sub> )	min(z)	$\langle z \rangle$	max(z)
CM	82	79	<1.0	3.9	18.6	<2.0	8.9	36.7	0.003	0.06	0.44
LOSVD	70	59	1.3	5.8	17.1	<2.0	8.8	39.0	0.01	0.06	0.44
X-ray	290	195	<1.0	26.1	>40.0	<2.0	7.2	26.2	0.003	0.22	1.41
WL	169	111	<1.0	12.4	>40.0	<2.0	8.1	64.5	0.02	0.48	1.45
WL+SL	113	58	<1.0	8.7	31.8	2.3	10.2	30.6	0.18	0.53	1.39
SL	19	11	3.2	24.3	>40.0	3.8	11.2	27.5	0.18	0.47	0.78

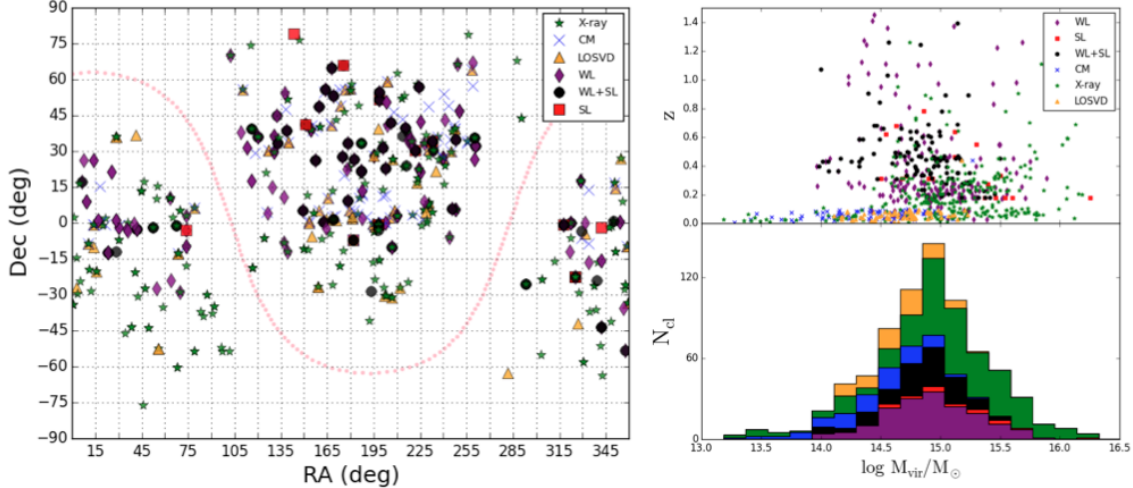


**Figure 3.1:** (Left) The distribution of clusters on the sky for each reconstruction method. The dotted line shows the location of the plane of the Milky Way galaxy. (Right) The range of redshift and cluster masses each method spans for the sample we have collected.

### 3.3.1 Normalization Procedure

Due to the nature of this study, cluster measurements must be properly normalized to ensure that they are compared to one another on equal footing. In this section, we discuss the steps taken to eliminate biases due to overdensity convention, assumed cosmology, and due to differences in the definitions of measurement uncertainty, respectively.

#### Convention

Under the assumption that the radial density profile follows an NFW profile, Hu & Kravtsov (2003) derive a procedure for the conversion of both concentration and mass between any two arbitrary characteristic radii. We apply these formulae as a first round of our normalization procedure.

#### Cosmology

Measurements taken from the literature do not always use the same fiducial cosmology, and thus are not immediately comparable. Because of this, we develop a procedure for converting measurements between any two arbitrary cosmologies. Appendix B outlines this procedure for general lensing methods.

For extreme cosmologies, the correction to the concentration parameter,  $c_{\text{vir}}$ , and mass,  $M_{\text{vir}}$ , are

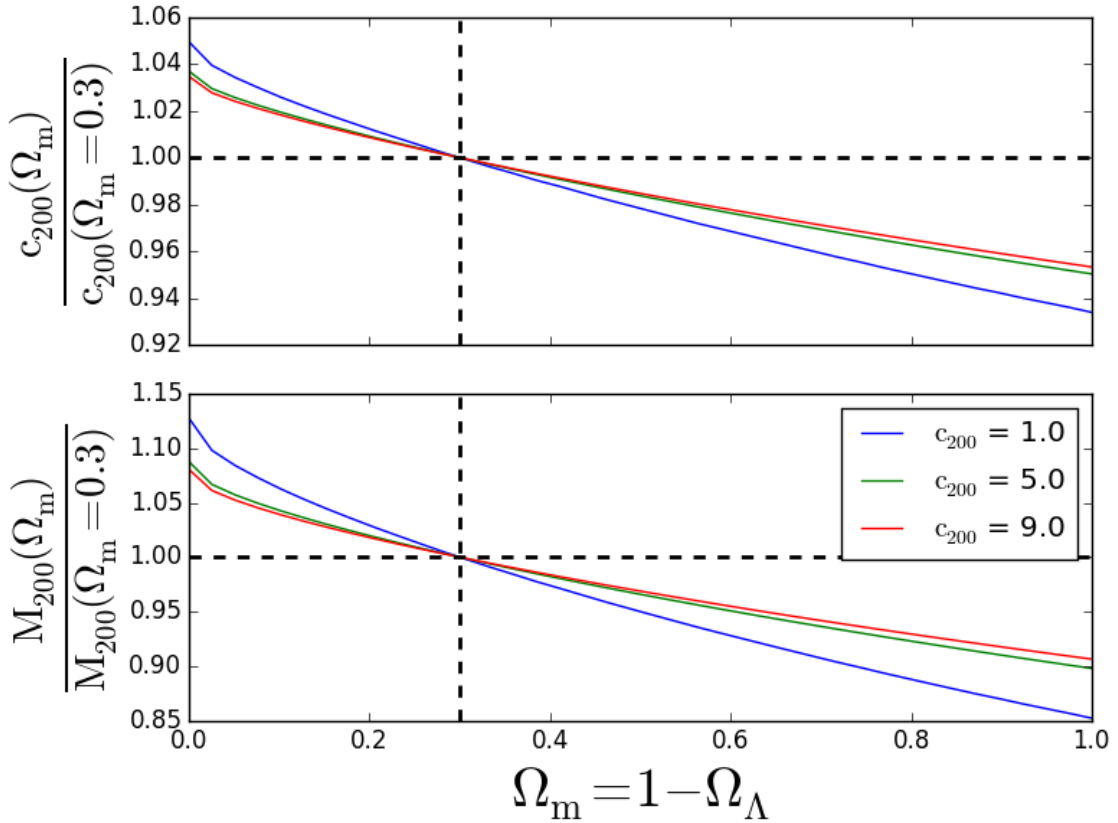


**Figure 3.2:** The fractional error in weak lensing concentration and mass measurements due to the conversion to an arbitrary cosmology (x-axis) from the fiducial cosmology used in this chapter.

approximately 5% and 10%, respectively. This correction is significantly smaller than other known effects. Moreover, the vast majority of all measurements we have collected assume flat cosmologies which lie in the range  $\Omega_\Lambda = 1 - \Omega_m = 0.73 - 0.68$ . The corrections to the concentration and mass in this range are  $\sim 1\%$ . Figure 3.2 shows the fractional error in concentration and mass, over the full range of flat cosmologies.

### Uncertainties

Another complication which must be accounted for is the usage of multiple definitions of measurement uncertainty on resulting mass and concentration estimates reported throughout the literature. Particularly, many fitting procedures (namely methods which involve brute force exploration of likelihood space) produce maximum-likelihood estimates of parameters of interest and corresponding

confidence intervals. However, most studies do not report the marginal distributions from their fitting procedures, and consequently, limits the utility of their measurements for those looking to compare or adopt their values.

Furthermore, the mathematical theorems which dictate the propagation of error of measurements rely on expected values and variances, rather than maximum-likelihood estimates and probability intervals. D'Agostini (2004) argues that the expected value and standard deviation should *always* be reported, and in the event of an asymmetric distribution, one should also report shape parameters or best-fit model parameters as well. Most importantly, any published result containing asymmetric uncertainties causes the value of the physical quantity of interest to be biased.

We follow the procedure outlined in D'Agostini (2004) for symmetrizing measurements with asymmetric uncertainties (to first order),  $\theta_m \xrightarrow{\Delta_+ - \Delta_-}$ , and apply this to both cluster mass and concentration measurements.

$$\sigma_\theta \approx \frac{\Delta_+ + \Delta_-}{2} \quad (3.6a)$$

$$E[\theta] \approx \theta_m + \mathcal{O}(\Delta_+ - \Delta_-) \quad (3.6b)$$

Additionally, many studies report measurements without uncertainties altogether. For these clusters, we apply uncertainty based upon the estimate of the average fractional uncertainty of all other measurements of its type. The most notable method having this issue is the caustic method, where virtually no measurements are accompanied by uncertainties. In this case, we apply the same fractional uncertainty to all measurements equally, and is derived from the average fractional error of LOSVD concentration and mass measurements.

Lastly, a large fraction of clusters represented in our database have multiple concentration and mass measurements, leading subsequent fits to be more sensitive to these particular objects. In order to prevent fits from being dominated by the most popular clusters (e.g. - Abell 1689, of which there are 26 measurements in total), we combine similar measurements using an uncertainty-weighted

average value.

### 3.4 The Observed Concentration-Mass Relation

In Figure 3.3, we show the full cluster dataset after applying the normalization procedures discussed in the previous section. Following this, we present here the results of our fitting procedure to these data. The typical prescription for modeling the c-M relation, is to use a double power-law model of the following form

$$c(M) = \frac{A}{(1+z)^\beta} \left( \frac{M}{M_*} \right)^\alpha \quad (3.7)$$

where the power-law indices,  $\alpha$  and  $\beta$ , control the dependence of the concentration with respect to mass and redshift. The model parameter,  $A$ , controls the normalization of the relation, once a suitable  $M_*$  has been chosen ( $M_* = 1.3 \times 10^{13} h^{-1} M_\odot = 1.857 \times 10^{13} M_\odot$ ).

We follow convention in using the above model, but in a slightly different form, with the power-law index,  $\beta$ , fixed to unity. We adapt this model to a linear model in the following way

$$\mathcal{Y} = m\mathcal{X} + b \pm \sigma_{\text{int}} \quad (3.8)$$

where variables and model parameters relate to the initial model in the following way:

$$\mathcal{Y} \equiv \log c(1+z) \quad (3.9a)$$

$$\mathcal{X} \equiv \log M \quad (3.9b)$$

$$m = \alpha \quad (3.9c)$$

$$b = \log A - \alpha \log M_* \quad (3.9d)$$

We introduce the intrinsic scatter,  $\sigma_{\text{int}}$ , as a fixed parameter, which we estimate from the data (independently from the fit itself), and is assumed to be constant over the full mass range:

$$\sigma_{\text{int}}^2 = \sigma_{\text{res}}^2 - \langle \sigma_{\mathcal{Y}}^2 \rangle \quad (3.10)$$

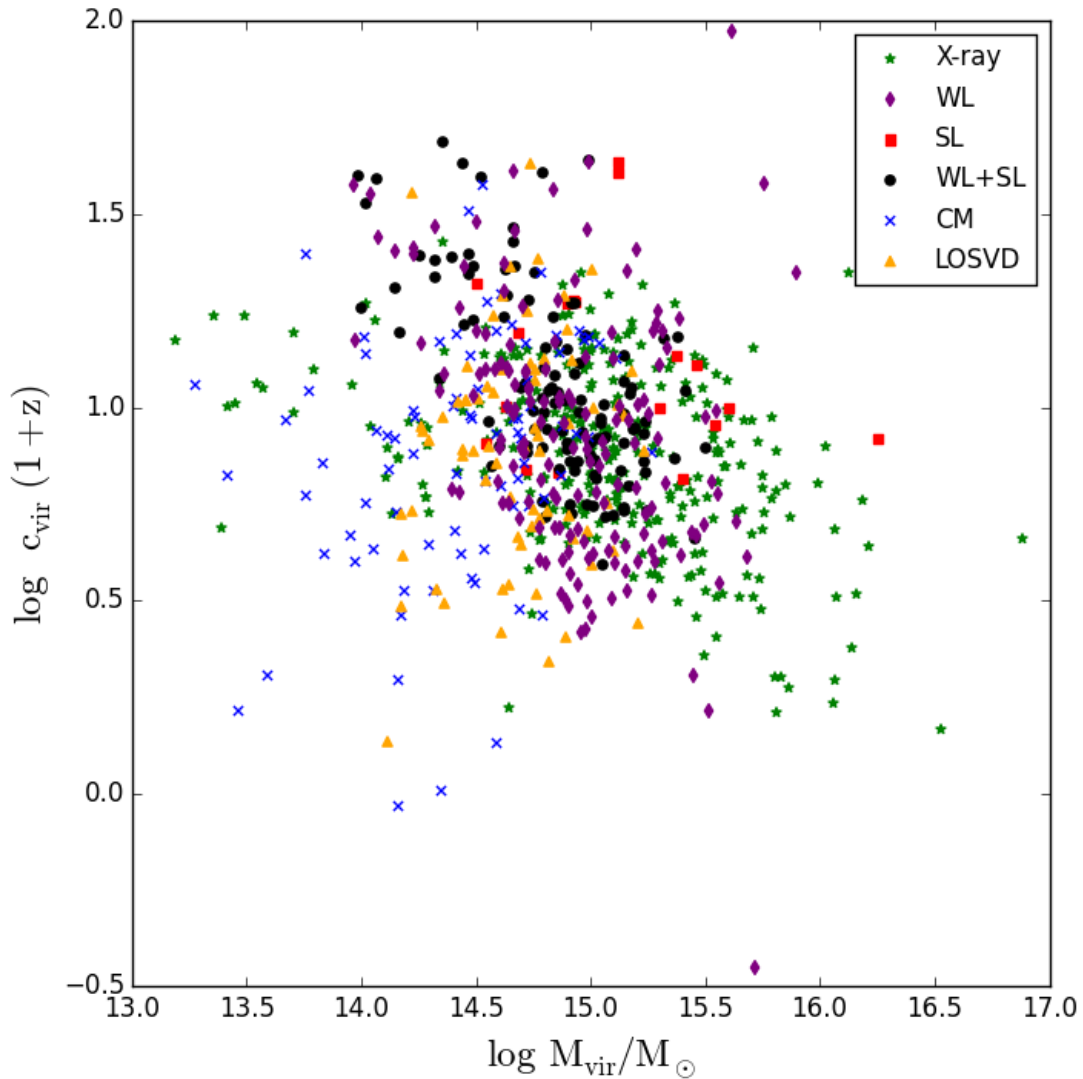


**Figure 3.3:** The full normalized observational cluster sample, colored by method. Uncertainties have been omitted here for clarity.

where  $\sigma_{\text{res}}$  is the scatter in the residual between the data and the best-fit model, and  $\langle \sigma_{\mathcal{Y}}^2 \rangle$  is the average squared-uncertainty in the dependent variable. The idea here is that the scatter in the residual must be accounted for by a combination of scatter due to the intrinsic relation itself as well as the uncertainties in the measurements of the observables. We also note that although the value of the redshift for any given cluster has an effect on the uncertainty of the variable  $\mathcal{Y}$ , the uncertainty in the measured redshifts themselves do not contribute much to the overall uncertainty of the best-fit model parameters.

After measurements have been normalized, we eliminate extreme values of mass and concentration. Simulations tell us that the most massive clusters which exist at present are approximately a few times  $10^{15} M_{\odot}$ . Accordingly, we remove masses which are larger than  $4 \times 10^{15} M_{\odot}$ . We also remove masses lower than  $1 \times 10^{14} M_{\odot}$ , as these are more typical masses of groups. Lastly, concentrations which are lower than 2, indicate rather poor NFW fits to the density profile, and will bias our inferred parameters.

In Table 3.2, we present our best-fit linear model parameters, and their mapping back to the original power-law model. In Figure 3.4, individual fits to each subsample are shown alongside normalized data points. Lensing (WL and WL+SL) and X-ray relations show a clear trend consistent with concentration decreasing with increasing mass. We also include a bootstrap analysis of these fits, to reveal the sensitivity of the fits to the data.

Though seemingly well-constrained, the bootstrap analysis reveals that our strong lensing c-M relation is highly sensitive to the dataset (due to the very small sample size), and so the best-fit model parameters are likely untrustworthy.

General agreement between concentration and mass measurements of all methods can be seen in the range  $10^{14.5} - 10^{15} M_{\odot}$ , which we also point out, is the region we find most consistent with simulation results.

**Table 3.2:** Best-Fit Concentration-Mass Relation Parameters

Method	Bootstrap →														
	N <sub>cl</sub>	m <sup>a</sup>	σ <sub>m</sub> <sup>b</sup>	b	σ <sub>b</sub>	A <sup>c</sup>	σ <sub>A</sub> <sup>d</sup>	σ <sub>int</sub> <sup>e</sup>	χ <sub>red</sub> <sup>2</sup>	m	σ <sub>m</sub>	b	σ <sub>b</sub>	A	σ <sub>A</sub>
CM	63	0.280	0.003	-3.138	0.038	3.778	0.677	0.242	0.327	0.28	0.19	-3.16	2.73	3.59	43.43
LOSVD	58	0.010	0.002	0.728	0.025	7.256	0.861	0.228	1.000	0.13	0.17	-1.00	2.55	5.31	58.74
X-ray	149	-0.105	0.001	2.494	0.010	12.612	0.676	0.160	1.224	-0.17	0.03	3.38	0.44	13.32	25.69
WL	93	-0.379	0.001	6.576	0.014	35.246	2.213	0.118	1.302	-0.43	0.11	7.35	1.62	44.10	312.68
WL+SL	57	-0.534	0.001	8.977	0.016	77.882	5.249	0.130	1.070	-0.54	0.10	9.10	1.46	86.06	552.28
SL	10	0.097	0.004	-0.422	0.062	7.236	1.951	0.254	1.003	0.11	0.23	-0.60	3.49	7.24	109.02
All (This Work)	293	-0.152	0.001	3.195	0.007	15.071	0.703	0.146	1.354	-0.16	0.03	3.26	0.44	13.71	26.45
All (CO07.1)	62	-0.14	0.12	—	—	14.8	6.1	0.15	—	—	—	—	—	—	—

<sup>a</sup>The slope, m, of the linear model is exactly equivalent to the power-law index  $\alpha$ .

<sup>b</sup> $\sigma_m = \sigma_\alpha$

<sup>c</sup>The normalization parameter, A, depends upon both m and b:  $A = 10^{b+m \log M_*}$

<sup>d</sup>Uncertainty was propagated through the expression in [3].

<sup>e</sup>Equivalent to the scatter in  $\log c_{\text{vir}}$  reported in previous studies.

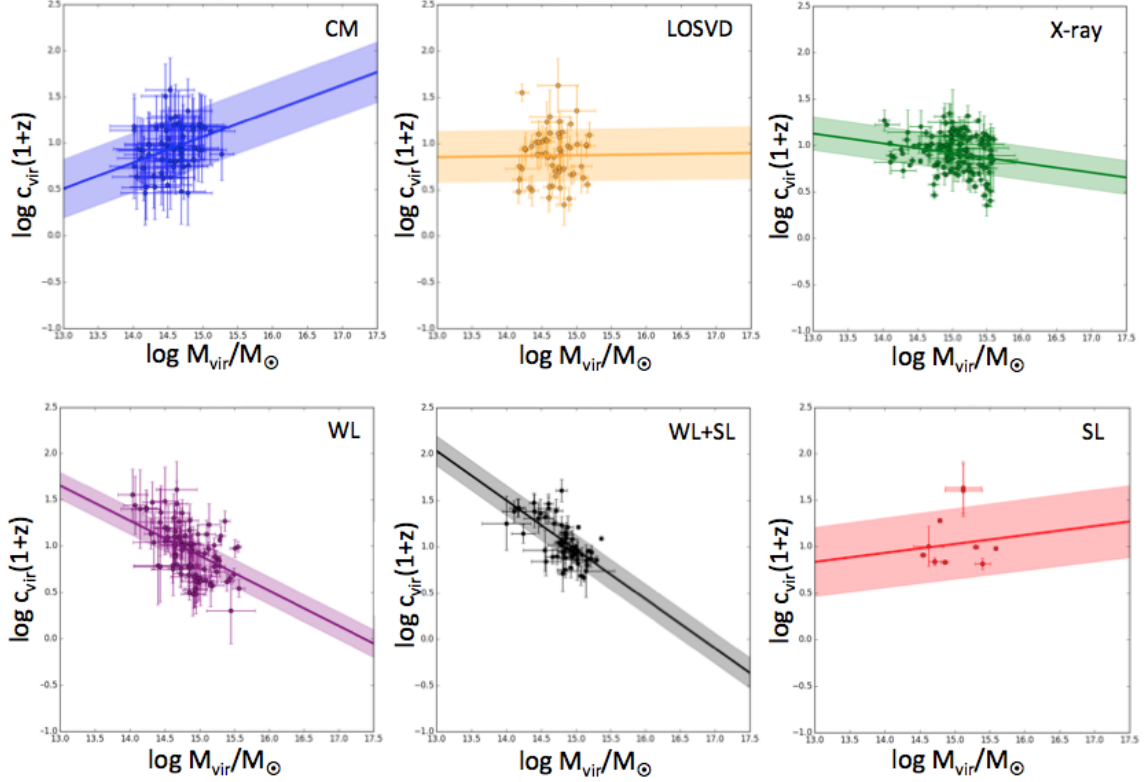


**Figure 3.4:** Upper left to lower right: Individual fits to CM, LOSVD, X-ray, WL, WL+SL, and SL. The shaded regions represent the  $1-\sigma$  uncertainty in the best-fit parameters, and includes the intrinsic scatter,  $\sigma_{\text{int}}$ . These relations are extrapolated over the full range of cluster masses for illustration purposes only.

We also compare our results to the c-M relation studied by CLASH, which use a combined weak and strong lensing technique for 19 X-ray selected galaxy clusters. The relation they fit,

$$c_{200} = A \left( \frac{1.37}{1+z} \right)^B \left( \frac{M_{200}}{8 \times 10^{14} h^{-1} M_{\odot}} \right)^C \quad (3.11)$$

with best-fit values of  $A = 3.66 \pm 0.16$ ,  $B = -0.14 \pm 0.52$ , and  $-0.32 \pm 0.18$ , agrees well with projected simulations, after accounting for the X-ray selection function. Figure 3.5 shows the comparison of the CLASH c-M relation to the the lensing relations, WL and WL+SL. Our relations are significantly steeper, and have higher normalizations<sup>2</sup>, though it should be noted that we do not account for the lensing selection function, which we would expect to lower both parameters.

<sup>2</sup>Due to the addition of a third model parameter, the CLASH normalization is not directly comparable to ours. However, visual inspection of Fig. 3.5 shows that their value is certainly lower than ours.

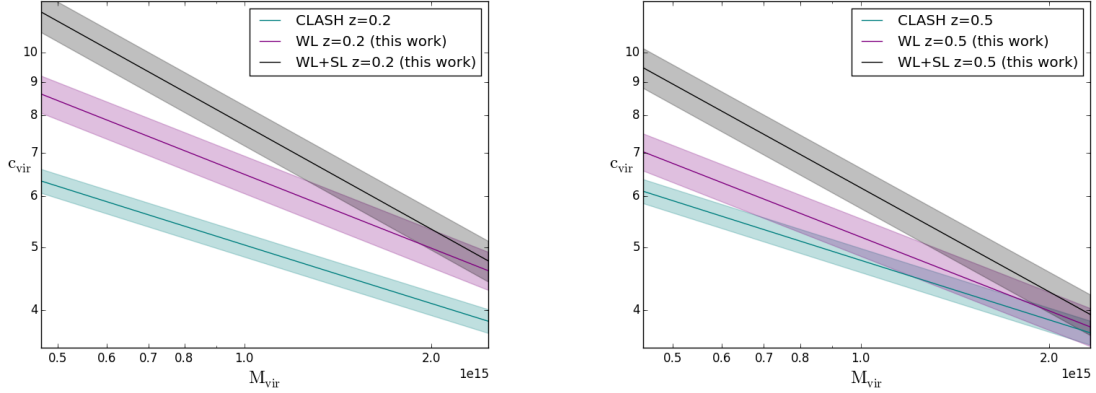


**Figure 3.5:** A direct comparison of the concentration-Mass relations for lensing based methods (WL and WL+SL) with results from CLASH (Merten et al., 2014). The left panel shows these relations at a redshift of  $z = 0.2$ , whereas the right panel is at a higher redshift  $z = 0.5$  (approximately the average redshift of WL and WL+SL measurements in our sample). Conversion from  $c_{200}$  to  $c_{\text{vir}}$  was necessary for comparison purposes.

### 3.5 Projection, Shape, And A Direct Comparison Of Reconstruction Techniques

When regarded as a single population of measurements, a linear fit to the full dataset of cluster mass and concentration pairs can be said to be, at face value, consistent with the results from simulations (albeit only marginally). In Figure 3.6, we show the best-fit linear model to the full dataset, with results from Groener & Goldberg (2014) (Chapter 2) plotted in pink. We also find very good agreement with Comerford & Natarajan (2007b), who find a best-fit model of  $c_{\text{vir}} = \frac{14.8 \pm 6.1}{(1+z)} (M_{\text{vir}}/M_*)^{-0.14 \pm 0.12}$ .

When the projection of triaxial halos is taken into account, simulations become more consistent with the lensing observations. Figure 3.7 compares WL and WL+SL relations to intrinsic halo concentrations (pink) and 2D concentrations due to line-of-sight projection (cyan) of MultiDark MDR1 simulation halos found previously in Groener & Goldberg (2014). While projected halos in this figure represent a perfectly elongated cluster sample, it is unlikely that *all* clusters with lensing analyses performed to date are oriented in this way. Thus, projected concentrations presented here can be interpreted as an upper limit, and constrains the ability of line-of-sight projection in easing

the tension between simulations and lensing observations. Bahé et al. (2012b) also confirm that mock weak lensing reconstructions of Millennium Simulation halos produce concentrations of upwards of a factor of 2 for line-of-sight orientation, congruent with our analytical treatment. However, this fails to completely account for the factor of  $\sim 3$  ( $\sim 4$ ) which we find for WL (WL+SL) clusters of mass  $\sim 10^{14} M_\odot$ .

In Figure 3.8 (*Left*), we compare our lensing relations to ones obtained through dissipative  $N$ -body simulations found in the literature. Median simulation relations are shown over the mass range defined by our lensing samples ( $1 \times 10^{14} - 3 \times 10^{15} M_\odot$ ), and are evaluated at a redshift corresponding to the average lensing redshift ( $z = 0.5$ ). The intrinsic scatter in concentration is not shown here, but is assumed to follow a log-normal distribution with a magnitude of  $\Delta(\log c_{\text{vir}}) \sim 0.18$  (Bullock et al., 2001a). The relation found by Prada et al. (2012b) shows the prominent upturn feature in concentration, while other relations are monotonically decreasing functions of mass. Simulation relations and ones obtained in this study stand in stark contrast with one another for lower mass clusters ( $\lesssim 1 \times 10^{14} M_\odot$ ), however, projection must be first be accounted for before any conclusions can be drawn. In the right panel, we compare analytical projections of simulation relations (using the method outlined in Groener & Goldberg 2014; see section 2.2) with WL and WL+SL relations. For the purposes of understanding the magnitude of this effect, halo shapes are assumed to be well-described by prolate spheroidal isodensities with axis ratios of  $q = 0.65$  (Jing & Suto, 2002c), with major axes in the line-of-sight direction. Increased scatter in projected relations are expected to be caused by the actual distributions of shapes and orientations (which we do not account for here). Direct statistical comparisons of these relations is non-trivial, due to the differences in relation models. However, the projection of triaxial halos was thought to be a sufficient explanation for fully describing the existence of differing observed and simulated cluster concentrations. It is clear that it is unlikely to be the sole contributing factor.

We also observe that the concentration-mass relation for combined WL+SL is steeper than WL alone (though both relations are consistent at the  $1-\sigma$  level). Cluster halo isodensities which are more prolate in the inner regions can produce larger projected concentrations for line-of-sight halos,

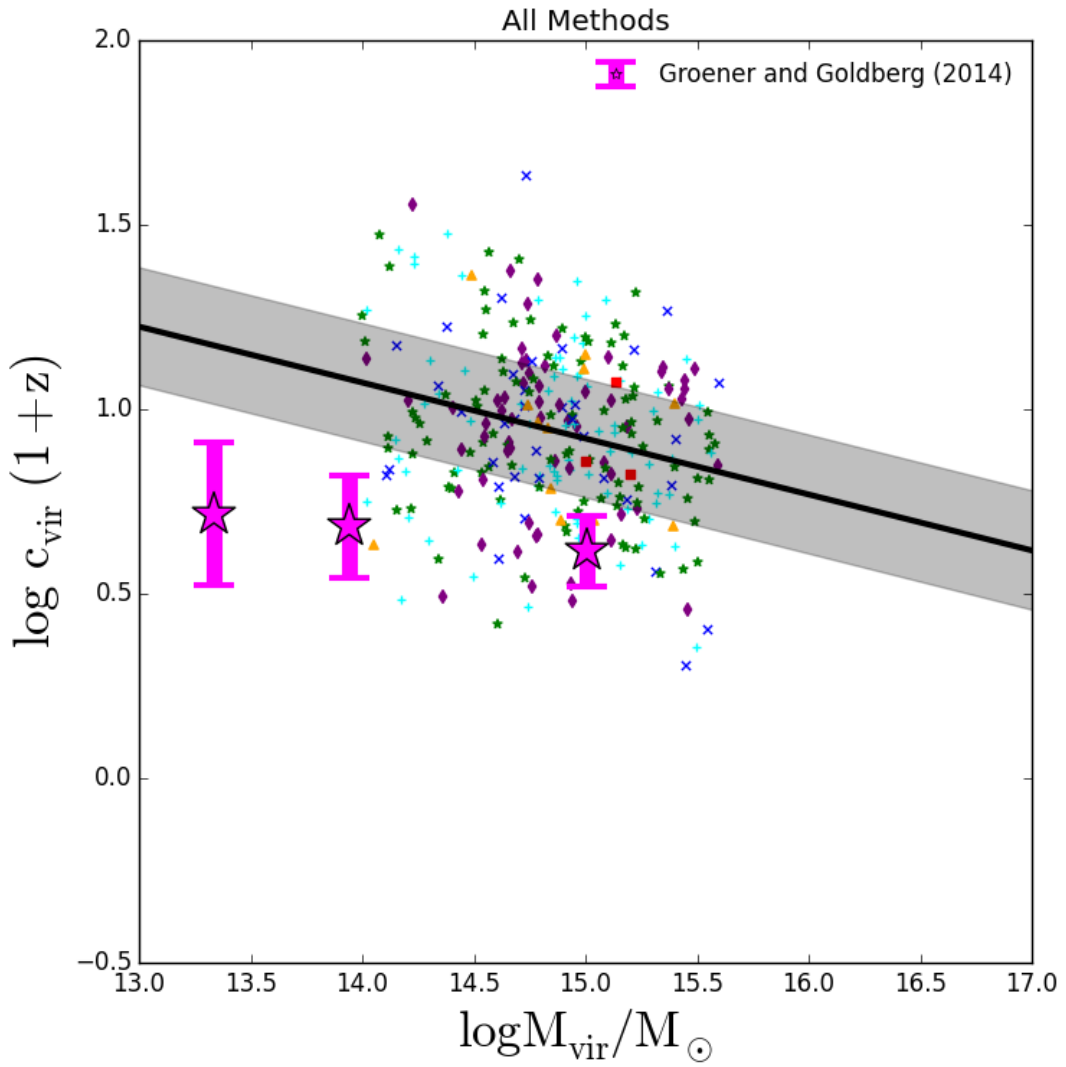


**Figure 3.6:** The concentration-mass relation (black line) with 1-sigma uncertainty region (grey shaded) observed for the full cluster dataset. Color scheme is the same, though cyan data points represent co-added cluster measurements where more than one category of reconstruction method was used. Errorbars have been omitted here for clarity.

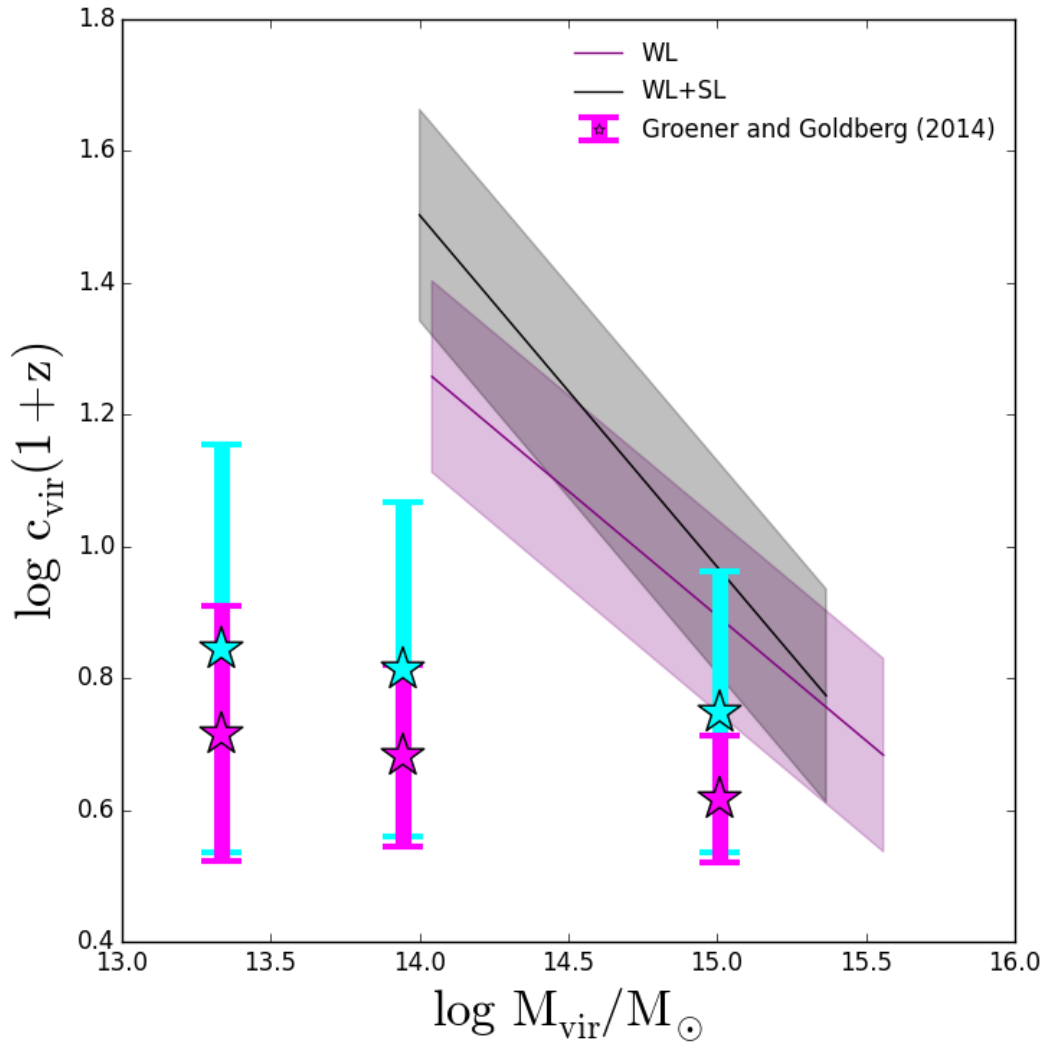


**Figure 3.7:** WL and WL+SL relations plotted with MultiDark MDR1 Simulation results found by Groener & Goldberg (2014). Pink data points represent intrinsic 3D concentrations found in three mass bins, and cyan data points are corresponding 2D concentrations due to the projection of line-of-sight oriented halos.

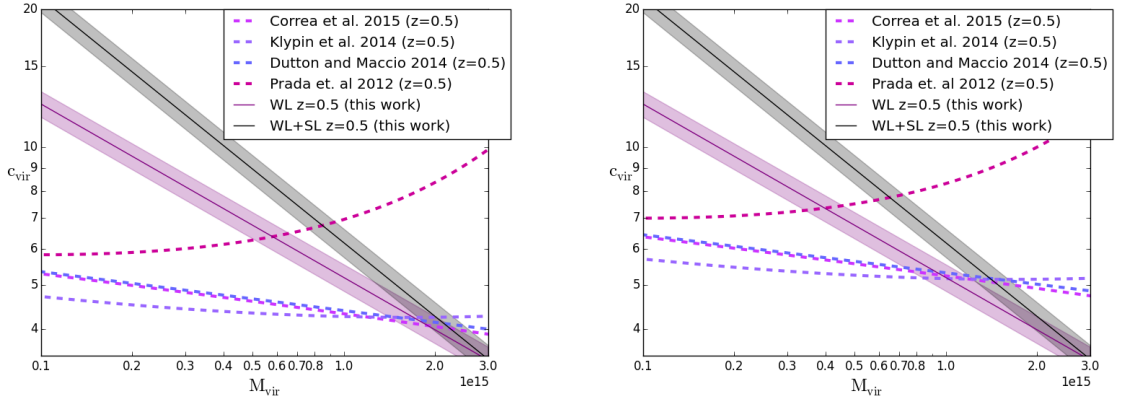


**Figure 3.8:** *Left:* Concentration-mass relations from recent simulations (Prada et al. 2012b, Dutton & Macciò 2014, Klypin et al. 2014, and Correa et al. 2015a), along with lensing (WL and WL+SL) relations found in this study. All relations are evaluated at a redshift of  $z = 0.5$ . *Right:* Simulation relations after projection effects have been taken into account. Halos are assumed to be prolate spheroidal ( $q=0.65$ ), oriented along the line-of-sight direction.

and thus any method which makes use of information on this scale may stand to be biased high because of it. We find that the sign of this difference is in the right direction for this effect, and we cannot rule out shape as one of the underlying causes.

Though we do not possess a complete volume-limited sample of galaxy clusters for which all measurement methods have been performed, we can begin to understand any systematic effects present in clusters with concentrations and masses present for various combinations. In Figures 3.9–3.11, we show clusters whose profiles have been estimated using the following pairwise combinations of methods: i) WL and WL+SL, ii) X-ray and WL, and iii) CM and LOSVD. We do not detect any discernable trend in the way concentrations or masses are overestimated or underestimated in each comparison, however, we show the magnitude of the potential discrepancy. WL and WL+SL mass measurements are generally in very good agreement with one another (with a few notable exceptions), however, differences in concentration do exist which are upwards of a factor of  $\sim 2$  in magnitude. X-ray and WL comparisons show discrepancies in mass (concentration) which can reach as high as a factor of  $\sim 9$  times ( $\sim 6$  times) larger, with X-ray mass estimates tending to be larger than WL. Galaxy-based reconstruction techniques (LOSVD/CM) tend to agree less in both mass

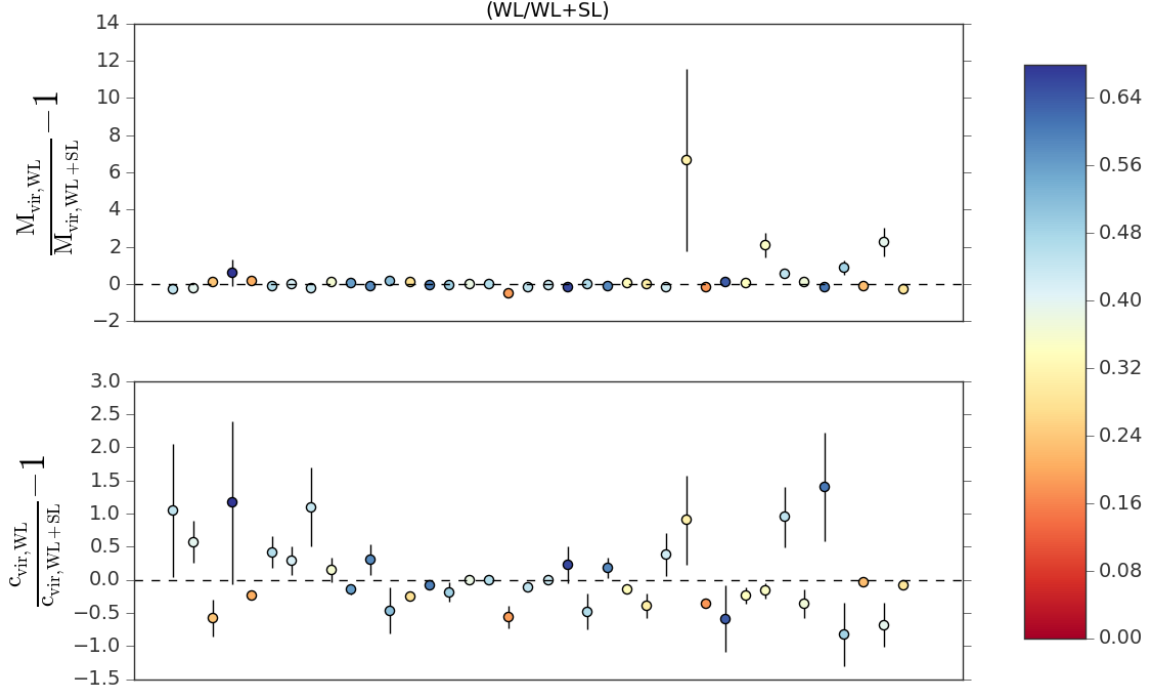


**Figure 3.9:** Comparisons of concentrations and masses for clusters measured using both WL and WL+SL methods. The color of the scatter point indicates redshift.

and concentration, with uncertainties which are quite large.

### 3.6 Conclusions And Discussions

In this chapter, we have studied the observed concentration-mass relation using all known cluster measurements to date. We also model individual relations for the most commonly used reconstruction techniques. In the present section, we discuss our results of this study.

- There is an inconsistency between lensing (WL and WL+SL) concentrations and theoretical expectations from simulations. Low to medium mass lensing measurements ( $\sim 10^{14} M_\odot$ ) are inconsistent with simulation results, even when projection is taken into account. It is very likely the case that some of this difference can be generated by the existence of a strong orientation bias in the lensing cluster population, however, the magnitude of this effect (quantified by previous studies) cannot completely explain the difference we observe here.
- We find that the concentration-mass relation from strong lensing clusters remains virtually

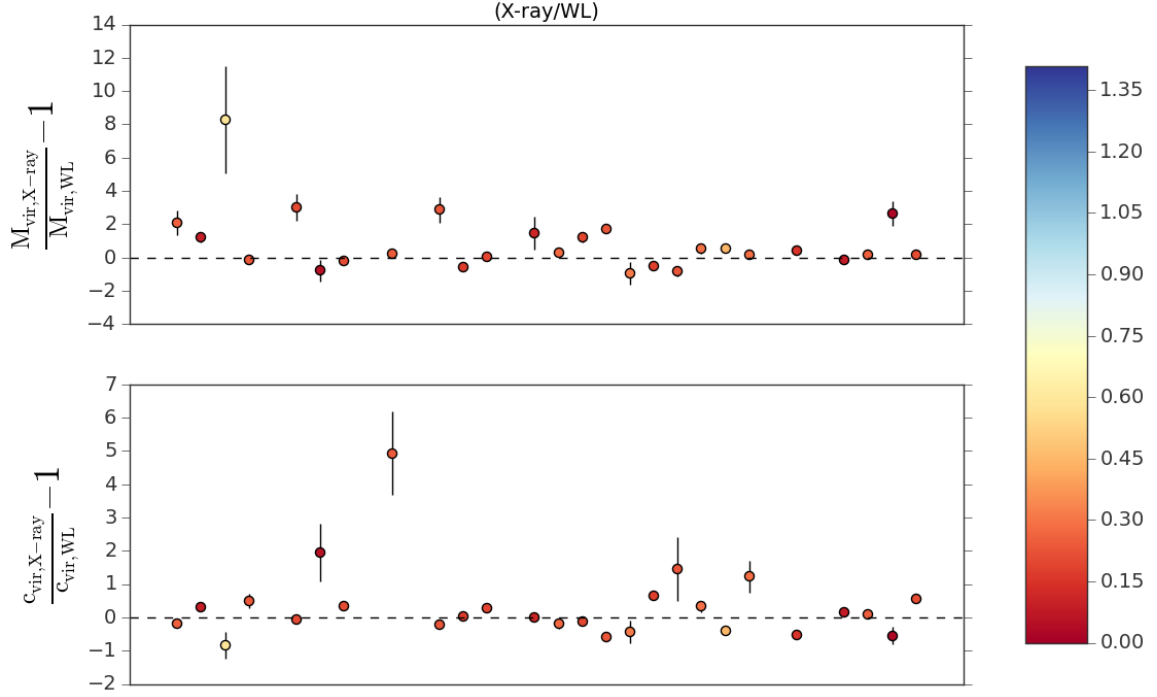


**Figure 3.10:** Comparisons of concentrations and masses for clusters measured using both X-ray and WL methods. The color of the scatter point indicates redshift.

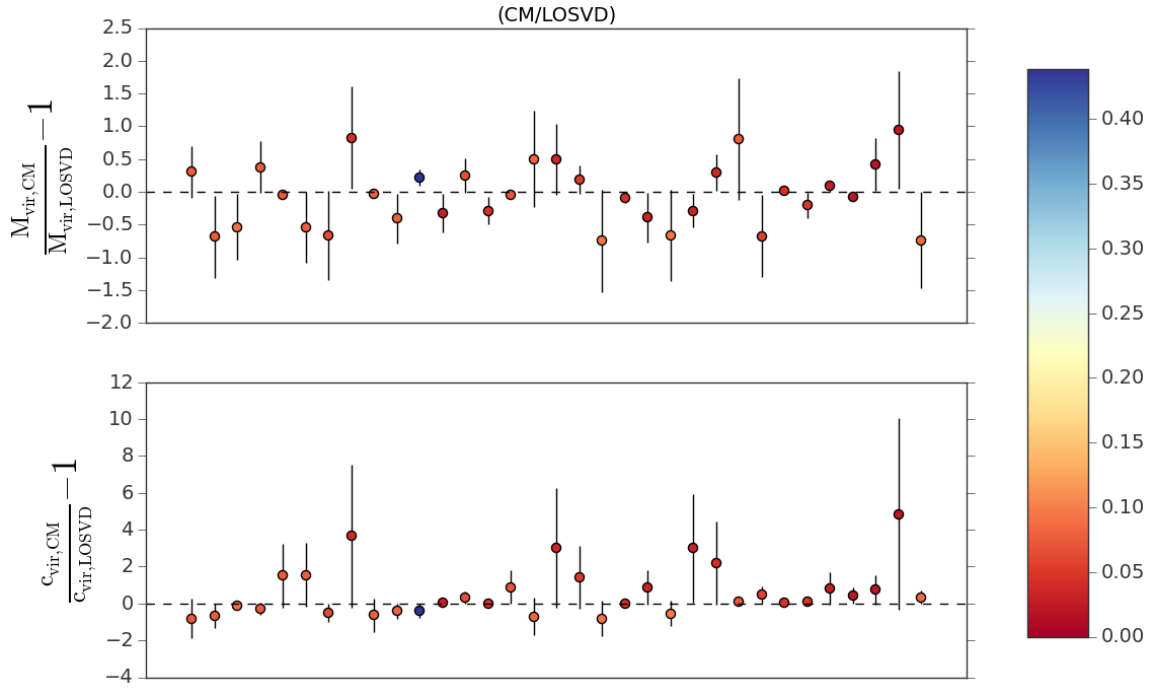


**Figure 3.11:** Comparisons of concentrations and masses for clusters measured using both CM and LOSVD methods. The color of the scatter point indicates redshift.

unconstrained, due to the small size of the sample, as well as the insensitivity of SL reconstructions to the outer region of clusters.

- The slope of the WL+SL relation is found to be higher (though still consistent) with WL alone over the lower half of the mass range, and may point to the existence of a new physical feature of clusters. However, when we only look at clusters with *both* measurements, we find no evidence that concentrations generated by WL+SL methods are in excess of WL. Most likely, this tells us that the selection effects for WL+SL is most likely the cause of this difference. Moreover, the intrinsic scatter of the concentration parameter on all mass scales is observed to be larger than the proposed difference in projected concentration due to shape, making this effect difficult to measure.
- Lensing (WL and WL+SL) concentrations are systematically higher than those made with X-ray methods. In the mass range of  $\sim (1 - 3) \times 10^{14} M_{\odot}$ , the WL+SL relation is marginally inconsistent with X-ray measurements. Reasons for a flatter X-ray relation as compared lensing methods are numerous. The gas distribution is rounder than the dark matter mass distribution, causing projection effects to be less severe for X-ray samples. X-ray masses are also biased low due to temperature and hydrostatic equilibrium biases. For the same nominal value of the mass ( $M_{WL} = M_X$ ), X-ray clusters are more massive than the WL sample. Because lower concentrations correlate with larger masses, these lower values are assigned to lower masses, causing a bias toward flatness. Lastly, at very high masses, selection effects are less critical to the c-M relation, since all high massive clusters are likely to pass observational thresholds, and thus are included in samples.
- Out of all reconstruction methods, we also find that lensing (WL and WL+SL) relations are the *most* inconsistent with a power-law index of zero.
- Methods which depend upon using galaxies as tracers of the mass show a neutral (LOSVD) or positive (CM) correlation between concentration and mass. The sensitivity of the slope of the caustic method c-M relation to the uncertainties is minimal. Disregarding uncertain-

ties in either mass or concentration, we find a best fit slope and intercept of  $m = 0.207$  and  $b = -2.103$ .

- We find the c-M relation of our X-ray sample to be consistent with results from DM only simulations, though with a higher normalization, and slightly higher slope. However, direct comparison of these results with simulations which include baryons, feedback, and star formation is necessary. Rasia et al. (2013) performed such a study, and found that the dependence of the c-M relation on the radial range used to derive the relation, the baryonic physics included in simulations, and the selection of clusters based on X-ray luminosity all work to alleviate tensions between simulations and observations which existed previously. Though, they also find that including AGN feedback brings the relation more in line with DM only simulations, and it remains unclear whether or not all tensions between these relations have been identified and accounted for.

One potential source of error in the inference of the slope of the c-M relation which we do not account for in this study is the covariance of the mass and concentration measurements themselves (Sereno et al., 2015b). Auger et al. (2013) discovered they were unable to constrain the slope of the c-M relation of a sample of 26 strongly-lensed clusters with richness information, due to the intrinsic covariance of their mass and concentration estimates, in addition to a limited dynamic range of halo masses. Furthermore, improper modeling of the distribution of halo masses can also significantly alter the inferred relation (i.e. - it is sensitive to the prior).

Selection effects can strongly steepen the slope of the c-M relation, especially for lensing clusters (Merten et al., 2014; Meneghetti et al., 2014). The slopes of relations for clusters from CLASH, LOCUSS, SGAS, and a high redshift sample (also included in this study), were all found to be much steeper than that of the relation characterizing dark-matter only clusters (Sereno et al., 2015b). For fixed mass, the most highly concentrated clusters are most likely to show SL features, and thus are most likely to be included in SL selected samples (Oguri & Blandford, 2009b). In all cases, the selection process of clusters tend to prefer over-concentrated halos, and depends strongly on observational selection thresholds (Einstein radius, X-ray luminosity, morphology, etc.).

Another consideration is the mis-modeling of the halo profile. Recently,  $N$ -body simulations have shown that Einasto profiles provide an even more accurate representation of the density profiles of dark matter halos compared to the NFW profile (Dutton & Macciò, 2014; Klypin et al., 2014; Meneghetti et al., 2014). Sereno et al. (2015a) find that WL masses and concentrations for very massive structures ( $\gtrsim 10^{15}h^{-1}M_{\odot}$ ) can be overestimated and underestimated, respectively, by about  $\sim 10\%$ , if an NFW model is incorrectly assumed. Though this does not fix the mismatch in the concentration parameter we have discussed here, it could perhaps artificially steepen the overall slope of the relation by reducing the concentrations of the most massive clusters.

Another plausible explanation for the existence of this new over-concentration discrepancy for clusters is that dark matter only simulations lack important cluster physics which is present in real clusters. Feedback from AGN and supernovae, and gas cooling are mechanisms which may cause (or prevent) further concentration of dark matter within the cores of clusters, and have a strong effect on their lensing efficiency (Puchwein et al., 2005b; Wambsganss et al., 2008b; Rozo et al., 2008b). Mead et al. (2010b) find that strong lensing cross-sections for high mass clusters are boosted by up to 2-3 times, when including gas cooling with star formation in simulations. Furthermore, they find that by adding AGN feedback into the mix, this cross-section (and also the concentration parameter) decreases, as energy is injected back into the baryonic component.

There is a strong need to obtain low-mass ( $< 1 \times 10^{14}M_{\odot}$ ) lensing measurements, since our most contentious conclusion is that, if the relation we have found holds in the galaxy group region, we expect cluster concentrations to be even less consistent with theory than they already are. Clearly this trend cannot continue indefinitely, but it remains to be seen how this model breaks down. An ideal study would contain a large, complete, and volume-limited sample of clusters, which can be studied in each reconstruction method. In this way, we could hope to eliminate the dependence of the selection function of clusters on the concentration-mass relation we would measure. Lastly, since selection effects are quite difficult to model, it is worth extending this study to as large of a sample as possible. Heterogeneous datasets (such as the one compiled in this study) have the ability to compensate for selection biases (Gott et al., 2001; Piffaretti et al., 2011; Sereno & Ettori, 2015).

## Chapter 4: The Impact of the Large Scale Environment Upon Cluster Observables

### 4.1 Introduction

Galaxy cluster halos are prolate spheroidal in shape, with major axes oriented along large scale structures (Colberg et al., 2005; Kasun & Evrard, 2005b; Basilakos et al., 2006; Allgood et al., 2006b; Altay et al., 2006; Aragon-Calvo et al., 2007; Bett et al., 2007b; Zhang et al., 2009; Paz et al., 2011). Through the study of cosmological simulations, this connection between clusters and their environment is largely caused by the redirection of the dark matter halo axes along the direction of the last major merger event (van Haarlem & van de Weygaert, 1993; Splinter et al., 1997).

It has also been well-established that cluster properties, like mass and concentration, are highly sensitive to projection of non-spherical distributions of mass, particularly for the various flavors of gravitational lensing (Comerford & Natarajan, 2007a; Sereno et al., 2010a). This effect has also been shown to be important in X-ray reconstructions (Buote et al., 2007; Schmidt & Allen, 2007; Ettori et al., 2011), as well as the caustic method (Svensmark et al., 2015). Reconstructing the 3-dimensional mass distribution within the cluster is currently a highly degenerate procedure, in that an infinite number of distributions may lead to the same mass map projected on the sky. Consequently, it becomes incredibly important to look for other clues which may help us assign likelihood to the orientation and shape of the cluster halos in 3-dimensional space.

Using galaxies as tracers of the large-scale structure (by means of redshift surveys), the cluster environment can be fully mapped out in 3-dimensions and studied alongside their 2-dimensional radial density profile properties. Since galaxy clusters are expected to point along filaments, a strong correlation between the orientation of the filament and the values of the concentration and mass *should* exist. For an environment consistent with line-of-sight structure, we expect to see higher cluster concentration and mass measurements.

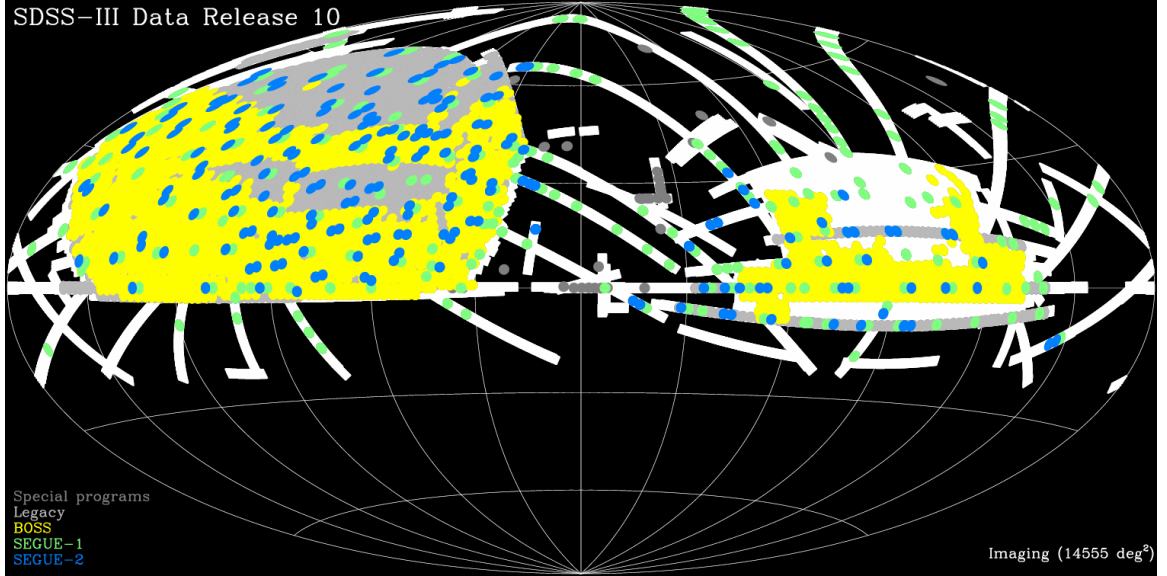


**Figure 4.1:** Image: [www.sdss3.org](http://www.sdss3.org). The SDSS DR10 survey footprint. In total, there are 1,848,851 spectroscopically confirmed galaxies within the dataset, out to a redshift of approximately  $z \approx 1$ .

## 4.2 Data

In order to study the relationship between cluster observables and the surrounding large scale structure, we require overlapping cluster and galaxy datasets. We use the locations of spectroscopically confirmed galaxies from Sloan Digital Sky Survey (SDSS) Data Release 10 (Fig 4.1) to trace out the large scale structure. In total, the survey covers 14,555 square degrees of the sky, with a magnitude limit of around 22. From this data release, we obtain the spectroscopic redshift, right ascension, and declination measurements of just under 1.4 million galaxies within an area on the sky defined by the following right ascension and declination bounds:  $100^\circ \leq \alpha \leq 270^\circ$  and  $-10^\circ \leq \delta \leq 70^\circ$  (Fig 4.2).

Cluster concentration and mass measurements, redshifts, and their locations on the sky, are taken from Chapter 3. It should be noted that these measurements have been normalized over overdensity convention, cosmology, and uncertainty convention (see Section 3.3.1). Starting with 361 unique clusters, a sub-sample of 203 is selected, based upon the constraint that they must exist within the SDSS survey volume outlined above.

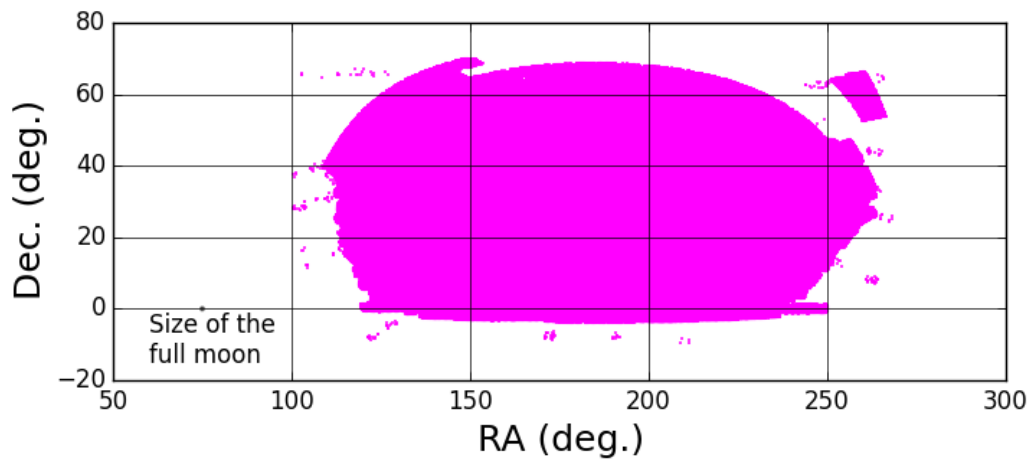


**Figure 4.2:** The subset of SDSS galaxies we use for our study have been selected between RA  $100^\circ \leq \alpha \leq 270^\circ$ , and a declination of  $-10^\circ \leq \delta \leq 70^\circ$ .

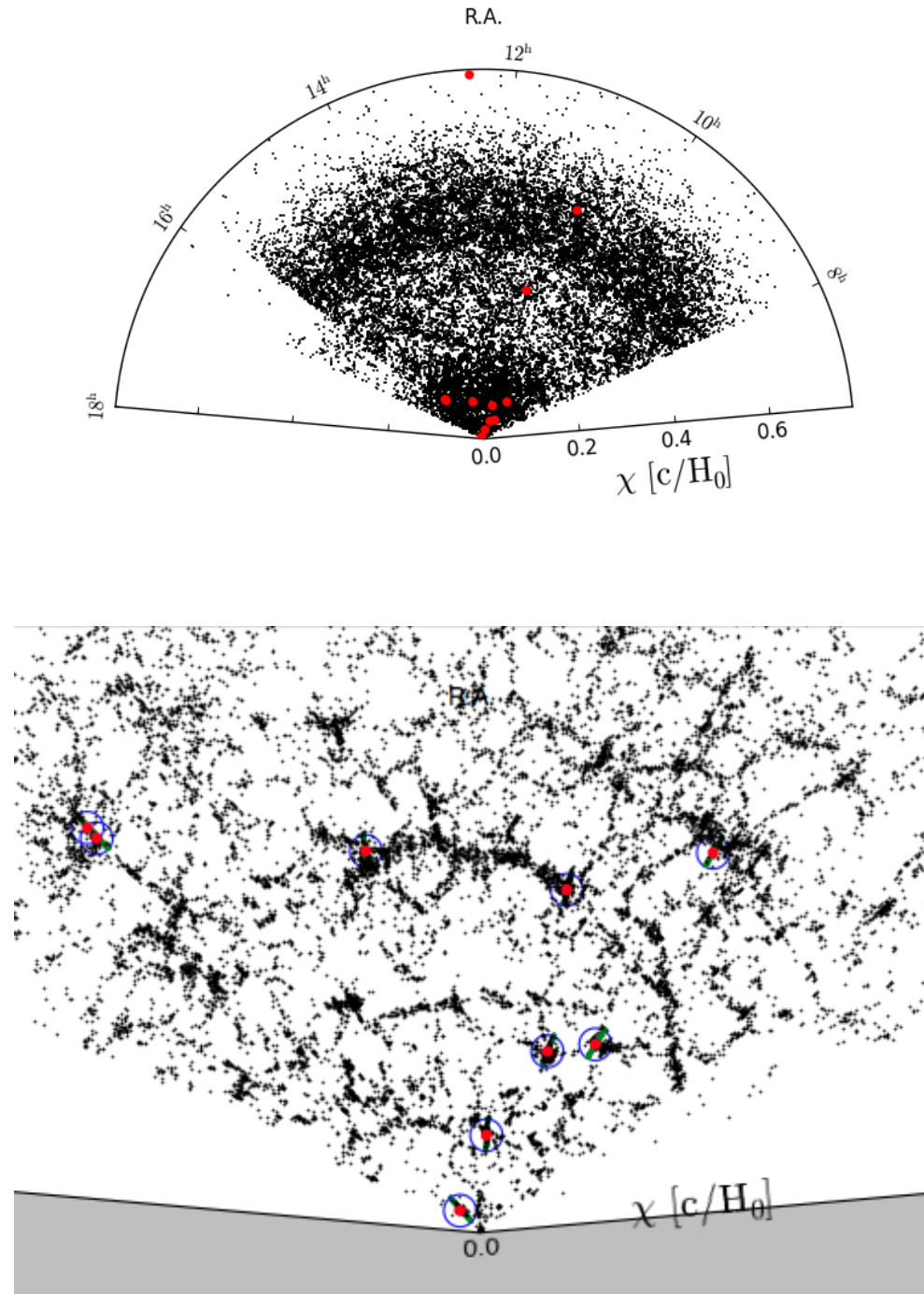


**Figure 4.3:** *Top:* A 2 degree slice in declination of the SDSS galaxy population (black), with clusters (red) obtained from [CITE GR15.1]. The observer is located at the origin. *Bottom:* A blown-up version of the top panel, showing the filamentary-like structure of the universe. Blue circles give scale ( $10h^{-1}$  Mpc), and green bars show the line-of-sight direction at the location of each cluster.

### 4.3 Obtaining Large-Scale Structure Around Clusters

Isolating SDSS galaxies around each cluster becomes our first major step in determining the effects of the large-scale environment upon cluster measurements. Since cluster alignment is said to correlate with the direction of filaments on scales up to  $30h^{-1}$  Mpc, we select an outer radius of  $10h^{-1}$  Mpc, which is nearly an order of magnitude larger than the outer radii of typical clusters,  $\sim 1.5h^{-1}$  Mpc (Fig. 4.3).

To keep the volume roughly the same around clusters at all redshifts, we use the following condition for the association of galaxies to a given cluster. Firstly, the spherical coordinates of the  $i^{\text{th}}$  cluster are:

$$\vec{r}_i = \langle \chi_i, \alpha_i, \delta_i \rangle \quad (4.1)$$

where  $\chi_i$  is the comoving distance to the  $i^{\text{th}}$  cluster at redshift  $z_i$

$$\chi_i = \frac{c}{H_0} \int_0^{z_i} \frac{dz}{\sqrt{\Omega_{m,0}(1+z)^3 + \Omega_\Lambda}} \quad (4.2)$$

with the Hubble distance being  $c/H_0 = 3000h^{-1}$  Mpc, and where  $\alpha_i$  and  $\delta_i$  represent the right ascension and declination of the cluster (in radians).

We then calculate the coordinates of every SDSS galaxy in the sample by placing the  $i^{\text{th}}$  cluster at the origin of a new spherical coordinate system. For the  $j^{\text{th}}$  galaxy, these coordinates would look like:

$$\vec{r}_{ij} = \langle x_{ij}^1, x_{ij}^2, x_{ij}^3 \rangle \quad (4.3)$$

where

$$x_{ij}^1 = \chi_j - \chi_i \quad (4.4a)$$

$$x_{ij}^2 = (\alpha_j - \alpha_i) \cos \delta_i D_{A,i} \quad (4.4b)$$

$$x^3_{ij} = (\delta_j - \delta_i) D_{A,i} \quad (4.4c)$$

A new distance measure is introduced here, the angular diameter distance,  $D_A$ , which is defined in terms of the comoving distance,  $\chi$ .

$$D_A = \frac{\chi}{1+z} \quad (4.5)$$

Selecting galaxies within a radius of  $R = 10h^{-1}$  Mpc becomes a straightforward condition to check:

$$(x^1_{ij})^2 + (x^2_{ij})^2 + (x^3_{ij})^2 \leq R^2 \quad (4.6)$$

As an example of this procedure, Figure 4.4 shows SDSS galaxies selected around the cluster Abell 1238.

Lastly, we enforce a threshold of  $N_{\text{gal}} \geq 100$  in order to ensure that only clusters with a sufficiently dense tracing of its environment are used for further study. This cuts our sample from 203 unique clusters down to 92.

### 4.3.1 Quantifying Structure

We are looking to understand if line-of-sight large-scale structure has an impact on cluster concentration and mass measurements. Our first attempt at quantifying the structures we find around clusters is to focus on the distributions of azimuthal ( $\theta$ ) and polar ( $\phi$ ) angles.

$$\theta = \tan^{-1} \left( \frac{y}{x} \right) \quad (4.7a)$$

$$\phi = \cos^{-1} \left( \frac{z}{r} \right) \quad (4.7b)$$

where we define  $\{x \equiv x^2, y \equiv x^3, z \equiv x^1\}$ , and where  $r = \sqrt{(x^1)^2 + (x^2)^2 + (x^3)^2}$ .

From these angles, we can make use of spherical harmonic functions, which are commonly used special functions defined on the surface of a sphere. Due to their orthogonal nature, any arbitrary

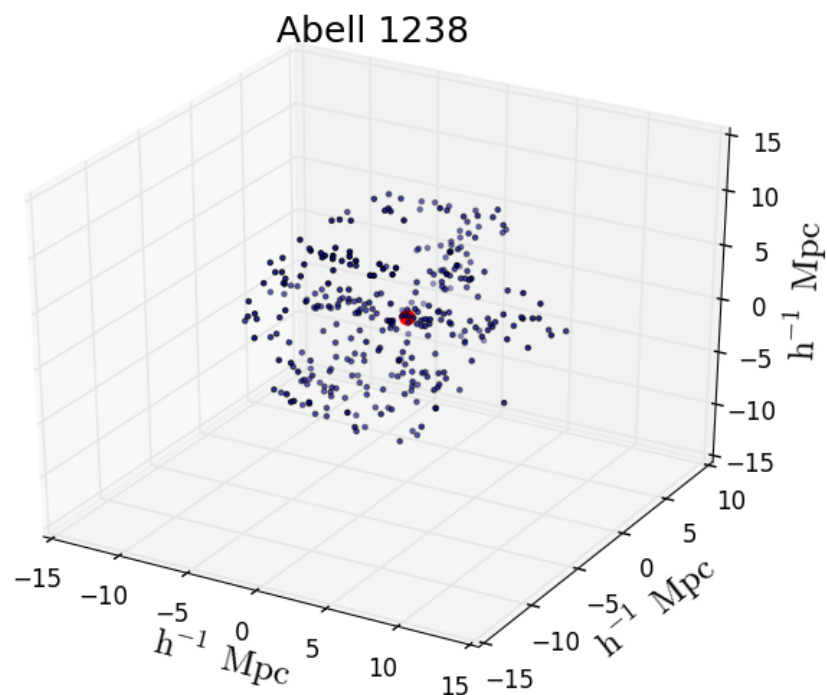


**Figure 4.4:** Shown here are the 322 spectroscopically confirmed SDSS galaxies (black scatter points) around the galaxy cluster Abell 1238 (red), located at a redshift of  $z = 0.0733$ .

angular function can be expressed as a linear combination of spherical harmonics.

$$f(\theta, \phi) = \sum_{l=0}^{\infty} \sum_{m=0}^l A_l^m Y_l^m(\theta, \phi) \quad (4.8)$$

Spherical harmonics are defined by a set of integers,  $l$  and  $m$  ( $m = -l, \dots, l$ ), roughly corresponding to the shape of the function and the orientation of the function, respectively.

The coefficients of this series can then generally be computed as follows:

$$A_l^m = \int_0^{2\pi} \int_0^\pi f(\theta, \phi) \tilde{Y}_l^m(\theta, \phi) \sin \theta d\theta d\phi \quad (4.9)$$

where  $\tilde{Y}_l^m(\theta, \phi)$  is the complex conjugate of the spherical harmonic function,  $Y_l^m(\theta, \phi)$ .

However, in our case, the function  $f(\theta, \phi)$  is discrete rather than continuous, leading us to compute coefficients in the following way:

$$A_l^m = \frac{4\pi}{N} \sum_{i=1}^{N_{\text{gal}}} \tilde{Y}_l^m(\theta_i, \phi_i) \quad (4.10)$$

Since we expect roughly triaxial or filamentary-like large-scale structure, we pay specific attention to the modes  $\{l = 1, m = -1, 0, 1\}$ .

$$Y_1^1 = -\sqrt{\frac{3}{8\pi}} \sin \theta e^{i\phi} \quad (4.11a)$$

$$Y_1^0 = \sqrt{\frac{3}{4\pi}} \cos \theta \quad (4.11b)$$

$$Y_1^{-1} = \sqrt{\frac{3}{8\pi}} \sin \theta e^{-i\phi} \quad (4.11c)$$

These spherical harmonics give us an idea about the elongation of structure along the primary axes. Most importantly is the value of  $A_1^0$  (line-of-sight direction,  $z$ ) relative to  $A_1^1$  and  $A_1^{-1}$  (in  $x$ -

and  $y$ -directions, respectively). From these coefficients, the statistic we compute is:

$$\frac{A_1^0}{\sqrt{A_1^{02} + A_1^{02}}} \quad (4.12)$$

#### 4.4 Results And Future Work

In this section, we present the results of our correlation tests between the line-of-sight statistic (4.12), with cluster mass  $M_{\text{vir}}$  (Figure 4.5), concentration  $c_{\text{vir}}$  (Figure 4.6), and the redshift-scaled concentration  $c_{\text{vir}}(1+z)$  (Figure 4.7). In all cases, we find no discernable correlation between cluster observables and line-of-sight orientation of its surrounding environment on scales of up to  $10h^{-1}\text{Mpc}$ . In each figure, we also highlight clusters which contain measurements which were made with weak lensing.

With a sample size of 92 clusters, it is difficult for us to completely reject the idea that angular information about galaxies around clusters (out to sufficient distances) *can* tell us about the true inclination of clusters with respect to the line-of-sight. Keeping this in mind, characterizing the large-scale galaxy distribution is made in a number of ways, many of which we have not yet attempted with our sample. Including radial information may prove useful, however, we would truly benefit the most by having a much larger cluster sample (for instance, the maxBCG sample Koester et al. 2007, which contains 13,823 galaxies found within SDSS).

The breakdown by method of cluster concentrations and masses measured for our 92 clusters are the following (remembering that some clusters are measured multiple times):

- LOSVD: 34
- CM: 62
- X-ray: 33
- WL: 5

Redshift-based distance measurements of galaxies are sensitive to two general effects, arising from their peculiar velocities (additional motion which is not defined by the Hubble flow). The first

effect is called the “finger of God” effect, whereby distances to galaxies are over-estimated (under-estimated) due to their radial motion away from (toward) the observer while orbiting within the cluster. This effect becomes important once typical peculiar velocities for galaxies around clusters ( $v_{\text{pec}} \approx 300 \text{ km/s}$ ) are comparable to their recession speed due to the expansion of the universe ( $v_{\text{exp}} = cz$  for relatively low redshifts). Nearby clusters suffer an elongation of their structure along the direction of observation. A much smaller effect than the “finger of God” effect, entitled the Kaiser effect, is caused by the coherent motions of galaxies as they fall toward clusters as they assemble. Instead of an elongation along the line-of-sight, structures are flattened perpendicular to this direction, creating pancake-like structures. Their combined effects are seen in the correlation function of galaxies in surveys like the two degree field galaxy redshift survey (2dFGRS) (Hawkins et al., 2003). Redshift space distortions become important once the distributions around clusters are quantified in any way. Careful subtraction of cluster members is therefore the only way to mitigate these effects upon our final result. In order to do this however, we require catalogs of cluster members.

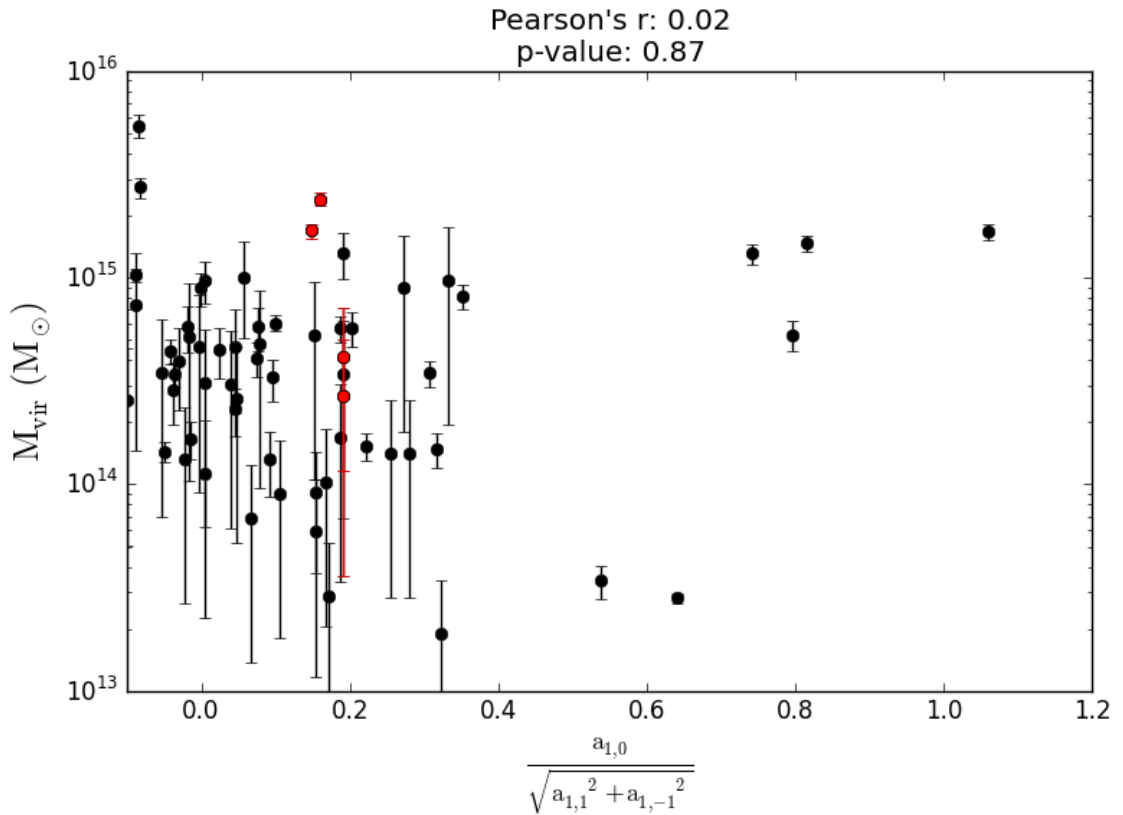


**Figure 4.5:** The correlation between the total cluster halo mass,  $M_{\text{vir}}$ , and the measure of line-of-sight orientation of environmental structure using the spherical harmonic coefficients,  $A_l^m$ . Larger values indicate more line-of-sight structure relative to perpendicular structure. Red points indicate clusters which make use of weak lensing (WL) measurements.

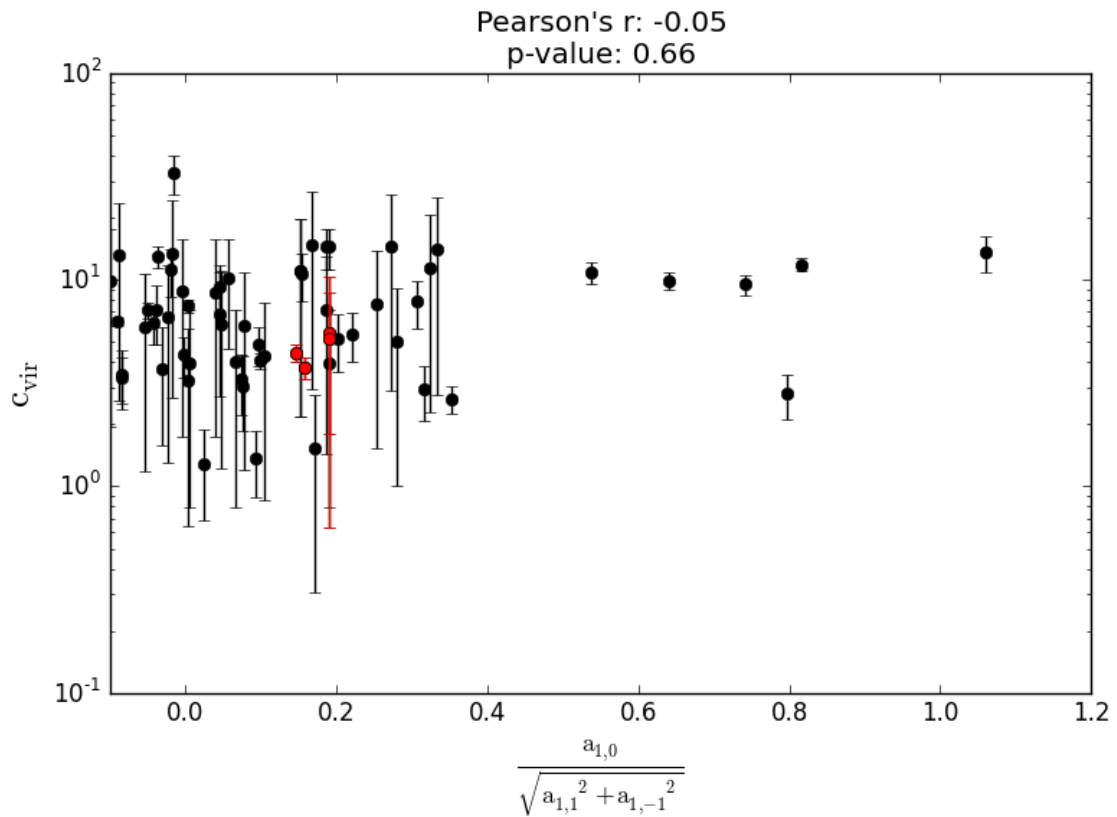


**Figure 4.6:** The correlation between the cluster concentration,  $c_{\text{vir}}$ , and the measure of line-of-sight orientation of environmental structure using the spherical harmonic coefficients,  $A_l^m$ . Larger values indicate more line-of-sight structure relative to perpendicular structure. Red points indicate clusters which make use of weak lensing (WL) measurements.

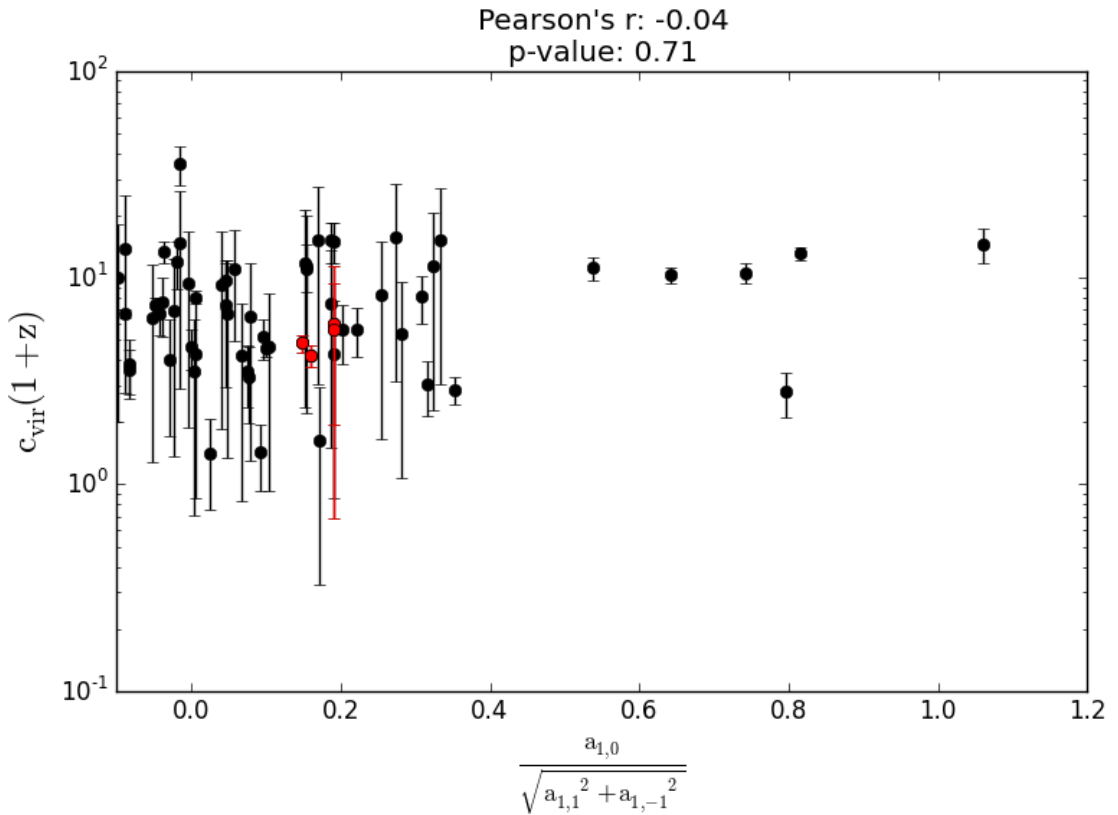


**Figure 4.7:** The correlation between the redshift-scaled cluster concentration,  $c_{\text{vir}}(1+z)$ , and the measure of line-of-sight orientation of environmental structure using the spherical harmonic coefficients,  $A_1^m$ . Larger values indicate more line-of-sight structure relative to perpendicular structure. Red points indicate clusters which make use of weak lensing (WL) measurements.

## Chapter 5: Conclusions

The internal distribution of mass within galaxy clusters is a crucial test of physics on the largest scales in the universe. Maps of clusters can be made in numerous ways, however, direct comparison becomes hard to make for a few reasons. Methods which depend upon galaxies to trace the mass (e.g. - the caustic method, and line-of-sight velocity dispersion), gravitational lensing (weak, strong, and weak+strong), and methods which relate the hot X-ray emitting gas to the total mass of the cluster, each come with their own set of assumptions, and probe varying masses, orientations, and concentrations from the cosmic population.

Furthermore, the relationship between the cluster concentration and mass (profile properties which the aforementioned techniques aim to measure), has been observed to be significantly different between large-scale, dissipationless  $N$ -body simulations and observations. This problem has been dubbed, “The over-concentration problem”, and is the primary motivation for the work we have done.

By studying galaxy clusters forming in the MultiDark MDR1 cosmological simulation (Chapter 2), we are able to observe their intrinsic 3-dimensional density profiles. This vantage point is not currently available observationally. We find that dynamically relaxed clusters are generally well-fit by the universal NFW profile, with co-aligned isodensities. However, upon projection along the line-of-sight direction, we find that the concentration becomes an aperture-based quantity, caused by one very important feature of clusters. Cluster isodensities, while remaining largely coaxial with one another, are not the same shape on all radial scales throughout the halo. This difference in shape can cause an upward bias of  $\sim 20\%$  in 2-dimensional concentrations on strong lensing scales ( $\sim 0.5 \cdot r_{200}$ ) as compared to weak lensing scales ( $\sim r_{200}$ ), when halos are viewed along their major axes. This rise in galaxy cluster axis ratios is something studies do not currently account for, and has the potential to cause systematic biases within the concentration-mass relations generated by different observational reconstruction techniques.

Motivated by this prediction, we then look for this novel characteristic difference in the concentration-mass relations of a sample of observational measurements in Chapter 3. We collect all known concentration and mass measurements from the literature, for which we quantify the c-M relation for each of six common reconstruction techniques (X-ray, WL, SL, WL+SL, CM, and LOSVD; see section 3.2). Though we cannot constrain the relation for strong lensing clusters (due to a lack of data), we do indeed find a somewhat steeper slope for WL+SL than we do for WL alone. However, observational relations are subject to an additional potential bias as compared to ones generated by simulations. Specific instruments or reconstruction techniques carry with them observational thresholds (e.g. - X-ray luminosity,  $L_X$ ). This means that a steeper WL+SL relation cannot necessarily be attributed to a changing of cluster shape with radius. The requirement for one to see strong lensing features around a cluster is a fairly strong selection effect, since chance alignment of background galaxies are more likely for higher masses with elongation along the line-of-sight. Nonetheless, we conclude that WL and WL+SL relations remain inconsistent with those from simulations, if projection is assumed to be the sole cause of differences in concentration.

Lastly, in Chapter 4, we explore the relationship between 2-dimensional measurements of mass and concentration (from clusters collected in Chapter 3) with the angular structure of the large-scale environment. Galaxy clusters populate the densest environments in the universe, often times living at the intersections of large-scale filamentary structures. These super-highways of galaxies trace out a cosmic web of structure, from which galaxy clusters tend to align themselves along. If this is in fact true, we would naively expect that having knowledge of the direction of large-scale structure around clusters may be able to tell us about the 3-dimensional orientation of the cluster, and therefore break the degenerate nature of the deprojection of mass along the line-of-sight. We use 1,391,449 spectroscopically confirmed galaxies obtained from the Sloan Digital Sky Survey (SDSS) Data Release 10 to trace out the large-scale structure around 92 galaxy clusters within the survey volume. We find essentially no dependence of cluster mass or concentration measurements with line-of-sight orientation of the large-scale structure surrounding them. However, we note that the concentration measurements used for this study are almost exclusively made with the caustic method

and line-of-sight velocity dispersion, rather than with lensing or X-ray methods. In Chapter 3, we saw evidence that these particular c-M relations were the most prone to projection effects.

Future work will include additional measures of quantifying structure around clusters, as well as the identification of cluster members. This will allow us to mitigate the effects of redshift space distortions, and more accurately map out cluster environments. Ultimately, if a strong connection is found between the orientation of large scale structure and the over-concentration of clusters, we would work toward the development of a procedure to constrain 3-dimensional cluster properties. We also aim to measure the profile properties of a large, volume limited sample of clusters in each major reconstruction technique available. This future project would require optical imaging and spectra (for lensing and galaxy-based methods), in addition to X-ray imaging. With selection effects essentially marginalized over, this would allow us to calibrate reconstruction techniques against one another, and truly understand physical biases which may exist between them.

Throughout this work, we have discussed the details and importance of measuring density profile properties of galaxy clusters, in both 2- and 3-dimensions. With larger and more sophisticated simulations and major survey projects like LSST on the horizon, it will soon be possible to study with much higher precision how shape, orientation, and the large-scale environment alter our perception of the largest bound structures in the universe.

## Bibliography

- Abdullah, M. H., Ali, G. B., Ismail, H. A., & Rassem, M. A. 2011, MNRAS, 416, 2027
- Allen, S. W., Schmidt, R. W., Fabian, A. C., & Ebeling, H. 2003, MNRAS, 342, 287
- Allgood, B., Flores, R. A., Primack, J. R., et al. 2006a, MNRAS, 367, 1781
- . 2006b, MNRAS, 367, 1781
- Altay, G., Colberg, J. M., & Croft, R. A. C. 2006, MNRAS, 370, 1422
- Ameglio, S., Borgani, S., Pierpaoli, E., & Dolag, K. 2007, MNRAS, 382, 397
- Andersson, K. E., & Madejski, G. M. 2004, ApJ, 607, 190
- Aragón-Calvo, M. A., van de Weygaert, R., Jones, B. J. T., & van der Hulst, J. M. 2007, ApJ, 655, L5
- Auger, M. W., Budzynski, J. M., Belokurov, V., Koposov, S. E., & McCarthy, I. 2013, ArXiv e-prints, arXiv:1308.6286 [astro-ph.CO]
- Babyk, Y. V., Del Popolo, A., & Vavilova, I. B. 2014, Astronomy Reports, 58, 587
- Bahé, Y. M., McCarthy, I. G., & King, L. J. 2012a, MNRAS, 421, 1073
- . 2012b, MNRAS, 421, 1073
- Bailin, J., & Steinmetz, M. 2004, ApJ, 616, 27
- . 2005, ApJ, 627, 647
- Bardeau, S., Kneib, J.-P., Czoske, O., et al. 2005, A&A, 434, 433
- Bardeau, S., Soucail, G., Kneib, J.-P., et al. 2007, A&A, 470, 449
- Bartelmann, M. 1996, A&A, 313, 697
- Bartelmann, M., & Schneider, P. 2001, Phys. Rep., 340, 291
- Basilakos, S., Plionis, M., Yepes, G., Gottlöber, S., & Turchaninov, V. 2006, MNRAS, 365, 539
- Becker, M. R., & Kravtsov, A. V. 2011, ApJ, 740, 25
- Bett, P., Eke, V., Frenk, C. S., et al. 2007a, MNRAS, 376, 215
- . 2007b, MNRAS, 376, 215
- Binggeli, B. 1980, A&A, 82, 289
- . 1982, A&A, 107, 338
- Birkinshaw, M. 1999, Phys. Rep., 310, 97
- Biviano, A., Rosati, P., Balestra, I., et al. 2013, A&A, 558, A1
- Bond, J. R., Cole, S., Efstathiou, G., & Kaiser, N. 1991, ApJ, 379, 440
- Borgani, S., & Guzzo, L. 2001, Nature, 409, 39

- Broadhurst, T., Takada, M., Umetsu, K., et al. 2005a, ApJ, 619, L143  
—. 2005b, ApJ, 619, L143
- Broadhurst, T., Umetsu, K., Medezinski, E., Oguri, M., & Rephaeli, Y. 2008a, ApJ, 685, L9  
—. 2008b, ApJ, 685, L9
- Broadhurst, T., Benítez, N., Coe, D., et al. 2005c, ApJ, 621, 53
- Brunino, R., Trujillo, I., Pearce, F. R., & Thomas, P. A. 2007, MNRAS, 375, 184
- Bryan, G. L., & Norman, M. L. 1998, ApJ, 495, 80
- Buckley-Geer, E. J., Lin, H., Drabek, E. R., et al. 2011, ApJ, 742, 48
- Bullock, J. S., Kolatt, T. S., Sigad, Y., et al. 2001a, MNRAS, 321, 559  
—. 2001b, MNRAS, 321, 559
- Buote, D. A., Gastaldello, F., Humphrey, P. J., et al. 2007, ApJ, 664, 123
- Buote, D. A., Humphrey, P. J., & Stocke, J. T. 2005, ApJ, 630, 750
- Buote, D. A., & Lewis, A. D. 2004, ApJ, 604, 116
- Carter, D., & Metcalfe, N. 1980, MNRAS, 191, 325
- Clowe, D. 2003, in Astronomical Society of the Pacific Conference Series, Vol. 301, Matter and Energy in Clusters of Galaxies, ed. S. Bowyer & C.-Y. Hwang, 271
- Clowe, D., & Schneider, P. 2001a, ArXiv Astrophysics e-prints, astro-ph/0109260  
—. 2001b, A&A, 379, 384  
—. 2002, A&A, 395, 385
- Coe, D., Benítez, N., Broadhurst, T., & Moustakas, L. A. 2010, ApJ, 723, 1678
- Colberg, J. M., Krughoff, K. S., & Connolly, A. J. 2005, MNRAS, 359, 272
- Cole, S., & Lacey, C. 1996a, MNRAS, 281, 716  
—. 1996b, MNRAS, 281, 716
- Comerford, J. M., & Natarajan, P. 2007a, MNRAS, 379, 190  
—. 2007b, MNRAS, 379, 190
- Corless, V. L., King, L. J., & Clowe, D. 2009, MNRAS, 393, 1235
- Correa, C. A., Wyithe, J. S. B., Schaye, J., & Duffy, A. R. 2015a, MNRAS, 452, 1217  
—. 2015b, ArXiv e-prints, arXiv:1501.04382
- Craig, M. W. 1997, PhD thesis, UNIVERSITY OF CALIFORNIA, BERKELEY
- D'Agostini, G. 2004, ArXiv Physics e-prints, physics/0403086
- Dalal, N., White, M., Bond, J. R., & Shirokov, A. 2008, ApJ, 687, 12
- David, L. P., Nulsen, P. E. J., McNamara, B. R., et al. 2001, ApJ, 557, 546
- Deb, S., Morandi, A., Pedersen, K., et al. 2012, ArXiv e-prints, arXiv:1201.3636 [astro-ph.CO]

- Démocles, J., Pratt, G. W., Pierini, D., et al. 2010, A&A, 517, A52
- Despali, G., Giocoli, C., & Tormen, G. 2014, MNRAS, 443, 3208
- Despali, G., Tormen, G., & Sheth, R. K. 2013, MNRAS, 431, 1143
- Diaferio, A. 1999, MNRAS, 309, 610
- Diaferio, A., & Geller, M. J. 1997, ApJ, 481, 633
- Diemer, B., & Kravtsov, A. V. 2015, ApJ, 799, 108
- Donnarumma, A., Ettori, S., Meneghetti, M., & Moscardini, L. 2009, MNRAS, 398, 438
- Doroshkevich, A. G. 1970, Astrophysics, 6, 320
- Dubinski, J., & Carlberg, R. G. 1991a, ApJ, 378, 496
- . 1991b, ApJ, 378, 496
- Dutton, A. A., & Macciò, A. V. 2014, MNRAS, 441, 3359
- Eichner, T., Seitz, S., Suyu, S. H., et al. 2013, ApJ, 774, 124
- Ettori, S., Gastaldello, F., Leccardi, A., et al. 2011, A&A, 526, C1
- Evans, A. K. D., & Bridle, S. 2009, ApJ, 695, 1446
- Evrard, A. E., Metzler, C. A., & Navarro, J. F. 1996, ApJ, 469, 494
- Fabian, A. C. 1991, MNRAS, 253, 29P
- Fabricant, D., Rybicki, G., & Gorenstein, P. 1985, in X-ray Astronomy '84, ed. M. Oda & R. Giacconi, 381
- Frenk, C. S., White, S. D. M., Davis, M., & Efstathiou, G. 1988a, ApJ, 327, 507
- . 1988b, ApJ, 327, 507
- Fukunaga, K., & Hostetler, L. 1975, Information Theory, IEEE Transactions on, 21, 32
- Gao, L., Navarro, J. F., Frenk, C. S., et al. 2012, MNRAS, 425, 2169
- Gastaldello, F., Buote, D. A., Humphrey, P. J., et al. 2007a, ApJ, 669, 158
- . 2007b, ApJ, 662, 923
- Gastaldello, F., Trevese, D., Vagnetti, F., & Fusco-Femiano, R. 2008, ApJ, 673, 176
- Gavazzi, R. 2002, NAR, 46, 783
- . 2005, A&A, 443, 793
- Gavazzi, R., Adami, C., Durret, F., et al. 2009, A&A, 498, L33
- Gavazzi, R., Fort, B., Mellier, Y., Pelló, R., & Dantel-Fort, M. 2003, A&A, 403, 11
- Ghigna, S., Moore, B., Governato, F., et al. 2000, ApJ, 544, 616
- Giocoli, C., Meneghetti, M., Ettori, S., & Moscardini, L. 2012, MNRAS, 426, 1558
- Giocoli, C., Meneghetti, M., Metcalf, R. B., Ettori, S., & Moscardini, L. 2014, MNRAS, 440, 1899
- Giodini, S., Lovisari, L., Pointecouteau, E., et al. 2013, Space Sci. Rev., 177, 247

- Gott, III, J. R., Vogeley, M. S., Podariu, S., & Ratra, B. 2001, ApJ, 549, 1
- Groener, A. M., & Goldberg, D. M. 2014, ApJ, 795, 153
- Gruen, D., Brimioule, F., Seitz, S., et al. 2013, MNRAS, 432, 1455
- Halkola, A., Seitz, S., & Pannella, M. 2006a, MNRAS, 372, 1425
- . 2006b, MNRAS, 372, 1425
- Hartigan, J. A., & Wong, M. A. 1979, Journal of the Royal Statistical Society. Series C (Applied Statistics), 28, 100
- Hawkins, E., Maddox, S., Cole, S., et al. 2003, MNRAS, 346, 78
- Hayashi, E., Navarro, J. F., & Springel, V. 2007a, MNRAS, 377, 50
- . 2007b, MNRAS, 377, 50
- Hennawi, J. F., Dalal, N., Bode, P., & Ostriker, J. P. 2007a, ApJ, 654, 714
- . 2007b, ApJ, 654, 714
- Hoekstra, H., & Jain, B. 2008, Annual Review of Nuclear and Particle Science, 58, 99
- Hopkins, P. F., Bahcall, N. A., & Bode, P. 2005, ApJ, 618, 1
- Hu, W., & Kravtsov, A. V. 2003, ApJ, 584, 702
- Israel, H., Erben, T., Reiprich, T. H., et al. 2010, A&A, 520, A58
- Jing, Y. P., & Suto, Y. 2002a, ApJ, 574, 538
- . 2002b, ApJ, 574, 538
- . 2002c, ApJ, 574, 538
- Kaiser, N. 1987, MNRAS, 227, 1
- Kasun, S. F., & Evrard, A. E. 2005a, ApJ, 629, 781
- . 2005b, ApJ, 629, 781
- Kauffmann, G., White, S. D. M., & Guiderdoni, B. 1993, MNRAS, 264, 201
- Kazantzidis, S., Kravtsov, A. V., Zentner, A. R., et al. 2004, ApJ, 611, L73
- Kelson, D. D., Zabludoff, A. I., Williams, K. A., et al. 2002, ApJ, 576, 720
- Khosroshahi, H. G., Maughan, B. J., Ponman, T. J., & Jones, L. R. 2006, MNRAS, 369, 1211
- Killedar, M., Borgani, S., Meneghetti, M., et al. 2012, MNRAS, 427, 533
- King, L. J., Clowe, D. I., & Schneider, P. 2002, A&A, 383, 118
- Kling, T. P., Dell'Antonio, I., Wittman, D., & Tyson, J. A. 2005, ApJ, 625, 643
- Klypin, A., Yepes, G., Gottlöber, S., Prada, F., & Hess, S. 2014, ArXiv e-prints, arXiv:1411.4001
- Klypin, A. A., Trujillo-Gomez, S., & Primack, J. 2011, ApJ, 740, 102
- Knebe, A., Knollmann, S. R., Muldrew, S. I., et al. 2011, MNRAS, 415, 2293
- Kneib, J.-P., Hudelet, P., Ellis, R. S., et al. 2003, ApJ, 598, 804

- Koester, B. P., McKay, T. A., Annis, J., et al. 2007, *ApJ*, 660, 239
- Kravtsov, A. V., Klypin, A. A., & Khokhlov, A. M. 1997a, *ApJS*, 111, 73
- . 1997b, *ApJS*, 111, 73
- Kubo, J. M., Stebbins, A., Annis, J., et al. 2007, *ApJ*, 671, 1466
- Lacey, C., & Cole, S. 1993a, *MNRAS*, 262, 627
- . 1993b, *MNRAS*, 262, 627
- Lau, E. T., Nagai, D., Kravtsov, A. V., Vikhlinin, A., & Zentner, A. R. 2012, *ApJ*, 755, 116
- Lemze, D., Barkana, R., Broadhurst, T. J., & Rephaeli, Y. 2008, *MNRAS*, 386, 1092
- Lerchster, M., Seitz, S., Brimioule, F., et al. 2011, *MNRAS*, 411, 2667
- Lewis, A. D., Buote, D. A., & Stocke, J. T. 2003, *ApJ*, 586, 135
- Limousin, M., Morandi, A., Sereno, M., et al. 2013a, *Space Sci. Rev.*, 177, 155
- . 2013b, *Space Sci. Rev.*, 177, 155
- Limousin, M., Richard, J., Jullo, E., et al. 2007a, *ApJ*, 668, 643
- . 2007b, *ApJ*, 668, 643
- Lokas, E. L. 2002, *MNRAS*, 333, 697
- Lokas, E. L., & Mamon, G. A. 2003, *MNRAS*, 343, 401
- Lokas, E. L., Wojtak, R., Gottlöber, S., Mamon, G. A., & Prada, F. 2006, *MNRAS*, 367, 1463
- Ludlow, A. D., Navarro, J. F., Li, M., et al. 2012, *MNRAS*, 427, 1322
- Macciò, A. V., Dutton, A. A., & van den Bosch, F. C. 2008, *MNRAS*, 391, 1940
- Mantz, A., Allen, S. W., Rapetti, D., & Ebeling, H. 2010, *MNRAS*, 406, 1759
- Mantz, A. B., Allen, S. W., Morris, R. G., et al. 2014, *MNRAS*, 440, 2077
- Markevitch, M., Vikhlinin, A., Forman, W. R., & Sarazin, C. L. 1999, *ApJ*, 527, 545
- Maughan, B. J., Jones, C., Jones, L. R., & Van Speybroeck, L. 2007, *ApJ*, 659, 1125
- McLaughlin, D. E. 1999, *ApJ*, 512, L9
- Mead, J. M. G., King, L. J., Sijacki, D., et al. 2010a, *MNRAS*, 406, 434
- . 2010b, *MNRAS*, 406, 434
- Medezinski, E., Broadhurst, T., Umetsu, K., et al. 2007, *ApJ*, 663, 717
- Meneghetti, M., Argazzi, R., Pace, F., et al. 2007, *A&A*, 461, 25
- Meneghetti, M., & Rasia, E. 2013, ArXiv e-prints, arXiv:1303.6158 [astro-ph.CO]
- Meneghetti, M., Rasia, E., Merten, J., et al. 2010, *A&A*, 514, A93
- Meneghetti, M., Rasia, E., Vega, J., et al. 2014, *ApJ*, 797, 34
- Merten, J., Meneghetti, M., Postman, M., et al. 2014, ArXiv e-prints, arXiv:1404.1376
- Molikawa, K., Hattori, M., Kneib, J.-P., & Yamashita, K. 1999, *A&A*, 351, 413

- Moore, B., Quinn, T., Governato, F., Stadel, J., & Lake, G. 1999, MNRAS, 310, 1147
- Moscardini, L., Matarrese, S., & Mo, H. J. 2001, MNRAS, 327, 422
- Muñoz-Cuartas, J. C., Macciò, A. V., Gottlöber, S., & Dutton, A. A. 2011, MNRAS, 411, 584
- Navarro, J. F., Frenk, C. S., & White, S. D. M. 1996, ApJ, 462, 563
- . 1997, ApJ, 490, 493
- Navarro, J. F., Hayashi, E., Power, C., et al. 2004, MNRAS, 349, 1039
- Oaxaca Wright, C., & Brainerd, T. G. 1999, ArXiv Astrophysics e-prints, astro-ph/9908213
- Oguri, M., Bayliss, M. B., Dahle, H., et al. 2012a, MNRAS, 420, 3213
- . 2012b, MNRAS, 420, 3213
- Oguri, M., & Blandford, R. D. 2009a, MNRAS, 392, 930
- . 2009b, MNRAS, 392, 930
- Oguri, M., Takada, M., Okabe, N., & Smith, G. P. 2010, MNRAS, 405, 2215
- Oguri, M., Takada, M., Umetsu, K., & Broadhurst, T. 2005a, ApJ, 632, 841
- . 2005b, ApJ, 632, 841
- Oguri, M., Hennawi, J. F., Gladders, M. D., et al. 2009a, ApJ, 699, 1038
- . 2009b, ApJ, 699, 1038
- Oguri, M., Schrabback, T., Jullo, E., et al. 2013, MNRAS, 429, 482
- Okabe, N., Bourdin, H., Mazzotta, P., & Maurogordato, S. 2011, ApJ, 741, 116
- Okabe, N., Futamase, T., Kajisawa, M., & Kuroshima, R. 2014, ApJ, 784, 90
- Okabe, N., Takada, M., Umetsu, K., Futamase, T., & Smith, G. P. 2010, PASJ, 62, 811
- Okabe, N., & Umetsu, K. 2008, PASJ, 60, 345
- Okabe, N., Umetsu, K., Tamura, T., et al. 2015, ArXiv e-prints, arXiv:1503.04412
- Old, L., Skibba, R. A., Pearce, F. R., et al. 2014, MNRAS, 441, 1513
- Patiri, S. G., Cuesta, A. J., Prada, F., Betancort-Rijo, J., & Klypin, A. 2006, ApJ, 652, L75
- Paulin-Henriksson, S., Antonuccio-Delogu, V., Haines, C. P., et al. 2007, A&A, 467, 427
- Paz, D. J., Lambas, D. G., Padilla, N., & Merchán, M. 2006, MNRAS, 366, 1503
- Paz, D. J., Sgró, M. A., Merchán, M., & Padilla, N. 2011, MNRAS, 414, 2029
- Piffaretti, R., Arnaud, M., Pratt, G. W., Pointecouteau, E., & Melin, J.-B. 2011, A&A, 534, A109
- Planck Collaboration, Ade, P. A. R., Aghanim, N., et al. 2015, ArXiv e-prints, arXiv:1502.01589
- Pointecouteau, E., Arnaud, M., Kaastra, J., & de Plaa, J. 2004, A&A, 423, 33
- Pointecouteau, E., Arnaud, M., & Pratt, G. W. 2005, A&A, 435, 1
- Prada, F., Klypin, A. A., Cuesta, A. J., Betancort-Rijo, J. E., & Primack, J. 2012a, MNRAS, 423, 3018

- . 2012b, MNRAS, 423, 3018
- Pratt, G. W., & Arnaud, M. 2005, A&A, 429, 791
- Press, W. H., & Schechter, P. 1974, ApJ, 187, 425
- Puchwein, E., Bartelmann, M., Dolag, K., & Meneghetti, M. 2005a, A&A, 442, 405
- . 2005b, A&A, 442, 405
- Puchwein, E., & Hilbert, S. 2009, MNRAS, 398, 1298
- Rasia, E., Borgani, S., Ettori, S., Mazzotta, P., & Meneghetti, M. 2013, ApJ, 776, 39
- Rasia, E., Meneghetti, M., Martino, R., et al. 2012, New Journal of Physics, 14, 055018
- Redlich, M., Bartelmann, M., Waizmann, J.-C., & Fedeli, C. 2012, A&A, 547, A66
- Regos, E., & Geller, M. J. 1989, AJ, 98, 755
- Riebe, K., Partl, A. M., Enke, H., et al. 2013, Astronomische Nachrichten, 334, 691
- Rines, K., & Diaferio, A. 2006, AJ, 132, 1275
- Rines, K., Geller, M. J., Diaferio, A., & Kurtz, M. J. 2013, ApJ, 767, 15
- Rines, K., Geller, M. J., Kurtz, M. J., & Diaferio, A. 2003, AJ, 126, 2152
- Rosati, P., Borgani, S., & Norman, C. 2002, ARA&A, 40, 539
- Rozo, E., Nagai, D., Keeton, C., & Kravtsov, A. 2008a, ApJ, 687, 22
- . 2008b, ApJ, 687, 22
- Rozo, E., Wechsler, R. H., Rykoff, E. S., et al. 2010, ApJ, 708, 645
- Schirmer, M., Suyu, S., Schrabback, T., et al. 2010, A&A, 514, A60
- Schmidt, R. W., & Allen, S. W. 2007, MNRAS, 379, 209
- Schneider, P., & Seitz, C. 1995, A&A, 294, 411
- Sereno, M., & Ettori, S. 2014, ArXiv e-prints, arXiv:1407.7868
- . 2015, MNRAS, 450, 3675
- Sereno, M., Ettori, S., & Baldi, A. 2012, MNRAS, 419, 2646
- Sereno, M., Fedeli, C., & Moscardini, L. 2015a, ArXiv e-prints, arXiv:1504.05183
- Sereno, M., Giocoli, C., Ettori, S., & Moscardini, L. 2014, ArXiv e-prints, arXiv:1410.4568
- . 2015b, MNRAS, 449, 2024
- Sereno, M., Jetzer, P., & Lubini, M. 2010a, MNRAS, 403, 2077
- Sereno, M., Lubini, M., & Jetzer, P. 2010b, A&A, 518, A55
- . 2010c, A&A, 518, A55
- Sereno, M., & Umetsu, K. 2011, MNRAS, 416, 3187
- Shaw, L. D., Weller, J., Ostriker, J. P., & Bode, P. 2006, ApJ, 646, 815
- Soucail, G., Fort, B., Mellier, Y., & Picat, J. P. 1987, A&A, 172, L14

- Splinter, R. J., Melott, A. L., Linn, A. M., Buck, C., & Tinker, J. 1997, *ApJ*, 479, 632
- Springel, V., White, S. D. M., Jenkins, A., et al. 2005, *Nature*, 435, 629
- Stanek, R., Rasia, E., Evrard, A. E., Pearce, F., & Gazzola, L. 2010, *ApJ*, 715, 1508
- Sunyaev, R. A., & Zeldovich, Y. B. 1972, *Comments on Astrophysics and Space Physics*, 4, 173
- Svensmark, J., Wojtak, R., & Hansen, S. H. 2015, *MNRAS*, 448, 1644
- Thanjavur, K., Crampton, D., & Willis, J. 2010, *ApJ*, 714, 1355
- Umetsu, K., & Broadhurst, T. 2008, *ApJ*, 684, 177
- Umetsu, K., Broadhurst, T., Zitrin, A., et al. 2011a, *ApJ*, 738, 41
- Umetsu, K., Broadhurst, T., Zitrin, A., Medezinski, E., & Hsu, L.-Y. 2011b, *ApJ*, 729, 127
- Umetsu, K., Birkinshaw, M., Liu, G.-C., et al. 2009, *ApJ*, 694, 1643
- Umetsu, K., Sereno, M., Medezinski, E., et al. 2015, ArXiv e-prints, arXiv:1503.01482
- van Haarlem, M., & van de Weygaert, R. 1993, *ApJ*, 418, 544
- Verdugo, T., Motta, V., Muñoz, R. P., et al. 2011, *A&A*, 527, A124
- Vikhlinin, A., Kravtsov, A., Forman, W., et al. 2006, *ApJ*, 640, 691
- Vikhlinin, A., Burenin, R. A., Ebeling, H., et al. 2009a, *ApJ*, 692, 1033
- Vikhlinin, A., Kravtsov, A. V., Burenin, R. A., et al. 2009b, *ApJ*, 692, 1060
- Voigt, L. M., & Fabian, A. C. 2006, *MNRAS*, 368, 518
- Voit, G. M. 2005, *Reviews of Modern Physics*, 77, 207
- Wambsganss, J., Ostriker, J. P., & Bode, P. 2008a, *ApJ*, 676, 753
- . 2008b, *ApJ*, 676, 753
- Wang, Y., Xu, H., Zhang, Z., et al. 2005, *ApJ*, 631, 197
- Warren, M. S., Quinn, P. J., Salmon, J. K., & Zurek, W. H. 1992a, *ApJ*, 399, 405
- . 1992b, *ApJ*, 399, 405
- Wechsler, R. H., Bullock, J. S., Primack, J. R., Kravtsov, A. V., & Dekel, A. 2002, *ApJ*, 568, 52
- White, S. D. M., & Frenk, C. S. 1991, *ApJ*, 379, 52
- White, S. D. M., Navarro, J. F., Evrard, A. E., & Frenk, C. S. 1993, *Nature*, 366, 429
- Williams, L. L. R., & Saha, P. 2004, ArXiv Astrophysics e-prints, astro-ph/0412445
- Wojtak, R., & Lokas, E. L. 2010, *MNRAS*, 408, 2442
- Xu, H., Jin, G., & Wu, X.-P. 2001, *ApJ*, 553, 78
- Zekser, K. C., White, R. L., Broadhurst, T. J., et al. 2006, *ApJ*, 640, 639
- Zhang, Y., Yang, X., Faltenbacher, A., et al. 2009, *ApJ*, 706, 747
- Zhao, D. H., Jing, Y. P., Mo, H. J., & Börner, G. 2003, *ApJ*, 597, L9
- Zitrin, A., Broadhurst, T., Umetsu, K., et al. 2010, *MNRAS*, 408, 1916
- Zitrin, A., Broadhurst, T., Coe, D., et al. 2011, *ApJ*, 742, 117

## Appendix A: Analytical Projection of Prolate Spheroidal Halos

The analytic form of the projected concentration is derived with the assumption that the surface mass density remains a constant (that is, the combination of shape and radial profile must change in such a way as to keep the original 2-dimensional distribution the same). We start with the scale convergence of a triaxial NFW halo as described in Sereno et al. (2010b):

$$\kappa_s = \frac{f_{geo}}{\sqrt{e_P} \Sigma_{cr}} \rho_s r_{sP} \quad (\text{A.1})$$

where  $e_P$ ,  $r_{sP}$ , and  $f_{geo}$  are the projected inverse axis ratio (the inverse of Equation 9), projected scale radius, and a geometric elongation parameter, respectively.

$$f_{geo} = \frac{e_P^{1/2}}{e_\Delta} \quad (\text{A.2})$$

The inverse projected axis ratio of a 3-dimensional ellipsoid viewed at an arbitrary viewing angle has been worked out by Binggeli (1980) to be

$$e_P = \sqrt{\frac{j + l + \sqrt{(j - l)^2 + 4k^2}}{j + l - \sqrt{(j - l)^2 + 4k^2}}} \quad (\text{A.3})$$

where the intrinsic halo geometry ( $q$  is the semi-minor to semi-major axis ratio;  $p$  is the semi-intermediate to semi-major axis ratio) and viewing angle are input into:

$$j = q^2 \sin^2 \theta + p^2 \sin^2 \phi \cos^2 \theta + \cos^2 \phi \cos^2 \theta \quad (\text{A.4})$$

$$k = p^2 \cos^2 \phi + \sin^2 \phi$$

$$l = (1 - p^2) \sin \phi \cos \phi \cos \theta$$

The elongation parameter is defined in the following way:

$$e_\Delta = \left( \frac{e_P}{e_1 e_2} \right)^{1/2} f^{3/4} \quad (\text{A.5})$$

$$f = e_1^2 \sin^2 \theta \sin^2 \phi + e_2^2 \sin^2 \theta \cos^2 \phi + \cos^2 \theta \quad (\text{A.6})$$

Remembering that the scale density  $\rho_s$  is

$$\rho_s = \rho_{cr} \delta_c \quad (\text{A.7})$$

allows us to associate the extra geometric factor of  $1/e_\Delta$  in the scale convergence expression with the overdensity.

$$\delta_C = \frac{1}{e_\Delta} \delta_c \quad (\text{A.8})$$

$$\frac{C^3}{\log(1+C) - \frac{C}{1+C}} = \frac{1}{e_\Delta} \frac{c^3}{\log(1+c) - \frac{c}{1+c}} \quad (\text{A.9})$$

The extra geometric factor can be expressed in terms of the prolate spheroidal projected axis ratio  $Q$ , a function of the intrinsic axis ratio  $q$ , and the angle between the major axis and the line-of-sight. Above, we have conclude that the assumption of prolateness is proven to be a reasonable one, thus the surplus in concentration can be completely expressed in terms of prolate spheroidal .

$$\frac{1}{e_\Delta} = \frac{Q^2}{q} \quad (\text{A.10})$$

## Appendix B: Lensing Cosmology Correction

In this section, we derive the correction to the measured cluster concentration and mass (assuming an NFW profile), due to assumed cosmological model. Beginning with the total mass enclosed within a sphere of radius  $r$

$$M_{\text{NFW}}(\leq r) = 4\pi r_s^3 \rho_s \left[ \log(1 + r/r_s) - \frac{r/r_s}{1 + r/r_s} \right] \quad (\text{B.1})$$

where  $r_s$  is the scale radius, and is used to scale the radial coordinate which we will denote as  $x = r/r_s$ . In terms of projected quantities, following Sereno et al. (2010c) we can express the scale radius and scale density  $\rho_s$  as

$$\rho_s = \frac{\Sigma_{\text{cr}}}{r_s} \kappa_s \quad (\text{B.2})$$

$$r_s = D_d \theta_s \quad (\text{B.3})$$

where  $\kappa_s$  is the normalization,  $\Sigma_{\text{cr}}$  is the critical surface mass density for lensing,  $D_d$  is the angular diameter distance to the lens, and  $\theta_s$  is the angular scale radius.

$$\Sigma_{\text{cr}} = \frac{c^2 D_s}{4\pi G D_{ds} D_d} \quad (\text{B.4})$$

At this point it should be noted that the scale convergence and projected (angular) scale radius do not depend upon cosmology when fitting the shear profile. The mass within radius  $r_\Delta$  and its corresponding concentration  $c_\Delta$  can be expressed in terms of projected quantities

$$M_{\text{NFW}}(\leq r_\Delta) = \frac{c^2 D_d D_s \kappa_s \theta_s^2}{G D_{ds}} \left[ \log(1 + c_\Delta) - \frac{c_\Delta}{1 + c_\Delta} \right] \quad (\text{B.5})$$

$$c_\Delta = \frac{r_\Delta}{r_s} = \frac{1}{D_d \theta_s} \left[ \frac{2M_{\text{NFW}}(\leq r_\Delta)}{\Delta \cdot H^2} \right]^{1/3} \quad (\text{B.6})$$

where  $\Delta$  is the factor by which the density inside  $r_\Delta$  is  $\Delta \cdot \rho_{\text{cr}}$ , and  $H$  is the Hubble parameter. Next, by solving the former two expressions for  $\kappa_s$  and  $\theta_s$  (which are conserved measurements for any arbitrary choice of cosmology), we obtain a system of equations which then relate the lensing mass and concentration in any two cosmologies,  $\Omega_1$  and  $\Omega_2$ . In order to simplify the notation a bit, the mass and concentration corresponding to  $r_\Delta$  in cosmology  $\Omega_x$ , will henceforth be expressed as  $M_\Delta(\Omega_x)$  and  $c_\Delta(\Omega_x)$ , respectively.

$$\frac{c_\Delta(\Omega_2)^3}{M_\Delta(\Omega_2)} = \frac{c_\Delta(\Omega_1)^3}{M_\Delta(\Omega_1)} \cdot R \quad (\text{B.7})$$

$$\frac{f(c_\Delta(\Omega_2))}{M_\Delta(\Omega_2)} = \frac{f(c_\Delta(\Omega_1))}{M_\Delta(\Omega_1)} \cdot T \quad (\text{B.8})$$

The ratios  $R$  and  $T$ , and the function  $f$ , can be expressed in terms of the following cosmology dependent quantities:

$$R = \frac{D_d(\Omega_1)^3 H(\Omega_1)^2 \Delta(\Omega_1)}{D_d(\Omega_2)^3 H(\Omega_2)^2 \Delta(\Omega_2)} = \frac{D_d(\Omega_1)^3}{D_d(\Omega_2)^3} \cdot \frac{\Delta(\Omega_1) \rho_{\text{cr}}(\Omega_1)}{\Delta(\Omega_2) \rho_{\text{cr}}(\Omega_1)} \quad (\text{B.9})$$

$$T = \frac{D_s(\Omega_1) D_d(\Omega_1)}{D_{ds}(\Omega_1)} \frac{D_{ds}(\Omega_2)}{D_s(\Omega_2) D_d(\Omega_2)} = \frac{\Sigma_{\text{cr}}(\Omega_2)}{\Sigma_{\text{cr}}(\Omega_1)} \quad (\text{B.10})$$

$$f(x) = \log(x) - \frac{x}{1+x} \quad (\text{B.11})$$

Solving this system of equations, can be done by numerically solving for  $c_\Delta(\Omega_2)$

$$\frac{f(c_\Delta(\Omega_2))}{c_\Delta(\Omega_2)^3} = \frac{f(c_\Delta(\Omega_1))}{c_\Delta(\Omega_1)^3} \cdot \frac{T}{R} \quad (\text{B.12})$$

Lastly, the mass  $M_\Delta(\Omega_2)$  is obtained by direct substitution of the numerical result from (15).

## Appendix C: Full Observational Dataset

We discuss here the details of our measurement aggregation procedure.

- The overwhelming majority of measurements were reported in the one or both of the conventions shown in Table A-1<sup>1</sup> (200, and virial). Whenever possible, we report measurements made by the original paper, rather than relying on the conversion procedure outlined in Hu & Kravtsov (2003). For papers which report their results for only one (or neither) of the previously mentioned conventions, we apply the aforementioned conversion process.
- There are numerous definitions (and approximations) used throughout the literature for  $\delta_{\text{vir}}$  (also represented as  $\Delta_v$ ). All measurements reported using the virial overdensity convention have been converted to a consistent definition (Bryan & Norman, 1998), before being reported in Table A-1:

$$\Delta_v = 18\pi^2 + 82x - 39x^2 \quad (\text{C.1})$$

for a flat cosmology ( $\Omega_R = 0$ ), and where  $x = \Omega(z) - 1$ . Furthermore,

$$\Omega(z) = \frac{\Omega_0 (1+z)^3}{E(z)^2} \quad (\text{C.2})$$

with  $E(z)$  representing the Hubble function.

$$E(z)^2 = \Omega_0 (1+z)^3 + \Omega_R (1+z)^2 + \Omega_\Lambda \quad (\text{C.3})$$

This approximation is accurate to 1% within the range of  $\Omega(z) = 0.1 - 1$ .

- All data reported in Comerford & Natarajan (2007b), were also reported in this study using their original cosmological model (with the exception of King et al. (2002)). We follow this convention, and continued to report measurements in Table A-1 in the cosmology found in the

source paper.

- All new measurements added to the dataset which do not appear in Comerford & Natarajan (2007b) received redshifts from previous entries (if available; meaning that if the cluster already exists in the database, the first reported value of the redshift is used). Differences in these redshifts are minimal ( $\sim 1\%$ ), and do not contribute significant uncertainty to the inferred c-M relation. Right ascension (RA) and declination (Dec) measurements were almost exclusively obtained from NED<sup>2</sup>. Lastly, due to the plurality of cluster naming conventions (nearly one for each survey or study), cluster names were cross-matched with previous entries using NED in order to ensure that our cluster sample does not contain artificially over-represented objects.

---

<sup>1</sup>The raw data has been made publicly available (format: csv, xlsx) here:  
<http://www.physics.drexel.edu/~groenera/>

<sup>2</sup><https://ned.ipac.caltech.edu/>

**Table C.1:** Cluster concentrations and masses

Cluster	z	RA	Dec.	Method	$c_{200}$	$M_{200}$ ( $10^{14} M_\odot$ )	$c_{\text{vir}}$	$M_{\text{vir}}$ ( $10^{14} M_\odot$ )	Ref.	$\delta$	$\Omega_m/\Omega_\Lambda/h$
Virgo	0.003	12 30 47.3	+12 20 13	X-ray	$2.8^{+0.7}_{-0.7}$	$4.2^{+0.5}_{-0.5}$	$3.8^{+0.9}_{-0.9}$	$5.4^{+0.9}_{-0.9}$	McLaughlin (1999)	200	0.3/0.7/0.7
Virgo	0.003	12 30 47.3	+12 20 13	CM	0.92	2.4	1.35	3.87	Rines & Diaferio (2006)	200	0.3/0.7/None
NGC 4636	0.0031	12 42 49.8	+02 41 16	CM	8.64	0.16	11.41	0.19	Rines & Diaferio (2006)	200	0.3/0.7/None
NGC 5846	0.006	15 06 29.3	+01 36 20	CM	8.29	0.5	10.95	0.59	Rines & Diaferio (2006)	200	0.3/0.7/None
NGC 5044	0.009	13 15 24.0	-16 23 08	X-ray	$8.4^{+0.2}_{-0.2}$	$0.322^{+0.009}_{-0.009}$	$11.1^{+0.3}_{-0.3}$	$0.375^{+0.011}_{-0.011}$	Gastaldello et al. (2007a)	1250	0.3/0.7/0.7
Abell 1060	0.01	10 36 41.8	-27 31 28	LOSVD	$10.67^{+0.93}_{-2.52}$	$3.57^{+0.34}_{-0.31}$	$13.98^{+1.22}_{-3.31}$	$4.09^{+0.39}_{-0.36}$	Wojtak & Lokas (2010)	102	0.3/0.7/0.7
Abell 1060	0.01	10 36 41.8	-27 31 28	X-ray	$10.27^{+2.45}_{-2.17}$	$9.81^{+1.32}_{-1.16}$	$13.7^{+3.27}_{-2.89}$	$11.39^{+1.53}_{-1.35}$	Babyk et al. (2014)	200	0.27/0.73/0.73
Abell 1060	0.01	10 36 41.8	-27 31 28	LOSVD	$10.6^{+17.1}_{-7.7}$	$3.8^{+0.4}_{-0.7}$	$14.0^{+22.0}_{-10.0}$	$4.4^{+1.1}_{-1.0}$	Lokas et al. (2006)	virial	0.3/0.7/0.7
Abell 1060	0.01	10 36 41.8	-27 31 28	X-ray	$8.4^{+0.6}_{-0.6}$	—	$11.1^{+0.8}_{-0.8}$	—	Xu et al. (2001)	200	0.3/0.7/0.5
Abell 3526	0.011	12 48 47.9	-41 18 28	X-ray	$10.43^{+0.81}_{-0.83}$	$8.26^{+0.72}_{-0.28}$	$13.9^{+1.08}_{-1.11}$	$9.58^{+0.84}_{-0.32}$	Babyk et al. (2014)	200	0.27/0.73/0.73
NGC 1550	0.0124	04 19 37.9	+02 24 34	X-ray	$13.0^{+0.8}_{-0.8}$	$0.274^{+0.011}_{-0.011}$	$17.0^{+1.0}_{-1.0}$	$0.311^{+0.014}_{-0.014}$	Gastaldello et al. (2007a)	2500	0.3/0.7/0.7
Abell S805	0.0139	18 47 20.0	-63 20 13	LOSVD	$6.69^{+1.07}_{-2.3}$	$2.35^{+0.33}_{-0.34}$	$8.85^{+1.42}_{-3.04}$	$2.79^{+0.39}_{-0.4}$	Wojtak & Lokas (2010)	102	0.3/0.7/0.7
NGC 2563	0.0149	08 20 35.7	+21 04 04	X-ray	$7.5^{+2.7}_{-2.7}$	$0.224^{+0.06}_{-0.06}$	$9.9^{+3.4}_{-3.4}$	$0.263^{+0.078}_{-0.078}$	Gastaldello et al. (2007a)	2500	0.3/0.7/0.7
Abell 262	0.0163	01 52 46.8	+36 09 05	LOSVD	$7.94^{+1.91}_{-2.19}$	$2.14^{+0.37}_{-0.21}$	$10.45^{+2.52}_{-2.88}$	$2.51^{+0.43}_{-0.25}$	Wojtak & Lokas (2010)	102	0.3/0.7/0.7
Abell 262	0.0163	01 52 46.8	+36 09 05	X-ray	$10.11^{+1.02}_{-0.98}$	$2.93^{+0.73}_{-0.67}$	$13.46^{+1.36}_{-1.3}$	$3.4^{+0.85}_{-0.78}$	Babyk et al. (2014)	200	0.27/0.73/0.73
Abell 262	0.0163	01 52 46.8	+36 09 05	LOSVD	$3.1^{+8.7}_{-2.4}$	$2.1^{+0.2}_{-0.6}$	$4.2^{+11.3}_{-3.2}$	$2.7^{+1.2}_{-1.0}$	Lokas et al. (2006)	virial	0.3/0.7/0.7
Abell 262	0.0163	01 52 46.8	+36 09 05	X-ray	$6.7^{+0.5}_{-0.5}$	$0.927^{+0.077}_{-0.077}$	$8.8^{+0.7}_{-0.7}$	$1.099^{+0.099}_{-0.099}$	Gastaldello et al. (2007a)	2500	0.3/0.7/0.7
Abell 262	0.0163	01 52 46.8	+36 09 05	X-ray	$5.29^{+0.43}_{-0.43}$	—	$7.03^{+0.55}_{-0.55}$	—	Vikhlinin et al. (2006)	500	0.3/0.7/0.71
Abell 262	0.0163	01 52 46.8	+36 09 05	X-ray	$12.9^{+1.1}_{-1.1}$	—	$16.8^{+1.4}_{-1.4}$	—	Xu et al. (2001)	200	0.3/0.7/0.5
Abell 194	0.018	01 25 40.8	-01 24 26	CM	6.27	1.09	8.3	1.3	Rines et al. (2003)	200/turn	0.3/0.7/None
NGC 533	0.0185	01 25 31.3	+01 45 33	X-ray	$13.0^{+1.0}_{-1.0}$	$0.202^{+0.01}_{-0.01}$	$16.9^{+1.3}_{-1.3}$	$0.229^{+0.012}_{-0.012}$	Gastaldello et al. (2007a)	1250	0.3/0.7/0.7
MKW 4	0.02	12 03 57.7	+01 53 18	LOSVD	$7.91^{+1.05}_{-2.75}$	$1.55^{+0.23}_{-0.21}$	$10.4^{+1.38}_{-3.62}$	$1.81^{+0.27}_{-0.25}$	Wojtak & Lokas (2010)	102	0.3/0.7/0.7
MKW 4	0.02	12 03 57.7	+01 53 18	X-ray	$19.93^{+3.15}_{-3.17}$	$2.22^{+1.84}_{-2.1}$	$26.19^{+4.14}_{-4.17}$	$2.48^{+2.06}_{-2.35}$	Babyk et al. (2014)	200	0.27/0.73/0.73
MKW 4	0.02	12 03 57.7	+01 53 18	X-ray	$9.4^{+0.6}_{-0.6}$	$0.54^{+0.026}_{-0.026}$	$12.3^{+0.8}_{-0.8}$	$0.624^{+0.033}_{-0.033}$	Gastaldello et al. (2007a)	1250	0.3/0.7/0.7
MKW 4	0.02	12 03 57.7	+01 53 18	X-ray	$3.85^{+0.22}_{-0.22}$	$1.11^{+0.15}_{-0.15}$	$5.17^{+0.28}_{-0.28}$	$1.37^{+0.2}_{-0.2}$	Vikhlinin et al. (2006)	500	0.3/0.7/0.71
MKW 4	0.02	12 03 57.7	+01 53 18	CM	11.6	2.27	15.13	2.59	Rines & Diaferio (2006)	200	0.3/0.7/None
Abell 3581	0.0218	14 07 28.1	-27 00 55	LOSVD	$9.32^{+0.83}_{-4.62}$	$1.53^{+0.37}_{-0.27}$	$12.2^{+1.09}_{-6.05}$	$1.77^{+0.43}_{-0.31}$	Wojtak & Lokas (2010)	102	0.3/0.7/0.7
Abell 3581	0.0218	14 07 28.1	-27 00 55	X-ray	$9.81^{+6.3}_{-5.4}$	$0.39^{+2.23}_{-0.27}$	$12.8^{+8.1}_{-6.9}$	$0.45^{+2.76}_{-0.31}$	Voigt & Fabian (2006)	200/2E4	0.3/0.7/0.7
Abell 1367	0.022	11 44 36.5	+19 45 32	CM	16.9	5.46	21.9	6.11	Rines et al. (2003)	200/turn	0.3/0.7/None

Continued on next page

Table C.1 – *Continued*

Cluster	z	RA	Dec.	Method	$c_{200}$	$M_{200}$ ( $10^{14} M_\odot$ )	$c_{\text{vir}}$	$M_{\text{vir}}$ ( $10^{14} M_\odot$ )	Ref.	$\delta$	$\Omega_m/\Omega_\Lambda/h$
IC 1860	0.0223	02 49 33.7	-31 11 21	X-ray	$7.2^{+0.6}_{-0.6}$	$0.431^{+0.036}_{-0.036}$	$9.5^{+0.8}_{-0.8}$	$0.507^{+0.046}_{-0.046}$	Gastaldello et al. (2007a)	1250	0.3/0.7/0.7
MKW 11	0.0228	13 29 31.2	+11 47 19	CM	4.29	0.46	5.75	0.57	Rines & Diaferio (2006)	200	0.3/0.7/None
NGC 5129	0.023	13 24 10.0	+13 58 36	X-ray	$11.2^{+1.8}_{-1.8}$	$0.135^{+0.017}_{-0.017}$	$14.6^{+2.3}_{-2.3}$	$0.154^{+0.02}_{-0.02}$	Gastaldello et al. (2007a)	1250	0.3/0.7/0.7
Abell 1656	0.023	12 59 48.7	+27 58 50	WL	$2.55^{+1.17}_{-0.84}$	$8.9^{+3.61}_{-2.26}$	$3.57^{+1.54}_{-1.12}$	$12.03^{+5.96}_{-3.46}$	Okabe et al. (2014)	virial/200/500	0.27/0.73/None
Abell 1656	0.023	12 59 48.7	+27 58 50	WL	$3.84^{+13.16}_{-1.84}$	$18.8^{+6.5}_{-5.6}$	$5.17^{+17.72}_{-2.48}$	$23.62^{+8.17}_{-7.04}$	Kubo et al. (2007)	200	0.3/0.7/None
Abell 1656	0.023	12 59 48.7	+27 58 50	WL	$5.0^{+3.2}_{-2.5}$	$7.3^{+6.1}_{-3.0}$	$6.7^{+4.3}_{-3.4}$	$8.9^{+7.4}_{-3.7}$	Gavazzi et al. (2009)	200	0.3/0.7/0.7
Abell 1656	0.023	12 59 48.7	+27 58 50	X-ray	$1.37^{+0.25}_{-0.27}$	$41.94^{+4.72}_{-3.92}$	$1.98^{+0.36}_{-0.39}$	$62.86^{+7.07}_{-5.88}$	Babyk et al. (2014)	200	0.27/0.73/0.73
Abell 1656	0.023	12 59 48.7	+27 58 50	CM	10.0	11.2	13.1	12.9	Rines et al. (2003)	200/turn	0.3/0.7/None
Abell 1656	0.023	12 59 48.7	+27 58 50	LOSVD	7.0	$11.8^{+0.3}_{-0.3}$	9.3	$13.9^{+4.0}_{-4.0}$	Lokas & Mamon (2003)	virial	0.3/0.7/0.7
Abell 779	0.0233	09 19 49.2	+33 45 37	LOSVD	$6.1^{+4.0}_{-4.0}$	1.65	$8.0^{+5.1}_{-5.1}$	1.97	Abdullah et al. (2011)	virial	0.3/0.7/None
Abell 779	0.0233	09 19 49.2	+33 45 37	LOSVD	$4.35^{+0.8}_{-1.47}$	$1.29^{+0.15}_{-0.24}$	$5.82^{+1.08}_{-1.97}$	$1.59^{+0.18}_{-0.3}$	Wojtak & Lokas (2010)	102	0.3/0.7/0.7
Abell 779	0.0233	09 19 49.2	+33 45 37	CM	24.41	2.66	31.46	2.94	Rines & Diaferio (2006)	200	0.3/0.7/None
NGC 4325	0.0257	12 23 06.7	+10 37 16	CM	4.87	0.21	6.49	0.26	Rines & Diaferio (2006)	200	0.3/0.7/None
NGC 4325	0.0257	12 23 06.7	+10 37 16	X-ray	$8.6^{+1.1}_{-1.1}$	$0.301^{+0.054}_{-0.054}$	$11.2^{+1.4}_{-1.4}$	$0.349^{+0.065}_{-0.065}$	Gastaldello et al. (2007a)	2500	0.3/0.7/0.7
RXC J2214.8+1350	0.0264	22 14 52.7	+13 50 48	CM	6.85	0.4	9.03	0.47	Rines & Diaferio (2006)	200	0.3/0.7/None
RXC J2315.7-0222	0.0267	23 15 45.2	-02 22 37	X-ray	$11.66^{+1.19}_{-1.19}$	$0.442^{+0.036}_{-0.036}$	$15.18^{+1.55}_{-1.55}$	$0.504^{+0.041}_{-0.041}$	Démocles et al. (2010)	500	0.3/0.7/0.7
MKW 8	0.0271	14 40 38.2	+03 28 35	X-ray	$15.28^{+3.14}_{-3.16}$	$7.47^{+1.48}_{-2.57}$	$20.11^{+4.13}_{-4.16}$	$8.45^{+1.67}_{-2.91}$	Babyk et al. (2014)	200	0.27/0.73/0.73
MKW 8	0.0271	14 40 38.2	+03 28 35	CM	5.27	0.56	7.0	0.68	Rines & Diaferio (2006)	200	0.3/0.7/None
NGC 6338	0.0286	17 15 23.0	+57 24 40	CM	7.46	2.16	9.8	2.54	Rines & Diaferio (2006)	200	0.3/0.7/None
Abell 539	0.029	05 16 37.3	+06 26 16	LOSVD	$9.81^{+1.26}_{-3.55}$	$3.25^{+0.49}_{-0.46}$	$12.8^{+1.65}_{-4.64}$	$3.73^{+0.57}_{-0.53}$	Wojtak & Lokas (2010)	102	0.3/0.7/0.7
Abell 539	0.029	05 16 37.3	+06 26 16	X-ray	$10.37^{+2.04}_{-2.01}$	$8.38^{+1.46}_{-1.77}$	$13.74^{+2.7}_{-2.66}$	$9.69^{+1.69}_{-2.05}$	Babyk et al. (2014)	200	0.27/0.73/0.73
Abell 539	0.029	05 16 37.3	+06 26 16	CM	14.7	3.63	19.0	4.09	Rines et al. (2003)	200/turn	0.3/0.7/None
Abell 4038	0.03	23 47 43.2	-28 08 29	X-ray	$9.38^{+1.03}_{-1.01}$	$8.26^{+1.18}_{-0.92}$	$12.46^{+1.37}_{-1.34}$	$9.62^{+1.37}_{-1.07}$	Babyk et al. (2014)	200	0.27/0.73/0.73
Abell 2197	0.03	16 28 10.4	+40 54 26	CM	1.35	0.99	1.91	1.45	Rines & Diaferio (2006)	200	0.3/0.7/None
Abell 2199	0.03	16 28 38.0	+39 32 55	X-ray	$6.27^{+0.25}_{-0.26}$	$12.38^{+2.18}_{-1.29}$	$8.42^{+0.34}_{-0.35}$	$14.91^{+2.63}_{-1.55}$	Babyk et al. (2014)	200	0.27/0.73/0.73
Abell 2199	0.03	16 28 38.0	+39 32 55	CM	4.02	3.7	5.39	4.62	Rines & Diaferio (2006)	200	0.3/0.7/None
Abell 2199	0.03	16 28 38.0	+39 32 55	CM	7.47	4.67	9.8	5.47	Rines et al. (2003)	200/turn	0.3/0.7/None
Abell 2199	0.03	16 28 38.0	+39 32 55	LOSVD	$7.79^{+11.26}_{-6.02}$	$6.0^{+1.5}_{-1.8}$	$10.4^{+14.6}_{-7.9}$	$7.1^{+3.4}_{-2.4}$	Lokas et al. (2006)	virial	0.3/0.7/0.7
Abell 2199	0.03	16 28 38.0	+39 32 55	LOSVD	4.0	5.0	5.0	6.0	Kelson et al. (2002)	200	0.3/0.7/0.75
Abell 2199	0.03	16 28 38.0	+39 32 55	X-ray	$8.2^{+0.4}_{-0.4}$	—	$10.7^{+0.5}_{-0.5}$	—	Xu et al. (2001)	200	0.3/0.7/0.5

Continued on next page

Table C.1 – *Continued*

Cluster	z	RA	Dec.	Method	$c_{200}$	$M_{200}$ ( $10^{14} M_\odot$ )	$c_{\text{vir}}$	$M_{\text{vir}}$ ( $10^{14} M_\odot$ )	Ref.	$\delta$	$\Omega_m/\Omega_\Lambda/h$
Abell 2199	0.03	16 28 38.0	+39 32 55	X-ray	10.0	—	13.0	—	Markevitch et al. (1999)	200	0.3/0.7/0.50
Zw1665	0.0302	08 23 11.5	+04 21 21.6	CM	11.38	0.9	14.8	1.03	Rines & Diaferio (2006)	200	0.3/0.7/None
Abell 2634	0.031	23 38 25.7	+27 00 45	LOSVD	$7.37^{+0.89}_{-2.03}$	$4.95^{+0.62}_{-0.74}$	$9.67^{+1.17}_{-2.66}$	$5.81^{+0.73}_{-0.87}$	Wojtak & Lokas (2010)	102	0.3/0.7/0.7
Abell 2634	0.031	23 38 25.7	+27 00 45	X-ray	$11.38^{+2.17}_{-2.16}$	$11.88^{+2.15}_{-2.17}$	$15.04^{+2.87}_{-2.85}$	$13.65^{+2.47}_{-1.46}$	Babyk et al. (2014)	200	0.27/0.73/0.73
IIIIZw54	0.0311	03 41 17.6	+15 23 44	X-ray	$11.25^{+1.33}_{-1.38}$	$8.81^{+1.04}_{-0.93}$	$14.87^{+1.76}_{-1.82}$	$10.13^{+1.2}_{-1.07}$	Babyk et al. (2014)	200	0.27/0.73/0.73
NGC 6107	0.0311	16 17 20.1	+34 54 07	CM	6.96	1.46	9.16	1.72	Rines & Diaferio (2006)	200	0.3/0.7/None
ESO 5520200	0.0314	04 54 52.0	-18 06 56	X-ray	$5.8^{+0.6}_{-0.6}$	$1.089^{+0.146}_{-0.146}$	$7.6^{+0.8}_{-0.8}$	$1.303^{+0.187}_{-0.187}$	Gastaldello et al. (2007a)	1250	0.3/0.7/0.7
AWM 4	0.0317	16 04 57.0	+23 55 14	X-ray	$7.21^{+1.02}_{-1.03}$	$6.55^{+0.85}_{-0.37}$	$9.64^{+1.36}_{-1.38}$	$7.79^{+1.01}_{-0.44}$	Babyk et al. (2014)	200	0.27/0.73/0.73
AWM 4	0.0317	16 04 57.0	+23 55 14	X-ray	$6.8^{+0.6}_{-0.6}$	$1.374^{+0.156}_{-0.156}$	$8.9^{+0.8}_{-0.8}$	$1.622^{+0.196}_{-0.196}$	Gastaldello et al. (2007a)	1250	0.3/0.7/0.7
Abell 496	0.0329	04 33 38.4	-13 15 33	LOSVD	$3.53^{+0.47}_{-0.75}$	$3.75^{+0.55}_{-0.46}$	$4.75^{+0.63}_{-1.01}$	$4.73^{+0.7}_{-0.58}$	Wojtak & Lokas (2010)	102	0.3/0.7/0.7
Abell 496	0.0329	04 33 38.4	-13 15 33	X-ray	$11.26^{+0.83}_{-0.81}$	$9.1^{+1.19}_{-1.27}$	$14.88^{+1.1}_{-1.07}$	$10.46^{+1.37}_{-1.46}$	Babyk et al. (2014)	200	0.27/0.73/0.73
Abell 496	0.0329	04 33 38.4	-13 15 33	CM	14.0	3.13	18.1	3.53	Rines et al. (2003)	200/turn	0.3/0.7/None
Abell 496	0.0329	04 33 38.4	-13 15 33	LOSVD	$6.9^{+12.9}_{-4.8}$	$4.5^{+0.3}_{-0.7}$	$9.3^{+16.7}_{-6.3}$	$5.3^{+1.1}_{-1.1}$	Lokas et al. (2006)	virial	0.3/0.7/0.7
Abell 496	0.0329	04 33 38.4	-13 15 33	X-ray	$10.4^{+0.6}_{-0.6}$	—	$13.5^{+0.8}_{-0.8}$	—	Xu et al. (2001)	200	0.3/0.7/0.5
Abell 496	0.0329	04 33 38.4	-13 15 33	X-ray	6.0	—	8.0	—	Markevitch et al. (1999)	200	0.3/0.7/0.50
Abell 1314	0.0334	11 34 50.5	+49 03 28	LOSVD	$6.52^{+1.09}_{-2.03}$	$2.93^{+0.52}_{-0.4}$	$8.57^{+1.43}_{-2.67}$	$3.47^{+0.62}_{-0.47}$	Wojtak & Lokas (2010)	102	0.3/0.7/0.7
Abell 1314	0.0334	11 34 50.5	+49 03 28	CM	10.95	1.91	14.23	2.18	Rines & Diaferio (2006)	200	0.3/0.7/None
Abell 2063	0.0337	15 23 01.8	+08 38 22	LOSVD	$12.35^{+1.19}_{-4.37}$	$5.21^{+1.04}_{-0.67}$	$16.02^{+1.55}_{-5.67}$	$5.92^{+1.18}_{-0.77}$	Wojtak & Lokas (2010)	102	0.3/0.7/0.7
Abell 2063	0.0337	15 23 01.8	+08 38 22	X-ray	$7.36^{+0.38}_{-0.33}$	$10.3^{+1.94}_{-1.29}$	$9.82^{+0.51}_{-0.44}$	$12.22^{+2.3}_{-1.53}$	Babyk et al. (2014)	200	0.27/0.73/0.73
Abell 2063	0.0337	15 23 01.8	+08 38 22	X-ray	$5.1^{+0.3}_{-0.3}$	—	$6.8^{+0.4}_{-0.4}$	—	Xu et al. (2001)	200	0.3/0.7/0.5
2A 0335+096	0.0347	03 38 35.3	+09 57 55	X-ray	$8.18^{+18.83}_{-7.2}$	$1.4^{+115.5}_{-1.0}$	$10.7^{+23.9}_{-9.3}$	$1.6^{+175.4}_{-1.2}$	Voigt & Fabian (2006)	200/2E4	0.3/0.7/0.7
Abell 2052	0.0348	15 16 44.0	+07 01 07	LOSVD	$9.41^{+1.48}_{-3.68}$	$2.48^{+0.42}_{-0.42}$	$12.26^{+1.92}_{-4.8}$	$2.86^{+0.49}_{-0.49}$	Wojtak & Lokas (2010)	102	0.3/0.7/0.7
Abell 2052	0.0348	15 16 44.0	+07 01 07	X-ray	$10.33^{+1.39}_{-1.33}$	$9.12^{+1.26}_{-1.72}$	$13.66^{+1.84}_{-1.76}$	$10.54^{+1.46}_{-1.99}$	Babyk et al. (2014)	200	0.27/0.73/0.73
Abell 2052	0.0348	15 16 44.0	+07 01 07	X-ray	$9.7^{+0.7}_{-0.7}$	—	$12.6^{+0.9}_{-0.9}$	—	Xu et al. (2001)	200	0.3/0.7/0.5
Abell 1142	0.035	11 00 48.9	+10 33 35	LOSVD	$6.9^{+2.0}_{-2.0}$	1.92	$9.1^{+2.5}_{-2.5}$	2.26	Abdullah et al. (2011)	virial	0.3/0.7/None
Abell 1142	0.035	11 00 48.9	+10 33 35	CM	28.44	3.09	36.47	3.39	Rines & Diaferio (2006)	200	0.3/0.7/None
Abell 2147	0.035	16 02 18.7	+16 01 12	X-ray	$10.46^{+3.81}_{-4.27}$	$10.93^{+1.27}_{-1.28}$	$13.83^{+5.04}_{-5.65}$	$12.62^{+1.47}_{-1.48}$	Babyk et al. (2014)	200	0.27/0.73/0.73
ESO 3060170	0.0358	05 40 06.6	-40 50 12	X-ray	$6.7^{+0.8}_{-0.8}$	$1.542^{+0.397}_{-0.397}$	$8.8^{+1.0}_{-1.0}$	$1.82^{+0.487}_{-0.487}$	Gastaldello et al. (2007a)	2500	0.3/0.7/0.7
RGH89 080	0.0379	13 20 24.9	+33 12 17	X-ray	$7.6^{+0.7}_{-0.7}$	$0.241^{+0.012}_{-0.012}$	$9.9^{+0.9}_{-0.9}$	$0.282^{+0.016}_{-0.016}$	Gastaldello et al. (2007a)	500	0.3/0.7/0.7
MKW 9	0.0382	15 32 29.3	+04 40 54	X-ray	$5.41^{+0.67}_{-0.67}$	$1.2^{+0.3}_{-0.3}$	$7.14^{+0.86}_{-0.86}$	$1.44^{+0.38}_{-0.38}$	Pointecouteau et al. (2005)	200	0.3/0.7/0.7

Continued on next page

Table C.1 – *Continued*

Cluster	z	RA	Dec.	Method	$c_{200}$	$M_{200}$ ( $10^{14} M_\odot$ )	$c_{\text{vir}}$	$M_{\text{vir}}$ ( $10^{14} M_\odot$ )	Ref.	$\delta$	$\Omega_m/\Omega_\Lambda/h$
MKW 9	0.0382	15 32 29.3	+04 40 54	X-ray	$5.4^{+0.7}_{-0.7}$	1.2	$7.1^{+0.9}_{-0.9}$	1.44	Pratt & Arnaud (2005)	200	0.3/0.7/0.7
Abell 3571	0.039	13 47 28.4	-32 50 59	LOSVD	$8.05^{+1.46}_{-2.41}$	$9.26^{+1.03}_{-1.58}$	$10.52^{+1.9}_{-3.15}$	$10.77^{+1.19}_{-1.84}$	Wojtak & Lokas (2010)	102	0.3/0.7/0.7
Abell 3571	0.039	13 47 28.4	-32 50 59	X-ray	$8.92^{+1.98}_{-2.1}$	$30.41^{+3.75}_{-3.84}$	$11.82^{+2.62}_{-2.78}$	$35.49^{+4.38}_{-4.48}$	Babyk et al. (2014)	200	0.27/0.73/0.73
Abell 3571	0.039	13 47 28.4	-32 50 59	X-ray	$4.9^{+0.2}_{-0.2}$	–	$6.5^{+0.3}_{-0.3}$	–	Xu et al. (2001)	200	0.3/0.7/0.5
Abell 1139	0.0398	10 58 04.3	+01 29 56	LOSVD	$2.57^{+0.37}_{-0.91}$	$1.19^{+0.18}_{-0.26}$	$3.49^{+0.5}_{-1.24}$	$1.56^{+0.24}_{-0.34}$	Wojtak & Lokas (2010)	102	0.3/0.7/0.7
Abell 2657	0.04	23 44 51.0	+09 08 40	X-ray	$5.49^{+0.83}_{-0.81}$	$9.89^{+2.17}_{-1.28}$	$7.38^{+1.12}_{-1.09}$	$12.05^{+2.64}_{-1.56}$	Babyk et al. (2014)	200	0.27/0.73/0.73
Abell 576	0.04	07 21 24.1	+55 44 20	LOSVD	$3.52^{+0.61}_{-0.92}$	$6.47^{+1.04}_{-0.81}$	$4.72^{+0.82}_{-1.23}$	$8.15^{+1.31}_{-1.02}$	Wojtak & Lokas (2010)	102	0.3/0.7/0.7
Abell 576	0.04	07 21 24.1	+55 44 20	X-ray	$4.28^{+0.83}_{-0.81}$	$21.11^{+2.16}_{-1.19}$	$5.8^{+1.12}_{-1.1}$	$26.41^{+2.7}_{-1.49}$	Babyk et al. (2014)	200	0.27/0.73/0.73
Abell 576	0.04	07 21 24.1	+55 44 20	CM	10.9	9.51	14.1	10.85	Rines et al. (2003)	200/turn	0.3/0.7/None
Abell 2589	0.041	23 23 53.5	+16 48 32	CM	6.34	0.99	8.32	1.17	Rines & Diaferio (2006)	200	0.3/0.7/None
Abell 2589	0.041	23 23 53.5	+16 48 32	X-ray	$4.9^{+2.4}_{-2.4}$	–	$6.5^{+3.1}_{-3.1}$	–	Buote & Lewis (2004)	200	0.3/0.7/0.7
Abell 2589	0.041	23 23 53.5	+16 48 32	X-ray	$6.27^{+0.75}_{-0.72}$	$10.05^{+1.27}_{-1.29}$	$8.39^{+1.0}_{-0.96}$	$12.08^{+1.53}_{-1.55}$	Babyk et al. (2014)	200	0.27/0.73/0.73
Abell 2107	0.0411	15 39 38.4	+21 47 20	LOSVD	$11.87^{+1.61}_{-4.76}$	$2.42^{+0.55}_{-0.38}$	$15.36^{+2.08}_{-6.16}$	$2.75^{+0.63}_{-0.44}$	Wojtak & Lokas (2010)	102	0.3/0.7/0.7
Abell 2593	0.0415	23 24 20.2	+14 39 04	LOSVD	$2.59^{+0.49}_{-0.76}$	$1.57^{+0.28}_{-0.2}$	$3.52^{+0.66}_{-1.04}$	$2.07^{+0.37}_{-0.27}$	Wojtak & Lokas (2010)	102	0.3/0.7/0.7
Abell 2593	0.0415	23 24 20.2	+14 39 04	CM	11.64	3.44	15.07	3.91	Rines & Diaferio (2006)	200	0.3/0.7/None
Abell 295	0.0424	02 02 19.9	-01 07 13	CM	1.38	0.27	1.94	0.39	Rines & Diaferio (2006)	200	0.3/0.7/None
Abell 160	0.0432	01 12 51.4	+15 30 54	CM	10.14	0.91	13.16	1.04	Rines & Diaferio (2006)	200	0.3/0.7/None
Abell 1983	0.0442	14 52 44.0	+16 44 46	LOSVD	$3.54^{+0.69}_{-1.49}$	$1.19^{+0.28}_{-0.26}$	$4.74^{+0.93}_{-1.99}$	$1.5^{+0.36}_{-0.33}$	Wojtak & Lokas (2010)	102	0.3/0.7/0.7
Abell 1983	0.0442	14 52 44.0	+16 44 46	X-ray	$3.83^{+0.71}_{-0.71}$	$1.59^{+0.61}_{-0.61}$	$5.1^{+0.91}_{-0.91}$	$1.97^{+0.82}_{-0.82}$	Pointecouteau et al. (2005)	200	0.3/0.7/0.7
Abell 119	0.0446	00 56 18.3	-01 13 00	LOSVD	$3.4^{+0.58}_{-0.91}$	$3.97^{+0.57}_{-0.59}$	$4.56^{+0.78}_{-1.23}$	$5.02^{+0.73}_{-0.75}$	Wojtak & Lokas (2010)	102	0.3/0.7/0.7
Abell 119	0.0446	00 56 18.3	-01 13 00	X-ray	$4.12^{+0.25}_{-0.23}$	$24.06^{+4.16}_{-2.18}$	$5.59^{+0.34}_{-0.31}$	$30.2^{+5.22}_{-2.74}$	Babyk et al. (2014)	200	0.27/0.73/0.73
Abell 119	0.0446	00 56 18.3	-01 13 00	CM	6.29	4.07	8.25	4.81	Rines et al. (2003)	200/turn	0.3/0.7/None
Abell 119	0.0446	00 56 18.3	-01 13 00	CM	2.55	2.36	3.45	3.06	Rines & Diaferio (2006)	200	0.3/0.7/None
Abell 119	0.0446	00 56 18.3	-01 13 00	X-ray	$3.3^{+0.2}_{-0.2}$	–	$4.4^{+0.3}_{-0.3}$	–	Xu et al. (2001)	200	0.3/0.7/0.5
Abell 3376	0.045	06 01 45.7	-39 59 34	X-ray	$7.38^{+1.01}_{-1.03}$	$26.61^{+3.72}_{-2.91}$	$9.81^{+1.34}_{-1.37}$	$31.5^{+4.4}_{-3.44}$	Babyk et al. (2014)	200	0.27/0.73/0.73
MKW 3S	0.045	15 21 51.9	+07 42 31	X-ray	$11.37^{+2.18}_{-2.73}$	$12.02^{+2.47}_{-3.19}$	$14.96^{+2.87}_{-3.59}$	$13.78^{+2.83}_{-3.66}$	Babyk et al. (2014)	200	0.27/0.73/0.73
MKW 3S	0.045	15 21 51.9	+07 42 31	X-ray	$6.4^{+0.7}_{-0.7}$	–	$8.4^{+0.9}_{-0.9}$	–	Xu et al. (2001)	200	0.3/0.7/0.5
Abell 168	0.0451	01 15 12.0	+00 19 48	LOSVD	$5.6^{+2.0}_{-2.0}$	2.58	$7.4^{+2.6}_{-2.6}$	3.08	Abdullah et al. (2011)	virial	0.3/0.7/None
Abell 168	0.0451	01 15 12.0	+00 19 48	X-ray	$7.37^{+0.26}_{-0.27}$	$6.74^{+2.03}_{-1.78}$	$9.8^{+0.35}_{-0.36}$	$7.98^{+2.4}_{-2.11}$	Babyk et al. (2014)	200	0.27/0.73/0.73
Abell 168	0.0451	01 15 12.0	+00 19 48	CM	5.19	4.3	6.84	5.17	Rines et al. (2003)	200/turn	0.3/0.7/None

Continued on next page

Table C.1 – *Continued*

Cluster	z	RA	Dec.	Method	$c_{200}$	$M_{200}$ ( $10^{14} M_\odot$ )	$c_{\text{vir}}$	$M_{\text{vir}}$ ( $10^{14} M_\odot$ )	Ref.	$\delta$	$\Omega_m/\Omega_\Lambda/h$
Abell 168	0.0451	01 15 12.0	+00 19 48	CM	7.69	2.24	10.03	2.61	Rines & Diaferio (2006)	200	0.3/0.7/None
MS 0116.3-0115	0.0452	01 18 53.6	-01 00 07	X-ray	$4.8^{+1.4}_{-1.4}$	$1.055^{+0.514}_{-0.514}$	$6.3^{+1.8}_{-1.8}$	$1.283^{+0.671}_{-0.671}$	Gastaldello et al. (2007a)	1250	0.3/0.7/0.7
Abell 957	0.0455	10 13 40.3	-00 54 52	LOSVD	$9.91^{+1.33}_{-3.46}$	$3.1^{+0.47}_{-0.47}$	$12.85^{+1.73}_{-4.48}$	$3.56^{+0.54}_{-0.54}$	Wojtak & Lokas (2010)	102	0.3/0.7/0.7
Abell 957	0.0455	10 13 40.3	-00 54 52	CM	8.13	2.79	10.6	3.25	Rines & Diaferio (2006)	200	0.3/0.7/None
Abell 1736	0.046	13 26 54.0	-27 11 00	X-ray	$16.27^{+4.16}_{-4.13}$	$8.11^{+1.15}_{-1.18}$	$21.26^{+5.44}_{-5.4}$	$9.12^{+1.29}_{-1.33}$	Babyk et al. (2014)	200	0.27/0.73/0.73
Abell 1644	0.047	12 57 09.7	-17 24 01	X-ray	$15.35^{+3.89}_{-4.17}$	$14.6^{+1.47}_{-1.17}$	$20.07^{+5.09}_{-5.45}$	$16.47^{+1.66}_{-1.32}$	Babyk et al. (2014)	200	0.27/0.73/0.73
Abell 4059	0.0478	23 57 02.3	-34 45 38	LOSVD	$2.6^{+0.5}_{-0.7}$	$3.37^{+0.48}_{-0.47}$	$3.52^{+0.67}_{-0.95}$	$4.41^{+0.62}_{-0.61}$	Wojtak & Lokas (2010)	102	0.3/0.7/0.7
Abell 4059	0.0478	23 57 02.3	-34 45 38	X-ray	$9.36^{+2.02}_{-2.01}$	$10.72^{+0.92}_{-1.28}$	$12.36^{+2.67}_{-2.65}$	$12.45^{+1.07}_{-1.49}$	Babyk et al. (2014)	200	0.27/0.73/0.73
Abell 4059	0.0478	23 57 02.3	-34 45 38	X-ray	$4.8^{+0.2}_{-0.2}$	–	$6.3^{+0.3}_{-0.3}$	–	Xu et al. (2001)	200	0.3/0.7/0.5
Abell 3558	0.048	13 27 57.5	-31 30 09	X-ray	$8.37^{+0.78}_{-0.83}$	$21.27^{+3.27}_{-2.16}$	$11.08^{+1.03}_{-1.1}$	$24.91^{+3.83}_{-2.53}$	Babyk et al. (2014)	200	0.27/0.73/0.73
Abell 3558	0.048	13 27 57.5	-31 30 09	LOSVD	$1.9^{+4.0}_{-1.2}$	$9.0^{+0.3}_{-2.3}$	$2.7^{+5.3}_{-1.7}$	$12.5^{+3.5}_{-4.5}$	Lokas et al. (2006)	virial	0.3/0.7/0.7
Abell 3558	0.048	13 27 57.5	-31 30 09	X-ray	$4.0^{+0.2}_{-0.2}$	–	$5.3^{+0.3}_{-0.3}$	–	Xu et al. (2001)	200	0.3/0.7/0.5
Abell 376	0.0484	02 45 48.5	+36 51 36	LOSVD	$6.29^{+1.44}_{-2.38}$	$4.67^{+1.34}_{-0.76}$	$8.25^{+1.89}_{-3.12}$	$5.53^{+1.58}_{-0.91}$	Wojtak & Lokas (2010)	102	0.3/0.7/0.7
SHK 352	0.0484	11 21 40.3	+02 53 33	CM	6.83	4.09	8.94	4.82	Rines & Diaferio (2006)	200	0.3/0.7/None
Abell 2717	0.049	00 03 12.1	-35 55 38	X-ray	$6.12^{+0.84}_{-0.81}$	$12.94^{+2.11}_{-1.26}$	$8.17^{+1.12}_{-1.08}$	$15.56^{+2.54}_{-1.52}$	Babyk et al. (2014)	200	0.27/0.73/0.73
Abell 2717	0.049	00 03 12.1	-35 55 38	X-ray	$4.6^{+0.3}_{-0.3}$	$1.51^{+0.09}_{-0.09}$	$6.0^{+0.4}_{-0.4}$	$1.842^{+0.122}_{-0.122}$	Gastaldello et al. (2007a)	500	0.3/0.7/0.7
Abell 2717	0.049	00 03 12.1	-35 55 38	X-ray	$4.21^{+0.25}_{-0.25}$	$1.57^{+0.19}_{-0.19}$	$5.58^{+0.32}_{-0.32}$	$1.92^{+0.25}_{-0.25}$	Pointecouteau et al. (2005)	200	0.3/0.7/0.7
Abell 2717	0.049	00 03 12.1	-35 55 38	X-ray	$4.2^{+0.3}_{-0.3}$	1.57	$5.6^{+0.4}_{-0.4}$	1.92	Pratt & Arnaud (2005)	200	0.3/0.7/0.7
Abell 3562	0.0499	13 33 36.3	-31 39 40	X-ray	$8.26^{+0.25}_{-0.27}$	$14.05^{+1.56}_{-1.46}$	$10.93^{+0.33}_{-0.36}$	$16.46^{+1.83}_{-1.71}$	Babyk et al. (2014)	200	0.27/0.73/0.73
Abell 3562	0.0499	13 33 36.3	-31 39 40	X-ray	$5.4^{+0.8}_{-0.8}$	–	$7.1^{+1.0}_{-1.0}$	–	Xu et al. (2001)	200	0.3/0.7/0.5
Abell 3395	0.05	06 27 14.4	-54 28 12	X-ray	$3.74^{+0.35}_{-0.37}$	$33.67^{+4.27}_{-4.12}$	$5.08^{+0.48}_{-0.5}$	$42.7^{+5.42}_{-5.22}$	Babyk et al. (2014)	200	0.27/0.73/0.73
Abell 671	0.0503	08 28 29.3	+30 25 01	LOSVD	$17.9^{+5.5}_{-5.5}$	5.32	$23.0^{+7.0}_{-7.0}$	5.93	Abdullah et al. (2011)	virial	0.3/0.7/None
Abell 671	0.0503	08 28 29.3	+30 25 01	LOSVD	$11.85^{+1.13}_{-4.63}$	$4.85^{+0.88}_{-0.69}$	$15.3^{+1.46}_{-5.98}$	$5.51^{+1.0}_{-0.78}$	Wojtak & Lokas (2010)	102	0.3/0.7/0.7
Abell 671	0.0503	08 28 29.3	+30 25 01	CM	12.1	4.01	15.61	4.54	Rines & Diaferio (2006)	200	0.3/0.7/None
Abell 1291A	0.0508	11 32 19.6	+55 58 44.0	CM	4.96	1.09	6.55	1.32	Rines & Diaferio (2006)	200	0.3/0.7/None
Abell 3391	0.051	06 26 22.8	-53 41 44	X-ray	$9.26^{+1.14}_{-1.36}$	$18.91^{+1.25}_{-1.28}$	$12.22^{+1.5}_{-1.79}$	$21.97^{+1.45}_{-1.49}$	Babyk et al. (2014)	200	0.27/0.73/0.73
Abell 757	0.0514	09 12 47.3	+47 42 38	CM	2.96	0.54	3.98	0.69	Rines & Diaferio (2006)	200	0.3/0.7/None
Abell 1377	0.0515	11 46 57.9	+55 44 20	LOSVD	$0.9^{+0.4}_{-0.4}$	0.81	$1.3^{+0.5}_{-0.5}$	1.3	Abdullah et al. (2011)	virial	0.3/0.7/None
Abell 1377	0.0515	11 46 57.9	+55 44 20	CM	2.33	1.16	3.17	1.54	Rines & Diaferio (2006)	200	0.3/0.7/None
Abell 117	0.0535	00 56 00.9	-10 01 46	LOSVD	$7.7^{+3.1}_{-3.1}$	2.78	$10.0^{+4.0}_{-4.0}$	3.23	Abdullah et al. (2011)	virial	0.3/0.7/None

Continued on next page

Table C.1 – *Continued*

Cluster	z	RA	Dec.	Method	$c_{200}$	$M_{200}$ ( $10^{14} M_\odot$ )	$c_{\text{vir}}$	$M_{\text{vir}}$ ( $10^{14} M_\odot$ )	Ref.	$\delta$	$\Omega_m/\Omega_\Lambda/h$
Hydra A	0.0538	09 18 05.7	-12 05 44	WL	$3.32^{+2.17}_{-1.29}$	$3.65^{+2.17}_{-1.43}$	$4.52^{+2.95}_{-1.75}$	$4.66^{+2.77}_{-1.82}$	Okabe et al. (2015)	virial	0.27/0.73/0.70
Hydra A	0.0538	09 18 05.7	-12 05 44	X-ray	$12.3^{+0.18}_{-0.18}$	$1.02^{+0.41}_{-0.41}$	$15.9^{+0.23}_{-0.23}$	$1.15^{+0.47}_{-0.47}$	David et al. (2001)	200	0.3/0.7/0.7
Abell 754	0.054	09 09 08.4	-09 39 58	WL	$3.74^{+4.12}_{-4.12}$	$3.3^{+4.77}_{-4.77}$	$4.97^{+5.26}_{-5.26}$	$4.09^{+5.39}_{-5.39}$	Okabe & Umetsu (2008)	virial	0.3/0.7/0.7
Abell 754	0.054	09 09 08.4	-09 39 58	X-ray	$1.02^{+0.27}_{-0.22}$	$40.3^{+3.71}_{-3.16}$	$1.49^{+0.39}_{-0.32}$	$63.37^{+5.83}_{-4.97}$	Babyk et al. (2014)	200	0.27/0.73/0.73
Abell 978	0.0544	10 20 28.8	-06 31 11	LOSVD	$4.25^{+0.86}_{-1.81}$	$4.23^{+1.09}_{-0.68}$	$5.63^{+1.13}_{-2.4}$	$5.19^{+1.34}_{-0.83}$	Wojtak & Lokas (2010)	102	0.3/0.7/0.7
RXCJ1022.0+3830	0.0546	10 22 04.7	+38 30 43	CM	5.45	1.41	7.16	1.69	Rines & Diaferio (2006)	200	0.3/0.7/None
Abell 3667	0.055	20 12 30.5	-56 49 55	X-ray	$9.36^{+1.25}_{-1.36}$	$26.84^{+2.48}_{-2.46}$	$12.33^{+1.65}_{-1.79}$	$31.13^{+2.88}_{-2.85}$	Babyk et al. (2014)	200	0.27/0.73/0.73
Abell 85	0.0557	00 41 50.1	-09 18 07	LOSVD	$3.12^{+0.56}_{-0.7}$	$9.59^{+1.38}_{-1.04}$	$4.18^{+0.75}_{-0.94}$	$12.22^{+1.76}_{-1.33}$	Wojtak & Lokas (2010)	102	0.3/0.7/0.7
Abell 85	0.0557	00 41 50.1	-09 18 07	X-ray	$3.55^{+0.26}_{-0.22}$	$25.68^{+4.89}_{-3.18}$	$4.82^{+0.35}_{-0.3}$	$32.73^{+6.23}_{-4.05}$	Babyk et al. (2014)	200	0.27/0.73/0.73
Abell 85	0.0557	00 41 50.1	-09 18 07	CM	4.5	3.36	5.93	4.08	Rines & Diaferio (2006)	200	0.3/0.7/None
Abell 85	0.0557	00 41 50.1	-09 18 07	X-ray	$7.5^{+0.6}_{-0.6}$	—	$9.8^{+0.8}_{-0.8}$	—	Xu et al. (2001)	200	0.3/0.7/0.5
Sersic 159 03	0.0564	23 13 58.6	-42 44 02	X-ray	$6.16^{+3.42}_{-2.79}$	$2.3^{+7.9}_{-1.4}$	$8.05^{+4.34}_{-3.56}$	$2.7^{+10.0}_{-1.7}$	Voigt & Fabian (2006)	200/2E4	0.3/0.7/0.7
Abell 2319	0.0564	19 21 08.8	+43 57 30	X-ray	$1.28^{+0.27}_{-0.22}$	$46.0^{+4.57}_{-5.82}$	$1.83^{+0.39}_{-0.31}$	$68.86^{+6.84}_{-8.71}$	Babyk et al. (2014)	200	0.27/0.73/0.73
Abell 2319	0.0564	19 21 08.8	+43 57 30	X-ray	$5.8^{+0.2}_{-0.2}$	—	$7.6^{+0.3}_{-0.3}$	—	Xu et al. (2001)	200	0.3/0.7/0.5
Abell 133	0.0569	01 02 42.1	-21 52 25	LOSVD	$8.56^{+1.13}_{-4.31}$	$4.88^{+1.26}_{-0.95}$	$11.09^{+1.47}_{-5.59}$	$5.64^{+1.46}_{-1.1}$	Wojtak & Lokas (2010)	102	0.3/0.7/0.7
Abell 133	0.0569	01 02 42.1	-21 52 25	X-ray	$8.11^{+0.25}_{-0.26}$	$16.34^{+3.55}_{-2.17}$	$10.71^{+0.33}_{-0.34}$	$19.15^{+4.16}_{-2.54}$	Babyk et al. (2014)	200	0.27/0.73/0.73
Abell 133	0.0569	01 02 42.1	-21 52 25	X-ray	$4.77^{+0.42}_{-0.42}$	$4.41^{+0.59}_{-0.59}$	$6.28^{+0.53}_{-0.53}$	$5.33^{+0.77}_{-0.77}$	Vikhlinin et al. (2006)	500	0.3/0.7/0.71
Abell 2256	0.058	17 03 43.5	+78 43 03	X-ray	$1.16^{+0.37}_{-0.27}$	$47.78^{+5.37}_{-5.29}$	$1.67^{+0.53}_{-0.39}$	$72.93^{+8.2}_{-8.07}$	Babyk et al. (2014)	200	0.27/0.73/0.73
Abell 2415	0.0581	22 05 40.5	-05 35 36	LOSVD	$5.5^{+1.5}_{-1.94}$	$3.04^{+0.75}_{-0.48}$	$7.22^{+1.97}_{-2.54}$	$3.63^{+0.89}_{-0.58}$	Wojtak & Lokas (2010)	102	0.3/0.7/0.7
Abell 2399	0.0582	21 57 25.8	-07 47 41	CM	7.12	1.43	9.28	1.68	Rines & Diaferio (2006)	200	0.3/0.7/None
Abell 2169	0.0585	16 14 09.6	+49 09 11	CM	3.79	1.14	5.04	1.42	Rines & Diaferio (2006)	200	0.3/0.7/None
Abell 1991	0.0586	14 54 31.4	+18 38 31	X-ray	$5.78^{+0.35}_{-0.35}$	$1.63^{+0.18}_{-0.18}$	$7.56^{+0.45}_{-0.45}$	$1.94^{+0.22}_{-0.22}$	Pointecouteau et al. (2005)	200	0.3/0.7/0.7
Abell 1991	0.0586	14 54 31.4	+18 38 31	X-ray	$5.7^{+0.4}_{-0.3}$	1.63	$7.5^{+0.5}_{-0.4}$	1.94	Pratt & Arnaud (2005)	200	0.3/0.7/0.7
Abell 1991	0.0586	14 54 31.4	+18 38 31	X-ray	$6.4^{+0.46}_{-0.46}$	$1.65^{+0.24}_{-0.24}$	$8.35^{+0.58}_{-0.58}$	$1.94^{+0.3}_{-0.3}$	Vikhlinin et al. (2006)	500	0.3/0.7/0.71
Abell 3266	0.0594	04 31 24.1	-61 26 38	X-ray	$8.36^{+0.83}_{-0.81}$	$33.25^{+4.16}_{-3.27}$	$11.03^{+1.1}_{-1.07}$	$38.86^{+4.86}_{-3.82}$	Babyk et al. (2014)	200	0.27/0.73/0.73
Abell 3266	0.0594	04 31 24.1	-61 26 38	X-ray	$3.9^{+0.2}_{-0.2}$	—	$5.2^{+0.3}_{-0.3}$	—	Xu et al. (2001)	200	0.3/0.7/0.5
Abell 3158	0.0597	03 42 53.9	-53 38 07	LOSVD	$8.71^{+1.07}_{-2.82}$	$11.11^{+2.11}_{-1.62}$	$11.28^{+1.39}_{-3.65}$	$12.81^{+2.43}_{-1.87}$	Wojtak & Lokas (2010)	102	0.3/0.7/0.7
Abell 3158	0.0597	03 42 53.9	-53 38 07	X-ray	$2.19^{+0.8}_{-0.81}$	$25.8^{+3.17}_{-2.72}$	$3.04^{+1.11}_{-1.12}$	$35.1^{+4.31}_{-3.7}$	Babyk et al. (2014)	200	0.27/0.73/0.73
Abell 3158	0.0597	03 42 53.9	-53 38 07	LOSVD	$2.5^{+0.57}_{-1.8}$	$11.4^{+1.7}_{-3.0}$	$3.5^{+7.5}_{-2.5}$	$15.4^{+7.6}_{-5.4}$	Lokas et al. (2006)	virial	0.3/0.7/0.7
Abell 602	0.0606	07 53 24.2	+29 21 58	CM	10.12	6.41	13.06	7.33	Rines & Diaferio (2006)	200	0.3/0.7/None

Continued on next page

Table C.1 – *Continued*

Cluster	z	RA	Dec.	Method	$c_{200}$	$M_{200}$ ( $10^{14} M_\odot$ )	$c_{\text{vir}}$	$M_{\text{vir}}$ ( $10^{14} M_\odot$ )	Ref.	$\delta$	$\Omega_m/\Omega_\Lambda/h$
Abell 3809	0.0623	21 46 57.8	-43 54 36	LOSVD	$2.56^{+0.56}_{-1.08}$	$1.71^{+0.45}_{-0.38}$	$3.45^{+0.75}_{-1.45}$	$2.23^{+0.58}_{-0.49}$	Wojtak & Lokas (2010)	102	0.3/0.7/0.7
Abell 2734	0.0625	00 11 20.7	-28 51 18	LOSVD	$2.66^{+0.1}_{-1.21}$	$3.96^{+0.3}_{-1.42}$	$3.58^{+0.14}_{-1.63}$	$5.14^{+0.38}_{-1.84}$	Wojtak & Lokas (2010)	102	0.3/0.7/0.7
RXCJ1351.7+4622	0.063	13 51 45.6	+46 22 00	CM	2.8	0.73	3.76	0.94	Rines & Diaferio (2006)	200	0.3/0.7/None
Abell 1795	0.063	13 48 53.0	+26 35 44	LOSVD	$7.97^{+0.96}_{-2.76}$	$6.87^{+1.07}_{-0.94}$	$10.33^{+1.25}_{-2.16}$	$7.96^{+1.24}_{-1.09}$	Wojtak & Lokas (2010)	102	0.3/0.7/0.7
Abell 1795	0.063	13 48 53.0	+26 35 44	X-ray	$4.61^{+0.55}_{-0.88}$	$19.34^{+2.18}_{-2.16}$	$6.19^{+0.74}_{-1.18}$	$23.87^{+2.69}_{-2.67}$	Babyk et al. (2014)	200	0.27/0.73/0.73
Abell 1795	0.063	13 48 53.0	+26 35 44	X-ray	$4.45^{+0.86}_{-0.77}$	$7.48^{+2.32}_{-1.58}$	$5.86^{+1.09}_{-0.98}$	$9.07^{+3.03}_{-2.03}$	Schmidt & Allen (2007)	virial	0.3/0.7/0.7
Abell 1795	0.063	13 48 53.0	+26 35 44	X-ray	$4.28^{+2.23}_{-2.41}$	$8.9^{+54.5}_{-5.6}$	$5.64^{+2.84}_{-3.09}$	$10.8^{+74.4}_{-7.0}$	Voigt & Fabian (2006)	200/2E4	0.3/0.7/0.7
Abell 1795	0.063	13 48 53.0	+26 35 44	X-ray	$4.82^{+0.26}_{-0.26}$	$8.38^{+0.79}_{-0.79}$	$6.32^{+0.33}_{-0.33}$	$10.1^{+1.01}_{-1.01}$	Vikhlinin et al. (2006)	500	0.3/0.7/0.71
Abell 1795	0.063	13 48 53.0	+26 35 44	X-ray	$7.6^{+0.3}_{-0.3}$	–	$9.9^{+0.4}_{-0.4}$	–	Xu et al. (2001)	200	0.3/0.7/0.5
RXC J0216.7-4749	0.0635	02 16 42.3	-47 49 24	X-ray	$3.45^{+0.39}_{-0.39}$	$0.196^{+0.018}_{-0.016}$	$4.59^{+0.52}_{-0.52}$	$0.246^{+0.023}_{-0.021}$	Démocles et al. (2010)	500	0.3/0.7/0.7
Abell 1436	0.0648	12 00 22.0	+56 13 49	LOSVD	$4.2^{+0.9}_{-0.9}$	3.65	$5.5^{+1.2}_{-1.2}$	4.46	Abdullah et al. (2011)	virial	0.3/0.7/None
Abell 1436	0.0648	12 00 22.0	+56 13 49	CM	1.99	1.11	2.71	1.5	Rines & Diaferio (2006)	200	0.3/0.7/None
Abell 2124	0.065	15 45 00.0	+36 03 58	X-ray	$11.36^{+2.84}_{-2.81}$	$13.12^{+1.37}_{-1.27}$	$14.85^{+3.71}_{-3.67}$	$15.0^{+1.57}_{-1.45}$	Babyk et al. (2014)	200	0.27/0.73/0.73
Abell 2124	0.065	15 45 00.0	+36 03 58	CM	10.93	8.29	14.05	9.42	Rines & Diaferio (2006)	200	0.3/0.7/None
Abell 2149	0.0653	16 01 38.1	+53 52 43	CM	1.09	0.19	1.54	0.29	Rines & Diaferio (2006)	200	0.3/0.7/None
Abell 1066	0.0684	10 39 27.9	+05 10 46	LOSVD	$8.5^{+2.4}_{-2.4}$	4.96	$11.0^{+3.0}_{-3.0}$	5.72	Abdullah et al. (2011)	virial	0.3/0.7/None
Abell 1066	0.0684	10 39 27.9	+05 10 46	CM	11.13	6.27	14.3	7.12	Rines & Diaferio (2006)	200	0.3/0.7/None
RXCJ1115.5+5426	0.0701	11 15 32.8	+54 26 06	CM	6.73	3.91	8.75	4.6	Rines & Diaferio (2006)	200	0.3/0.7/None
Abell 644	0.0704	08 17 24.5	-07 30 46	X-ray	$2.19^{+0.25}_{-0.27}$	$32.55^{+3.51}_{-2.99}$	$3.03^{+0.35}_{-0.37}$	$44.13^{+4.76}_{-4.05}$	Babyk et al. (2014)	200	0.27/0.73/0.73
Abell 644	0.0704	08 17 24.5	-07 30 46	X-ray	$4.6^{+0.9}_{-0.9}$	7.0	$6.0^{+1.2}_{-1.2}$	8.0	Buote et al. (2005)	virial	0.3/0.7/0.7
Abell 644	0.0704	08 17 24.5	-07 30 46	X-ray	$4.6^{+0.2}_{-0.2}$	–	$6.0^{+0.3}_{-0.3}$	–	Xu et al. (2001)	200	0.3/0.7/0.5
Abell 1767	0.0714	13 36 06.1	+59 12 28	LOSVD	$3.7^{+1.1}_{-1.1}$	6.48	$4.9^{+1.4}_{-1.4}$	8.02	Abdullah et al. (2011)	virial	0.3/0.7/None
Abell 1767	0.0714	13 36 06.1	+59 12 28	LOSVD	$4.05^{+0.15}_{-1.87}$	$9.52^{+1.13}_{-2.89}$	$5.34^{+0.2}_{-2.46}$	$11.71^{+1.38}_{-3.56}$	Wojtak & Lokas (2010)	102	0.3/0.7/0.7
Abell 1767	0.0714	13 36 06.1	+59 12 28	CM	6.12	7.27	7.97	8.62	Rines & Diaferio (2006)	200	0.3/0.7/None
Abell 1691	0.072	13 11 23.2	+39 12 05	LOSVD	$2.65^{+0.67}_{-1.15}$	$4.07^{+1.28}_{-0.77}$	$3.56^{+0.9}_{-1.55}$	$5.27^{+1.66}_{-1.0}$	Wojtak & Lokas (2010)	102	0.3/0.7/0.7
Abell 399	0.072	02 57 56.4	+13 00 59	X-ray	$2.15^{+0.37}_{-0.33}$	$37.9^{+3.94}_{-4.11}$	$2.97^{+0.51}_{-0.46}$	$51.5^{+5.35}_{-5.58}$	Babyk et al. (2014)	200	0.27/0.73/0.73
RXJ1053.7+5450	0.0727	10 53 43.9	+54 52 20	CM	8.49	4.57	10.96	5.28	Rines & Diaferio (2006)	200	0.3/0.7/None
Abell 2462	0.073	22 39 16.4	-17 19 46	X-ray	$13.23^{+0.72}_{-0.67}$	$20.73^{+2.47}_{-2.49}$	$17.2^{+0.94}_{-0.87}$	$23.47^{+2.8}_{-2.82}$	Babyk et al. (2014)	200	0.27/0.73/0.73
Abell 2065	0.073	15 22 42.6	+27 43 21	X-ray	$2.38^{+0.64}_{-0.56}$	$39.43^{+5.82}_{-4.18}$	$3.27^{+0.88}_{-0.77}$	$52.76^{+7.79}_{-5.59}$	Babyk et al. (2014)	200	0.27/0.73/0.73
Abell 1238	0.0733	11 22 58.0	+01 05 32	LOSVD	$3.8^{+2.2}_{-2.2}$	1.35	$5.0^{+2.8}_{-2.8}$	1.66	Abdullah et al. (2011)	virial	0.3/0.7/None

Continued on next page

Table C.1 – *Continued*

Cluster	z	RA	Dec.	Method	$c_{200}$	$M_{200}$ ( $10^{14} M_\odot$ )	$c_{\text{vir}}$	$M_{\text{vir}}$ ( $10^{14} M_\odot$ )	Ref.	$\delta$	$\Omega_m/\Omega_\Lambda/h$
Abell 2067	0.0737	15 23 07.9	+30 50 42	CM	18.24	0.51	23.22	0.57	Rines & Diaferio (2006)	200	0.3/0.7/None
Abell 2064	0.0738	15 20 59.4	+48 38 17	CM	6.67	2.6	8.66	3.06	Rines & Diaferio (2006)	200	0.3/0.7/None
Abell 1569	0.074	12 36 18.7	+16 35 30	X-ray	$10.37^{+2.01}_{-2.04}$	$14.35^{+1.34}_{-1.11}$	$13.54^{+2.62}_{-2.66}$	$16.48^{+1.54}_{-1.27}$	Babyk et al. (2014)	200	0.27/0.73/0.73
Abell 401	0.0748	02 58 57.5	+13 34 46	X-ray	$3.19^{+0.38}_{-0.33}$	$37.97^{+4.16}_{-2.81}$	$4.32^{+0.51}_{-0.45}$	$48.79^{+5.35}_{-3.61}$	Babyk et al. (2014)	200	0.27/0.73/0.73
Abell 401	0.0748	02 58 57.5	+13 34 46	X-ray	$4.2^{+0.3}_{-0.3}$	—	$5.5^{+0.4}_{-0.4}$	—	Xu et al. (2001)	200	0.3/0.7/0.5
Abell 3112	0.075	03 17 58.5	-44 14 20	X-ray	$9.36^{+0.73}_{-0.73}$	$18.84^{+3.14}_{-2.16}$	$12.25^{+0.96}_{-0.96}$	$21.78^{+3.63}_{-2.5}$	Babyk et al. (2014)	200	0.27/0.73/0.73
Abell 3112	0.075	03 17 58.5	-44 14 20	X-ray	$7.06^{+3.62}_{-3.23}$	$2.9^{+13.5}_{-1.9}$	$9.14^{+2.82}_{-3.05}$	$3.4^{+16.4}_{-2.2}$	Voigt & Fabian (2006)	200/2E4	0.3/0.7/0.7
Abell 1424	0.0754	11 57 28.7	+05 03 46	LOSVD	$5.4^{+1.9}_{-1.9}$	2.32	$7.0^{+2.4}_{-2.4}$	2.76	Abdullah et al. (2011)	virial	0.3/0.7/None
Abell 1424	0.0754	11 57 28.7	+05 03 46	CM	5.92	4.21	7.71	5.0	Rines & Diaferio (2006)	200	0.3/0.7/None
Abell 1190	0.0755	11 11 38.5	+40 50 33	LOSVD	$2.93^{+0.44}_{-1.21}$	$3.49^{+0.45}_{-0.82}$	$3.91^{+0.59}_{-1.61}$	$4.46^{+0.58}_{-1.05}$	Wojtak & Lokas (2010)	102	0.3/0.7/0.7
Abell 1190	0.0755	11 11 38.5	+40 50 33	CM	6.08	3.29	7.91	3.9	Rines & Diaferio (2006)	200	0.3/0.7/None
Abell 1205	0.0756	11 13 20.7	+02 31 56	LOSVD	$12.5^{+6.3}_{-6.3}$	3.33	$16.0^{+8.0}_{-8.0}$	3.76	Abdullah et al. (2011)	virial	0.3/0.7/None
Abell 1205	0.0756	11 13 20.7	+02 31 56	CM	2.05	3.66	2.78	4.91	Rines & Diaferio (2006)	200	0.3/0.7/None
Abell 1173	0.076	11 09 18.8	+41 33 45	CM	5.9	1.19	7.68	1.41	Rines & Diaferio (2006)	200	0.3/0.7/None
Abell 2670	0.0761	23 54 13.7	-10 25 08	LOSVD	$14.1^{+3.2}_{-3.2}$	6.79	$18.0^{+4.0}_{-4.0}$	7.63	Abdullah et al. (2011)	virial	0.3/0.7/None
Abell 2670	0.0761	23 54 13.7	-10 25 08	LOSVD	$11.62^{+1.02}_{-3.67}$	$7.25^{+0.95}_{-0.79}$	$14.88^{+1.3}_{-4.7}$	$8.2^{+1.08}_{-0.89}$	Wojtak & Lokas (2010)	102	0.3/0.7/0.7
Abell 2670	0.0761	23 54 13.7	-10 25 08	X-ray	$5.33^{+1.11}_{-1.09}$	$16.62^{+1.25}_{-1.62}$	$7.08^{+1.47}_{-1.45}$	$20.15^{+1.52}_{-1.96}$	Babyk et al. (2014)	200	0.27/0.73/0.73
Abell 2670	0.0761	23 54 13.7	-10 25 08	CM	3.35	2.03	4.45	2.56	Rines & Diaferio (2006)	200	0.3/0.7/None
RXCJ1210.3+0523	0.0764	12 10 19.9	+05 22 25	CM	3.96	0.84	5.22	1.04	Rines & Diaferio (2006)	200	0.3/0.7/None
Abell 2029	0.0767	15 10 55.0	+05 43 12	X-ray	$6.99^{+0.41}_{-0.43}$	$33.43^{+3.71}_{-4.12}$	$9.21^{+0.54}_{-0.57}$	$39.52^{+4.39}_{-4.87}$	Babyk et al. (2014)	200	0.27/0.73/0.73
Abell 2029	0.0767	15 10 55.0	+05 43 12	X-ray	$6.64^{+0.34}_{-0.38}$	$7.66^{+0.77}_{-0.58}$	$8.6^{+0.42}_{-0.48}$	$8.97^{+0.94}_{-0.71}$	Schmidt & Allen (2007)	virial	0.3/0.7/0.7
Abell 2029	0.0767	15 10 55.0	+05 43 12	X-ray	$4.38^{+1.64}_{-1.76}$	$20.0^{+57.0}_{-16.0}$	$5.74^{+2.08}_{-2.24}$	$24.0^{+74.0}_{-20.0}$	Voigt & Fabian (2006)	200/2E4	0.3/0.7/0.7
Abell 2029	0.0767	15 10 55.0	+05 43 12	X-ray	$6.0^{+0.3}_{-0.3}$	$10.81^{+1.08}_{-1.08}$	$7.8^{+0.38}_{-0.38}$	$12.76^{+1.33}_{-1.33}$	Vikhlinin et al. (2006)	500	0.3/0.7/0.71
Abell 2029	0.0767	15 10 55.0	+05 43 12	X-ray	$4.4^{+0.9}_{-0.9}$	$12.0^{+2.0}_{-2.0}$	$5.8^{+1.1}_{-1.1}$	$15.0^{+3.0}_{-3.0}$	Lewis et al. (2003)	200	0.3/0.7/0.7
Abell 2029	0.0767	15 10 55.0	+05 43 12	X-ray	$8.4^{+0.6}_{-0.6}$	—	$10.8^{+0.8}_{-0.8}$	—	Xu et al. (2001)	200	0.3/0.7/0.5
ZwCl 1215.1+0400	0.0772	12 17 40.6	+03 39 45	X-ray	$5.62^{+0.42}_{-0.4}$	$33.71^{+4.17}_{-4.29}$	$7.45^{+0.56}_{-0.53}$	$40.65^{+5.03}_{-5.17}$	Babyk et al. (2014)	200	0.27/0.73/0.73
ZwCl 1215.1+0400	0.0772	12 17 40.6	+03 39 45	CM	6.78	2.54	8.79	2.98	Rines & Diaferio (2006)	200	0.3/0.7/None
Abell 1773	0.0782	13 42 05.5	+02 13 39	LOSVD	$3.89^{+1.18}_{-1.31}$	$5.07^{+1.13}_{-0.88}$	$5.12^{+1.55}_{-1.73}$	$6.25^{+1.39}_{-1.09}$	Wojtak & Lokas (2010)	102	0.3/0.7/0.7
Abell 1773	0.0782	13 42 05.5	+02 13 39	CM	9.83	2.61	12.63	2.98	Rines & Diaferio (2006)	200	0.3/0.7/None
Abell 2061	0.0783	15 21 17.0	+30 38 24	LOSVD	$9.3^{+2.4}_{-2.4}$	4.78	$12.0^{+3.0}_{-3.0}$	5.48	Abdullah et al. (2011)	virial	0.3/0.7/None

Continued on next page

Table C.1 – *Continued*

Cluster	z	RA	Dec.	Method	$c_{200}$	$M_{200}$ ( $10^{14} M_\odot$ )	$c_{\text{vir}}$	$M_{\text{vir}}$ ( $10^{14} M_\odot$ )	Ref.	$\delta$	$\Omega_m/\Omega_\Lambda/h$
Abell 2061	0.0783	15 21 17.0	+30 38 24	CM	6.35	6.41	8.24	7.56	Rines & Diaferio (2006)	200	0.3/0.7/None
Abell 1809	0.079	13 53 06.4	+05 08 59	LOSVD	$4.6^{+1.5}_{-1.5}$	2.88	$6.0^{+1.9}_{-1.9}$	3.47	Abdullah et al. (2011)	virial	0.3/0.7/None
Abell 1809	0.079	13 53 06.4	+05 08 59	LOSVD	$6.95^{+0.73}_{-2.42}$	$4.22^{+0.77}_{-0.55}$	$8.99^{+0.95}_{-3.13}$	$4.93^{+0.9}_{-0.64}$	Wojtak & Lokas (2010)	102	0.3/0.7/0.7
Abell 1809	0.079	13 53 06.4	+05 08 59	CM	2.9	2.13	3.87	2.73	Rines & Diaferio (2006)	200	0.3/0.7/None
Abell 1035B	0.0801	10 32 14.16	+40 14 49.2	CM	4.53	2.86	5.94	3.48	Rines & Diaferio (2006)	200	0.3/0.7/None
Abell 2255	0.0801	17 12 31.0	+64 05 33	LOSVD	$16.5^{+10.4}_{-10.4}$	9.06	$21.0^{+13.0}_{-13.0}$	10.1	Abdullah et al. (2011)	virial	0.3/0.7/None
Abell 2255	0.0801	17 12 31.0	+64 05 33	CM	5.96	8.24	7.75	9.77	Rines & Diaferio (2006)	200	0.3/0.7/None
RXJ1159.8+5531	0.081	11 59 51.4	+55 32 01	X-ray	$8.3^{+2.1}_{-2.1}$	$0.789^{+0.451}_{-0.451}$	$10.6^{+2.7}_{-2.7}$	$0.909^{+0.536}_{-0.536}$	Gastaldello et al. (2007a)	500	0.3/0.7/0.7
RXJ1159.8+5531	0.081	11 59 51.4	+55 32 01	X-ray	$2.63^{+0.43}_{-0.43}$	–	$3.51^{+0.55}_{-0.55}$	–	Vikhlinin et al. (2006)	500	0.3/0.7/0.71
Abell 1651	0.0825	12 59 21.5	-04 11 41	X-ray	$4.29^{+0.74}_{-0.71}$	$19.48^{+2.45}_{-2.17}$	$5.73^{+0.99}_{-0.95}$	$24.12^{+3.03}_{-2.69}$	Babyk et al. (2014)	200	0.27/0.73/0.73
Abell 1651	0.0825	12 59 21.5	-04 11 41	X-ray	$4.9^{+0.2}_{-0.2}$	–	$6.4^{+0.3}_{-0.3}$	–	Xu et al. (2001)	200	0.3/0.7/0.5
RXJ1326.2+0013	0.0827	13 26 17.6	+00 13 17	CM	2.98	0.89	3.97	1.13	Rines & Diaferio (2006)	200	0.3/0.7/None
MS 1306	0.0832	13 09 16.99	-01 36 45.0	CM	3.25	0.71	4.31	0.9	Rines & Diaferio (2006)	200	0.3/0.7/None
Abell 2428	0.0836	22 16 15.5	-09 20 24	CM	3.07	1.56	4.08	1.98	Rines & Diaferio (2006)	200	0.3/0.7/None
Abell 1663	0.0837	13 02 50.7	-02 30 22	LOSVD	$14.1^{+9.6}_{-9.6}$	3.7	$18.0^{+12.0}_{-12.0}$	4.15	Abdullah et al. (2011)	virial	0.3/0.7/None
Abell 1663	0.0837	13 02 50.7	-02 30 22	CM	4.06	5.07	5.34	6.24	Rines & Diaferio (2006)	200	0.3/0.7/None
Abell 1459	0.0839	12 04 15.7	+02 30 18	LOSVD	$26.1^{+5.6}_{-5.6}$	1.53	$33.0^{+7.0}_{-7.0}$	1.67	Abdullah et al. (2011)	virial	0.3/0.7/None
Abell 1650	0.0843	12 58 41.1	-01 45 25	LOSVD	$2.12^{+0.25}_{-0.78}$	$5.98^{+1.08}_{-1.23}$	$2.87^{+0.34}_{-1.05}$	$7.99^{+1.44}_{-1.65}$	Wojtak & Lokas (2010)	102	0.3/0.7/0.7
Abell 1650	0.0843	12 58 41.1	-01 45 25	X-ray	$2.03^{+0.35}_{-0.37}$	$39.44^{+3.74}_{-2.78}$	$2.8^{+0.48}_{-0.51}$	$53.84^{+5.11}_{-3.8}$	Babyk et al. (2014)	200	0.27/0.73/0.73
Abell 1650	0.0843	12 58 41.1	-01 45 25	CM	2.3	1.56	3.09	2.05	Rines & Diaferio (2006)	200	0.3/0.7/None
Abell 2597	0.0852	23 25 20.0	-12 07 38	X-ray	$8.28^{+1.27}_{-1.26}$	$10.76^{+1.27}_{-1.22}$	$10.83^{+1.66}_{-1.65}$	$12.53^{+1.48}_{-1.42}$	Babyk et al. (2014)	200	0.27/0.73/0.73
Abell 2597	0.0852	23 25 20.0	-12 07 38	X-ray	$5.86^{+0.5}_{-0.5}$	$3.0^{+0.33}_{-0.33}$	$7.59^{+0.63}_{-0.63}$	$3.54^{+0.42}_{-0.42}$	Pointecouteau et al. (2005)	200	0.3/0.7/0.7
Abell 2597	0.0852	23 25 20.0	-12 07 38	X-ray	$6.7^{+0.6}_{-0.6}$	–	$8.7^{+0.8}_{-0.8}$	–	Xu et al. (2001)	200	0.3/0.7/0.5
Abell 1750N	0.0856	13 30 49.9	-01 52 22	WL	$3.97^{+2.71}_{-2.71}$	$3.39^{+2.68}_{-2.68}$	$5.21^{+3.42}_{-3.42}$	$4.14^{+2.97}_{-2.97}$	Okabe & Umetsu (2008)	virial	0.3/0.7/0.7
Abell 1750C	0.0856	13 30 49.9	-01 52 22	WL	$4.22^{+3.87}_{-3.87}$	$2.21^{+2.13}_{-2.13}$	$5.52^{+4.89}_{-4.89}$	$2.69^{+2.33}_{-2.33}$	Okabe & Umetsu (2008)	virial	0.3/0.7/0.7
Abell 1750	0.0856	13 30 49.9	-01 52 22	CM	2.96	2.7	3.94	3.44	Rines & Diaferio (2006)	200	0.3/0.7/None
Abell 1552	0.0861	12 29 50.0	+11 44 26	CM	2.42	2.39	3.24	3.12	Rines & Diaferio (2006)	200	0.3/0.7/None
Abell 2249	0.0863	17 09 48.8	+34 26 26	CM	10.9	8.61	13.94	9.76	Rines & Diaferio (2006)	200	0.3/0.7/None
Abell 2245	0.0868	17 02 31.9	+33 30 47	CM	11.31	7.9	14.45	8.93	Rines & Diaferio (2006)	200	0.3/0.7/None
Abell 478	0.088	04 13 25.6	+10 28 01	WL	$3.4^{+1.25}_{-0.95}$	$13.06^{+4.52}_{-3.49}$	$4.56^{+1.67}_{-1.28}$	$16.48^{+5.7}_{-4.41}$	Okabe et al. (2015)	virial	0.27/0.73/0.70

Continued on next page

Table C.1 – *Continued*

Cluster	z	RA	Dec.	Method	$c_{200}$	$M_{200}$ ( $10^{14} M_\odot$ )	$c_{\text{vir}}$	$M_{\text{vir}}$ ( $10^{14} M_\odot$ )	Ref.	$\delta$	$\Omega_m/\Omega_\Lambda/h$
Abell 478	0.088	04 13 25.6	+10 28 01	X-ray	$4.51^{+0.51}_{-0.48}$	$23.35^{+2.62}_{-2.17}$	$6.01^{+0.68}_{-0.64}$	$28.72^{+3.22}_{-2.67}$	Babyk et al. (2014)	200	0.27/0.73/0.73
Abell 478	0.088	04 13 25.6	+10 28 01	X-ray	$3.92^{+0.36}_{-0.33}$	$13.1^{+2.3}_{-2.1}$	$5.13^{+0.45}_{-0.41}$	$16.0^{+3.0}_{-2.6}$	Schmidt & Allen (2007)	virial	0.3/0.7/0.7
Abell 478	0.088	04 13 25.6	+10 28 01	X-ray	$2.88^{+2.02}_{-2.88}$	$34.0^{+\infty}_{-26.0}$	$3.81^{+2.56}_{-3.81}$	$43.0^{+\infty}_{-33.0}$	Voigt & Fabian (2006)	200/2E4	0.3/0.7/0.7
Abell 478	0.088	04 13 25.6	+10 28 01	X-ray	$4.22^{+0.39}_{-0.39}$	$10.8^{+1.8}_{-1.8}$	$5.52^{+0.49}_{-0.49}$	$13.1^{+2.3}_{-2.3}$	Pointecouteau et al. (2005)	200	0.3/0.7/0.7
Abell 478	0.088	04 13 25.6	+10 28 01	X-ray	$5.33^{+0.39}_{-0.39}$	$10.53^{+1.51}_{-1.51}$	$6.92^{+0.49}_{-0.49}$	$12.51^{+1.88}_{-1.88}$	Vikhlinin et al. (2006)	500	0.3/0.7/0.71
Abell 478	0.088	04 13 25.6	+10 28 01	X-ray	$4.2^{+0.4}_{-0.4}$	11.0	$5.5^{+0.5}_{-0.5}$	13.0	Pointecouteau et al. (2004)	200	0.3/0.7/0.7
Abell 478	0.088	04 13 25.6	+10 28 01	X-ray	$3.67^{+0.31}_{-0.35}$	$18.4^{+4.8}_{-2.4}$	$4.82^{+0.39}_{-0.44}$	$22.6^{+6.2}_{-3.1}$	Allen et al. (2003)	200	0.3/0.7/0.5
Abell 478	0.088	04 13 25.6	+10 28 01	X-ray	$6.7^{+0.4}_{-0.4}$	–	$8.6^{+0.5}_{-0.5}$	–	Xu et al. (2001)	200	0.3/0.7/0.5
Abell 1885	0.0882	14 13 43.5	+43 39 48	CM	4.67	6.13	6.1	7.42	Rines & Diaferio (2006)	200	0.3/0.7/None
Abell 1728	0.0899	13 23 30.2	+11 17 46	CM	4.59	3.96	6.0	4.8	Rines & Diaferio (2006)	200	0.3/0.7/None
Abell 2142	0.0903	15 58 20.6	+27 13 37	LOSVD	$3.3^{+1.0}_{-1.0}$	7.77	$4.4^{+1.3}_{-1.3}$	9.69	Abdullah et al. (2011)	virial	0.3/0.7/None
Abell 2142	0.0903	15 58 20.6	+27 13 37	LOSVD	$2.24^{+0.3}_{-0.78}$	$12.32^{+1.78}_{-2.07}$	$3.01^{+0.41}_{-1.05}$	$16.29^{+2.35}_{-2.74}$	Wojtak & Lokas (2010)	102	0.3/0.7/0.7
Abell 2142	0.0903	15 58 20.6	+27 13 37	WL	$4.29^{+0.69}_{-0.61}$	$12.62^{+2.59}_{-1.89}$	$5.6^{+0.9}_{-0.8}$	$15.29^{+3.14}_{-2.29}$	Umetsu et al. (2009)	virial	0.3/0.7/0.7
Abell 2142	0.0903	15 58 20.6	+27 13 37	WL	$3.27^{+1.35}_{-1.35}$	$13.66^{+6.7}_{-6.7}$	$4.32^{+1.7}_{-1.7}$	$17.07^{+7.49}_{-7.49}$	Okabe & Umetsu (2008)	virial	0.3/0.7/0.7
Abell 2142	0.0903	15 58 20.6	+27 13 37	X-ray	$5.27^{+0.83}_{-0.79}$	$29.87^{+2.47}_{-3.17}$	$6.97^{+1.1}_{-1.04}$	$36.14^{+2.99}_{-3.84}$	Babyk et al. (2014)	200	0.27/0.73/0.73
Abell 2142	0.0903	15 58 20.6	+27 13 37	CM	1.97	4.56	2.66	6.13	Rines & Diaferio (2006)	200	0.3/0.7/None
Abell 2700	0.092	00 03 50.6	+02 03 48	X-ray	$8.06^{+1.52}_{-1.3}$	$1.9^{+0.23}_{-0.23}$	$10.35^{+1.95}_{-1.67}$	$2.19^{+0.27}_{-0.27}$	Ettori et al. (2011)	200	0.3/0.7/0.7
Abell 971	0.0923	10 19 46.7	+40 57 55	CM	10.49	4.57	13.4	5.19	Rines & Diaferio (2006)	200	0.3/0.7/None
Abell 954	0.0928	10 13 44.8	-00 06 31	LOSVD	$4.03^{+1.19}_{-1.49}$	$4.32^{+1.32}_{-0.95}$	$5.28^{+1.57}_{-1.95}$	$5.28^{+1.61}_{-1.16}$	Wojtak & Lokas (2010)	102	0.3/0.7/0.7
Abell 954	0.0928	10 13 44.8	-00 06 31	CM	0.58	0.84	0.85	1.44	Rines & Diaferio (2006)	200	0.3/0.7/None
Abell 3921	0.093	22 49 57.0	-64 25 46	X-ray	$5.27^{+0.73}_{-0.71}$	$29.61^{+2.15}_{-1.77}$	$6.97^{+0.97}_{-0.94}$	$35.81^{+2.6}_{-2.14}$	Babyk et al. (2014)	200	0.27/0.73/0.73
Abell 2175	0.0961	16 20 22.9	+29 54 54	LOSVD	$2.13^{+0.34}_{-1.2}$	$5.05^{+1.25}_{-1.33}$	$2.87^{+0.46}_{-1.62}$	$6.69^{+1.66}_{-1.77}$	Wojtak & Lokas (2010)	102	0.3/0.7/0.7
Abell 2175	0.0961	16 20 22.9	+29 54 54	CM	0.64	1.34	0.93	2.23	Rines & Diaferio (2006)	200	0.3/0.7/None
Abell 3911	0.097	22 46 18.6	-52 43 46	X-ray	$5.59^{+1.33}_{-1.39}$	$3.88^{+0.5}_{-0.5}$	$7.24^{+1.72}_{-1.8}$	$4.61^{+0.59}_{-0.59}$	Ettori et al. (2011)	200	0.3/0.7/0.7
Abell 2110	0.0971	15 39 48.7	+30 43 02	CM	4.69	2.14	6.11	2.59	Rines & Diaferio (2006)	200	0.3/0.7/None
Abell 2048	0.0972	15 15 17.8	+04 22 56	LOSVD	$31.0^{+20.9}_{-20.9}$	5.02	$39.0^{+26.0}_{-26.0}$	5.45	Abdullah et al. (2011)	virial	0.3/0.7/None
Abell 3827	0.098	22 01 56.0	-59 56 58	X-ray	$4.47^{+0.67}_{-0.64}$	$6.61^{+0.73}_{-0.73}$	$5.83^{+0.87}_{-0.83}$	$8.02^{+0.89}_{-0.89}$	Ettori et al. (2011)	200	0.3/0.7/0.7
Abell 3827	0.098	22 01 56.0	-59 56 58	X-ray	$4.45^{+0.67}_{-0.77}$	$78.9^{+5.26}_{-4.27}$	$5.91^{+0.89}_{-1.02}$	$96.98^{+6.47}_{-5.25}$	Babyk et al. (2014)	200	0.27/0.73/0.73
Abell 2244	0.0997	17 02 42.9	+34 03 43	X-ray	$2.43^{+0.84}_{-0.81}$	$36.52^{+3.16}_{-3.18}$	$3.3^{+1.14}_{-1.1}$	$48.31^{+4.18}_{-4.21}$	Babyk et al. (2014)	200	0.27/0.73/0.73
Abell 2244	0.0997	17 02 42.9	+34 03 43	CM	3.83	4.36	5.02	5.38	Rines & Diaferio (2006)	200	0.3/0.7/None

Continued on next page

Table C.1 – *Continued*

Cluster	z	RA	Dec.	Method	$c_{200}$	$M_{200}$ ( $10^{14} M_\odot$ )	$c_{\text{vir}}$	$M_{\text{vir}}$ ( $10^{14} M_\odot$ )	Ref.	$\delta$	$\Omega_m/\Omega_\Lambda/h$
PKS0745-191	0.103	07 47 31.3	-19 17 40	X-ray	$6.45^{+0.73}_{-0.61}$	$33.52^{+3.17}_{-3.17}$	$8.45^{+0.96}_{-0.8}$	$39.71^{+3.76}_{-3.76}$	Babyk et al. (2014)	200	0.27/0.73/0.73
PKS0745-191	0.103	07 47 31.3	-19 17 40	X-ray	$5.86^{+1.56}_{-1.07}$	$11.82^{+4.7}_{-3.55}$	$7.55^{+1.95}_{-1.34}$	$13.89^{+5.85}_{-1.07}$	Schmidt & Allen (2007)	virial	0.3/0.7/0.7
PKS0745-191	0.103	07 47 31.3	-19 17 40	X-ray	$5.46^{+3.22}_{-2.88}$	$9.7^{+52.2}_{-8.5}$	$7.05^{+4.04}_{-3.63}$	$11.0^{+67.0}_{-10.0}$	Voigt & Fabian (2006)	200/2E4	0.3/0.7/0.7
PKS0745-191	0.103	07 47 31.3	-19 17 40	X-ray	$5.12^{+0.4}_{-0.4}$	$10.0^{+1.2}_{-1.2}$	$6.62^{+0.5}_{-0.5}$	$11.9^{+1.5}_{-1.5}$	Pointecouteau et al. (2005)	200	0.3/0.7/0.7
PKS0745-191	0.103	07 47 31.3	-19 17 40	X-ray	$3.83^{+0.52}_{-0.27}$	$18.6^{+3.5}_{-4.0}$	$5.0^{+0.66}_{-0.34}$	$22.7^{+4.5}_{-5.1}$	Allen et al. (2003)	200	0.3/0.7/0.5
Abell 1446	0.104	12 01 51.5	+58 01 18	X-ray	$9.16^{+0.67}_{-0.72}$	$12.66^{+1.26}_{-1.15}$	$11.89^{+0.87}_{-0.93}$	$14.59^{+1.45}_{-1.33}$	Babyk et al. (2014)	200	0.27/0.73/0.73
RXCJ0049.4-2931	0.108	00 49 24.0	-29 31 28	X-ray	$12.77^{+3.8}_{-3.18}$	$0.94^{+0.16}_{-0.16}$	$16.17^{+4.81}_{-4.03}$	$1.05^{+0.18}_{-0.18}$	Ettori et al. (2011)	200	0.3/0.7/0.7
ZwCl0740.4+1740	0.1114	07 43 23.16	+17 33 40.0	WL	$1.8^{+1.5}_{-1.5}$	$7.0^{+4.4}_{-4.4}$	$2.4^{+1.9}_{-1.9}$	$9.5^{+7.1}_{-7.1}$	Sereno et al. (2014)	200	0.3/0.7/0.7
ZwCl0740.4+1740	0.1114	07 43 23.16	+17 33 40.0	WL	$2.09^{+1.49}_{-1.0}$	$4.36^{+4.06}_{-1.77}$	$2.85^{+2.03}_{-1.37}$	$5.89^{+5.48}_{-2.39}$	Okabe et al. (2010)	virial	0.27/0.73/0.72
Abell 2034	0.113	15 10 11.7	+33 30 53	X-ray	$2.46^{+0.81}_{-0.06}$	$17.64^{+2.17}_{-2.17}$	$3.26^{+1.07}_{-0.08}$	$22.82^{+2.81}_{-2.81}$	Ettori et al. (2011)	200	0.3/0.7/0.7
Abell 2034	0.113	15 10 11.7	+33 30 53	WL	$2.84^{+1.79}_{-1.79}$	$8.09^{+5.55}_{-5.55}$	$3.74^{+2.25}_{-2.25}$	$10.24^{+6.14}_{-6.14}$	Okabe & Umetsu (2008)	virial	0.3/0.7/0.7
Abell 2034	0.113	15 10 11.7	+33 30 53	X-ray	$2.46^{+0.59}_{-0.62}$	$19.98^{+2.54}_{-1.37}$	$3.33^{+0.8}_{-0.84}$	$26.28^{+3.34}_{-1.8}$	Babyk et al. (2014)	200	0.27/0.73/0.73
Abell 2051	0.115	15 16 34.0	-00 56 56	X-ray	$2.75^{+0.49}_{-0.06}$	$4.73^{+0.42}_{-0.42}$	$3.63^{+0.65}_{-0.08}$	$6.03^{+0.54}_{-0.54}$	Ettori et al. (2011)	200	0.3/0.7/0.7
Abell 1361	0.117	11 43 45.1	+46 21 21	X-ray	$7.28^{+0.83}_{-0.81}$	$11.07^{+1.34}_{-1.18}$	$9.46^{+1.08}_{-1.05}$	$12.95^{+1.57}_{-1.38}$	Babyk et al. (2014)	200	0.27/0.73/0.73
Abell 2050	0.118	15 16 19.2	+00 05 52	X-ray	$7.06^{+1.64}_{-1.54}$	$2.84^{+0.41}_{-0.41}$	$9.03^{+2.1}_{-1.97}$	$3.3^{+0.48}_{-0.48}$	Ettori et al. (2011)	200	0.3/0.7/0.7
Abell 3814	0.118	21 49 07.4	-30 41 55	X-ray	$4.79^{+0.43}_{-0.49}$	$2.21^{+0.21}_{-0.21}$	$6.19^{+0.56}_{-0.63}$	$2.65^{+0.25}_{-0.25}$	Ettori et al. (2011)	200	0.3/0.7/0.7
RXC J1141.4-1216	0.119	11 41 24.3	-12 16 20	X-ray	$3.15^{+0.19}_{-0.24}$	$4.88^{+0.37}_{-0.37}$	$4.13^{+0.25}_{-0.31}$	$6.12^{+0.46}_{-0.46}$	Ettori et al. (2011)	200	0.3/0.7/0.7
Abell 1664	0.128	13 03 41.8	-24 13 06	X-ray	$7.24^{+0.83}_{-0.81}$	$22.84^{+2.81}_{-2.19}$	$9.38^{+1.08}_{-1.05}$	$26.68^{+3.28}_{-2.56}$	Babyk et al. (2014)	200	0.27/0.73/0.73
Abell 1084	0.132	10 44 33.0	-07 04 22	X-ray	$4.56^{+0.34}_{-0.25}$	$2.86^{+0.18}_{-0.18}$	$5.88^{+0.44}_{-0.32}$	$3.44^{+0.22}_{-0.22}$	Ettori et al. (2011)	200	0.3/0.7/0.7
RXJ1416.4+2315	0.137	14 16 26.9	+23 15 31	X-ray	$11.2^{+4.5}_{-4.5}$	$3.1^{+1.0}_{-1.0}$	$14.1^{+5.6}_{-5.6}$	$3.5^{+1.3}_{-1.3}$	Khosroshahi et al. (2006)	200	0.3/0.7/0.7
Abell 1068	0.1375	10 40 43.9	+39 56 53	X-ray	$3.02^{+0.2}_{-0.22}$	$6.4^{+0.48}_{-0.48}$	$3.94^{+0.26}_{-0.29}$	$8.02^{+0.6}_{-0.6}$	Ettori et al. (2011)	200	0.3/0.7/0.7
Abell 1068	0.1375	10 40 43.9	+39 56 53	X-ray	$3.05^{+0.21}_{-0.22}$	$7.71^{+0.71}_{-0.78}$	$4.05^{+0.28}_{-0.29}$	$9.8^{+0.9}_{-0.99}$	Babyk et al. (2014)	200	0.27/0.73/0.73
Abell 1068	0.1375	10 40 43.9	+39 56 53	X-ray	$3.69^{+0.26}_{-0.26}$	$5.68^{+0.49}_{-0.49}$	$4.77^{+0.33}_{-0.33}$	$6.9^{+0.65}_{-0.65}$	Pointecouteau et al. (2005)	200	0.3/0.7/0.7
RXC J2218.6-3853	0.138	22 18 40.2	-38 53 51	X-ray	$3.16^{+0.85}_{-0.55}$	$8.76^{+1.62}_{-1.62}$	$4.12^{+1.11}_{-0.72}$	$10.92^{+2.02}_{-2.02}$	Ettori et al. (2011)	200	0.3/0.7/0.7
RXCJ0605.8-3518	0.141	06 05 52.8	-35 18 02	X-ray	$4.1^{+0.34}_{-0.34}$	$4.51^{+0.36}_{-0.36}$	$5.29^{+0.44}_{-0.44}$	$5.47^{+0.44}_{-0.44}$	Ettori et al. (2011)	200	0.3/0.7/0.7
RXCJ0605.8-3518	0.141	06 05 52.8	-35 18 02	X-ray	$4.14^{+0.33}_{-0.23}$	$6.37^{+0.75}_{-0.72}$	$5.43^{+0.43}_{-0.3}$	$7.81^{+0.92}_{-0.88}$	Babyk et al. (2014)	200	0.27/0.73/0.73
Abell 22	0.142	00 20 42.8	-25 42 37	X-ray	$4.17^{+1.41}_{-1.07}$	$10.03^{+2.67}_{-2.67}$	$5.37^{+1.82}_{-1.38}$	$12.14^{+3.23}_{-3.23}$	Ettori et al. (2011)	200	0.3/0.7/0.7
Abell 1413	0.143	11 55 18.9	+23 24 31	X-ray	$5.83^{+0.57}_{-0.35}$	$6.12^{+0.32}_{-0.32}$	$7.44^{+0.73}_{-0.45}$	$7.18^{+0.38}_{-0.38}$	Ettori et al. (2011)	200	0.3/0.7/0.7
Abell 1413	0.143	11 55 18.9	+23 24 31	X-ray	$5.85^{+0.67}_{-0.44}$	$8.53^{+1.18}_{-0.92}$	$7.59^{+0.87}_{-0.57}$	$10.12^{+1.4}_{-1.09}$	Babyk et al. (2014)	200	0.27/0.73/0.73
Abell 1413	0.143	11 55 18.9	+23 24 31	X-ray	$4.44^{+0.78}_{-0.75}$	$9.31^{+2.69}_{-1.77}$	$5.69^{+0.97}_{-0.94}$	$11.11^{+3.45}_{-2.23}$	Schmidt & Allen (2007)	virial	0.3/0.7/0.7

Continued on next page

Table C.1 – *Continued*

Cluster	z	RA	Dec.	Method	$c_{200}$	$M_{200}$ ( $10^{14} M_\odot$ )	$c_{\text{vir}}$	$M_{\text{vir}}$ ( $10^{14} M_\odot$ )	Ref.	$\delta$	$\Omega_m/\Omega_\Lambda/h$
Abell 1413	0.143	11 55 18.9	+23 24 31	X-ray	$5.82^{+0.5}_{-0.5}$	$6.5^{+0.65}_{-0.65}$	$7.41^{+0.62}_{-0.62}$	$7.59^{+0.82}_{-0.82}$	Pointecouteau et al. (2005)	200	0.3/0.7/0.7
Abell 1413	0.143	11 55 18.9	+23 24 31	X-ray	$4.42^{+0.24}_{-0.24}$	$10.67^{+1.17}_{-1.17}$	$5.66^{+0.3}_{-0.3}$	$12.73^{+1.47}_{-1.47}$	Vikhlinin et al. (2006)	500	0.3/0.7/0.71
Abell 2328	0.147	20 48 10.6	-17 50 38	X-ray	$2.23^{+1.63}_{-0.21}$	$5.96^{+1.12}_{-1.12}$	$2.94^{+2.15}_{-0.28}$	$7.73^{+1.45}_{-1.45}$	Ettori et al. (2011)	200	0.3/0.7/0.7
RXCJ0547.6-3152	0.148	05 47 38.2	-31 52 31	X-ray	$4.1^{+0.59}_{-1.17}$	$7.89^{+1.51}_{-1.51}$	$5.28^{+0.76}_{-1.51}$	$9.55^{+1.83}_{-1.83}$	Ettori et al. (2011)	200	0.3/0.7/0.7
RXCJ0547.6-3152	0.148	05 47 38.2	-31 52 31	X-ray	$4.14^{+0.57}_{-0.63}$	$11.06^{+1.17}_{-1.1}$	$5.42^{+0.75}_{-0.82}$	$13.55^{+1.43}_{-1.35}$	Babyk et al. (2014)	200	0.27/0.73/0.73
Abell 2204	0.152	16 32 46.5	+05 34 14	X-ray	$2.81^{+0.02}_{-0.28}$	$15.93^{+1.19}_{-1.19}$	$3.66^{+0.03}_{-0.36}$	$20.06^{+1.5}_{-1.5}$	Ettori et al. (2011)	200	0.3/0.7/0.7
Abell 2204	0.152	16 32 46.5	+05 34 14	WL	$7.1^{+6.2}_{-6.2}$	$7.2^{+2.7}_{-2.7}$	$9.0^{+7.9}_{-7.9}$	$8.3^{+3.1}_{-3.1}$	Corless et al. (2009)	200	0.3/0.7/0.7
Abell 2204	0.152	16 32 46.5	+05 34 14	X-ray	$2.83^{+0.32}_{-0.44}$	$23.35^{+3.16}_{-2.17}$	$3.76^{+0.43}_{-0.58}$	$29.83^{+4.04}_{-2.77}$	Babyk et al. (2014)	200	0.27/0.73/0.73
Abell 2204	0.152	16 32 46.5	+05 34 14	WL	6.3	–	8.0	–	Clowe (2003)	200	0.3/0.7/0.7
Abell 2204	0.152	16 32 46.5	+05 34 14	WL	6.3	$12.0^{+3.0}_{-2.0}$	8.0	$14.0^{+3.0}_{-2.0}$	Clowe & Schneider (2002)	200	0.3/0.7/None
Abell 2204	0.152	16 32 46.5	+05 34 14	WL	4.3	–	5.5	–	Clowe & Schneider (2001a)	200	0.3/0.7/0.7
Abell 2204	0.152	16 32 46.5	+05 34 14	X-ray	$9.75^{+2.92}_{-2.16}$	$7.48^{+2.63}_{-1.8}$	$12.2^{+3.6}_{-2.67}$	$8.44^{+3.14}_{-2.12}$	Schmidt & Allen (2007)	virial	0.3/0.7/0.7
Abell 2204	0.152	16 32 46.5	+05 34 14	X-ray	$4.59^{+0.37}_{-0.37}$	$11.8^{+1.3}_{-1.3}$	$5.86^{+0.46}_{-0.46}$	$14.0^{+1.7}_{-1.7}$	Pointecouteau et al. (2005)	200	0.3/0.7/0.7
Abell 3888	0.153	22 34 31.0	-37 44 06	X-ray	$4.28^{+2.31}_{-1.16}$	$13.42^{+4.15}_{-4.15}$	$5.49^{+2.96}_{-1.49}$	$16.16^{+5.0}_{-5.0}$	Ettori et al. (2011)	200	0.3/0.7/0.7
Abell 2009	0.153	15 00 20.40	+21 21 43.2	WL	$5.5^{+1.9}_{-1.9}$	$4.3^{+1.1}_{-1.1}$	$7.0^{+2.4}_{-2.4}$	$5.1^{+1.4}_{-1.4}$	Sereno et al. (2014)	200	0.3/0.7/0.7
Abell 2009	0.153	15 00 20.40	+21 21 43.2	WL	$5.09^{+1.85}_{-1.32}$	$3.24^{+1.01}_{-0.78}$	$6.59^{+2.4}_{-1.71}$	$3.86^{+1.2}_{-0.93}$	Okabe et al. (2010)	virial	0.27/0.73/0.72
Abell 907	0.1527	09 58 22.2	-11 03 35	X-ray	$2.39^{+0.42}_{-0.39}$	$11.94^{+2.02}_{-2.02}$	$3.13^{+0.55}_{-0.51}$	$15.33^{+2.59}_{-2.59}$	Ettori et al. (2011)	200	0.3/0.7/0.7
Abell 907	0.1527	09 58 22.2	-11 03 35	X-ray	$6.25^{+1.01}_{-0.89}$	$6.54^{+0.73}_{-0.72}$	$8.07^{+1.3}_{-1.15}$	$7.7^{+0.86}_{-0.85}$	Babyk et al. (2014)	200	0.27/0.73/0.73
Abell 907	0.1527	09 58 22.2	-11 03 35	X-ray	$5.21^{+0.6}_{-0.6}$	$6.28^{+0.63}_{-0.63}$	$6.61^{+0.75}_{-0.75}$	$7.37^{+0.82}_{-0.82}$	Vikhlinin et al. (2006)	500	0.3/0.7/0.71
Abell 1240	0.159	11 23 32.1	+43 06 32	X-ray	$6.38^{+0.28}_{-0.15}$	$7.34^{+0.94}_{-0.81}$	$8.22^{+0.36}_{-0.19}$	$8.62^{+1.1}_{-0.95}$	Babyk et al. (2014)	200	0.27/0.73/0.73
RXCJ2014.8-2430	0.161	20 14 49.7	-24 30 30	X-ray	$3.86^{+0.15}_{-0.3}$	$7.56^{+0.53}_{-0.53}$	$4.96^{+0.19}_{-0.39}$	$9.18^{+0.64}_{-0.64}$	Ettori et al. (2011)	200	0.3/0.7/0.7
RXCJ2014.8-2430	0.161	20 14 49.7	-24 30 30	X-ray	$3.88^{+0.54}_{-0.67}$	$10.53^{+1.48}_{-1.47}$	$5.07^{+0.71}_{-0.88}$	$12.95^{+1.82}_{-1.81}$	Babyk et al. (2014)	200	0.27/0.73/0.73
RXJ1720.1+2638	0.164	17 20 08.88	+26 38 06.0	WL	$8.5^{+4.1}_{-4.1}$	$4.6^{+1.4}_{-1.4}$	$10.7^{+5.0}_{-5.0}$	$5.2^{+1.8}_{-1.8}$	Sereno et al. (2014)	200	0.3/0.7/0.7
RXJ1720.1+2638	0.164	17 20 08.88	+26 38 06.0	WL	$6.81^{+4.37}_{-2.4}$	$3.5^{+1.42}_{-1.05}$	$8.73^{+5.6}_{-3.08}$	$4.07^{+1.65}_{-1.22}$	Okabe et al. (2010)	virial	0.27/0.73/0.72
Abell 3404	0.167	06 45 29.3	-54 13 08	X-ray	$4.58^{+1.06}_{-0.96}$	$7.08^{+1.12}_{-1.12}$	$5.84^{+1.35}_{-1.22}$	$8.45^{+1.34}_{-1.34}$	Ettori et al. (2011)	200	0.3/0.7/0.7
Abell 1201	0.169	11 12 54.9	+13 26 41	X-ray	$6.27^{+0.83}_{-0.81}$	$5.43^{+0.59}_{-0.66}$	$8.05^{+1.07}_{-1.04}$	$6.37^{+0.69}_{-0.77}$	Babyk et al. (2014)	200	0.27/0.73/0.73
Abell 586	0.171	07 32 22.32	+31 38 02.4	WL	$1.0^{+0.4}_{-0.4}$	$22.6^{+13.3}_{-13.3}$	$1.4^{+0.5}_{-0.5}$	$32.9^{+21.8}_{-21.8}$	Sereno et al. (2014)	200	0.3/0.7/0.7
Abell 586	0.171	07 32 22.32	+31 38 02.4	WL	$6.55^{+2.75}_{-1.97}$	$6.34^{+2.49}_{-1.79}$	$8.38^{+3.52}_{-2.52}$	$7.37^{+2.89}_{-2.08}$	Okabe et al. (2010)	virial	0.27/0.73/0.72
Abell 1914	0.171	14 26 01.6	+37 49 38	WL	$3.21^{+2.26}_{-2.26}$	$7.15^{+4.31}_{-4.31}$	$4.15^{+2.79}_{-2.79}$	$8.77^{+4.56}_{-4.56}$	Okabe & Umetsu (2008)	virial	0.3/0.7/0.7
Abell 1914	0.171	14 26 01.6	+37 49 38	X-ray	$1.04^{+0.36}_{-0.33}$	$76.85^{+5.81}_{-5.28}$	$1.44^{+0.5}_{-0.46}$	$113.86^{+8.61}_{-7.82}$	Babyk et al. (2014)	200	0.27/0.73/0.73

Continued on next page

Table C.1 – *Continued*

Cluster	z	RA	Dec.	Method	$c_{200}$	$M_{200}$ ( $10^{14} M_\odot$ )	$c_{\text{vir}}$	$M_{\text{vir}}$ ( $10^{14} M_\odot$ )	Ref.	$\delta$	$\Omega_m/\Omega_\Lambda/h$
Abell 2218	0.175	16 35 52.4	+66 12 52	X-ray	$6.26^{+2.46}_{-1.48}$	$4.76^{+0.74}_{-0.74}$	$7.9^{+3.1}_{-1.87}$	$5.52^{+0.86}_{-0.86}$	Ettori et al. (2011)	200	0.3/0.7/0.7
Abell 2218	0.175	16 35 52.4	+66 12 52	WL	$6.86^{+1.3}_{-1.3}$	$13.87^{+3.07}_{-3.07}$	$8.63^{+1.6}_{-1.6}$	$15.99^{+3.76}_{-3.76}$	Bardeau et al. (2007)	200	0.3/0.7/0.7
Abell 2218	0.175	16 35 52.4	+66 12 52	X-ray	$6.33^{+2.34}_{-1.55}$	$6.46^{+0.82}_{-0.83}$	$8.12^{+3.0}_{-1.99}$	$7.57^{+0.96}_{-0.97}$	Babyk et al. (2014)	200	0.27/0.73/0.73
Abell 2345	0.1765	21 27 11.0	-12 09 33	WL	$0.2^{+0.1}_{-0.1}$	$24.6^{+9.3}_{-9.3}$	$0.3^{+0.1}_{-0.1}$	$51.6^{+25.3}_{-25.3}$	Sereno et al. (2014)	200	0.3/0.7/0.7
Abell 750	0.18	09 09 06.7	+11 01 48	WL	$2.5^{+1.4}_{-1.4}$	$11.3^{+4.3}_{-4.3}$	$3.2^{+1.7}_{-1.7}$	$14.3^{+6.4}_{-6.4}$	Sereno et al. (2014)	200	0.3/0.7/0.7
Abell 1689	0.18	13 11 29.5	-01 20 17	WL	$10.7^{+4.5}_{-2.7}$	$17.6^{+2.0}_{-2.0}$	$13.4^{+5.4}_{-3.3}$	$19.7^{+2.0}_{-2.0}$	Umetsu & Broadhurst (2008)	200/virial	0.3/0.7/0.7
Abell 1689	0.18	13 11 29.5	-01 20 17	WL+SL	$10.1^{+0.8}_{-0.7}$	$18.6^{+1.6}_{-1.6}$	$12.7^{+1.0}_{-0.9}$	$21.0^{+1.7}_{-1.7}$	Umetsu & Broadhurst (2008)	200/virial	0.3/0.7/0.7
Abell 1689	0.18	13 11 29.5	-01 20 17	SL	$9.2^{+1.2}_{-1.2}$	$18.0^{+4.0}_{-3.0}$	$11.5^{+1.5}_{-1.4}$	$20.0^{+5.0}_{-0.3}$	Coe et al. (2010)	200/virial	0.3/0.7/0.7
Abell 1689	0.18	13 11 29.5	-01 20 17	WL	$10.7^{+2.85}_{-2.85}$	$18.3^{+3.7}_{-3.7}$	$13.32^{+3.48}_{-3.48}$	$20.5^{+4.4}_{-4.4}$	Umetsu et al. (2015)	200	0.3/0.7/0.7
Abell 1689	0.18	13 11 29.5	-01 20 17	SL	$8.69^{+1.26}_{-1.26}$	$25.6^{+4.4}_{-4.4}$	$10.86^{+1.54}_{-1.54}$	$29.0^{+5.3}_{-5.3}$	Umetsu et al. (2015)	200	0.3/0.7/0.7
Abell 1689	0.18	13 11 29.5	-01 20 17	WL+SL	$10.3^{+2.52}_{-2.52}$	$21.3^{+3.6}_{-3.6}$	$12.83^{+3.08}_{-3.08}$	$23.9^{+4.4}_{-4.4}$	Umetsu et al. (2015)	200	0.3/0.7/0.7
Abell 1689	0.18	13 11 29.5	-01 20 17	X-ray	$8.31^{+0.64}_{-0.63}$	$7.36^{+0.44}_{-0.44}$	$10.4^{+0.8}_{-0.79}$	$8.36^{+0.5}_{-0.5}$	Ettori et al. (2011)	200	0.3/0.7/0.7
Abell 1689	0.18	13 11 29.5	-01 20 17	WL	$15.4^{+9.0}_{-9.0}$	$13.1^{+2.8}_{-2.8}$	$19.1^{+11.2}_{-11.2}$	$14.4^{+3.1}_{-3.1}$	Corless et al. (2009)	200	0.3/0.7/0.7
Abell 1689	0.18	13 11 29.5	-01 20 17	WL	$12.56^{+3.86}_{-2.66}$	$13.99^{+2.31}_{-2.06}$	$15.6^{+4.8}_{-3.3}$	$15.57^{+2.57}_{-2.29}$	Umetsu et al. (2009)	virial	0.3/0.7/0.7
Abell 1689	0.18	13 11 29.5	-01 20 17	WL	$10.27^{+2.48}_{-1.93}$	$16.31^{+2.76}_{-2.24}$	$12.8^{+3.09}_{-2.41}$	$18.31^{+3.1}_{-2.51}$	Umetsu et al. (2011b)	virial	0.3/0.7/0.7
Abell 1689	0.18	13 11 29.5	-01 20 17	WL	$4.28^{+0.82}_{-0.82}$	$28.16^{+4.8}_{-4.8}$	$5.45^{+1.01}_{-1.01}$	$33.73^{+6.35}_{-6.35}$	Bardeau et al. (2007)	200	0.3/0.7/0.7
Abell 1689	0.18	13 11 29.5	-01 20 17	X-ray	$8.35^{+0.91}_{-0.85}$	$16.09^{+2.81}_{-1.73}$	$10.62^{+1.16}_{-1.08}$	$18.44^{+3.22}_{-1.98}$	Babyk et al. (2014)	200	0.27/0.73/0.73
Abell 1689	0.18	13 11 29.5	-01 20 17	SL	$6.0^{+0.5}_{-0.5}$	30.0	$7.6^{+0.6}_{-0.6}$	35.0	Halkola et al. (2006b)	200	0.3/0.7/0.7
Abell 1689	0.18	13 11 29.5	-01 20 17	SL	$5.7^{+0.34}_{-0.5}$	$130.0^{+88.0}_{-57.0}$	$7.18^{+0.42}_{-0.62}$	$151.0^{+104.0}_{-67.0}$	Zekser et al. (2006)	200	0.3/0.7/None
Abell 1689	0.18	13 11 29.5	-01 20 17	SL	$6.5^{+1.9}_{-1.6}$	$34.0^{+1.0}_{-2.0}$	$8.2^{+2.1}_{-1.8}$	$40.0^{+1.0}_{-1.0}$	Broadhurst et al. (2005c)	virial	0.3/0.7/0.7
Abell 1689	0.18	13 11 29.5	-01 20 17	WL	30.4	—	37.4	—	Halkola et al. (2006b)	200	0.3/0.7/0.7
Abell 1689	0.18	13 11 29.5	-01 20 17	WL	$22.1^{+2.9}_{-4.7}$	—	$27.2^{+3.5}_{-5.7}$	—	Medezinski et al. (2007)	virial	0.3/0.7/None
Abell 1689	0.18	13 11 29.5	-01 20 17	WL	$3.5^{+0.5}_{-0.3}$	$14.1^{+6.3}_{-4.7}$	$4.5^{+0.6}_{-0.4}$	$17.1^{+7.8}_{-5.8}$	Bardeau et al. (2005)	200	0.3/0.7/0.7
Abell 1689	0.18	13 11 29.5	-01 20 17	WL	$11.0^{+1.14}_{-0.9}$	$17.3^{+1.7}_{-1.7}$	$13.7^{+1.4}_{-1.1}$	$19.3^{+2.0}_{-2.0}$	Broadhurst et al. (2005b)	virial	0.3/0.7/0.7
Abell 1689	0.18	13 11 29.5	-01 20 17	WL	7.9	—	9.9	—	Clowe (2003)	200	0.3/0.7/0.7
Abell 1689	0.18	13 11 29.5	-01 20 17	WL	4.8	8.5	6.1	10.0	King et al. (2002)	200	1.0/0.0/None
Abell 1689	0.18	13 11 29.5	-01 20 17	WL	6.0	—	8.0	—	Clowe & Schneider (2001b)	200	0.3/0.7/None
Abell 1689	0.18	13 11 29.5	-01 20 17	WL	6.0	—	7.6	—	Clowe & Schneider (2001a)	200	0.3/0.7/0.7
Abell 1689	0.18	13 11 29.5	-01 20 17	WL+SL	$7.6^{+0.3}_{-0.5}$	23.0	$9.5^{+0.4}_{-0.6}$	26.0	Halkola et al. (2006b)	200	0.3/0.7/0.7
Abell 1689	0.18	13 11 29.5	-01 20 17	WL+SL	$7.6^{+1.6}_{-1.6}$	$13.2^{+2.0}_{-2.0}$	$9.5^{+2.0}_{-2.0}$	$15.1^{+2.0}_{-2.0}$	Limousin et al. (2007b)	200	0.3/0.7/0.7

Continued on next page

Table C.1 – *Continued*

Cluster	z	RA	Dec.	Method	$c_{200}$	$M_{200}$ ( $10^{14} M_\odot$ )	$c_{\text{vir}}$	$M_{\text{vir}}$ ( $10^{14} M_\odot$ )	Ref.	$\delta$	$\Omega_m/\Omega_\Lambda/h$
Abell 1689	0.18	13 11 29.5	-01 20 17	X-ray	$7.7^{+1.7}_{-2.6}$	—	$9.6^{+2.1}_{-3.2}$	—	Andersson & Madejski (2004)	200	0.3/0.7/0.7
Abell 383	0.188	02 48 02.00	-03 32 15.0	WL+SL	$7.01^{+0.54}_{-0.52}$	$6.71^{+1.2}_{-1.11}$	$8.77^{+0.67}_{-0.65}$	$7.67^{+1.37}_{-1.27}$	Zitrin et al. (2011)	virial	0.3/0.7/0.7
Abell 383	0.188	02 48 02.00	-03 32 15.0	X-ray	$3.4^{+0.03}_{-0.42}$	$4.43^{+0.37}_{-0.37}$	$4.35^{+0.04}_{-0.54}$	$5.42^{+0.45}_{-0.45}$	Ettori et al. (2011)	200	0.3/0.7/0.7
Abell 383	0.188	02 48 02.00	-03 32 15.0	WL	$7.7^{+3.7}_{-3.7}$	$4.1^{+1.0}_{-1.0}$	$9.6^{+4.5}_{-4.5}$	$4.7^{+1.3}_{-1.3}$	Sereno et al. (2014)	200	0.3/0.7/0.7
Abell 383	0.188	02 48 02.00	-03 32 15.0	WL	$7.0^{+1.2}_{-1.2}$	$7.9^{+2.1}_{-2.1}$	$8.8^{+1.5}_{-1.5}$	$9.1^{+2.5}_{-2.5}$	Sereno et al. (2014)	200	0.3/0.7/0.7
Abell 383	0.188	02 48 02.00	-03 32 15.0	WL	$2.62^{+0.69}_{-0.69}$	$5.99^{+2.09}_{-2.09}$	$3.38^{+0.86}_{-0.86}$	$7.53^{+2.85}_{-2.85}$	Bardeau et al. (2007)	200	0.3/0.7/0.7
Abell 383	0.188	02 48 02.00	-03 32 15.0	X-ray	$3.44^{+0.47}_{-0.36}$	$5.63^{+2.04}_{-1.19}$	$4.48^{+0.61}_{-0.47}$	$6.97^{+2.53}_{-1.47}$	Babyk et al. (2014)	200	0.27/0.73/0.73
Abell 383	0.188	02 48 02.00	-03 32 15.0	WL+SL	$4.4^{+1.0}_{-1.0}$	$8.7^{+0.7}_{-0.7}$	$5.6^{+1.3}_{-1.3}$	$10.4^{+0.7}_{-0.7}$	Merten et al. (2014)	2500/200/virial	0.27/0.73/0.7
Abell 383	0.188	02 48 02.00	-03 32 15.0	X-ray	$3.76^{+0.53}_{-0.68}$	$6.62^{+2.56}_{-1.34}$	$4.78^{+0.65}_{-0.84}$	$7.95^{+3.28}_{-1.68}$	Schmidt & Allen (2007)	virial	0.3/0.7/0.7
Abell 383	0.188	02 48 02.00	-03 32 15.0	X-ray	$6.41^{+0.57}_{-0.57}$	$4.1^{+0.47}_{-0.47}$	$8.03^{+0.7}_{-0.7}$	$4.72^{+0.57}_{-0.57}$	Vikhlinin et al. (2006)	500	0.3/0.7/0.71
Abell 383	0.188	02 48 02.00	-03 32 15.0	WL	$6.97^{+4.1}_{-2.4}$	$3.13^{+0.99}_{-0.74}$	$8.87^{+5.22}_{-3.05}$	$3.62^{+1.15}_{-0.86}$	Okabe et al. (2010)	virial	0.27/0.73/0.72
ZwCl0839.9+2937	0.194	08 42 56.07	+29 27 25.7	WL	$8.2^{+4.4}_{-4.4}$	$2.9^{+0.9}_{-0.9}$	$10.2^{+5.4}_{-5.4}$	$3.3^{+1.1}_{-1.1}$	Sereno et al. (2014)	200	0.3/0.7/0.7
ZwCl0839.9+2937	0.194	08 42 56.07	+29 27 25.7	WL	$5.67^{+3.95}_{-2.13}$	$2.49^{+0.92}_{-0.7}$	$7.24^{+5.04}_{-2.72}$	$2.91^{+1.08}_{-0.82}$	Okabe et al. (2010)	virial	0.27/0.73/0.72
ZwCl0839.9+2937	0.194	08 42 56.07	+29 27 25.7	X-ray	$6.5^{+0.1}_{-0.1}$	6.1	$8.1^{+0.1}_{-0.1}$	7.0	Wang et al. (2005)	200	0.3/0.7/0.7
Abell 291	0.196	02 01 44.20	-02 12 03.0	WL	$1.8^{+0.9}_{-0.9}$	$7.7^{+2.3}_{-2.3}$	$2.4^{+1.1}_{-1.1}$	$10.1^{+3.7}_{-3.7}$	Sereno et al. (2014)	200	0.3/0.7/0.7
Abell 291	0.196	02 01 44.20	-02 12 03.0	WL	$1.76^{+1.0}_{-0.7}$	$5.19^{+2.29}_{-1.52}$	$2.36^{+1.34}_{-0.94}$	$7.02^{+3.1}_{-2.06}$	Okabe et al. (2010)	virial	0.27/0.73/0.72
Abell 115	0.1971	00 55 59.76	+26 22 40.8	WL	$2.7^{+2.7}_{-2.7}$	$6.4^{+4.0}_{-4.0}$	$3.5^{+3.3}_{-3.3}$	$8.0^{+5.9}_{-5.9}$	Sereno et al. (2014)	200	0.3/0.7/0.7
Abell 115	0.1971	00 55 59.76	+26 22 40.8	WL	$2.83^{+3.86}_{-1.56}$	$4.26^{+3.24}_{-1.95}$	$3.69^{+5.03}_{-2.04}$	$5.36^{+4.08}_{-2.45}$	Okabe et al. (2010)	virial	0.27/0.73/0.72
Abell 520	0.199	04 54 19.0	+02 56 49	WL	$2.24^{+1.48}_{-1.48}$	$6.86^{+3.32}_{-3.32}$	$2.9^{+1.82}_{-1.82}$	$8.77^{+3.4}_{-3.4}$	Okabe & Umetsu (2008)	virial	0.3/0.7/0.7
Abell 520	0.199	04 54 19.0	+02 56 49	X-ray	3.79	129.0	4.8	154.0	Molikawa et al. (1999)	virial	0.3/0.7/0.5
Abell 2163	0.203	16 15 34.1	-06 07 26	WL	$2.18^{+0.57}_{-0.5}$	$26.94^{+5.7}_{-4.53}$	$2.84^{+0.71}_{-0.61}$	$34.63^{+8.57}_{-6.5}$	Okabe et al. (2011)	200/virial	0.3/0.7/None
Abell 2163	0.203	16 15 34.1	-06 07 26	X-ray	$2.04^{+0.37}_{-0.33}$	$111.18^{+5.92}_{-7.38}$	$2.7^{+0.49}_{-0.44}$	$145.93^{+7.77}_{-9.69}$	Babyk et al. (2014)	200	0.27/0.73/0.73
Abell 209	0.206	01 31 53.00	-13 36 34.0	WL	$3.4^{+3.1}_{-1.6}$	$7.7^{+4.3}_{-2.7}$	$4.4^{+4.0}_{-2.1}$	$9.5^{+5.3}_{-3.3}$	Paulin-Henriksson et al. (2007)	200	0.27/0.73/0.7
Abell 209	0.206	01 31 53.00	-13 36 34.0	X-ray	$3.03^{+0.67}_{-0.77}$	$8.6^{+1.23}_{-1.23}$	$3.87^{+0.86}_{-0.98}$	$10.59^{+1.51}_{-1.51}$	Ettori et al. (2011)	200	0.3/0.7/0.7
Abell 209	0.206	01 31 53.00	-13 36 34.0	WL	$2.1^{+0.5}_{-0.5}$	$14.4^{+2.7}_{-2.7}$	$2.7^{+0.6}_{-0.6}$	$18.5^{+4.0}_{-4.0}$	Sereno et al. (2014)	200	0.3/0.7/0.7
Abell 209	0.206	01 31 53.00	-13 36 34.0	WL	$3.0^{+0.3}_{-0.3}$	$23.1^{+3.7}_{-3.7}$	$3.8^{+0.4}_{-0.4}$	$28.5^{+4.9}_{-4.9}$	Sereno et al. (2014)	200	0.3/0.7/0.7
Abell 209	0.206	01 31 53.00	-13 36 34.0	WL	$3.0^{+0.92}_{-0.92}$	$10.27^{+2.91}_{-2.91}$	$3.83^{+1.13}_{-1.13}$	$12.66^{+3.99}_{-3.99}$	Bardeau et al. (2007)	200	0.3/0.7/0.7
Abell 209	0.206	01 31 53.00	-13 36 34.0	X-ray	$3.11^{+0.77}_{-0.67}$	$12.05^{+2.34}_{-2.11}$	$4.04^{+1.0}_{-0.87}$	$15.01^{+2.91}_{-2.63}$	Babyk et al. (2014)	200	0.27/0.73/0.73
Abell 209	0.206	01 31 53.00	-13 36 34.0	WL+SL	$3.2^{+0.9}_{-0.9}$	$9.5^{+0.7}_{-0.7}$	$4.3^{+1.1}_{-1.1}$	$11.7^{+0.7}_{-0.7}$	Merten et al. (2014)	2500/200/virial	0.27/0.73/0.7
Abell 209	0.206	01 31 53.00	-13 36 34.0	WL	$2.05^{+0.52}_{-0.45}$	$10.65^{+2.52}_{-1.98}$	$2.71^{+0.69}_{-0.6}$	$14.0^{+3.31}_{-2.6}$	Okabe et al. (2010)	virial	0.27/0.73/0.72

Continued on next page

Table C.1 – *Continued*

Cluster	z	RA	Dec.	Method	$c_{200}$	$M_{200}$ ( $10^{14} M_\odot$ )	$c_{\text{vir}}$	$M_{\text{vir}}$ ( $10^{14} M_\odot$ )	Ref.	$\delta$	$\Omega_m/\Omega_\Lambda/h$
Abell 963	0.206	10 17 13.9	+39 01 31	X-ray	$4.35^{+0.94}_{-0.76}$	$6.17^{+0.83}_{-0.83}$	$5.49^{+1.19}_{-0.96}$	$7.34^{+0.99}_{-0.99}$	Ettori et al. (2011)	200	0.3/0.7/0.7
Abell 963	0.206	10 17 13.9	+39 01 31	WL	$2.0^{+0.7}_{-0.7}$	$7.4^{+1.6}_{-1.6}$	$2.6^{+0.9}_{-0.9}$	$9.6^{+2.5}_{-2.5}$	Sereno et al. (2014)	200	0.3/0.7/0.7
Abell 963	0.206	10 17 13.9	+39 01 31	WL	$8.35^{+1.25}_{-1.25}$	$5.66^{+1.29}_{-1.29}$	$10.37^{+1.52}_{-1.52}$	$6.41^{+1.52}_{-1.52}$	Bardeau et al. (2007)	200	0.3/0.7/0.7
Abell 963	0.206	10 17 13.9	+39 01 31	X-ray	$4.35^{+1.01}_{-0.99}$	$8.22^{+1.24}_{-0.91}$	$5.59^{+1.3}_{-1.27}$	$9.9^{+1.49}_{-1.1}$	Babyk et al. (2014)	200	0.27/0.73/0.73
Abell 963	0.206	10 17 13.9	+39 01 31	WL	$1.94^{+0.75}_{-0.6}$	$5.25^{+1.64}_{-1.2}$	$2.57^{+1.0}_{-0.79}$	$6.96^{+2.17}_{-1.59}$	Okabe et al. (2010)	virial	0.27/0.73/0.72
Abell 963	0.206	10 17 13.9	+39 01 31	X-ray	$4.39^{+0.88}_{-0.88}$	$7.47^{+3.05}_{-1.8}$	$5.53^{+1.07}_{-1.08}$	$8.81^{+3.84}_{-2.21}$	Schmidt & Allen (2007)	virial	0.3/0.7/0.7
Abell 963	0.206	10 17 13.9	+39 01 31	X-ray	$5.72^{+0.78}_{-1.07}$	$7.04^{+1.96}_{-1.26}$	$7.16^{+0.95}_{-1.31}$	$8.14^{+2.43}_{-1.51}$	Allen et al. (2003)	200	0.3/0.7/0.5
RXJ0439.0+0520	0.208	04 39 02.2	+05 20 43	X-ray	$7.71^{+1.27}_{-1.77}$	$9.11^{+1.75}_{-2.27}$	$9.74^{+1.6}_{-2.24}$	$10.45^{+2.01}_{-2.6}$	Babyk et al. (2014)	200	0.27/0.73/0.73
RX J0439.0+0520	0.208	04 39 02.2	+05 20 43	X-ray	$6.66^{+1.53}_{-1.21}$	$3.97^{+1.78}_{-1.19}$	$8.3^{+1.87}_{-1.48}$	$4.54^{+2.13}_{-1.4}$	Schmidt & Allen (2007)	virial	0.3/0.7/0.7
RX J1504.1-0248	0.215	15 04 07.5	-02 48 16	X-ray	$3.77^{+1.05}_{-1.09}$	$17.5^{+13.5}_{-5.6}$	$4.75^{+1.28}_{-1.34}$	$20.9^{+17.3}_{-6.97}$	Schmidt & Allen (2007)	virial	0.3/0.7/0.7
MS 0735.6+7421	0.216	07 41 44.8	+74 14 52	X-ray	6.85	22.0	8.51	25.0	Molikawa et al. (1999)	virial	0.3/0.7/0.5
Abell 773	0.217	09 17 59.4	+51 42 23	X-ray	$3.27^{+1.49}_{-1.05}$	$10.94^{+3.12}_{-3.12}$	$4.15^{+1.89}_{-1.33}$	$13.34^{+3.8}_{-3.8}$	Ettori et al. (2011)	200	0.3/0.7/0.7
Abell 773	0.217	09 17 59.4	+51 42 23	X-ray	$3.33^{+0.61}_{-0.53}$	$14.09^{+1.72}_{-1.28}$	$4.3^{+0.79}_{-0.68}$	$17.38^{+2.12}_{-1.58}$	Babyk et al. (2014)	200	0.27/0.73/0.73
MS 1006.0+1202	0.221	10 08 47.9	+11 47 33	X-ray	4.19	31.0	5.26	36.0	Molikawa et al. (1999)	virial	0.3/0.7/0.5
Abell 2261	0.224	17 22 27.60	+32 07 37.2	WL	$4.1^{+0.6}_{-0.6}$	$17.7^{+1.1}_{-1.1}$	$5.2^{+0.7}_{-0.7}$	$21.1^{+1.6}_{-1.6}$	Sereno et al. (2014)	200	0.3/0.7/0.7
Abell 2261	0.224	17 22 27.60	+32 07 37.2	WL	$4.8^{+0.5}_{-0.5}$	$19.7^{+2.4}_{-2.4}$	$6.0^{+0.6}_{-0.6}$	$23.2^{+3.0}_{-3.0}$	Sereno et al. (2014)	200	0.3/0.7/0.7
Abell 2261	0.224	17 22 27.60	+32 07 37.2	WL	$5.13^{+1.52}_{-1.12}$	$16.62^{+3.2}_{-2.71}$	$6.4^{+1.9}_{-1.4}$	$19.29^{+3.71}_{-3.14}$	Umetsu et al. (2009)	virial	0.3/0.7/0.7
Abell 2261	0.224	17 22 27.60	+32 07 37.2	WL+SL	$3.4^{+1.4}_{-1.4}$	$14.2^{+1.7}_{-1.7}$	$4.4^{+1.8}_{-1.8}$	$17.6^{+1.8}_{-1.8}$	Merten et al. (2014)	2500/200/virial	0.27/0.73/0.7
Abell 2261	0.224	17 22 27.60	+32 07 37.2	WL	$4.75^{+1.34}_{-1.03}$	$8.04^{+1.7}_{-1.43}$	$6.04^{+1.71}_{-1.31}$	$9.49^{+2.01}_{-1.69}$	Okabe et al. (2010)	virial	0.27/0.73/0.72
ZwCl 0823.2+0425	0.2248	08 25 59.3	+04 15 47	WL	$2.6^{+1.2}_{-1.2}$	$7.9^{+2.1}_{-2.1}$	$3.3^{+1.5}_{-1.5}$	$9.8^{+3.1}_{-3.1}$	Sereno et al. (2014)	200	0.3/0.7/0.7
Abell 1763	0.228	13 35 18.2	+40 59 49	X-ray	$7.5^{+2.3}_{-3.41}$	$4.25^{+0.74}_{-0.74}$	$9.28^{+2.85}_{-4.22}$	$4.83^{+0.84}_{-0.84}$	Ettori et al. (2011)	200	0.3/0.7/0.7
Abell 1763	0.228	13 35 18.2	+40 59 49	WL	$2.63^{+0.63}_{-0.63}$	$19.8^{+3.76}_{-3.76}$	$3.36^{+0.77}_{-0.77}$	$24.62^{+5.31}_{-5.31}$	Bardeau et al. (2007)	200	0.3/0.7/0.7
Abell 2219	0.2281	16 40 21.4	+46 42 21	WL	$6.6^{+2.9}_{-2.9}$	$11.7^{+2.7}_{-2.7}$	$8.2^{+3.5}_{-3.5}$	$13.4^{+3.5}_{-3.5}$	Sereno et al. (2014)	200	0.3/0.7/0.7
Abell 2219	0.2281	16 40 21.4	+46 42 21	WL	$3.84^{+0.99}_{-0.99}$	$29.91^{+6.21}_{-6.21}$	$4.84^{+1.21}_{-1.21}$	$35.83^{+8.29}_{-8.29}$	Bardeau et al. (2007)	200	0.3/0.7/0.7
Abell 2219	0.2281	16 40 21.4	+46 42 21	X-ray	$3.44^{+0.73}_{-0.73}$	$36.49^{+4.92}_{-3.39}$	$4.42^{+0.94}_{-0.94}$	$44.75^{+6.03}_{-4.16}$	Babyk et al. (2014)	200	0.27/0.73/0.73
Abell 2219	0.2281	16 40 21.4	+46 42 21	WL	$5.44^{+2.7}_{-1.71}$	$7.8^{+2.17}_{-1.76}$	$6.88^{+3.42}_{-2.16}$	$9.11^{+2.54}_{-2.06}$	Okabe et al. (2010)	virial	0.27/0.73/0.72
Abell 267	0.23	01 52 48.72	+01 01 08.4	WL	$5.1^{+1.8}_{-1.8}$	$4.3^{+1.0}_{-1.0}$	$6.4^{+2.2}_{-2.2}$	$5.0^{+1.3}_{-1.3}$	Sereno et al. (2014)	200	0.3/0.7/0.7
Abell 267	0.23	01 52 48.72	+01 01 08.4	WL	$4.54^{+2.01}_{-2.01}$	$3.89^{+2.09}_{-2.09}$	$5.69^{+2.45}_{-2.45}$	$4.59^{+2.64}_{-2.64}$	Bardeau et al. (2007)	200	0.3/0.7/0.7
Abell 267	0.23	01 52 48.72	+01 01 08.4	WL	$4.73^{+1.66}_{-1.25}$	$3.26^{+0.91}_{-0.75}$	$6.0^{+2.11}_{-1.58}$	$3.85^{+1.08}_{-0.88}$	Okabe et al. (2010)	virial	0.27/0.73/0.72
Abell 2390	0.23	21 53 35.5	+17 41 12	X-ray	$2.06^{+0.12}_{-0.04}$	$24.71^{+1.16}_{-1.16}$	$2.65^{+0.15}_{-0.05}$	$31.57^{+1.48}_{-1.48}$	Ettori et al. (2011)	200	0.3/0.7/0.7

Continued on next page

Table C.1 – *Continued*

Cluster	z	RA	Dec.	Method	$c_{200}$	$M_{200}$ ( $10^{14} M_\odot$ )	$c_{\text{vir}}$	$M_{\text{vir}}$ ( $10^{14} M_\odot$ )	Ref.	$\delta$	$\Omega_m/\Omega_\Lambda/h$
Abell 2390	0.23	21 53 35.5	+17 41 12	WL	$5.3^{+1.3}_{-1.3}$	$9.7^{+2.1}_{-2.1}$	$6.6^{+1.6}_{-1.6}$	$11.3^{+2.7}_{-2.7}$	Sereno et al. (2014)	200	0.3/0.7/0.7
Abell 2390	0.23	21 53 35.5	+17 41 12	WL	$5.55^{+1.85}_{-1.21}$	$11.15^{+1.86}_{-1.73}$	$6.9^{+2.3}_{-1.5}$	$12.86^{+2.14}_{-2.0}$	Umetsu et al. (2009)	virial	0.3/0.7/0.7
Abell 2390	0.23	21 53 35.5	+17 41 12	WL	$5.26^{+1.43}_{-1.43}$	$13.47^{+3.51}_{-3.51}$	$6.56^{+1.74}_{-1.74}$	$15.7^{+4.43}_{-4.43}$	Bardeau et al. (2007)	200	0.3/0.7/0.7
Abell 2390	0.23	21 53 35.5	+17 41 12	X-ray	$2.11^{+0.52}_{-0.62}$	$28.21^{+3.15}_{-2.39}$	$2.76^{+0.68}_{-0.81}$	$36.57^{+4.08}_{-3.1}$	Babyk et al. (2014)	200	0.27/0.73/0.73
Abell 2390	0.23	21 53 35.5	+17 41 12	WL	$4.89^{+1.21}_{-1.01}$	$6.97^{+1.64}_{-1.39}$	$6.2^{+1.53}_{-1.28}$	$8.2^{+1.93}_{-1.63}$	Okabe et al. (2010)	virial	0.27/0.73/0.72
Abell 2390	0.23	21 53 35.5	+17 41 12	X-ray	$2.58^{+0.19}_{-0.19}$	$16.58^{+1.93}_{-1.93}$	$3.28^{+0.23}_{-0.23}$	$20.45^{+2.57}_{-2.57}$	Vikhlinin et al. (2006)	500	0.3/0.7/0.71
Abell 2390	0.23	21 53 35.5	+17 41 12	X-ray	$3.2^{+1.79}_{-1.57}$	$20.6^{+59.7}_{-11.6}$	$4.04^{+2.18}_{-1.93}$	$24.9^{+79.7}_{-14.4}$	Allen et al. (2003)	200	0.3/0.7/0.5
Abell 2667	0.233	23 51 40.7	-26 05 01	X-ray	$2.24^{+0.08}_{-0.02}$	$15.88^{+0.45}_{-0.45}$	$2.87^{+0.1}_{-0.03}$	$20.08^{+0.57}_{-0.57}$	Ettori et al. (2011)	200	0.3/0.7/0.7
Abell 2667	0.233	23 51 40.7	-26 05 01	X-ray	$2.25^{+0.17}_{-0.15}$	$19.71^{+2.61}_{-1.27}$	$2.94^{+0.22}_{-0.2}$	$25.32^{+3.35}_{-1.63}$	Babyk et al. (2014)	200	0.27/0.73/0.73
Abell 2667	0.233	23 51 40.7	-26 05 01	X-ray	$3.02^{+0.74}_{-0.85}$	$13.6^{+10.6}_{-4.6}$	$3.82^{+0.9}_{-1.04}$	$16.5^{+13.9}_{-5.8}$	Allen et al. (2003)	200	0.3/0.7/0.5
RXJ2129.6+0005	0.235	21 29 37.92	+00 05 38.4	X-ray	$3.71^{+0.27}_{-0.38}$	$5.4^{+0.44}_{-0.44}$	$4.67^{+0.34}_{-0.48}$	$6.48^{+0.53}_{-0.53}$	Ettori et al. (2011)	200	0.3/0.7/0.7
RXJ2129.6+0005	0.235	21 29 37.92	+00 05 38.4	WL	$2.0^{+1.2}_{-1.2}$	$9.7^{+3.6}_{-3.6}$	$2.6^{+1.5}_{-1.5}$	$12.4^{+5.5}_{-5.5}$	Sereno et al. (2014)	200	0.3/0.7/0.7
RXJ2129.6+0005	0.235	21 29 37.92	+00 05 38.4	WL	$6.7^{+0.9}_{-0.9}$	$6.1^{+1.1}_{-1.1}$	$8.3^{+1.1}_{-1.1}$	$7.0^{+1.3}_{-1.3}$	Sereno et al. (2014)	200	0.3/0.7/0.7
RXJ2129.6+0005	0.235	21 29 37.92	+00 05 38.4	X-ray	$3.77^{+0.38}_{-0.33}$	$8.46^{+0.94}_{-1.1}$	$4.82^{+0.49}_{-0.42}$	$10.26^{+1.14}_{-1.33}$	Babyk et al. (2014)	200	0.27/0.73/0.73
RXJ2129.6+0005	0.235	21 29 37.92	+00 05 38.4	WL+SL	$4.3^{+1.4}_{-1.4}$	$6.1^{+0.6}_{-0.6}$	$5.6^{+1.7}_{-1.7}$	$7.3^{+0.7}_{-0.7}$	Merten et al. (2014)	2500/200/virial	0.27/0.73/0.7
RXJ2129.6+0005	0.235	21 29 37.92	+00 05 38.4	WL	$2.56^{+1.67}_{-1.03}$	$5.32^{+2.16}_{-1.55}$	$3.32^{+2.16}_{-1.34}$	$6.71^{+2.73}_{-1.96}$	Okabe et al. (2010)	virial	0.27/0.73/0.72
RXJ2129.6+0005	0.235	21 29 37.92	+00 05 38.4	X-ray	$4.07^{+2.31}_{-1.97}$	$6.46^{+12.6}_{-3.14}$	$5.09^{+2.8}_{-2.41}$	$7.63^{+16.3}_{-3.83}$	Schmidt & Allen (2007)	virial	0.3/0.7/0.7
ZwCl 1305.4+2941	0.241	13 07 49.2	+29 25 48	X-ray	$6.39^{+0.41}_{-0.41}$	$2.43^{+0.19}_{-0.19}$	$7.9^{+0.5}_{-0.5}$	$2.77^{+0.21}_{-0.21}$	Gastaldello et al. (2008)	virial	0.3/0.7/0.7
MS 1910.5+6736	0.246	19 10 27.3	+67 41 27	X-ray	4.65	8.7	5.78	10.0	Molikawa et al. (1999)	virial	0.3/0.7/0.5
Abell 2485	0.2472	22 48 31.13	-16 06 25.6	WL	$3.1^{+1.8}_{-1.8}$	$4.9^{+1.7}_{-1.7}$	$3.9^{+2.2}_{-2.2}$	$6.0^{+2.4}_{-2.4}$	Sereno et al. (2014)	200	0.3/0.7/0.7
Abell 2485	0.2472	22 48 31.13	-16 06 25.6	WL	$2.73^{+1.74}_{-1.12}$	$3.66^{+1.48}_{-1.11}$	$3.52^{+2.24}_{-1.44}$	$4.56^{+1.84}_{-1.38}$	Okabe et al. (2010)	virial	0.27/0.73/0.72
Abell 521	0.2475	04 54 09.1	-10 14 19	WL	$1.6^{+0.4}_{-0.4}$	$6.9^{+1.7}_{-1.7}$	$2.1^{+0.5}_{-0.5}$	$9.1^{+2.5}_{-2.5}$	Sereno et al. (2014)	200	0.3/0.7/0.7
Abell 521	0.2475	04 54 09.1	-10 14 19	X-ray	$11.26^{+0.83}_{-0.78}$	$7.21^{+1.16}_{-1.13}$	$13.97^{+1.03}_{-0.97}$	$8.04^{+1.29}_{-1.26}$	Babyk et al. (2014)	200	0.27/0.73/0.73
Abell 521	0.2475	04 54 09.1	-10 14 19	WL	$2.36^{+0.78}_{-0.61}$	$4.6^{+1.14}_{-0.96}$	$3.06^{+1.01}_{-0.79}$	$5.85^{+1.45}_{-1.22}$	Okabe et al. (2010)	virial	0.27/0.73/0.72
Abell 1835	0.2528	14 01 02.3	+02 52 48	X-ray	$2.64^{+0.34}_{-0.09}$	$17.53^{+1.41}_{-1.41}$	$3.34^{+0.43}_{-0.11}$	$21.66^{+1.74}_{-1.74}$	Ettori et al. (2011)	200	0.3/0.7/0.7
Abell 1835	0.2528	14 01 02.3	+02 52 48	WL	$8.0^{+10.9}_{-8.0}$	$11.0^{+4.3}_{-4.3}$	$9.8^{+13.4}_{-9.8}$	$12.4^{+4.8}_{-4.8}$	Corless et al. (2009)	200	0.3/0.7/0.7
Abell 1835	0.2528	14 01 02.3	+02 52 48	WL	$2.7^{+0.8}_{-0.8}$	$15.0^{+3.3}_{-3.3}$	$3.4^{+1.0}_{-1.0}$	$18.5^{+4.6}_{-4.6}$	Sereno et al. (2014)	200	0.3/0.7/0.7
Abell 1835	0.2528	14 01 02.3	+02 52 48	WL	$2.58^{+0.48}_{-0.48}$	$38.67^{+5.91}_{-5.91}$	$3.27^{+0.59}_{-0.59}$	$47.85^{+8.25}_{-8.25}$	Bardeau et al. (2007)	200	0.3/0.7/0.7
Abell 1835	0.2528	14 01 02.3	+02 52 48	X-ray	$2.66^{+0.35}_{-0.44}$	$22.86^{+2.86}_{-3.11}$	$3.43^{+0.45}_{-0.57}$	$28.65^{+3.58}_{-3.9}$	Babyk et al. (2014)	200	0.27/0.73/0.73
Abell 1835	0.2528	14 01 02.3	+02 52 48	WL	$2.6^{+0.77}_{-0.61}$	$10.92^{+2.91}_{-2.28}$	$3.35^{+0.99}_{-0.79}$	$13.69^{+3.65}_{-2.86}$	Okabe et al. (2010)	virial	0.27/0.73/0.72

Continued on next page

Table C.1 – *Continued*

Cluster	z	RA	Dec.	Method	$c_{200}$	$M_{200}$ ( $10^{14} M_\odot$ )	$c_{\text{vir}}$	$M_{\text{vir}}$ ( $10^{14} M_\odot$ )	Ref.	$\delta$	$\Omega_m/\Omega_\Lambda/h$
Abell 1835	0.252	14 01 02.3	+02 52 48	WL	2.9	—	3.7	—	Clowe (2003)	200	0.3/0.7/0.7
Abell 1835	0.252	14 01 02.3	+02 52 48	WL	2.96	$23.8^{+3.5}_{-3.2}$	3.72	$28.8^{+4.2}_{-3.9}$	Clowe & Schneider (2002)	200	0.3/0.7/None
Abell 1835	0.252	14 01 02.3	+02 52 48	WL	4.8	—	5.96	—	Clowe & Schneider (2001a)	200	0.3/0.7/0.7
Abell 1835	0.252	14 01 02.3	+02 52 48	X-ray	$3.42^{+0.45}_{-0.31}$	$21.2^{+4.62}_{-5.03}$	$4.28^{+0.55}_{-0.37}$	$25.3^{+5.78}_{-6.21}$	Schmidt & Allen (2007)	virial	0.3/0.7/0.7
Abell 1835	0.252	14 01 02.3	+02 52 48	X-ray	$3.13^{+1.37}_{-1.44}$	$24.0^{+104.0}_{-16.0}$	$3.93^{+1.66}_{-1.76}$	$29.0^{+136.0}_{-20.0}$	Voigt & Fabian (2006)	200/2E4	0.3/0.7/0.7
Abell 1835	0.252	14 01 02.3	+02 52 48	X-ray	$4.21^{+0.53}_{-0.61}$	$18.2^{+8.4}_{-3.0}$	$5.24^{+0.64}_{-0.74}$	$21.4^{+10.3}_{-3.7}$	Allen et al. (2003)	200	0.3/0.7/0.5
RXCJ0307.0-2840	0.253	03 07 04.1	-28 40 14	X-ray	$3.15^{+0.88}_{-0.78}$	$10.44^{+2.39}_{-2.39}$	$3.97^{+1.11}_{-0.98}$	$12.67^{+2.9}_{-2.9}$	Ettori et al. (2011)	200	0.3/0.7/0.7
RXCJ0307.0-2840	0.253	03 07 04.1	-28 40 14	X-ray	$3.22^{+0.88}_{-0.77}$	$12.62^{+1.72}_{-1.82}$	$4.12^{+1.13}_{-0.99}$	$15.5^{+2.11}_{-2.24}$	Babyk et al. (2014)	200	0.27/0.73/0.73
ZwCl0104.4+0048	0.2545	01 06 48.48	+01 02 42.0	WL	$7.9^{+4.7}_{-4.7}$	$2.0^{+0.6}_{-0.6}$	$9.7^{+5.7}_{-5.7}$	$2.3^{+0.8}_{-0.8}$	Sereno et al. (2014)	200	0.3/0.7/0.7
ZwCl0104.4+0048	0.2545	01 06 48.48	+01 02 42.0	WL	$6.46^{+6.56}_{-2.74}$	$1.51^{+0.51}_{-0.41}$	$8.08^{+8.2}_{-3.43}$	$1.73^{+0.58}_{-0.47}$	Okabe et al. (2010)	virial	0.27/0.73/0.72
Abell 68	0.2546	00 37 05.28	+09 09 10.8	X-ray	$2.65^{+0.82}_{-0.06}$	$15.96^{+1.97}_{-1.97}$	$3.38^{+1.04}_{-0.08}$	$19.7^{+2.43}_{-2.43}$	Ettori et al. (2011)	200	0.3/0.7/0.7
Abell 68	0.2546	00 37 05.28	+09 09 10.8	WL	$4.9^{+3.8}_{-3.8}$	$4.4^{+1.7}_{-1.7}$	$6.1^{+4.6}_{-4.6}$	$5.1^{+2.3}_{-2.3}$	Sereno et al. (2014)	200	0.3/0.7/0.7
Abell 68	0.2546	00 37 05.28	+09 09 10.8	WL	$3.84^{+1.13}_{-1.13}$	$8.86^{+2.81}_{-2.81}$	$4.8^{+1.37}_{-1.37}$	$10.56^{+3.62}_{-3.62}$	Bardeau et al. (2007)	200	0.3/0.7/0.7
Abell 68	0.2546	00 37 05.28	+09 09 10.8	WL	$3.15^{+2.63}_{-1.43}$	$4.49^{+2.09}_{-1.48}$	$4.02^{+3.36}_{-1.82}$	$5.49^{+2.56}_{-1.81}$	Okabe et al. (2010)	virial	0.27/0.73/0.72
ZwCl1454.8+2233	0.2578	14 57 14.40	+22 20 38.4	WL	$3.6^{+2.8}_{-2.8}$	$3.7^{+2.0}_{-2.0}$	$4.5^{+3.4}_{-3.4}$	$4.4^{+2.7}_{-2.7}$	Sereno et al. (2014)	200	0.3/0.7/0.7
ZwCl1454.8+2233	0.2578	14 57 14.40	+22 20 38.4	WL	$3.14^{+2.69}_{-1.53}$	$2.82^{+1.65}_{-1.11}$	$4.01^{+3.44}_{-1.96}$	$3.45^{+2.02}_{-1.36}$	Okabe et al. (2010)	virial	0.27/0.73/0.72
MS 1455.0+2232	0.259	14 57 15.1	+22 20 34	X-ray	$6.32^{+0.53}_{-0.51}$	$3.66^{+0.29}_{-0.29}$	$7.79^{+0.65}_{-0.63}$	$4.19^{+0.33}_{-0.33}$	Ettori et al. (2011)	200	0.3/0.7/0.7
MS 1455.0+2232	0.259	14 57 15.1	+22 20 34	X-ray	10.9	14.0	13.2	15.0	Molikawa et al. (1999)	virial	0.3/0.7/0.5
J0454-0309	0.26	04 54 10.0	-03 09 00	WL	$9.5^{+4.8}_{-4.8}$	$0.84^{+0.66}_{-0.66}$	$11.79^{+5.84}_{-5.84}$	$0.94^{+0.77}_{-0.77}$	Schirmer et al. (2010)	200	0.27/0.73/0.7
RXCJ2337.6+0016	0.273	23 37 40.6	+00 16 36	X-ray	$4.99^{+3.52}_{-2.18}$	$6.81^{+1.91}_{-1.91}$	$6.17^{+4.35}_{-2.7}$	$7.91^{+2.22}_{-2.22}$	Ettori et al. (2011)	200	0.3/0.7/0.7
RXCJ2337.6+0016	0.273	23 37 40.6	+00 16 36	WL	$6.6^{+2.5}_{-2.5}$	$6.4^{+1.1}_{-1.1}$	$8.1^{+3.0}_{-3.0}$	$7.3^{+1.4}_{-1.4}$	Sereno et al. (2014)	200	0.3/0.7/0.7
RXCJ2337.6+0016	0.273	23 37 40.6	+00 16 36	X-ray	$5.02^{+1.55}_{-1.77}$	$8.5^{+1.01}_{-0.89}$	$6.3^{+1.95}_{-2.22}$	$9.98^{+1.19}_{-1.04}$	Babyk et al. (2014)	200	0.27/0.73/0.73
RXCJ0303.8-7752	0.274	03 03 46.4	-77 52 09	X-ray	$1.85^{+1.04}_{-0.09}$	$13.21^{+2.33}_{-2.33}$	$2.36^{+1.33}_{-0.11}$	$16.88^{+2.98}_{-2.98}$	Ettori et al. (2011)	200	0.3/0.7/0.7
RXCJ0532.9-3701	0.275	05 32 56.0	-37 01 34	X-ray	$5.97^{+2.43}_{-1.82}$	$6.88^{+1.83}_{-1.83}$	$7.34^{+2.99}_{-2.24}$	$7.88^{+2.1}_{-2.1}$	Ettori et al. (2011)	200	0.3/0.7/0.7
Abell 1703	0.277	13 15 05.24	+51 49 02.6	SL	$4.0^{+0.5}_{-0.5}$	$20.2^{+5.9}_{-4.9}$	$5.1^{+0.7}_{-0.7}$	$24.1^{+7.0}_{-5.8}$	Oguri et al. (2009b)	virial	0.26/0.74/0.72
Abell 1703	0.277	13 15 05.24	+51 49 02.6	WL	$2.6^{+1.1}_{-0.9}$	$15.5^{+5.2}_{-4.0}$	$3.3^{+1.4}_{-1.1}$	$19.5^{+6.5}_{-5.0}$	Oguri et al. (2009b)	virial	0.26/0.74/0.72
Abell 1703	0.277	13 15 05.24	+51 49 02.6	WL+SL	$5.2^{+1.0}_{-0.6}$	$12.9^{+3.4}_{-3.0}$	$6.5^{+1.2}_{-0.7}$	$15.0^{+4.0}_{-3.5}$	Oguri et al. (2009b)	virial	0.26/0.74/0.72
Abell 1703	0.277	13 15 05.24	+51 49 02.6	WL+SL	$5.8^{+0.4}_{-0.4}$	$15.3^{+1.8}_{-1.8}$	$7.15^{+0.5}_{-0.5}$	$17.4^{+2.1}_{-2.1}$	Zitrin et al. (2010)	virial	0.3/0.7/0.7
Abell 1703	0.277	13 15 05.24	+51 49 02.6	WL	$6.3^{+1.8}_{-1.4}$	$14.4^{+3.5}_{-2.7}$	$7.71^{+2.22}_{-1.66}$	$16.4^{+4.0}_{-3.1}$	Zitrin et al. (2010)	virial	0.3/0.7/0.7
Abell 1703	0.277	13 15 05.24	+51 49 02.6	WL	$5.6^{+0.8}_{-0.8}$	$13.6^{+2.0}_{-2.0}$	$6.9^{+1.0}_{-1.0}$	$15.7^{+2.5}_{-2.5}$	Sereno et al. (2014)	200	0.3/0.7/0.7

Continued on next page

Table C.1 – *Continued*

Cluster	z	RA	Dec.	Method	$c_{200}$	$M_{200}$ ( $10^{14} M_\odot$ )	$c_{\text{vir}}$	$M_{\text{vir}}$ ( $10^{14} M_\odot$ )	Ref.	$\delta$	$\Omega_m/\Omega_\Lambda/h$
Abell 1703	0.277	13 15 05.24	+51 49 02.6	WL	$5.72^{+1.92}_{-1.39}$	$15.41^{+3.06}_{-2.55}$	$7.02^{+2.36}_{-1.7}$	$17.6^{+3.49}_{-2.91}$	Umetsu et al. (2011b)	virial	0.3/0.7/0.7
Abell 1703	0.277	13 15 05.24	+51 49 02.6	WL	$3.81^{+0.99}_{-0.82}$	$10.82^{+2.19}_{-1.82}$	$4.79^{+1.24}_{-1.03}$	$12.88^{+2.61}_{-2.17}$	Oguri et al. (2012b)	virial	0.275/0.725/0.702
Abell 1703	0.277	13 15 05.24	+51 49 02.6	WL+SL	$5.69^{+0.92}_{-0.68}$	$9.52^{+1.67}_{-1.42}$	$7.08^{+1.14}_{-0.84}$	$10.96^{+1.92}_{-1.63}$	Oguri et al. (2012b)	virial	0.275/0.725/0.702
Abell 2631	0.278	23 37 40.08	+00 16 33.6	WL	$6.3^{+2.84}_{-1.83}$	$4.57^{+1.0}_{-0.85}$	$7.84^{+3.54}_{-2.28}$	$5.24^{+1.15}_{-0.98}$	Okabe et al. (2010)	virial	0.27/0.73/0.72
Abell 1758N	0.279	13 32 32.1	+50 30 37	WL	$0.16^{+0.68}_{-0.68}$	$3.74^{+6.8}_{-6.8}$	$0.24^{+0.95}_{-0.95}$	$7.51^{+8.14}_{-8.14}$	Okabe & Umetsu (2008)	virial	0.3/0.7/0.7
Abell 1758S	0.279	13 32 32.1	+50 30 37	WL	$3.13^{+5.41}_{-5.41}$	$1.42^{+1.63}_{-1.63}$	$3.91^{+6.51}_{-6.51}$	$1.71^{+1.64}_{-1.64}$	Okabe & Umetsu (2008)	virial	0.3/0.7/0.7
Abell 689	0.2793	08 37 25.4	+14 58 59	WL	$1.5^{+1.6}_{-1.6}$	$1.6^{+0.9}_{-0.9}$	$1.9^{+2.0}_{-2.0}$	$2.1^{+1.5}_{-1.5}$	Sereno et al. (2014)	200	0.3/0.7/0.7
RXJ0142.0+2131	0.2803	01 42 02.64	+21 31 19.2	WL	$5.4^{+1.6}_{-1.6}$	$6.0^{+1.3}_{-1.3}$	$6.6^{+1.9}_{-1.9}$	$6.9^{+1.7}_{-1.7}$	Sereno et al. (2014)	200	0.3/0.7/0.7
RXJ0142.0+2131	0.2803	01 42 02.64	+21 31 19.2	WL	$5.71^{+2.17}_{-1.52}$	$3.89^{+1.07}_{-0.88}$	$7.12^{+2.71}_{-1.89}$	$4.49^{+1.23}_{-1.01}$	Okabe et al. (2010)	virial	0.27/0.73/0.72
XMMU J131359.7-162735	0.281	13 13 59.7	-16 27 35	X-ray	$5.5^{+0.3}_{-0.3}$	$3.4^{+0.32}_{-0.32}$	$6.7^{+0.4}_{-0.4}$	$3.89^{+0.35}_{-0.35}$	Gastaldello et al. (2007b)	virial	0.3/0.7/0.7
Abell 697	0.282	08 42 56.7	+36 21 45	WL	$2.5^{+0.7}_{-0.7}$	$13.1^{+2.4}_{-2.4}$	$3.1^{+0.9}_{-0.9}$	$16.2^{+3.4}_{-3.4}$	Sereno et al. (2014)	200	0.3/0.7/0.7
Abell 697	0.282	08 42 56.7	+36 21 45	X-ray	$5.58^{+1.11}_{-1.22}$	$13.56^{+1.27}_{-1.14}$	$6.97^{+1.39}_{-1.52}$	$15.76^{+1.48}_{-1.32}$	Babyk et al. (2014)	200	0.27/0.73/0.73
Abell 697	0.282	08 42 56.7	+36 21 45	WL	$2.31^{+0.66}_{-0.54}$	$9.78^{+2.12}_{-1.75}$	$2.97^{+0.85}_{-0.69}$	$12.36^{+2.68}_{-2.21}$	Okabe et al. (2010)	virial	0.27/0.73/0.72
RXCJ0232.2-4420	0.283	02 32 18.7	-44 20 41	X-ray	$1.8^{+0.66}_{-0.04}$	$14.28^{+1.9}_{-1.9}$	$2.29^{+0.84}_{-0.05}$	$18.26^{+2.43}_{-2.43}$	Ettori et al. (2011)	200	0.3/0.7/0.7
RXCJ0232.2-4420	0.283	02 32 18.7	-44 20 41	X-ray	$1.88^{+0.67}_{-0.66}$	$18.25^{+2.16}_{-1.82}$	$2.43^{+0.87}_{-0.85}$	$23.64^{+2.8}_{-2.36}$	Babyk et al. (2014)	200	0.27/0.73/0.73
Abell 611	0.288	08 00 58.9	+36 02 50	WL	$3.7^{+1.4}_{-1.4}$	$7.4^{+1.7}_{-1.7}$	$4.6^{+1.7}_{-1.7}$	$8.8^{+2.3}_{-2.3}$	Sereno et al. (2014)	200	0.3/0.7/0.7
Abell 611	0.288	08 00 58.9	+36 02 50	WL	$4.5^{+0.8}_{-0.8}$	$14.6^{+3.6}_{-3.6}$	$5.6^{+1.0}_{-1.0}$	$17.1^{+4.4}_{-4.4}$	Sereno et al. (2014)	200	0.3/0.7/0.7
Abell 611	0.288	08 00 58.9	+36 02 50	WL+SL	$3.4^{+0.9}_{-0.9}$	$8.5^{+0.5}_{-0.5}$	$4.3^{+1.1}_{-1.1}$	$10.3^{+0.7}_{-0.7}$	Merten et al. (2014)	2500/200/virial	0.27/0.73/0.7
Abell 611	0.288	08 00 58.9	+36 02 50	WL	$3.35^{+1.4}_{-0.97}$	$5.51^{+1.45}_{-1.18}$	$4.23^{+1.77}_{-1.23}$	$6.65^{+1.75}_{-1.42}$	Okabe et al. (2010)	virial	0.27/0.73/0.72
Abell 611	0.288	08 00 58.9	+36 02 50	X-ray	$5.08^{+1.72}_{-1.61}$	$6.81^{+4.68}_{-2.11}$	$6.24^{+2.06}_{-1.94}$	$7.83^{+5.78}_{-2.53}$	Schmidt & Allen (2007)	virial	0.3/0.7/0.7
Abell 611	0.288	08 00 58.9	+36 02 50	X-ray	$4.58^{+2.36}_{-2.22}$	$9.4^{+16.6}_{-3.9}$	$5.64^{+2.83}_{-2.68}$	$11.0^{+21.0}_{-5.0}$	Allen et al. (2003)	200	0.3/0.7/0.5
ZwCl1459.4+4240	0.2897	15 01 23.13	+42 20 39.6	WL	$8.3^{+3.9}_{-3.9}$	$3.7^{+1.1}_{-1.1}$	$10.1^{+4.7}_{-4.7}$	$4.1^{+1.3}_{-1.3}$	Sereno et al. (2014)	200	0.3/0.7/0.7
ZwCl1459.4+4240	0.2897	15 01 23.13	+42 20 39.6	WL	$5.26^{+2.68}_{-1.75}$	$3.8^{+1.3}_{-1.04}$	$6.55^{+3.34}_{-2.18}$	$4.4^{+1.5}_{-1.2}$	Okabe et al. (2010)	virial	0.27/0.73/0.72
Zwicky 3146	0.291	10 23 39.6	+04 11 10	X-ray	$3.37^{+0.15}_{-0.26}$	$7.79^{+0.49}_{-0.49}$	$4.19^{+0.19}_{-0.32}$	$9.32^{+0.59}_{-0.59}$	Ettori et al. (2011)	200	0.3/0.7/0.7
Zwicky 3146	0.291	10 23 39.6	+04 11 10	X-ray	$2.32^{+2.31}_{-2.32}$	$28.1^{+\infty}_{-16.3}$	$2.91^{+2.78}_{-2.91}$	$34.5^{+\infty}_{-20.9}$	Schmidt & Allen (2007)	virial	0.3/0.7/0.7
RXCJ0043.4-2037	0.292	00 43 24.4	-20 37 17	X-ray	$7.8^{+5.05}_{-3.51}$	$4.7^{+1.24}_{-1.24}$	$9.5^{+6.15}_{-4.27}$	$5.28^{+1.39}_{-1.39}$	Ettori et al. (2011)	200	0.3/0.7/0.7
RXCJ0043.4-2037	0.292	00 43 24.4	-20 37 17	X-ray	$8.01^{+3.89}_{-3.03}$	$6.38^{+0.82}_{-0.84}$	$9.9^{+4.81}_{-3.74}$	$7.22^{+0.93}_{-0.95}$	Babyk et al. (2014)	200	0.27/0.73/0.73
RXCJ0516.7-5430	0.294	05 16 35.2	-54 16 37	X-ray	$2.41^{+2.82}_{-0.75}$	$10.44^{+2.88}_{-2.88}$	$3.03^{+3.55}_{-0.94}$	$12.89^{+3.56}_{-3.56}$	Ettori et al. (2011)	200	0.3/0.7/0.7
RXCJ0516.7-5430	0.294	05 16 35.2	-54 16 37	X-ray	$2.45^{+1.55}_{-0.77}$	$13.96^{+1.54}_{-1.22}$	$3.13^{+1.98}_{-0.98}$	$17.48^{+1.93}_{-1.53}$	Babyk et al. (2014)	200	0.27/0.73/0.73
Abell 2537	0.295	23 08 23.2	-02 11 31	X-ray	$4.88^{+0.24}_{-0.24}$	$16.12^{+2.16}_{-2.19}$	$6.1^{+0.3}_{-0.3}$	$18.89^{+2.53}_{-2.57}$	Babyk et al. (2014)	200	0.27/0.73/0.73

Continued on next page

Table C.1 – *Continued*

Cluster	z	RA	Dec.	Method	$c_{200}$	$M_{200}$ ( $10^{14} M_\odot$ )	$c_{\text{vir}}$	$M_{\text{vir}}$ ( $10^{14} M_\odot$ )	Ref.	$\delta$	$\Omega_m/\Omega_\Lambda/h$
Abell 2537	0.295	23 08 23.2	-02 11 31	X-ray	$4.83^{+2.32}_{-1.59}$	$7.58^{+5.88}_{-3.04}$	$5.93^{+2.78}_{-1.91}$	$8.74^{+7.28}_{-3.64}$	Schmidt & Allen (2007)	virial	0.3/0.7/0.7
MS 1008.1-1224	0.301	10 10 32.2	-12 39 55	X-ray	4.4	34.0	5.4	39.0	Molikawa et al. (1999)	virial	0.3/0.7/0.5
RXCJ1131.9-1955	0.307	11 31 54.4	-19 55 42	X-ray	$2.43^{+1.16}_{-0.76}$	$11.31^{+2.5}_{-2.5}$	$3.04^{+1.45}_{-0.95}$	$13.91^{+3.07}_{-3.07}$	Ettori et al. (2011)	200	0.3/0.7/0.7
RXCJ1131.9-1955	0.307	11 31 54.4	-19 55 42	X-ray	$2.55^{+1.24}_{-1.67}$	$15.43^{+1.45}_{-1.66}$	$3.24^{+1.58}_{-1.12}$	$19.17^{+1.8}_{-2.06}$	Babyk et al. (2014)	200	0.27/0.73/0.73
Abell 2744	0.308	00 14 18.9	-30 23 22	X-ray	$1.72^{+0.15}_{-0.17}$	$22.17^{+2.14}_{-2.26}$	$2.22^{+0.19}_{-0.22}$	$28.83^{+2.78}_{-2.94}$	Babyk et al. (2014)	200	0.27/0.73/0.73
GHO132029+3155	0.308	13 22 48.77	+31 39 17.8	WL	$12.3^{+3.2}_{-3.2}$	$3.9^{+0.6}_{-0.6}$	$14.8^{+3.8}_{-3.8}$	$4.3^{+0.7}_{-0.7}$	Sereno et al. (2014)	200	0.3/0.7/0.7
GHO132029+3155	0.308	13 22 48.77	+31 39 17.8	WL	$7.17^{+2.73}_{-1.91}$	$3.03^{+0.57}_{-0.51}$	$8.81^{+3.35}_{-2.35}$	$3.43^{+0.65}_{-0.58}$	Oguri et al. (2012b)	virial	0.275/0.725/0.702
GHO132029+3155	0.308	13 22 48.77	+31 39 17.8	WL+SL	$12.86^{+3.71}_{-2.29}$	$2.68^{+0.47}_{-0.45}$	$15.67^{+4.52}_{-2.79}$	$2.95^{+0.52}_{-0.5}$	Oguri et al. (2012b)	virial	0.275/0.725/0.702
MS 2137.3-2353	0.313	21 40 15.2	-23 39 40	SL	$9.5^{+1.29}_{-0.87}$	$4.11^{+0.75}_{-0.46}$	$11.47^{+1.56}_{-1.05}$	$4.55^{+0.83}_{-0.51}$	Donnarumma et al. (2009)	200	0.3/0.7/0.7
MS 2137.3-2353	0.313	21 40 15.2	-23 39 40	X-ray	$8.68^{+0.71}_{-0.91}$	$4.43^{+0.25}_{-0.25}$	$10.49^{+0.86}_{-1.1}$	$4.93^{+0.28}_{-0.28}$	Donnarumma et al. (2009)	200	0.3/0.7/0.7
MS 2137.3-2353	0.313	21 40 15.2	-23 39 40	WL	$5.2^{+0.9}_{-0.9}$	$10.5^{+2.4}_{-2.4}$	$6.4^{+1.1}_{-1.1}$	$11.7^{+2.9}_{-2.9}$	Sereno et al. (2014)	200	0.3/0.7/0.7
MS 2137.3-2353	0.313	21 40 15.2	-23 39 40	WL+SL	$3.1^{+0.6}_{-0.6}$	$10.4^{+0.6}_{-0.6}$	$4.0^{+0.7}_{-0.7}$	$12.6^{+0.6}_{-0.6}$	Merten et al. (2014)	2500/200/virial	0.27/0.73/0.7
MS 2137.3-2353	0.313	21 40 15.2	-23 39 40	SL	$13.0^{+1.0}_{-1.0}$	$2.9^{+0.4}_{-0.4}$	$16.0^{+1.0}_{-1.0}$	$3.2^{+0.4}_{-0.4}$	Comerford & Natarajan (2007b)	200/virial	0.3/0.7/0.7
MS 2137.3-2353	0.313	21 40 15.2	-23 39 40	SL	$11.92^{+0.77}_{-0.74}$	$7.56^{+0.63}_{-0.54}$	$14.34^{+0.91}_{-0.88}$	$8.29^{+0.71}_{-0.61}$	Gavazzi (2005)	200	0.3/0.7/0.7
MS 2137.3-2353	0.313	21 40 15.2	-23 39 40	SL	$12.5^{+5.0}_{-6.0}$	7.9	$15.0^{+6.0}_{-7.0}$	8.6	Gavazzi et al. (2003)	200	0.3/0.7/None
MS 2137.3-2353	0.313	21 40 15.2	-23 39 40	SL	$11.7^{+2.1}_{-2.1}$	$7.23^{+1.9}_{-1.9}$	$14.1^{+2.5}_{-2.5}$	$7.93^{+2.17}_{-2.17}$	Gavazzi (2002)	200	0.3/0.7/None
MS 2137.3-2353	0.313	21 40 15.2	-23 39 40	WL	$12.0^{+12.0}_{-8.0}$	$9.3^{+85.4}_{-7.8}$	$14.0^{+14.0}_{-10.0}$	$10.0^{+100.0}_{-9.0}$	Gavazzi et al. (2003)	200	0.3/0.7/None
MS 2137.3-2353	0.313	21 40 15.2	-23 39 40	WL+SL	$11.73^{+0.55}_{-0.55}$	$7.72^{+0.47}_{-0.42}$	$14.11^{+0.65}_{-0.65}$	$8.47^{+0.53}_{-0.48}$	Gavazzi (2005)	200	0.3/0.7/0.7
MS 2137.3-2353	0.313	21 40 15.2	-23 39 40	X-ray	$7.21^{+0.58}_{-0.59}$	$4.7^{+0.81}_{-0.56}$	$8.75^{+0.69}_{-0.71}$	$5.27^{+0.94}_{-0.65}$	Schmidt & Allen (2007)	virial	0.3/0.7/0.7
MS 2137.3-2353	0.313	21 40 15.2	-23 39 40	X-ray	$5.28^{+2.41}_{-2.52}$	$8.0^{+32.0}_{-4.8}$	$6.44^{+2.87}_{-3.02}$	$9.1^{+39.0}_{-5.6}$	Voigt & Fabian (2006)	200/2E4	0.3/0.7/0.7
MS 2137.3-2353	0.313	21 40 15.2	-23 39 40	X-ray	$8.71^{+1.22}_{-0.92}$	$4.25^{+0.84}_{-0.88}$	$10.5^{+1.5}_{-1.1}$	$4.72^{+0.96}_{-1.0}$	Allen et al. (2003)	200	0.3/0.7/0.5
MS 2137.3-2353	0.313	21 40 15.2	-23 39 40	X-ray	12.4	11.0	14.9	12.0	Molikawa et al. (1999)	virial	0.3/0.7/0.5
MACSJ0242.6-2132	0.314	02 42 35.9	-21 32 26	X-ray	$7.88^{+1.64}_{-1.23}$	$27.44^{+1.99}_{-2.19}$	$9.69^{+2.02}_{-1.51}$	$30.97^{+2.25}_{-2.47}$	Babyk et al. (2014)	200	0.27/0.73/0.73
MACSJ0242.6-2132	0.314	02 42 35.9	-21 32 26	X-ray	$6.69^{+1.23}_{-0.92}$	$4.85^{+1.64}_{-1.31}$	$8.12^{+1.46}_{-1.09}$	$5.47^{+1.92}_{-1.51}$	Schmidt & Allen (2007)	virial	0.3/0.7/0.7
MACSJ1427.6-2521	0.318	14 27 39.4	-25 21 02	X-ray	$8.28^{+1.99}_{-1.77}$	$25.04^{+2.36}_{-2.26}$	$10.16^{+2.44}_{-2.17}$	$28.16^{+2.65}_{-2.54}$	Babyk et al. (2014)	200	0.27/0.73/0.73
Abell 1995	0.318	14 52 56.1	+58 02 56	X-ray	$3.17^{+0.38}_{-0.33}$	$45.32^{+5.16}_{-3.18}$	$3.99^{+0.48}_{-0.42}$	$54.96^{+6.26}_{-3.86}$	Babyk et al. (2014)	200	0.27/0.73/0.73
MS 0353.6-3642	0.32	03 55 33.3	-36 34 18	X-ray	4.84	32.0	5.91	36.0	Molikawa et al. (1999)	virial	0.3/0.7/0.5
MACSJ2229.8-2756	0.324	22 29 45.2	-27 55 37	X-ray	$8.54^{+1.67}_{-1.36}$	$46.06^{+4.92}_{-5.17}$	$10.46^{+2.05}_{-1.67}$	$51.67^{+5.52}_{-5.8}$	Babyk et al. (2014)	200	0.27/0.73/0.73
MACSJ2229.8-2756	0.324	22 29 45.2	-27 55 37	X-ray	$7.7^{+3.66}_{-2.62}$	$2.74^{+2.02}_{-1.0}$	$9.3^{+4.34}_{-3.11}$	$3.06^{+2.38}_{-1.15}$	Schmidt & Allen (2007)	virial	0.3/0.7/0.7
MS 1224.7+2007	0.327	12 27 13.5	+19 50 55	X-ray	11.3	9.2	13.5	10.0	Molikawa et al. (1999)	virial	0.3/0.7/0.5

Continued on next page

Table C.1 – *Continued*

Cluster	z	RA	Dec.	Method	$c_{200}$	$M_{200}$ ( $10^{14} M_\odot$ )	$c_{\text{vir}}$	$M_{\text{vir}}$ ( $10^{14} M_\odot$ )	Ref.	$\delta$	$\Omega_m/\Omega_\Lambda/h$
MS 1358.4+6245	0.328	13 59 53.1	+62 31 16	X-ray	5.84	26.0	7.09	29.0	Molikawa et al. (1999)	virial	0.3/0.7/0.5
CL 2244-0221	0.33	22 47 12.6	-02 05 40	SL	$4.3^{+0.4}_{-0.4}$	$4.5^{+0.9}_{-0.9}$	$5.2^{+0.5}_{-0.5}$	$5.2^{+1.1}_{-1.1}$	Comerford & Natarajan (2007b)	200/virial	0.3/0.7/0.7
RCSJ2156+0123	0.335	15 47 34.2	+26 38 29.0	X-ray	$1.23^{+0.41}_{-0.3}$	$22.8^{+3.28}_{-2.88}$	$1.6^{+0.53}_{-0.39}$	$30.75^{+4.43}_{-3.89}$	Babyk et al. (2014)	200	0.27/0.73/0.73
SDSSJ1531+3414	0.335	15 31 10.60	+34 14 25.0	SL	$2.4^{+10.4}_{-0.6}$	$35.1^{+20.9}_{-34.0}$	$3.0^{+13.0}_{-0.7}$	$43.9^{+26.1}_{-42.5}$	Oguri et al. (2009b)	virial	0.26/0.74/0.72
SDSSJ1531+3414	0.335	15 31 10.60	+34 14 25.0	WL	$9.4^{+23.3}_{-6.0}$	$5.3^{+3.5}_{-2.3}$	$11.5^{+28.5}_{-7.4}$	$5.9^{+3.9}_{-2.6}$	Oguri et al. (2009b)	virial	0.26/0.74/0.72
SDSSJ1531+3414	0.335	15 31 10.60	+34 14 25.0	WL+SL	$6.4^{+2.4}_{-1.2}$	$5.8^{+2.5}_{-2.1}$	$7.9^{+3.0}_{-1.5}$	$6.6^{+2.9}_{-2.4}$	Oguri et al. (2009b)	virial	0.26/0.74/0.72
SDSSJ1531+3414	0.335	15 31 10.60	+34 14 25.0	WL	$6.8^{+1.2}_{-1.2}$	$6.4^{+1.6}_{-1.6}$	$8.2^{+1.4}_{-1.4}$	$7.2^{+1.9}_{-1.9}$	Sereno et al. (2014)	200	0.3/0.7/0.7
SDSSJ1531+3414	0.335	15 31 10.60	+34 14 25.0	WL	$4.84^{+2.66}_{-1.68}$	$4.98^{+1.58}_{-1.25}$	$5.96^{+3.27}_{-2.07}$	$5.75^{+1.83}_{-1.44}$	Oguri et al. (2012b)	virial	0.275/0.725/0.702
SDSSJ1531+3414	0.335	15 31 10.60	+34 14 25.0	WL+SL	$6.81^{+1.29}_{-0.95}$	$4.54^{+1.18}_{-1.05}$	$8.32^{+1.57}_{-1.16}$	$5.13^{+1.33}_{-1.19}$	Oguri et al. (2012b)	virial	0.275/0.725/0.702
SDSSJ1621+0607	0.342	16 21 32.36	+06 07 19.0	WL	$4.4^{+1.0}_{-1.0}$	$7.1^{+2.3}_{-2.3}$	$5.4^{+1.2}_{-1.2}$	$8.2^{+2.8}_{-2.8}$	Sereno et al. (2014)	200	0.3/0.7/0.7
SDSSJ1621+0607	0.342	16 21 32.36	+06 07 19.0	WL	$3.17^{+1.52}_{-1.12}$	$5.58^{+2.12}_{-1.68}$	$3.94^{+1.89}_{-1.39}$	$6.68^{+2.54}_{-2.01}$	Oguri et al. (2012b)	virial	0.275/0.725/0.702
SDSSJ1621+0607	0.342	16 21 32.36	+06 07 19.0	WL+SL	$4.52^{+1.17}_{-0.85}$	$5.08^{+1.77}_{-1.44}$	$5.56^{+1.44}_{-1.04}$	$5.89^{+2.05}_{-1.67}$	Oguri et al. (2012b)	virial	0.275/0.725/0.702
MACSJ0947.2+7623	0.345	09 47 13.0	+76 23 14	X-ray	$5.41^{+1.86}_{-1.51}$	$10.69^{+8.41}_{-4.04}$	$6.54^{+2.2}_{-1.79}$	$12.15^{+10.04}_{-4.71}$	Schmidt & Allen (2007)	virial	0.3/0.7/0.7
RXCJ2248.7-4431	0.348	22 48 43.5	-44 31 44	WL	$2.6^{+1.5}_{-1.0}$	$33.1^{+9.6}_{-6.8}$	$3.3^{+1.9}_{-1.3}$	$40.7^{+11.8}_{-8.4}$	Gruen et al. (2013)	200	0.27/0.73/0.72
RXCJ2248.7-4431	0.348	22 48 43.5	-44 31 44	WL	$7.1^{+2.6}_{-2.6}$	$12.6^{+4.3}_{-4.3}$	$8.6^{+3.1}_{-3.1}$	$14.1^{+5.1}_{-5.1}$	Sereno et al. (2014)	200	0.3/0.7/0.7
RXCJ2248.7-4431	0.348	22 48 43.5	-44 31 44	WL+SL	$3.2^{+0.9}_{-0.9}$	$11.6^{+1.2}_{-1.2}$	$4.0^{+1.1}_{-1.1}$	$14.0^{+1.2}_{-1.2}$	Merten et al. (2014)	2500/200/virial	0.27/0.73/0.7
MACSJ1115.8+0129	0.352	11 15 52.0	+01 29 55	WL	$4.1^{+0.8}_{-0.8}$	$15.0^{+3.9}_{-3.9}$	$5.0^{+1.9}_{-1.9}$	$17.5^{+4.8}_{-4.8}$	Sereno et al. (2014)	200	0.3/0.7/0.7
MACSJ1115.8+0129	0.352	11 15 52.0	+01 29 55	X-ray	$2.23^{+0.53}_{-0.55}$	$23.59^{+4.17}_{-3.18}$	$2.81^{+0.67}_{-0.69}$	$29.42^{+5.2}_{-3.97}$	Babyk et al. (2014)	200	0.27/0.73/0.73
MACSJ1115.8+0129	0.352	11 15 52.0	+01 29 55	WL+SL	$2.3^{+0.7}_{-0.7}$	$9.0^{+0.9}_{-0.9}$	$2.9^{+0.9}_{-0.9}$	$11.3^{+1.0}_{-1.0}$	Merten et al. (2014)	2500/200/virial	0.27/0.73/0.7
MACSJ1931.8-2635	0.352	19 31 49.6	-26 34 34	WL	$5.9^{+3.3}_{-3.3}$	$12.3^{+7.7}_{-7.7}$	$7.1^{+3.9}_{-3.9}$	$14.0^{+9.3}_{-9.3}$	Sereno et al. (2014)	200	0.3/0.7/0.7
MACSJ1931.8-2635	0.352	19 31 49.6	-26 34 34	X-ray	$4.11^{+0.36}_{-0.24}$	$32.78^{+3.91}_{-4.19}$	$5.09^{+0.45}_{-0.3}$	$38.59^{+4.6}_{-4.93}$	Babyk et al. (2014)	200	0.27/0.73/0.73
MACSJ1931.8-2635	0.352	19 31 49.6	-26 34 34	WL+SL	$3.2^{+0.9}_{-0.9}$	$6.9^{+0.5}_{-0.5}$	$3.9^{+1.1}_{-1.1}$	$8.3^{+0.6}_{-0.6}$	Merten et al. (2014)	2500/200/virial	0.27/0.73/0.7
MACSJ1931.8-2635	0.352	19 31 49.6	-26 34 34	X-ray	$3.11^{+1.87}_{-1.88}$	$16.2^{+\infty}_{-8.6}$	$3.81^{+2.22}_{-2.25}$	$19.2^{+\infty}_{-10.5}$	Schmidt & Allen (2007)	virial	0.3/0.7/0.7
RXJ1532.9+3021	0.3615	15 32 53.8	+30 20 58	WL	$7.5^{+2.3}_{-2.3}$	$4.7^{+1.6}_{-1.6}$	$9.0^{+2.7}_{-2.7}$	$5.2^{+1.9}_{-1.9}$	Sereno et al. (2014)	200	0.3/0.7/0.7
RXJ1532.9+3021	0.3615	15 32 53.8	+30 20 58	X-ray	$2.77^{+2.28}_{-2.28}$	$19.0^{+675.0}_{-16.0}$	$3.4^{+2.7}_{-2.75}$	$23.0^{+1006.0}_{-19.0}$	Voigt & Fabian (2006)	200/2E4	0.3/0.7/0.7
SDSSJ1152+3313	0.362	11 52 00.15	+33 13 42.1	WL	$12.5^{+4.0}_{-4.0}$	$1.3^{+0.6}_{-0.6}$	$14.9^{+4.7}_{-4.7}$	$1.4^{+0.7}_{-0.7}$	Sereno et al. (2014)	200	0.3/0.7/0.7
SDSSJ1152+3313	0.362	11 52 00.15	+33 13 42.1	WL	$23.02^{+10.26}_{-20.29}$	$0.68^{+1.24}_{-0.41}$	$27.54^{+12.27}_{-24.27}$	$0.73^{+1.33}_{-0.44}$	Oguri et al. (2012b)	virial	0.275/0.725/0.702
SDSSJ1152+3313	0.362	11 52 00.15	+33 13 42.1	WL+SL	$14.45^{+18.65}_{-6.14}$	$0.75^{+0.86}_{-0.44}$	$17.38^{+22.43}_{-7.38}$	$0.82^{+0.94}_{-0.48}$	Oguri et al. (2012b)	virial	0.275/0.725/0.702
MACSJ1532.9+3021	0.363	15 32 53.8	+30 20 58	WL+SL	$3.0^{+1.4}_{-1.4}$	$5.3^{+0.8}_{-0.8}$	$3.8^{+1.7}_{-1.7}$	$6.4^{+0.9}_{-0.9}$	Merten et al. (2014)	2500/200/virial	0.27/0.73/0.7
MACSJ1532.9+3021	0.363	15 32 53.8	+30 20 58	X-ray	$4.71^{+1.32}_{-1.25}$	$8.46^{+5.96}_{-2.73}$	$5.69^{+1.56}_{-1.47}$	$9.67^{+7.19}_{-3.22}$	Schmidt & Allen (2007)	virial	0.3/0.7/0.7

Continued on next page

Table C.1 – *Continued*

Cluster	z	RA	Dec.	Method	$c_{200}$	$M_{200}$ ( $10^{14} M_\odot$ )	$c_{\text{vir}}$	$M_{\text{vir}}$ ( $10^{14} M_\odot$ )	Ref.	$\delta$	$\Omega_m/\Omega_\Lambda/h$
SDSSJ0851+3331	0.37	08 51 38.86	+33 31 06.1	WL	$8.6^{+2.6}_{-2.6}$	$7.1^{+2.0}_{-2.0}$	$10.3^{+3.1}_{-3.1}$	$7.9^{+2.3}_{-2.3}$	Sereno et al. (2014)	200	0.3/0.7/0.7
SDSSJ0851+3331	0.37	08 51 38.86	+33 31 06.1	WL	$4.6^{+2.77}_{-1.66}$	$6.36^{+2.12}_{-1.7}$	$5.62^{+3.39}_{-2.03}$	$7.33^{+2.44}_{-1.96}$	Oguri et al. (2012b)	virial	0.275/0.725/0.702
SDSSJ0851+3331	0.37	08 51 38.86	+33 31 06.1	WL+SL	$7.8^{+2.6}_{-1.53}$	$5.59^{+1.61}_{-1.44}$	$9.44^{+3.15}_{-1.85}$	$6.24^{+1.8}_{-1.61}$	Oguri et al. (2012b)	virial	0.275/0.725/0.702
MS 1512.4+3647	0.372	15 14 25.1	+36 36 30	X-ray	7.82	7.2	9.35	7.9	Molikawa et al. (1999)	virial	0.3/0.7/0.5
Abell 370	0.375	02 39 50.5	-01 35 08	WL	$5.83^{+0.91}_{-0.77}$	$31.14^{+3.92}_{-3.33}$	$7.0^{+1.09}_{-0.92}$	$35.01^{+4.41}_{-3.74}$	Umetsu et al. (2011b)	virial	0.3/0.7/0.7
MACSJ0011.7-1523	0.379	00 11 42.9	-15 23 22	X-ray	$4.01^{+0.23}_{-0.33}$	$48.34^{+3.82}_{-4.15}$	$4.94^{+0.28}_{-0.41}$	$56.76^{+4.49}_{-4.87}$	Babyk et al. (2014)	200	0.27/0.73/0.73
BCS J2352-5452	0.3838	23 51 38.0	-54 52 53	WL	$4.9^{+3.9}_{-2.2}$	$5.0^{+2.9}_{-2.3}$	$5.9^{+4.7}_{-2.6}$	$5.7^{+3.3}_{-2.6}$	Buckley-Geer et al. (2011)	200	0.3/0.7/0.7
BCS J2352-5452	0.3838	23 51 38.0	-54 52 53	WL+SL	$5.5^{+2.7}_{-1.6}$	$4.9^{+2.9}_{-2.2}$	$6.6^{+3.2}_{-1.9}$	$5.6^{+3.3}_{-2.5}$	Buckley-Geer et al. (2011)	200	0.3/0.7/0.7
MACSJ1720.3+3536	0.391	17 20 16.8	+35 36 26	WL	$6.1^{+1.5}_{-1.5}$	$10.1^{+2.6}_{-2.6}$	$7.3^{+1.8}_{-1.8}$	$11.4^{+3.1}_{-3.1}$	Sereno et al. (2014)	200	0.3/0.7/0.7
MACSJ1720.3+3536	0.391	17 20 16.8	+35 36 26	X-ray	$5.25^{+0.61}_{-0.36}$	$40.7^{+5.17}_{-4.92}$	$6.4^{+0.74}_{-0.44}$	$46.72^{+5.93}_{-5.65}$	Babyk et al. (2014)	200	0.27/0.73/0.73
MACSJ1720.3+3536	0.391	17 20 16.8	+35 36 26	WL+SL	$4.3^{+1.4}_{-1.4}$	$7.5^{+0.8}_{-0.8}$	$5.2^{+1.7}_{-1.7}$	$8.8^{+0.8}_{-0.8}$	Merten et al. (2014)	2500/200/virial	0.27/0.73/0.7
MACSJ1720.3+3536	0.391	17 20 16.8	+35 36 26	X-ray	$4.37^{+1.21}_{-0.88}$	$9.01^{+4.63}_{-3.3}$	$5.26^{+1.42}_{-1.04}$	$10.31^{+5.55}_{-3.87}$	Schmidt & Allen (2007)	virial	0.3/0.7/0.7
ZwCl 0024.0+1652	0.395	00 26 35.7	+17 09 46	WL	$7.41^{+1.89}_{-1.41}$	$17.74^{+3.0}_{-2.59}$	$8.82^{+2.25}_{-1.68}$	$19.66^{+3.32}_{-2.87}$	Umetsu et al. (2011b)	virial	0.3/0.7/0.7
ZwCl 0024.0+1652	0.395	00 26 35.7	+17 09 46	WL+SL	$22.0^{+9.0}_{-5.0}$	$5.7^{+1.1}_{-1.0}$	$26.0^{+10.0}_{-6.0}$	$6.1^{+1.2}_{-1.1}$	Kneib et al. (2003)	200	0.3/0.7/0.65
SDSSJ0915+3826	0.397	09 15 39.00	+38 26 58.5	WL	$13.2^{+3.8}_{-3.8}$	$1.9^{+0.7}_{-0.7}$	$15.6^{+4.4}_{-4.4}$	$2.1^{+0.8}_{-0.8}$	Sereno et al. (2014)	200	0.3/0.7/0.7
SDSSJ0915+3826	0.397	09 15 39.00	+38 26 58.5	WL	$33.62^{+0.0}_{-14.49}$	$0.86^{+0.28}_{-0.26}$	$39.81^{+0.0}_{-17.16}$	$0.91^{+0.3}_{-0.28}$	Oguri et al. (2012b)	virial	0.275/0.725/0.702
SDSSJ0915+3826	0.397	09 15 39.00	+38 26 58.5	WL+SL	$22.65^{+10.85}_{-9.15}$	$0.75^{+0.47}_{-0.25}$	$26.92^{+12.9}_{-10.88}$	$0.8^{+0.5}_{-0.27}$	Oguri et al. (2012b)	virial	0.275/0.725/0.702
MACSJ0429.6-0253	0.399	04 29 36.0	-02 53 08	WL	$5.8^{+1.4}_{-1.4}$	$7.9^{+2.4}_{-2.4}$	$6.9^{+1.6}_{-1.6}$	$8.9^{+2.8}_{-2.8}$	Sereno et al. (2014)	200	0.3/0.7/0.7
MACSJ0429.6-0253	0.399	04 29 36.0	-02 53 08	X-ray	$3.36^{+1.76}_{-1.65}$	$18.5^{+1.82}_{-1.63}$	$4.14^{+2.17}_{-2.03}$	$21.97^{+2.16}_{-1.94}$	Babyk et al. (2014)	200	0.27/0.73/0.73
MACSJ0429.6-0253	0.399	04 29 36.0	-02 53 08	WL+SL	$3.3^{+1.3}_{-1.3}$	$8.0^{+1.4}_{-1.4}$	$4.0^{+1.6}_{-1.6}$	$9.6^{+1.4}_{-1.4}$	Merten et al. (2014)	2500/200/virial	0.27/0.73/0.7
MACSJ0429.6-0253	0.399	04 29 36.0	-02 53 08	X-ray	$7.64^{+1.57}_{-1.1}$	$3.66^{+1.11}_{-0.97}$	$9.09^{+1.84}_{-1.29}$	$4.05^{+1.27}_{-1.1}$	Schmidt & Allen (2007)	virial	0.3/0.7/0.7
MACSJ0159.8-0849	0.405	01 59 49.4	-08 49 59	X-ray	$5.35^{+0.82}_{-0.72}$	$44.0^{+4.84}_{-4.44}$	$6.5^{+1.0}_{-0.87}$	$50.34^{+5.54}_{-5.08}$	Babyk et al. (2014)	200	0.27/0.73/0.73
MACSJ0159.8-0849	0.405	01 59 49.4	-08 49 59	X-ray	$4.93^{+1.01}_{-1.07}$	$11.59^{+6.29}_{-3.3}$	$5.9^{+1.18}_{-1.25}$	$13.13^{+7.46}_{-3.84}$	Schmidt & Allen (2007)	virial	0.3/0.7/0.7
SDSSJ1343+4155	0.418	13 43 32.85	+41 55 03.4	WL	$4.5^{+1.3}_{-1.3}$	$4.6^{+1.6}_{-1.6}$	$5.4^{+1.5}_{-1.5}$	$5.3^{+1.9}_{-1.9}$	Sereno et al. (2014)	200	0.3/0.7/0.7
SDSSJ1343+4155	0.418	13 43 32.85	+41 55 03.4	WL	$3.76^{+4.66}_{-1.92}$	$3.35^{+1.78}_{-1.26}$	$4.57^{+5.66}_{-2.33}$	$3.89^{+2.07}_{-1.46}$	Oguri et al. (2012b)	virial	0.275/0.725/0.702
SDSSJ1343+4155	0.418	13 43 32.85	+41 55 03.4	WL+SL	$4.18^{+1.39}_{-0.82}$	$3.26^{+1.34}_{-1.08}$	$5.07^{+1.69}_{-1.0}$	$3.76^{+1.55}_{-1.25}$	Oguri et al. (2012b)	virial	0.275/0.725/0.702
MACS J0416.1-2403	0.42	04 16 09.9	-24 03 58	WL	$8.0^{+1.7}_{-1.7}$	$8.6^{+1.4}_{-1.4}$	$9.5^{+2.0}_{-2.0}$	$9.5^{+1.7}_{-1.7}$	Sereno et al. (2014)	200	0.3/0.7/0.7
MS 0302.7+1658	0.426	03 05 31.7	+17 10 03	X-ray	7.39	8.5	8.75	9.4	Molikawa et al. (1999)	virial	0.3/0.7/0.5
SDSSJ1038+4849	0.43	10 38 42.90	+48 49 18.7	WL	$14.8^{+3.5}_{-3.5}$	$1.7^{+0.4}_{-0.4}$	$17.3^{+4.1}_{-4.1}$	$1.8^{+0.4}_{-0.4}$	Sereno et al. (2014)	200	0.3/0.7/0.7
SDSSJ1038+4849	0.43	10 38 42.90	+48 49 18.7	WL	$17.65^{+15.99}_{-11.46}$	$0.8^{+0.66}_{-0.36}$	$20.89^{+18.92}_{-13.56}$	$0.86^{+0.71}_{-0.39}$	Oguri et al. (2012b)	virial	0.275/0.725/0.702

Continued on next page

Table C.1 – *Continued*

Cluster	z	RA	Dec.	Method	$c_{200}$	$M_{200}$ ( $10^{14} M_\odot$ )	$c_{\text{vir}}$	$M_{\text{vir}}$ ( $10^{14} M_\odot$ )	Ref.	$\delta$	$\Omega_m/\Omega_\Lambda/h$
SDSSJ1038+4849	0.43	10 38 42.90	+48 49 18.7	WL+SL	$33.83^{+0.0}_{-18.36}$	$0.7^{+0.49}_{-0.11}$	$39.81^{+0.0}_{-21.61}$	$0.74^{+0.52}_{-0.12}$	Oguri et al. (2012b)	virial	0.275/0.725/0.702
SDSSJ1226+2152	0.43	12 26 51.70	+21 52 26.0	WL	$6.2^{+5.8}_{-5.8}$	$1.9^{+2.1}_{-2.1}$	$7.4^{+6.8}_{-6.8}$	$2.1^{+2.5}_{-2.5}$	Sereno et al. (2014)	200	0.3/0.7/0.7
SDSSJ1226+2152	0.43	12 26 51.70	+21 52 26.0	WL	$5.7^{+27.48}_{-5.69}$	$0.71^{+66.61}_{-0.62}$	$6.84^{+32.97}_{-6.83}$	$0.8^{+75.05}_{-0.7}$	Oguri et al. (2012b)	virial	0.275/0.725/0.702
SDSSJ1226+2152	0.43	12 26 51.70	+21 52 26.0	WL+SL	$33.83^{+0.0}_{-28.15}$	$0.37^{+1.2}_{-0.24}$	$39.81^{+0.0}_{-33.13}$	$0.39^{+1.27}_{-0.25}$	Oguri et al. (2012b)	virial	0.275/0.725/0.702
SDSSJ1226+2149	0.435	12 26 51.11	+21 49 52.3	WL	$4.9^{+1.5}_{-1.5}$	$10.0^{+3.4}_{-3.4}$	$5.8^{+1.7}_{-1.7}$	$11.4^{+4.1}_{-4.1}$	Sereno et al. (2014)	200	0.3/0.7/0.7
SDSSJ1226+2149	0.435	12 26 51.11	+21 49 52.3	WL	$4.35^{+2.08}_{-1.44}$	$7.65^{+3.17}_{-2.3}$	$5.25^{+2.51}_{-1.74}$	$8.81^{+3.63}_{-2.64}$	Oguri et al. (2012b)	virial	0.275/0.725/0.702
SDSSJ1226+2149	0.435	12 26 51.11	+21 49 52.3	WL+SL	$4.61^{+1.4}_{-0.95}$	$7.55^{+2.88}_{-2.14}$	$5.56^{+1.69}_{-1.14}$	$8.61^{+3.28}_{-2.44}$	Oguri et al. (2012b)	virial	0.275/0.725/0.702
MACS J1206.2-0847	0.439	12 06 12.2	-08 48 01	SL	$3.7^{+0.2}_{-0.2}$	—	$4.4^{+0.2}_{-0.2}$	—	Eichner et al. (2013)	200	0.272/0.728/0.702
MACS J1206.2-0847	0.439	12 06 12.2	-08 48 01	LOSVD	$7.3^{+2.4}_{-2.4}$	$13.7^{+1.8}_{-1.8}$	$8.6^{+2.8}_{-2.8}$	$15.2^{+2.3}_{-2.3}$	Biviano et al. (2013)	200	0.3/0.7/0.7
MACS J1206.2-0847	0.439	12 06 12.2	-08 48 01	CM	$4.4^{+3.0}_{-3.0}$	$16.3^{+5.8}_{-5.8}$	$5.3^{+3.5}_{-3.5}$	$18.6^{+7.5}_{-7.5}$	Biviano et al. (2013)	200	0.3/0.7/0.7
MACS J1206.2-0847	0.439	12 06 12.2	-08 48 01	WL	$6.3^{+1.8}_{-1.8}$	$13.3^{+3.3}_{-3.3}$	$7.5^{+2.1}_{-2.1}$	$14.9^{+3.9}_{-3.9}$	Sereno et al. (2014)	200	0.3/0.7/0.7
MACS J1206.2-0847	0.439	12 06 12.2	-08 48 01	WL+SL	$4.3^{+1.5}_{-1.5}$	$8.6^{+1.1}_{-1.1}$	$5.2^{+1.7}_{-1.7}$	$10.0^{+1.1}_{-1.1}$	Merten et al. (2014)	2500/200/virial	0.27/0.73/0.7
SDSSJ1329+2243	0.443	13 29 34.49	+22 43 16.2	WL	$5.0^{+0.9}_{-0.9}$	$6.7^{+1.3}_{-1.3}$	$6.0^{+1.0}_{-1.0}$	$7.6^{+1.6}_{-1.6}$	Sereno et al. (2014)	200	0.3/0.7/0.7
SDSSJ1329+2243	0.443	13 29 34.49	+22 43 16.2	WL	$8.31^{+6.13}_{-3.01}$	$4.44^{+1.21}_{-1.03}$	$9.89^{+7.29}_{-3.58}$	$4.9^{+1.34}_{-1.14}$	Oguri et al. (2012b)	virial	0.275/0.725/0.702
SDSSJ1329+2243	0.443	13 29 34.49	+22 43 16.2	WL+SL	$4.84^{+0.98}_{-0.67}$	$4.95^{+1.22}_{-1.07}$	$5.82^{+1.18}_{-0.81}$	$5.62^{+1.38}_{-1.21}$	Oguri et al. (2012b)	virial	0.275/0.725/0.702
SDSSJ0957+0509	0.448	09 57 39.19	+05 09 31.9	WL	$6.9^{+2.6}_{-2.6}$	$2.0^{+1.1}_{-1.1}$	$8.2^{+3.0}_{-3.0}$	$2.2^{+1.3}_{-1.3}$	Sereno et al. (2014)	200	0.3/0.7/0.7
SDSSJ0957+0509	0.448	09 57 39.19	+05 09 31.9	WL	$33.94^{+0.0}_{-23.57}$	$0.92^{+0.57}_{-0.29}$	$39.81^{+0.0}_{-27.65}$	$0.97^{+0.6}_{-0.31}$	Oguri et al. (2012b)	virial	0.275/0.725/0.702
SDSSJ0957+0509	0.448	09 57 39.19	+05 09 31.9	WL+SL	$7.57^{+3.75}_{-1.83}$	$1.16^{+0.76}_{-0.55}$	$9.02^{+4.47}_{-2.18}$	$1.29^{+0.85}_{-0.61}$	Oguri et al. (2012b)	virial	0.275/0.725/0.702
MACSJ0329.7-0212	0.45	03 29 41.5	-02 11 46	WL	$9.0^{+2.3}_{-2.3}$	$8.7^{+1.6}_{-1.6}$	$10.6^{+2.7}_{-2.7}$	$9.5^{+1.9}_{-1.9}$	Sereno et al. (2014)	200	0.3/0.7/0.7
MACSJ0329.7-0212	0.45	03 29 41.5	-02 11 46	WL+SL	$3.8^{+1.6}_{-1.6}$	$7.3^{+1.0}_{-1.0}$	$4.7^{+1.9}_{-1.9}$	$8.6^{+1.1}_{-1.1}$	Merten et al. (2014)	2500/200/virial	0.27/0.73/0.7
MACSJ0329.7-0212	0.45	03 29 41.5	-02 11 46	X-ray	$4.74^{+0.75}_{-0.78}$	$6.62^{+2.57}_{-1.56}$	$5.62^{+0.88}_{-0.91}$	$7.48^{+3.03}_{-1.81}$	Schmidt & Allen (2007)	virial	0.3/0.7/0.7
SDSSJ1138+2754	0.451	11 38 08.95	+27 54 30.7	WL	$3.6^{+0.3}_{-0.3}$	$12.7^{+0.7}_{-0.7}$	$4.3^{+0.4}_{-0.4}$	$14.7^{+0.9}_{-0.9}$	Sereno et al. (2014)	200	0.3/0.7/0.7
SDSSJ1138+2754	0.451	11 38 08.95	+27 54 30.7	WL	$2.92^{+1.25}_{-0.9}$	$9.49^{+2.18}_{-1.95}$	$3.55^{+1.52}_{-1.09}$	$11.22^{+2.58}_{-2.31}$	Oguri et al. (2012b)	virial	0.275/0.725/0.702
SDSSJ1138+2754	0.451	11 38 08.95	+27 54 30.7	WL+SL	$3.7^{+0.5}_{-0.44}$	$8.94^{+1.81}_{-1.59}$	$4.47^{+0.6}_{-0.53}$	$10.35^{+2.09}_{-1.84}$	Oguri et al. (2012b)	virial	0.275/0.725/0.702
RXJ1347.5-1145	0.451	13 47 30.6	-11 45 10	WL	$4.5^{+1.2}_{-1.2}$	$27.9^{+7.1}_{-7.1}$	$5.4^{+1.4}_{-1.4}$	$31.8^{+8.7}_{-8.7}$	Sereno et al. (2014)	200	0.3/0.7/0.7
RXJ1347.5-1145	0.451	13 47 30.6	-11 45 10	WL	$7.71^{+2.67}_{-1.84}$	$19.33^{+3.6}_{-3.17}$	$9.08^{+3.14}_{-2.17}$	$21.20^{+3.96}_{-3.49}$	Umetsu et al. (2011b)	virial	0.3/0.7/0.7
RXJ1347.5-1145	0.451	13 47 30.6	-11 45 10	WL+SL	$3.9^{+1.5}_{-1.5}$	$11.6^{+1.9}_{-1.9}$	$4.7^{+1.8}_{-1.8}$	$13.5^{+1.9}_{-1.9}$	Merten et al. (2014)	2500/200/virial	0.27/0.73/0.7
RXJ1347.5-1145	0.451	13 47 30.6	-11 45 10	WL	$15.0^{+64.0}_{-10.0}$	$27.0^{+26.0}_{-14.0}$	$18.0^{+74.0}_{-12.0}$	$29.0^{+31.0}_{-15.0}$	Kling et al. (2005)	200	0.3/0.7/0.5
RXJ1347.5-1145	0.451	13 47 30.6	-11 45 10	X-ray	$4.79^{+0.68}_{-0.37}$	$32.0^{+6.1}_{-8.2}$	$5.68^{+0.79}_{-0.43}$	$36.1^{+7.1}_{-9.5}$	Schmidt & Allen (2007)	virial	0.3/0.7/0.7
RXJ1347.5-1145	0.451	13 47 30.6	-11 45 10	X-ray	$4.37^{+1.39}_{-1.24}$	$33.0^{+48.0}_{-18.0}$	$5.2^{+1.62}_{-1.45}$	$37.0^{+57.0}_{-21.0}$	Voigt & Fabian (2006)	200/2E4	0.3/0.7/0.7

Continued on next page

Table C.1 – *Continued*

Cluster	z	RA	Dec.	Method	$c_{200}$	$M_{200}$ ( $10^{14} M_\odot$ )	$c_{\text{vir}}$	$M_{\text{vir}}$ ( $10^{14} M_\odot$ )	Ref.	$\delta$	$\Omega_m/\Omega_\Lambda/h$
RXJ1347.5-1145	0.451	13 47 30.6	-11 45 10	X-ray	$6.34^{+1.61}_{-1.35}$	$23.7^{+14.2}_{-9.3}$	$7.49^{+1.87}_{-1.57}$	$26.3^{+16.3}_{-10.5}$	Allen et al. (2003)	200	0.3/0.7/0.5
3C 295	0.461	14 11 20.5	+52 12 10	X-ray	$7.79^{+1.04}_{-0.9}$	$3.57^{+0.81}_{-0.65}$	$9.15^{+1.2}_{-0.9}$	$3.93^{+0.92}_{-0.73}$	Schmidt & Allen (2007)	virial	0.3/0.7/0.7
3C 295	0.461	14 11 20.5	+52 12 10	X-ray	$7.9^{+1.71}_{-1.72}$	$3.76^{+1.59}_{-1.02}$	$9.29^{+2.01}_{-2.02}$	$4.14^{+1.75}_{-1.12}$	Allen et al. (2003)	200	0.3/0.7/0.5
MACSJ1621.6+3810	0.461	16 21 36.0	+38 10 00	X-ray	$5.97^{+2.95}_{-1.94}$	$7.1^{+5.33}_{-2.9}$	$7.05^{+3.42}_{-2.26}$	$7.91^{+6.25}_{-3.31}$	Schmidt & Allen (2007)	virial	0.3/0.7/0.7
SDSSJ1446+3032	0.464	14 46 34.02	+30 32 58.2	SL	$9.8^{+23.7}_{-6.0}$	$4.8^{+12.1}_{-2.5}$	$11.7^{+28.3}_{-7.2}$	$5.3^{+13.4}_{-2.8}$	Oguri et al. (2009b)	virial	0.26/0.74/0.72
SDSSJ1446+3032	0.464	14 46 34.02	+30 32 58.2	WL	$7.6^{+9.5}_{-3.4}$	$7.5^{+2.6}_{-2.3}$	$9.1^{+11.4}_{-4.1}$	$8.3^{+2.9}_{-2.5}$	Oguri et al. (2009b)	virial	0.26/0.74/0.72
SDSSJ1446+3032	0.464	14 46 34.02	+30 32 58.2	WL+SL	$6.9^{+3.2}_{-2.6}$	$7.4^{+2.7}_{-2.0}$	$8.3^{+3.9}_{-3.1}$	$8.3^{+3.0}_{-2.2}$	Oguri et al. (2009b)	virial	0.26/0.74/0.72
SDSSJ1446+3032	0.464	14 46 34.02	+30 32 58.2	WL	$10.0^{+3.9}_{-3.9}$	$6.3^{+1.6}_{-1.6}$	$11.7^{+4.5}_{-4.5}$	$6.9^{+1.9}_{-1.9}$	Sereno et al. (2014)	200	0.3/0.7/0.7
SDSSJ1446+3032	0.464	14 46 34.02	+30 32 58.2	WL	$10.65^{+7.65}_{-3.7}$	$3.73^{+1.07}_{-0.9}$	$12.59^{+9.04}_{-4.37}$	$4.07^{+1.17}_{-0.98}$	Oguri et al. (2012b)	virial	0.275/0.725/0.702
SDSSJ1446+3032	0.464	14 46 34.02	+30 32 58.2	WL+SL	$10.16^{+7.09}_{-3.21}$	$3.77^{+1.09}_{-0.91}$	$12.02^{+8.39}_{-3.8}$	$4.12^{+1.19}_{-0.99}$	Oguri et al. (2012b)	virial	0.275/0.725/0.702
SDSSJ1115+5319	0.466	11 15 14.85	+53 19 54.6	WL	$4.6^{+1.7}_{-1.7}$	$12.4^{+3.6}_{-3.6}$	$5.5^{+2.0}_{-2.0}$	$14.1^{+4.4}_{-4.4}$	Sereno et al. (2014)	200	0.3/0.7/0.7
SDSSJ1115+5319	0.466	11 15 14.85	+53 19 54.6	WL	$2.17^{+1.0}_{-0.73}$	$9.52^{+2.89}_{-2.38}$	$2.66^{+1.23}_{-0.9}$	$11.61^{+3.52}_{-2.9}$	Oguri et al. (2012b)	virial	0.275/0.725/0.702
SDSSJ1115+5319	0.466	11 15 14.85	+53 19 54.6	WL+SL	$4.38^{+1.26}_{-0.82}$	$9.29^{+2.68}_{-2.4}$	$5.25^{+1.51}_{-0.98}$	$10.59^{+3.05}_{-2.74}$	Oguri et al. (2012b)	virial	0.275/0.725/0.702
RCS2J1055+5548	0.466	10 55 04.59	+55 48 23.3	WL	$6.4^{+1.1}_{-1.1}$	$5.9^{+1.4}_{-1.4}$	$7.5^{+1.3}_{-1.3}$	$6.6^{+1.6}_{-1.6}$	Sereno et al. (2014)	200	0.3/0.7/0.7
RCS2J1055+5548	0.466	10 55 04.59	+55 48 23.3	WL	$5.16^{+3.4}_{-1.86}$	$4.55^{+1.52}_{-1.18}$	$6.17^{+4.07}_{-2.23}$	$5.13^{+1.71}_{-1.33}$	Oguri et al. (2012b)	virial	0.275/0.725/0.702
RCS2J1055+5548	0.466	10 55 04.59	+55 48 23.3	WL+SL	$6.22^{+1.18}_{-0.92}$	$4.29^{+1.17}_{-0.96}$	$7.41^{+1.4}_{-1.1}$	$4.79^{+1.31}_{-1.07}$	Oguri et al. (2012b)	virial	0.275/0.725/0.702
SDSSJ1456+5702	0.484	14 56 00.78	+57 02 20.3	WL	$15.6^{+2.8}_{-2.8}$	$4.3^{+0.7}_{-0.7}$	$18.1^{+3.2}_{-3.2}$	$4.6^{+0.8}_{-0.8}$	Sereno et al. (2014)	200	0.3/0.7/0.7
SDSSJ1456+5702	0.484	14 56 00.78	+57 02 20.3	WL	$2.4^{+1.36}_{-0.95}$	$5.56^{+1.69}_{-1.39}$	$2.92^{+1.65}_{-1.16}$	$6.68^{+2.03}_{-1.67}$	Oguri et al. (2012b)	virial	0.275/0.725/0.702
SDSSJ1456+5702	0.484	14 56 00.78	+57 02 20.3	WL+SL	$19.33^{+12.38}_{-5.33}$	$2.51^{+0.8}_{-0.71}$	$22.65^{+14.51}_{-6.24}$	$2.69^{+0.86}_{-0.76}$	Oguri et al. (2012b)	virial	0.275/0.725/0.702
SDSSJ1632+3500	0.49	16 32 10.26	+35 00 29.7	WL	$10.9^{+4.4}_{-4.4}$	$5.0^{+1.4}_{-1.4}$	$12.7^{+5.1}_{-5.1}$	$5.4^{+1.6}_{-1.6}$	Sereno et al. (2014)	200	0.3/0.7/0.7
SDSSJ1632+3500	0.49	16 32 10.26	+35 00 29.7	WL	$5.5^{+6.12}_{-2.58}$	$3.77^{+1.55}_{-1.25}$	$6.53^{+7.27}_{-3.06}$	$4.22^{+1.74}_{-1.4}$	Oguri et al. (2012b)	virial	0.275/0.725/0.702
SDSSJ1632+3500	0.49	16 32 10.26	+35 00 29.7	WL+SL	$7.2^{+5.03}_{-1.73}$	$3.6^{+1.43}_{-1.14}$	$8.51^{+5.94}_{-2.05}$	$3.98^{+1.58}_{-1.26}$	Oguri et al. (2012b)	virial	0.275/0.725/0.702
MACSJ1311.0-0311	0.494	13 11 01.9	-03 10 36	X-ray	$5.01^{+0.73}_{-0.35}$	$55.11^{+5.58}_{-5.58}$	$5.99^{+0.87}_{-0.42}$	$62.6^{+5.5}_{-6.34}$	Babyk et al. (2014)	200	0.27/0.73/0.73
MACSJ1311.0-0311	0.494	13 11 01.9	-03 10 36	WL+SL	$4.4^{+1.0}_{-1.0}$	$4.6^{+0.3}_{-0.3}$	$5.3^{+1.1}_{-1.1}$	$5.3^{+0.4}_{-0.4}$	Merten et al. (2014)	2500/200/virial	0.27/0.73/0.7
MACSJ1311.0-0311	0.494	13 11 01.9	-03 10 36	X-ray	$4.42^{+1.39}_{-1.05}$	$6.22^{+3.71}_{-2.15}$	$5.22^{+1.6}_{-1.22}$	$7.02^{+4.38}_{-2.49}$	Schmidt & Allen (2007)	virial	0.3/0.7/0.7
WARP J0030.5+2618	0.5	00 30 33.2	+26 18 19	WL	$2.0^{+1.8}_{-1.2}$	$7.2^{+3.6}_{-2.9}$	$2.4^{+2.2}_{-1.4}$	$8.7^{+4.3}_{-3.5}$	Israel et al. (2010)	200	0.3/0.7/0.72
SDSSJ1152+0930	0.517	11 52 47.38	+09 30 14.7	WL	$3.1^{+1.6}_{-1.6}$	$7.0^{+2.6}_{-2.6}$	$3.7^{+1.9}_{-1.9}$	$8.1^{+3.3}_{-3.3}$	Sereno et al. (2014)	200	0.3/0.7/0.7
SDSSJ1152+0930	0.517	11 52 47.38	+09 30 14.7	WL	$1.34^{+1.07}_{-0.7}$	$5.64^{+2.8}_{-2.0}$	$1.66^{+1.33}_{-0.87}$	$7.24^{+3.59}_{-2.57}$	Oguri et al. (2012b)	virial	0.275/0.725/0.702
SDSSJ1152+0930	0.517	11 52 47.38	+09 30 14.7	WL+SL	$2.96^{+0.77}_{-0.55}$	$4.92^{+2.19}_{-1.67}$	$3.55^{+0.92}_{-0.66}$	$5.75^{+2.56}_{-1.95}$	Oguri et al. (2012b)	virial	0.275/0.725/0.702
MACSJ1423.8+2404	0.543	14 23 47.6	+24 04 40	X-ray	$3.33^{+0.65}_{-0.63}$	$48.21^{+4.72}_{-4.71}$	$3.98^{+0.78}_{-0.75}$	$55.97^{+5.48}_{-5.47}$	Babyk et al. (2014)	200	0.27/0.73/0.73

Continued on next page

Table C.1 – *Continued*

Cluster	z	RA	Dec.	Method	$c_{200}$	$M_{200}$ ( $10^{14} M_\odot$ )	$c_{\text{vir}}$	$M_{\text{vir}}$ ( $10^{14} M_\odot$ )	Ref.	$\delta$	$\Omega_m/\Omega_\Lambda/h$
MACSJ1423.8+2404	0.543	14 23 47.6	+24 04 40	WL+SL	$4.7^{+1.2}_{-1.2}$	$5.7^{+1.0}_{-1.0}$	$5.7^{+2.8}_{-2.8}$	$6.5^{+1.1}_{-1.1}$	Merten et al. (2014)	2500/200/virial	0.27/0.73/0.7
MACSJ1423.8+2404	0.543	14 23 47.6	+24 04 40	X-ray	$7.69^{+0.7}_{-0.79}$	$5.28^{+1.13}_{-0.76}$	$8.92^{+0.81}_{-0.91}$	$5.77^{+1.27}_{-0.84}$	Schmidt & Allen (2007)	virial	0.3/0.7/0.7
MACS J1149.5+2223	0.544	11 49 35.1	+22 24 11	WL	$2.7^{+0.4}_{-0.4}$	$26.6^{+4.7}_{-4.7}$	$3.2^{+0.5}_{-0.5}$	$31.0^{+5.8}_{-5.8}$	Sereno et al. (2014)	200	0.3/0.7/0.7
MACS J0717.5+3745	0.546	07 17 30.9	+37 45 30	WL	$5.2^{+1.2}_{-1.2}$	$28.4^{+4.1}_{-4.1}$	$6.1^{+1.4}_{-1.4}$	$31.7^{+5.0}_{-5.0}$	Sereno et al. (2014)	200	0.3/0.7/0.7
MS 0015.9+1609	0.546	00 18 33.8	+16 26 17	X-ray	4.37	93.3	5.11	105.0	Molikawa et al. (1999)	virial	0.3/0.7/0.5
MS 0451.6-0305	0.55	04 54 11.1	-03 00 54	SL	$5.5^{+0.3}_{-0.3}$	$18.0^{+2.0}_{-2.0}$	$6.4^{+0.3}_{-0.3}$	$20.0^{+2.0}_{-2.0}$	Comerford & Natarajan (2007b)	200/virial	0.3/0.7/0.7
SDSSJ1209+2640	0.561	12 09 23.68	+26 40 46.7	WL	$6.7^{+1.3}_{-1.3}$	$7.7^{+2.1}_{-2.1}$	$7.8^{+1.5}_{-1.5}$	$8.5^{+2.4}_{-2.4}$	Sereno et al. (2014)	200	0.3/0.7/0.7
SDSSJ1209+2640	0.561	12 09 23.68	+26 40 46.7	WL+SL	$4.89^{+3.14}_{-1.91}$	$6.19^{+2.25}_{-1.81}$	$5.75^{+3.69}_{-2.25}$	$6.92^{+2.52}_{-2.02}$	Oguri et al. (2012b)	virial	0.275/0.725/0.702
SDSSJ1209+2640	0.561	12 09 23.68	+26 40 46.7	WL+SL	$6.71^{+1.36}_{-1.07}$	$5.48^{+1.66}_{-1.32}$	$7.85^{+1.59}_{-1.25}$	$6.03^{+1.83}_{-1.45}$	Oguri et al. (2012b)	virial	0.275/0.725/0.702
RXJ0848.7+4456	0.57	08 48 47.2	+44 56 17	X-ray	$0.82^{+0.05}_{-0.01}$	$3.32^{+0.73}_{-0.77}$	$1.02^{+0.06}_{-0.01}$	$4.42^{+0.97}_{-1.03}$	Babyk et al. (2014)	200	0.27/0.73/0.73
SDSSJ1029+2623	0.584	10 29 12.48	+26 23 32.0	WL+SL	$22.31^{+12.24}_{-6.51}$	$2.08^{+0.54}_{-0.47}$	$25.7^{+14.1}_{-7.5}$	$2.21^{+0.57}_{-0.5}$	Oguri et al. (2013)	virial	0.275/0.725/0.702
SDSSJ1029+2623	0.584	10 29 12.48	+26 23 32.0	WL	$9.2^{+4.3}_{-4.3}$	$2.9^{+0.7}_{-0.7}$	$10.6^{+4.9}_{-4.9}$	$3.1^{+0.8}_{-0.8}$	Sereno et al. (2014)	200	0.3/0.7/0.7
SDSSJ1029+2623	0.584	10 29 12.48	+26 23 32.0	WL	$9.89^{+12.51}_{-4.32}$	$1.85^{+0.68}_{-0.56}$	$11.48^{+14.52}_{-5.02}$	$2.0^{+0.73}_{-0.6}$	Oguri et al. (2012b)	virial	0.275/0.725/0.702
SDSSJ1029+2623	0.584	10 29 12.48	+26 23 32.0	WL+SL	$9.56^{+8.24}_{-3.59}$	$1.86^{+0.62}_{-0.52}$	$11.09^{+9.56}_{-4.17}$	$2.02^{+0.67}_{-0.57}$	Oguri et al. (2012b)	virial	0.275/0.725/0.702
SDSSJ1315+5439	0.588	13 15 09.30	+54 37 51.8	WL	$12.3^{+4.5}_{-4.5}$	$5.3^{+1.4}_{-1.4}$	$14.1^{+5.1}_{-5.1}$	$5.7^{+1.6}_{-1.6}$	Sereno et al. (2014)	200	0.3/0.7/0.7
SDSSJ1315+5439	0.588	13 15 09.30	+54 37 51.8	WL	$8.12^{+13.74}_{-3.96}$	$4.06^{+1.67}_{-1.34}$	$9.44^{+15.97}_{-4.6}$	$4.42^{+1.82}_{-1.46}$	Oguri et al. (2012b)	virial	0.275/0.725/0.702
SDSSJ1315+5439	0.588	13 15 09.30	+54 37 51.8	WL+SL	$8.32^{+12.34}_{-2.43}$	$4.01^{+1.52}_{-1.27}$	$9.66^{+14.33}_{-2.82}$	$4.37^{+1.66}_{-1.38}$	Oguri et al. (2012b)	virial	0.275/0.725/0.702
MACSJ2129.4-0741	0.589	21 29 26.2	-07 41 26	X-ray	$1.7^{+0.38}_{-0.41}$	$96.66^{+10.26}_{-10.15}$	$2.05^{+0.46}_{-0.49}$	$117.61^{+12.48}_{-12.35}$	Babyk et al. (2014)	200	0.27/0.73/0.73
MACSJ0647.7+7015	0.59	06 47 50.5	+70 14 55	WL	$7.3^{+2.6}_{-2.6}$	$11.4^{+3.0}_{-3.0}$	$8.4^{+3.0}_{-3.0}$	$12.5^{+3.5}_{-3.5}$	Sereno et al. (2014)	200	0.3/0.7/0.7
MACSJ0647.7+7015	0.59	06 47 50.5	+70 14 55	X-ray	$1.0^{+0.12}_{-0.11}$	$89.51^{+10.14}_{-9.28}$	$1.23^{+0.15}_{-0.14}$	$115.37^{+13.07}_{-11.96}$	Babyk et al. (2014)	200	0.27/0.73/0.73
SDSSJ1050+0017	0.6	10 50 39.90	+00 17 07.1	WL	$10.1^{+4.3}_{-4.3}$	$7.7^{+1.9}_{-1.9}$	$11.6^{+4.9}_{-4.9}$	$8.3^{+2.2}_{-2.2}$	Sereno et al. (2014)	200	0.3/0.7/0.7
SDSSJ1050+0017	0.6	10 50 39.90	+00 17 07.1	WL	$6.22^{+4.59}_{-2.29}$	$6.22^{+1.79}_{-1.55}$	$7.24^{+5.34}_{-2.67}$	$6.84^{+1.97}_{-1.71}$	Oguri et al. (2012b)	virial	0.275/0.725/0.702
SDSSJ1050+0017	0.6	10 50 39.90	+00 17 07.1	WL+SL	$6.15^{+4.17}_{-1.8}$	$6.21^{+1.79}_{-1.5}$	$7.16^{+4.86}_{-2.09}$	$6.84^{+1.97}_{-1.65}$	Oguri et al. (2012b)	virial	0.275/0.725/0.702
SDSSJ1420+3955	0.607	14 20 40.33	+39 55 09.8	WL	$4.3^{+1.1}_{-1.1}$	$8.9^{+2.7}_{-2.7}$	$5.0^{+1.3}_{-1.3}$	$10.0^{+3.2}_{-3.2}$	Sereno et al. (2014)	200	0.3/0.7/0.7
SDSSJ1420+3955	0.607	14 20 40.33	+39 55 09.8	WL	$8.24^{+5.44}_{-2.86}$	$6.36^{+2.02}_{-1.65}$	$9.55^{+6.3}_{-3.31}$	$6.92^{+2.2}_{-1.79}$	Oguri et al. (2012b)	virial	0.275/0.725/0.702
SDSSJ1420+3955	0.607	14 20 40.33	+39 55 09.8	WL+SL	$3.9^{+1.13}_{-0.84}$	$6.73^{+2.24}_{-1.8}$	$4.57^{+1.32}_{-0.98}$	$7.59^{+2.53}_{-2.03}$	Oguri et al. (2012b)	virial	0.275/0.725/0.702
3C 220.1	0.62	09 32 39.6	+79 06 32	SL	$4.3^{+0.2}_{-0.2}$	$3.1^{+0.3}_{-0.3}$	$5.0^{+0.2}_{-0.2}$	$3.5^{+0.3}_{-0.3}$	Comerford & Natarajan (2007b)	200/virial	0.3/0.7/0.7
SDSSJ2111-0114	0.638	21 11 19.34	-01 14 23.5	SL	$13.9^{+20.9}_{-8.8}$	$5.1^{+12.1}_{-2.5}$	$16.0^{+24.0}_{-10.1}$	$5.5^{+13.0}_{-2.7}$	Oguri et al. (2009b)	virial	0.26/0.74/0.72
SDSSJ2111-0114	0.638	21 11 19.34	-01 14 23.5	WL	$12.2^{+22.4}_{-8.2}$	$8.5^{+3.8}_{-3.0}$	$14.1^{+25.9}_{-9.5}$	$9.2^{+4.1}_{-3.2}$	Oguri et al. (2009b)	virial	0.26/0.74/0.72
SDSSJ2111-0114	0.638	21 11 19.34	-01 14 23.5	WL+SL	$12.2^{+22.4}_{-8.0}$	$8.5^{+3.8}_{-3.0}$	$14.1^{+25.9}_{-9.3}$	$9.2^{+4.1}_{-3.2}$	Oguri et al. (2009b)	virial	0.26/0.74/0.72

Continued on next page

Table C.1 – *Continued*

Cluster	z	RA	Dec.	Method	$c_{200}$	$M_{200}$ ( $10^{14} M_\odot$ )	$c_{\text{vir}}$	$M_{\text{vir}}$ ( $10^{14} M_\odot$ )	Ref.	$\delta$	$\Omega_m/\Omega_\Lambda/h$
SDSSJ2111-0114	0.638	21 11 19.34	-01 14 23.5	WL	$5.1^{+3.8}_{-3.8}$	$5.7^{+2.7}_{-2.7}$	$5.9^{+4.3}_{-4.3}$	$6.3^{+3.2}_{-3.2}$	Sereno et al. (2014)	200	0.3/0.7/0.7
SDSSJ2111-0114	0.638	21 11 19.34	-01 14 23.5	WL	$1.59^{+1.4}_{-0.84}$	$4.92^{+2.11}_{-1.75}$	$1.91^{+1.68}_{-1.01}$	$6.03^{+2.58}_{-2.14}$	Oguri et al. (2012b)	virial	0.275/0.725/0.702
SDSSJ2111-0114	0.638	21 11 19.34	-01 14 23.5	WL+SL	$4.11^{+2.71}_{-1.39}$	$4.69^{+2.17}_{-1.73}$	$4.79^{+3.16}_{-1.62}$	$5.25^{+2.43}_{-1.94}$	Oguri et al. (2012b)	virial	0.275/0.725/0.702
RCSJ1419.2+5326	0.64	14 19 12.0	+53 26 00	X-ray	$6.24^{+0.73}_{-0.71}$	$12.91^{+1.64}_{-1.72}$	$7.25^{+0.85}_{-0.82}$	$14.25^{+1.81}_{-1.9}$	Babyk et al. (2014)	200	0.27/0.73/0.73
SDSSJ1110+6459	0.659	11 10 17.70	+64 59 47.8	WL	$12.2^{+4.9}_{-4.9}$	$4.4^{+1.9}_{-1.9}$	$13.9^{+5.5}_{-5.5}$	$4.7^{+2.1}_{-2.1}$	Sereno et al. (2014)	200	0.3/0.7/0.7
SDSSJ1110+6459	0.659	11 10 17.70	+64 59 47.8	WL	$31.55^{+3.45}_{-24.16}$	$1.97^{+2.05}_{-0.64}$	$35.89^{+3.92}_{-27.48}$	$2.07^{+2.15}_{-0.67}$	Oguri et al. (2012b)	virial	0.275/0.725/0.702
SDSSJ1110+6459	0.659	11 10 17.70	+64 59 47.8	WL+SL	$19.61^{+15.26}_{-13.75}$	$2.13^{+2.27}_{-0.9}$	$22.39^{+17.42}_{-15.7}$	$2.26^{+2.41}_{-0.96}$	Oguri et al. (2012b)	virial	0.275/0.725/0.702
SDSSJ1004+4112	0.68	10 04 34.18	+41 12 43.5	WL	$8.5^{+4.4}_{-4.4}$	$2.6^{+1.9}_{-1.9}$	$9.7^{+4.9}_{-4.9}$	$2.8^{+2.1}_{-2.1}$	Sereno et al. (2014)	200	0.3/0.7/0.7
SDSSJ1004+4112	0.68	10 04 34.18	+41 12 43.5	WL	$3.81^{+26.08}_{-3.22}$	$2.52^{+3.88}_{-1.72}$	$4.42^{+30.26}_{-3.74}$	$2.82^{+4.34}_{-1.92}$	Oguri et al. (2012b)	virial	0.275/0.725/0.702
SDSSJ1004+4112	0.68	10 04 34.18	+41 12 43.5	WL+SL	$7.24^{+10.33}_{-2.72}$	$2.03^{+2.21}_{-1.31}$	$8.32^{+11.87}_{-3.13}$	$2.21^{+2.41}_{-1.43}$	Oguri et al. (2012b)	virial	0.275/0.725/0.702
SDSSJ1004+4112	0.68	10 04 34.18	+41 12 43.5	SL	5.0	3.87	6.0	4.25	Williams & Saha (2004)	200	0.3/0.7/0.7
MACSJ0744.9+3927	0.686	07 44 52.5	+39 27 27	WL	$7.1^{+2.6}_{-2.6}$	$12.9^{+3.3}_{-3.3}$	$8.1^{+2.9}_{-2.9}$	$14.0^{+3.8}_{-3.8}$	Sereno et al. (2014)	200	0.3/0.7/0.7
MACSJ0744.9+3927	0.686	07 44 52.5	+39 27 27	X-ray	$1.01^{+0.37}_{-0.16}$	$106.48^{+8.82}_{-6.18}$	$1.22^{+0.45}_{-0.19}$	$134.02^{+11.1}_{-7.78}$	Babyk et al. (2014)	200	0.27/0.73/0.73
MACSJ0744.9+3927	0.686	07 44 52.5	+39 27 27	WL+SL	$4.1^{+1.0}_{-1.0}$	$7.0^{+0.4}_{-0.4}$	$4.8^{+1.1}_{-1.1}$	$7.9^{+0.4}_{-0.4}$	Merten et al. (2014)	2500/200/virial	0.27/0.73/0.7
MACSJ0744.9+3927	0.686	07 44 52.5	+39 27 27	X-ray	$4.32^{+1.43}_{-1.06}$	$8.83^{+4.84}_{-3.16}$	$4.95^{+1.61}_{-1.2}$	$9.78^{+5.6}_{-3.58}$	Schmidt & Allen (2007)	virial	0.3/0.7/0.7
RXJ1221.4+4918	0.7	12 21 24.5	+49 18 13	X-ray	$2.39^{+0.37}_{-0.35}$	$46.64^{+5.22}_{-3.49}$	$2.81^{+0.44}_{-0.41}$	$54.23^{+6.07}_{-4.06}$	Babyk et al. (2014)	200	0.27/0.73/0.73
RXJ1113.1-2615	0.72	11 13 05.2	-26 15 26	X-ray	$3.28^{+0.73}_{-0.71}$	$5.3^{+0.73}_{-0.48}$	$3.81^{+0.85}_{-0.82}$	$6.02^{+0.83}_{-0.55}$	Babyk et al. (2014)	200	0.27/0.73/0.73
RCSJ1107.3-0523	0.735	11 07 22.8	-05 23 49	X-ray	$3.15^{+0.56}_{-0.45}$	$5.27^{+0.74}_{-0.45}$	$3.66^{+0.65}_{-0.52}$	$5.99^{+0.84}_{-0.51}$	Babyk et al. (2014)	200	0.27/0.73/0.73
RCSJ0224-0002	0.778	02 24 00.0	-00 02 00	X-ray	$2.78^{+0.25}_{-0.25}$	$10.51^{+1.11}_{-1.28}$	$3.22^{+0.29}_{-0.29}$	$11.99^{+1.27}_{-1.46}$	Babyk et al. (2014)	200	0.27/0.73/0.73
CLG 1137.5+6625	0.78	11 40 23.9	+66 08 19	WL	$3.6^{+1.9}_{-1.9}$	$9.3^{+4.6}_{-4.6}$	$4.1^{+2.1}_{-2.1}$	$10.4^{+5.4}_{-5.4}$	Sereno et al. (2014)	200	0.3/0.7/0.7
RCSJ2318.5+0034	0.78	23 18 31.5	+00 34 18	X-ray	$1.18^{+0.19}_{-0.17}$	$28.37^{+4.11}_{-3.18}$	$1.4^{+0.23}_{-0.2}$	$34.49^{+5.0}_{-3.87}$	Babyk et al. (2014)	200	0.27/0.73/0.73
MS 1137.5+6625	0.783	11 40 23.9	+66 08 19	SL	$3.3^{+0.2}_{-0.2}$	$6.5^{+0.7}_{-0.7}$	$3.8^{+0.2}_{-0.2}$	$7.2^{+0.8}_{-0.8}$	Comerford & Natarajan (2007b)	200/virial	0.3/0.7/0.7
RX J1716.6+6708	0.81	17 16 49.6	+67 08 30	WL	$5.0^{+4.7}_{-4.7}$	$5.0^{+3.4}_{-3.4}$	$5.7^{+5.2}_{-5.2}$	$5.5^{+4.0}_{-4.0}$	Sereno et al. (2014)	200	0.3/0.7/0.7
MS 1054-0321	0.83	10 56 59.5	-03 37 28	WL	$0.9^{+0.8}_{-0.8}$	$23.0^{+16.4}_{-16.4}$	$1.1^{+0.9}_{-0.9}$	$28.1^{+22.5}_{-22.5}$	Sereno et al. (2014)	200	0.3/0.7/0.7
CL J0152-1357	0.84	01 52 41.0	-13 57 45	WL	$11.3^{+3.9}_{-3.9}$	$2.9^{+0.6}_{-0.6}$	$12.6^{+4.3}_{-4.3}$	$3.1^{+0.7}_{-0.7}$	Sereno et al. (2014)	200	0.3/0.7/0.7
RCSJ1620.2+2929	0.87	16 20 12.0	+29 29 00	X-ray	$4.38^{+0.72}_{-0.71}$	$7.57^{+1.02}_{-1.04}$	$4.98^{+0.82}_{-0.81}$	$8.35^{+1.13}_{-1.15}$	Babyk et al. (2014)	200	0.27/0.73/0.73
CLJ 1226.9+3332	0.89	12 26 58.0	+33 32 54	WL	$4.3^{+1.1}_{-1.1}$	$10.1^{+2.3}_{-2.3}$	$4.8^{+1.2}_{-1.2}$	$11.1^{+2.6}_{-2.6}$	Sereno et al. (2014)	200	0.3/0.7/0.7
CLJ 1226.9+3332	0.89	12 26 58.0	+33 32 54	WL+SL	$4.0^{+0.9}_{-0.9}$	$15.6^{+1.0}_{-1.0}$	$4.5^{+1.1}_{-1.1}$	$17.2^{+1.1}_{-1.1}$	Merten et al. (2014)	2500/200/virial	0.27/0.73/0.7
CLJ 1226.9+3332	0.89	12 26 58.0	+33 32 54	X-ray	$2.04^{+0.32}_{-0.36}$	$143.19^{+15.26}_{-17.26}$	$2.35^{+0.37}_{-0.41}$	$164.38^{+17.52}_{-19.81}$	Babyk et al. (2014)	200	0.27/0.73/0.73
CLJ 1226.9+3332	0.89	12 26 58.0	+33 32 54	X-ray	$7.9^{+1.7}_{-1.4}$	$6.8^{+1.6}_{-1.2}$	$8.8^{+1.9}_{-1.5}$	$7.2^{+1.7}_{-1.3}$	Maughan et al. (2007)	200	0.3/0.7/0.7

Continued on next page

Table C.1 – *Continued*

Cluster	z	RA	Dec.	Method	$c_{200}$	$M_{200}$ ( $10^{14} M_\odot$ )	$c_{\text{vir}}$	$M_{\text{vir}}$ ( $10^{14} M_\odot$ )	Ref.	$\delta$	$\Omega_m/\Omega_\Lambda/h$
CLJ1604+4304	0.9	16 04 25.1	+43 04 53	WL	$9.4^{+5.8}_{-5.8}$	$4.0^{+2.4}_{-2.4}$	$10.5^{+6.4}_{-6.4}$	$4.2^{+2.6}_{-2.6}$	Sereno et al. (2014)	200	0.3/0.7/0.7
RCS J2319.8+0038	0.904	23 19 53.3	+00 38 13	X-ray	$3.27^{+0.56}_{-0.55}$	$40.96^{+4.25}_{-5.22}$	$3.72^{+0.64}_{-0.63}$	$45.74^{+4.75}_{-5.83}$	Babyk et al. (2014)	200	0.27/0.73/0.73
RCS J2319.8+0038	0.904	23 19 53.3	+00 38 13	WL	$11.5^{+4.8}_{-4.8}$	$2.4^{+0.9}_{-0.9}$	$12.8^{+5.3}_{-5.3}$	$2.5^{+1.0}_{-1.0}$	Sereno et al. (2014)	200	0.3/0.7/0.7
RCSJ0439-2904	0.951	04 39 38.0	-29 04 55	WL	$7.3^{+4.9}_{-4.9}$	$3.0^{+1.3}_{-1.3}$	$8.1^{+5.4}_{-5.4}$	$3.2^{+1.5}_{-1.5}$	Sereno et al. (2014)	200	0.3/0.7/0.7
RCSJ0439-2904	0.951	04 39 38.0	-29 04 55	X-ray	$4.12^{+0.25}_{-0.21}$	$3.79^{+0.56}_{-0.27}$	$4.65^{+0.28}_{-0.24}$	$4.17^{+0.62}_{-0.3}$	Babyk et al. (2014)	200	0.27/0.73/0.73
XMMU J1230.3+1339	0.97	12 30 17.0	+13 39 01	WL	$4.0^{+14.0}_{-2.0}$	$8.8^{+4.2}_{-4.2}$	$4.5^{+15.8}_{-2.3}$	$9.7^{+4.6}_{-4.6}$	Lerchster et al. (2011)	200	0.27/0.73/0.72
XMMU J1230.3+1339	0.97	12 30 17.0	+13 39 01	WL	$2.1^{+2.1}_{-2.1}$	$24.4^{+15.4}_{-15.4}$	$2.4^{+2.3}_{-2.3}$	$27.5^{+18.8}_{-18.8}$	Sereno et al. (2014)	200	0.3/0.7/0.7
RCS J1511.0+0903	0.97	15 11 03.8	+09 03 15	WL	$11.4^{+5.5}_{-5.5}$	$1.6^{+0.7}_{-0.7}$	$12.6^{+6.0}_{-6.0}$	$1.7^{+0.8}_{-0.8}$	Sereno et al. (2014)	200	0.3/0.7/0.7
XMMU J1229.4+0151	0.98	12 29 28.8	+01 51 34	WL	$0.5^{+0.6}_{-0.6}$	$34.1^{+22.9}_{-22.9}$	$0.6^{+0.7}_{-0.7}$	$43.3^{+35.2}_{-35.2}$	Sereno et al. (2014)	200	0.3/0.7/0.7
RCS 0221-0321	1.02	02 21 41	-03 21 47	WL	$11.6^{+5.2}_{-5.2}$	$1.6^{+0.6}_{-0.6}$	$12.8^{+5.7}_{-5.7}$	$1.7^{+0.6}_{-0.6}$	Sereno et al. (2014)	200	0.3/0.7/0.7
RCS J0220.9-0333	1.03	02 20 55.7	-03 33 10	WL	$5.6^{+4.4}_{-4.4}$	$4.0^{+2.1}_{-2.1}$	$6.2^{+4.8}_{-4.8}$	$4.3^{+2.4}_{-2.4}$	Sereno et al. (2014)	200	0.3/0.7/0.7
WARP J1415.1+3612	1.03	14 15 11.1	+36 12 03	WL	$4.0^{+2.1}_{-2.1}$	$3.3^{+2.3}_{-2.3}$	$4.5^{+2.3}_{-2.3}$	$3.6^{+2.6}_{-2.6}$	Sereno et al. (2014)	200	0.3/0.7/0.7
RCS J2345-3632	1.04	23 45 27.3	-36 32 50	WL	$2.7^{+2.6}_{-2.6}$	$2.3^{+1.7}_{-1.7}$	$3.0^{+2.9}_{-2.9}$	$2.5^{+2.0}_{-2.0}$	Sereno et al. (2014)	200	0.3/0.7/0.7
RCS J2156.7-0448	1.07	21 56 42.1	-04 48 04	WL	$7.9^{+5.4}_{-5.4}$	$0.9^{+0.7}_{-0.7}$	$8.7^{+5.9}_{-5.9}$	$1.0^{+0.8}_{-0.8}$	Sereno et al. (2014)	200	0.3/0.7/0.7
RCS J0337-2844	1.1	03 37 50.4	-28 44 28	WL	$3.3^{+3.9}_{-3.9}$	$5.9^{+5.3}_{-5.3}$	$3.7^{+4.3}_{-4.3}$	$6.5^{+6.1}_{-6.1}$	Sereno et al. (2014)	200	0.3/0.7/0.7
RXJ0910.7+5422	1.11	09 10 45.0	+54 22 08	X-ray	$2.64^{+0.25}_{-0.21}$	$64.92^{+5.67}_{-7.34}$	$2.96^{+0.28}_{-0.24}$	$72.15^{+6.3}_{-8.16}$	Babyk et al. (2014)	200	0.27/0.73/0.73
RXJ0910.7+5422	1.11	09 10 45.0	+54 22 08	WL	$6.6^{+3.9}_{-3.9}$	$3.3^{+1.3}_{-1.3}$	$7.3^{+4.2}_{-4.2}$	$3.5^{+1.5}_{-1.5}$	Sereno et al. (2014)	200	0.3/0.7/0.7
ISCS J1432.4+3332	1.11	14 32 29.1	+33 32 48	WL	$2.0^{+1.5}_{-1.5}$	$7.3^{+5.3}_{-5.3}$	$2.2^{+1.7}_{-1.7}$	$8.2^{+6.2}_{-6.2}$	Sereno et al. (2014)	200	0.3/0.7/0.7
XMMU J2205.8-0159	1.12	22 05 50.2	-01 59 29	WL	$4.7^{+3.3}_{-3.3}$	$2.0^{+1.3}_{-1.3}$	$5.2^{+3.6}_{-3.6}$	$2.2^{+1.5}_{-1.5}$	Sereno et al. (2014)	200	0.3/0.7/0.7
XLSS J0223-0436	1.22	02 23 03	-04 36 18	WL	$0.8^{+0.9}_{-0.9}$	$25.4^{+21.6}_{-21.6}$	$0.9^{+1.0}_{-1.0}$	$29.8^{+28.2}_{-28.2}$	Sereno et al. (2014)	200	0.3/0.7/0.7
RDCS J1252-2927	1.24	12 52 54.4	-29 27 17	WL	$4.6^{+1.7}_{-1.7}$	$6.3^{+1.7}_{-1.7}$	$5.0^{+1.8}_{-1.8}$	$6.8^{+1.9}_{-1.9}$	Sereno et al. (2014)	200	0.3/0.7/0.7
ISCS J1434.5+3427	1.24	14 34 28.5	+34 26 22	WL	$5.9^{+6.1}_{-6.1}$	$2.3^{+1.9}_{-1.9}$	$6.5^{+6.6}_{-6.6}$	$2.4^{+2.1}_{-2.1}$	Sereno et al. (2014)	200	0.3/0.7/0.7
RDCS J0849+4452	1.26	08 48 56.2	+44 52 00	WL	$2.8^{+1.0}_{-1.0}$	$3.4^{+1.6}_{-1.6}$	$3.1^{+1.1}_{-1.1}$	$3.7^{+1.8}_{-1.8}$	Sereno et al. (2014)	200	0.3/0.7/0.7
ISCS J1429.3+3437	1.26	14 29 18.5	+34 37 25	WL	$0.4^{+0.5}_{-0.5}$	$39.0^{+28.1}_{-28.1}$	$0.5^{+0.6}_{-0.6}$	$48.8^{+41.4}_{-41.4}$	Sereno et al. (2014)	200	0.3/0.7/0.7
RXJ0849+4452	1.26	08 53 43.6	+35 45 53.8	X-ray	$1.14^{+0.11}_{-0.1}$	$4.67^{+0.66}_{-0.47}$	$1.28^{+0.12}_{-0.11}$	$5.37^{+0.76}_{-0.54}$	Babyk et al. (2014)	200	0.27/0.73/0.73
RDCS J0848+4453	1.27	08 48 34.2	+44 53 35	WL	$2.8^{+4.4}_{-4.4}$	$2.1^{+2.4}_{-2.4}$	$3.1^{+4.8}_{-4.8}$	$2.3^{+2.8}_{-2.8}$	Sereno et al. (2014)	200	0.3/0.7/0.7
ISCS J1432.6+3436	1.36	14 32 38.3	+34 36 49	WL	$5.3^{+5.5}_{-5.5}$	$3.4^{+2.7}_{-2.7}$	$5.8^{+5.9}_{-5.9}$	$3.6^{+3.0}_{-3.0}$	Sereno et al. (2014)	200	0.3/0.7/0.7
ISCS J1434.7+3519	1.37	14 34 46.3	+35 19 45	WL	$0.7^{+0.9}_{-0.9}$	$11.1^{+15.9}_{-15.9}$	$0.8^{+1.0}_{-1.0}$	$13.0^{+20.1}_{-20.1}$	Sereno et al. (2014)	200	0.3/0.7/0.7
XMMU J2235.3-2557	1.39	22 35 20.6	-25 57 42	WL	$2.1^{+1.4}_{-1.4}$	$12.7^{+11.7}_{-11.7}$	$2.3^{+1.5}_{-1.5}$	$13.9^{+13.2}_{-13.2}$	Sereno et al. (2014)	200	0.3/0.7/0.7
ISCS J1438.1+3414	1.41	14 38 09.5	+34 14 19	WL	$6.9^{+5.9}_{-5.9}$	$2.6^{+2.0}_{-2.0}$	$7.5^{+6.3}_{-6.3}$	$2.7^{+2.2}_{-2.2}$	Sereno et al. (2014)	200	0.3/0.7/0.7

Continued on next page

Table C.1 – *Continued*

Cluster	z	RA	Dec.	Method	$c_{200}$	$M_{200}$ ( $10^{14} M_\odot$ )	$c_{\text{vir}}$	$M_{\text{vir}}$ ( $10^{14} M_\odot$ )	Ref.	$\delta$	$\Omega_m/\Omega_\Lambda/h$
ISCS J1438.1+3414	1.41	14 38 09.5	+34 14 19	X-ray	$0.55^{+0.05}_{-0.08}$	$293.15^{+18.27}_{-36.84}$	$0.63^{+0.06}_{-0.09}$	$353.98^{+22.06}_{-44.48}$	Babyk et al. (2014)	200	$0.27/0.73/0.73$
XMMXCS J2215.9-1738	1.45	22 15 58.5	-17 38 02	WL	$8.7^{+5.9}_{-5.9}$	$2.7^{+1.6}_{-1.6}$	$9.4^{+6.3}_{-6.3}$	$2.8^{+1.7}_{-1.7}$	Sereno et al. (2014)	200	$0.3/0.7/0.7$

**Table C.2:** A Summary of The References

Reference	# Measurements	# Clusters (Unique)	Method(s)
Babyk et al. (2014)	128	128	X-ray
Sereno et al. (2014)	109	104	WL
Rines & Diaferio (2006)	72	72	CM
Oguri et al. (2012b)	56	28	WL+SL, WL
Ettori et al. (2011)	44	44	X-ray
Wojtak & Łokas (2010)	41	41	LOSVD
Schmidt & Allen (2007)	31	31	X-ray
Okabe et al. (2010)	26	26	WL
Xu et al. (2001)	22	22	X-ray
Abdullah et al. (2011)	20	20	LOSVD
Merten et al. (2014)	19	19	WL+SL
Gastaldello et al. (2007a)	16	16	X-ray
Molikawa et al. (1999)	13	13	X-ray
Voigt & Fabian (2006)	12	12	X-ray
Vikhlinin et al. (2006)	12	12	X-ray
Oguri et al. (2009b)	12	4	WL+SL, SL, WL
Bardeau et al. (2007)	11	11	WL
Pointecouteau et al. (2005)	10	10	X-ray
Allen et al. (2003)	10	10	X-ray
Rines et al. (2003)	9	9	CM
Okabe & Umetsu (2008)	9	9	WL
Łokas et al. (2006)	6	6	LOSVD
Umetsu et al. (2011b)	5	5	WL

*Continued on next page*

Table C.2 – *Continued from previous page*

Reference	# Measurements	# Clusters (Unique)	Method(s)
Comerford & Natarajan (2007b)	5	5	SL
Umetsu et al. (2009)	4	4	WL
Umetsu et al. (2015)	3	1	WL+SL, SL, WL
Pratt & Arnaud (2005)	3	3	X-ray
Halkola et al. (2006b)	3	1	WL+SL, SL, WL
Corless et al. (2009)	3	3	WL
Clowe (2003)	3	3	WL
Clowe & Schneider (2001a)	3	3	WL
Zitrin et al. (2010)	2	1	WL+SL, WL
Umetsu & Broadhurst (2008)	2	1	WL+SL, WL
Okabe et al. (2015)	2	2	WL
Markevitch et al. (1999)	2	2	X-ray
Gavazzi (2005)	2	1	WL+SL, SL
Gavazzi et al. (2003)	2	1	SL, WL
Donnarumma et al. (2009)	2	1	X-ray, SL
Démocles et al. (2010)	2	2	X-ray
Clowe & Schneider (2002)	2	2	WL
Buckley-Geer et al. (2011)	2	1	WL+SL, WL
Biviano et al. (2013)	2	1	CM, LOSVD
Zitrin et al. (2011)	1	1	WL+SL
Zekser et al. (2006)	1	1	SL
Williams & Saha (2004)	1	1	SL
Wang et al. (2005)	1	1	X-ray
Schirmer et al. (2010)	1	1	WL

*Continued on next page*

Table C.2 – *Continued from previous page*

Reference	# Measurements	# Clusters (Unique)	Method(s)
Pointecouteau et al. (2004)	1	1	X-ray
Paulin-Henriksson et al. (2007)	1	1	WL
Okabe et al. (2014)	1	1	WL
Okabe et al. (2011)	1	1	WL
Oguri et al. (2013)	1	1	WL+SL
Medezinski et al. (2007)	1	1	WL
McLaughlin (1999)	1	1	X-ray
Maughan et al. (2007)	1	1	X-ray
Lokas & Mamon (2003)	1	1	LOSVD
Limousin et al. (2007b)	1	1	WL+SL
Lerchster et al. (2011)	1	1	WL
Lewis et al. (2003)	1	1	X-ray
Kubo et al. (2007)	1	1	WL
Kneib et al. (2003)	1	1	WL+SL
Kling et al. (2005)	1	1	WL
King et al. (2002)	1	1	WL
Khosroshahi et al. (2006)	1	1	X-ray
Kelson et al. (2002)	1	1	LOSVD
Israel et al. (2010)	1	1	WL
Gruen et al. (2013)	1	1	WL
Gavazzi et al. (2009)	1	1	WL
Gastaldello et al. (2008)	1	1	X-ray
Gastaldello et al. (2007b)	1	1	X-ray
Gavazzi (2002)	1	1	SL

*Continued on next page*

Table C.2 – *Continued from previous page*

Reference	# Measurements	# Clusters (Unique)	Method(s)
Eichner et al. (2013)	1	1	SL
David et al. (2001)	1	1	X-ray
Coe et al. (2010)	1	1	SL
Clowe & Schneider (2001b)	1	1	WL
Buote et al. (2005)	1	1	X-ray
Buote & Lewis (2004)	1	1	X-ray
Broadhurst et al. (2005c)	1	1	SL
Broadhurst et al. (2005b)	1	1	WL
Bardeau et al. (2005)	1	1	WL
Andersson & Madejski (2004)	1	1	X-ray

## Vita

### Austen M. Groener

#### Education

- Drexel University, Philadelphia, Pennsylvania USA
  - Ph.D., Physics, September 2015
  - M.S., Physics, June 2011
- Hartwick College, Oneonta, New York USA
  - B.A., Physics, May 2009

#### Publications

- “The Galaxy Cluster Concentration-Mass Scaling Relation”, 2015
- “Shape Profiles and Orientation Bias for Weak and Strong Lensing Cluster Halos”, ApJ, 795, 2, 2014

#### Awards

- Drexel University Outstanding Teaching Assistant Honorable Mention, 2012
- Drexel College of Arts and Sciences Research Award, 2011
- Hartwick College Service Award, 2009
- Hartwick College Faculty Scholar, 2008

#### Teaching Experience

- **Grader.** Physics 432/532: Cosmology, Drexel University
- **Grader.** Physics 631: General Relativity, Drexel University
- **Teaching Assistant/Telescope Operator.** Physics 232: Observational Astronomy, Drexel University, *The Lynch Observatory*
- **Teaching Assistant.** Physics 113, 114, 115: Contemporary Physics I, II, III, Drexel University
- **Teaching Assistant.** Physics 152, 153, 154: Introductory Physics I, II, III, Drexel University
- **Teaching Assistant.** Physics 135: How Things Work, Drexel University
- **Teaching Assistant.** Physics 101, 102: Fundamentals of Physics I, II, Drexel University
- **Supplemental Instructor/Private Tutor.** Physics 201, 202: General Physics I, II, Hartwick College
- **Supplemental Instructor/Private Tutor.** Physics 163: General Astronomy, Hartwick College

#### Public Outreach

- **Dragons Code**
- **Volunteer at the Lynch Observatory**

*October 2014 to March 2015*  
*September 2009 to December 2014*

